The potential of remote sensing technologies for monitoring the productivity of dry season irrigated rice

A thesis submitted to The University of Manchester for the degree of Doctor of Philosophy in the Faculty of Humanities

By

Oluseun A. Adeluyi

2020

Department of Geography

School of Education, Environment and Development

‘Blank page’

Contents

Word count: 51,051

Abstract

Rice is an important staple crop and significantly contributes to the dietary needs of the global population. From the African context, Nigeria and most sub-Saharan countries rely on rice importation to meet the rising consumption demands, mainly due to low yield returns. As such, monitoring rice yield and yield indicators (e.g. Leaf Area Index, biomass) in order to understand patterns and trends of rice growth is fundamental to improve yield outcomes. In this PhD rice yield and yield indicators were monitored using a combination of proximal, airborne and satellite sensors, across a range of spatial scales with the overall aim of furthering our understanding of the dynamics of irrigated rice yields. The first main objective of the thesis investigated the relative merits of structural and multispectral information for estimating centimetre scale rice above ground biomass from very high spatial resolution drone imagery. The focus was the reproductive and ripening stages of rice growth due to the strong relationship between biomass and yield at these stages. Results indicated that crop structural information, derived from a consumer-grade RGB camera, was of greater importance for rice biomass estimation than multispectral information. The second object of the thesis explored the potential of a hybrid gaussian process regression (GPR) - radiative transfer model (RTM) to estimate the phenological dynamics of rice Leaf Area Index (LAI). Sentinel-2 spectral bands were simulated from field spectroscopy data and combined with extensive *in situ* field measurement to develop and test a hybrid LAI prediction model. Results were also compared with the satellite-derived Sentinel-2 LAI standard. The findings demonstrated the potential of the proposed hybrid model for predicting within-season dynamics of rice LAI. The third objective of the thesis determined the relative importance of the spatial and spectral resolution of Sentinel-2 for estimating rice yield across a range of spatial extents. This section investigated the suitability of Sentinel-2 for predicting within and between field yield variability across varying spatial extents. The results demonstrated that the spatial resolution of Sentinel-2 data was more important than the spectral resolution for predicting within field yields. Results also demonstrated the potential of Sentinel-2 data for estimating rice yields across smallholder rice farms.

Declaration

No portion of the work referred to in the thesis has been submitted in support of an application for another degree or qualification of this or any other university or other institute of learning.

Copyright Statement

The following four notes on copyright and the ownership of intellectual property rights must be included as written below:

i. The author of this thesis (including any appendices and/or schedules to this thesis) owns certain copyright or related rights in it (the "Copyright") and s/he has given The University of Manchester certain rights to use such Copyright, including for administrative purposes.

ii. Copies of this thesis, either in full or in extracts and whether in hard or electronic copy, may be made only in accordance with the Copyright, Designs and Patents Act 1988 (as amended) and regulations issued under it or, where appropriate, in accordance with licensing agreements which the University has from time to time. This page must form part of any such copies made.

iii. The ownership of certain Copyright, patents, designs, trademarks and other intellectual property (the "Intellectual Property") and any reproductions of copyright works in the thesis, for example graphs and tables ("Reproductions"), which may be described in this thesis, may not be owned by the author and may be owned by third parties. Such Intellectual Property and Reproductions cannot and must not be made available for use without the prior written permission of the owner(s) of the relevant Intellectual Property and/or Reproductions.

iv. Further information on the conditions under which disclosure, publication and commercialisation of this thesis, the Copyright and any Intellectual Property and/or Reproductions described in it may take place is available in the University IP Policy (seehttp://documents.manchester.ac.uk/DocuInfo.aspx?DocID=24420), in any relevant Thesis restriction declarations deposited in the University Library, The University Library's regulations (seehttp://www.library.manchester.ac.uk/about/regulations/) and in The University's policy on Presentation of Theses

Dedication

I dedicate this thesis to God Almighty who has been my eternal rock and source of refuge. I also dedicate this thesis to my wife, Marian, my daughter, Temilayo, my parents (Mr and Mrs Adeluyi), my siblings (Dr Femi Adeluyi, Mrs Bola Orewole and Mr Tunde Adeluyi), to my extended family members and all well-wishers.

Acknowledgement

First and foremost, I would like to thank my research supervisors, Angela Harris, Gareth Clay and Timothy Foster. Without their assistance and dedicated involvement in every step of the PhD process, this thesis would have never been accomplished. I use this opportunity to sincerely thank you for your mentorship, support, encouragement and understanding over the past four years.

The Petroleum Technology Development Fund funded this research under scholarship number PTDF/ED/PHD/AOA/909/16. I will like to appreciate Mark Mclean and Olam International for funding my fieldwork, providing stipend for my field assistants and catering for our accommodation during the fieldwork at Olam rice farm. I will like to acknowledge N8 Agri-food for providing funding for training and logistics during the course of my study. I am also grateful to the management of the National Space Research and Development Agency for the support offered through a study leave. Without these funding bodies, it would have been impossible to undertake research of this magnitude.

Getting through my thesis required more than academic and financial support, and I have a couple of people to thank for listening to and, at times, having to tolerate me during the study. I will like to appreciate my field assistances, Rotji Golu and Joshua Adebayo, who ensured the field study continued when I was away for the birth of my daughter. I want to appreciate Darrel and John Salter from Korec for offering to exchange their drone camera when mine developed issues and also providing support remotely. I'll like to appreciate Peter Kabano for encouraging me during some difficult periods during the study. I also want to specially appreciate Gail Millin-Chalabi for providing a work station for me to process my drone data and for being very accommodating during the PhD program. I want to thank the staff and PhD students in the Geography department for providing an enabling environment to work and thrive. It was a pleasure knowing each one of you.

And finally, I appreciate my family for their patience and support through my study period, especially my wife, Marian and daughter, Temilayo. Thank you for your encouragement, sacrifice, love and unwavering selflessness.

Key Words

AGB	-	Above ground Biomass
ANN	-	Artificial Neural Network
AWMD	-	Alternate Wetting and Moderate Drying
AWSD	-	Alternate Wetting and Severe Drying
B	-	Block
CF	-	Continuous Flooding
Chl	-	Chlorophyll
CI-EDGE	-	Chlorophyll Red Edge
DAS	-	Days After Sowing
DSM	-	Digital Surface Model
EO	-	Earth Observation
ESA	-	European Space Agency
GCP	-	Ground Control Point
GLCM	-	Gray Level Co-occurrence Matrix
GNDVI	-	Green Normalised Difference Vegetation Index
GPR	-	Gaussian Process Regression
Ha	-	Hectares
HN	-	High Nitrogen
KRR	-	Kernel Ridge Regression
LAI	-	Leaf Area Index
LN	-	Low Nitrogen
LUT	-	Look-up Table
MAE	-	Mean Absolute Error
MLRA	-	Machine Learning Regression Algorithm
MSI	-	Multispectral Imager
NDRE	-	Normalised Difference Red Edge
NDVI	-	Normalised Difference Vegetation Index
NERICA	-	New Rice for Africa
NIR	-	Near Infrared
NN	-	Normal Nitrogen

OSAVI	-	Optimised Soil Vegetation Index
P	-	Plot
PH	-	Plant Height
PROSAIL	-	PROSPECT and SAIL
PROSAIL-GPR-		PROSPECT and SAIL – Gaussian Process Regression
RF	-	Random Forest
RMSE	-	Root Mean Square Error
RGB	-	Red Green Blue
RS	-	Remote Sensing
SLM	-	Simple Linear Model
SE	-	Standard Error
SNAP	-	Sentinel-2 Application Platform
SP	-	Sub-Plot
t/ha	-	Tonnes per Hectare
TM	-	Texture Metrics
TOC	-	Top Of Canopy
VI	-	Vegetation Indices
UAV	-	Unmanned Aerial Vehicle

Chapter 1 Introduction

Summary

This chapter outlines the overarching research context and rationale to the research. The chapter begins by discussing the global importance of rice as a global staple food source, before focusing on rice consumption and farming in sub-Saharan Africa, and specifically in a Nigerian context. The chapter also identifies the limitations of current monitoring and management practices within Nigeria, which has led to low rice crop yields, despite Nigeria's government decision to prioritise the rice and agricultural sector. The potential of remote sensing for improving the monitoring of irrigated dry season rice farming in this region of Africa is also discussed. Finally, the chapter presents the overarching aim and objectives of the PhD research, as well as the briefly explaining the methodological rationale and thesis structure.

1.1 Research Context

Rice is characterised as a semi-aquatic plant with two important species for human consumption: Asian rice (*Oryza sativa*), which was first cultivated in Southeast Asia (somewhere around India, Myanmar, Thailand, North Vietnam, or China) and African rice (*Oryza glaberrima*) found/first cultivated in west-Africa (somewhere around Nigeria and Ghana). With almost 500 million metric tons of rice produced at a global scale and cultivated on 167.13 million hectares of land (Statistica, 2020a), rice is considered a major staple food of more than half of the world's population (Khir and Pan, 2019). Its growth and cultivation cuts across all continents except for Antarctica (Brady, 1981). According to Global Rice Science Partnership (GRiSP,2013), rice contributes more than 20% of people's global daily calories, 19% of global human per capita energy and 13% of per capita protein, thereby making rice significant towards attain the 2nd objective of the Sustainable Development goals (zero hunger).

In the context of sub-Saharan Africa, rice consumption has increased by almost 300% between 1961 and 2013 (11 kg and 28 kg, respectively; OECD-FAO, 2019). Increasing trends in rice consumption are primarily caused by high rates of population growth and consumer preferences. Such increase in rice demand have led to the need to import rice in large quantities (30million tonnes) at great economic cost to the sub-Saharan region. For example, over £3.5 billion was spent on importing rice in 2008 (GRiSP, 2013). The demand for rice is highest in west African countries where studies show an annual per capita rise in rice

consumption from 10kg in 1961 to 54kg in 2017 (Soullier et al., 2020), with rice consumption rates in Guinea, Guinea-Bissau, Liberia and Sierra Leone consuming more than 90 kg per capita per year. In particular, rice consumption has risen rapidly in both Nigeria and Ghana (by 2.3% and 1.8% 2017 respectively), considered two of the most populated countries in the sub-Saharan region (Soullier et al., 2020). Increases in rice consumption across both countries is primarily driven by population growth and increased levels of urbanisation (Mendez del Villar and Lançon, 2015).

Consumption figures confirm the importance of rice as a panacea to tackling food insecurity globally and particularly in developing regions like sub-Saharan Africa(Ittersum et al., 2016). However, shortfalls exist between current levels of rice production and the amount needed to feed the population of sub-Saharan Africa and Nigeria in years to come. (OECD-FAO, 2019) projections state that sub-Saharan population is expected to double by 2050, with a growth rate of 2.3% per annum, while Nigeria population is expected to rise to 400 million people -– about 200 million more mouths to feed than in 2020. At the same time, urgency is needed to cut greenhouse gas emissions from rice production to optimize the production of rice without the conversion of forests to agriculture. Similarly, due to the water demands, rice is a major user of irrigation water, accounting for approximately 40 per cent of irrigated water demand (Sustainable Rice Platform (SRP), 2019). The future challenge for the sub-Saharan rice industry is to foster substantial growth, needed to satisfy the growing demand, in a way that aligns with the consumer-driven environmental constraints (Okpiaifo et al., 2020). For countries like Nigeria with vast arable land, the call for sustainable ways of growing rice and boosting production will foster the charge to combat hunger and poverty and to meet the objectives of the African Development Fund, whose 1st and 2nd Objectives are to end poverty in Africa.

After years of neglect in the rice and agricultural sector as a result of the oil boom in the 1970s, usually referred to as the dutch-disease (Okotie, 2018), within the last two decades, the Nigerian government has taken the initiative to improve the production and yield potential of rice grown within Nigeria. In the words of the former Nigerian Minister of Agriculture, Akinwumi Adesina (Forum, 2013),

> *"Nigeria was largely self-sufficient in food in the 1960s. Then, we discovered oil and became too dependent on this resource as the economic driver of growth, export income and development. We abandoned our farmers. Yields stagnated. Investments in infrastructure were redirected. Rural communities slid into*

poverty. We became a food-importing country, spending an average $11 billion a year on wheat, rice, sugar and fish imports alone.

And yet we have an abundance of resources - 34 million hectares of arable land, two of Africa's largest rivers, and a large and young workforce to support agricultural intensification. Plus, we have 167 million consumers to support increased food production and processing".

To this end, current approaches adopted by the Nigeria government to boost rice production have included encouraging the growth of genetically enhanced strains of rice (known as New Rice for Africa (NERICA) varieties), which have been developed as part of the Asian and African rice initiative, to improve yield potential (Gridley et al., 2002; Jones et al., 1997). In addition, the Agricultural Transformation Agenda (ATA) in 2011 was initiated to help boost rice production through measures such as infrastructure development, the training of farmers in modern sowing practice, the provision of fertiliser at subsidised rates and the provision of loans for farming (Ugalahi et al., 2016). With the increasing demand for rice farming all year round, there has also been emphasis on the production of irrigated rice during the dry season months. The potential for irrigation farming in Nigeria is fostered by the presence of two of the largest rivers in west Africa, which pass through the country, local groundwater in shallow alluvial (FADAMA) aquifers adjacent to major rivers (Ugalahi et al., 2016), extensive ground waters in eight hydrological areas, permeable (sedimentary aquifers) groundwater is distributed in about ten provinces in Nigeria and over 200 dams and 83 water projects (ongoing and proposed).

Despite the strategies and policies put in place by the government since early 2000s, to improve rice yield especially during the dry season months, poor farming practices persist in many farms (Ismaila et al., 2012). These farming practices often involve an unsuitable or sub-optimal rice varieties based on the soil and water requirements, wrong timing of sowing and harvesting, leading to poor/inaccurate monitoring of yield indicators during the growing season and forecasting of yield amongst others have contributed to the grossly low rice yield in Nigeria (Akintayo et al., 2011; Reuters, 2020; Ugalahi et al., 2016). In addition, the current approaches that have been adopted for monitoring and estimating yield are time-consuming and prone to significant discrepancies as a result of insufficient ground observations, leading to poor production assessment(Mosleh et al., 2015a).

In a bid to find sustainable approaches to bridge the yield gaps, in 1999, Nigeria adopted similar strategies to USA, China and Europe on the importance to competitiveness, technological innovation and sustainable growth of rice and other crops (Njoku, 2018). One

such advancement is the adoption of remote sensing-based solutions to address agricultural challenges that face the country. This is demonstrated in the establishment of commissioned agencies charged with remote sensing research and development, including the National Space Research and Development Agency (NASRDA), National Centre for Remote Sensing (NCRS) and the African Regional Centre for Space Science and Technology Education in English (ARCSSTEE). Remote sensing techniques are well suited to monitoring rice yield and yield indicators in the sense that it is capable of providing repeated and complete coverage for different growing seasons and across multiple scales, spanning from small fields to landscapes and regions(Dong and Xiao, 2016; Alex Okiemute Onojeghuo et al., 2018a). Remotely sensed data can provide important information on the growth stage of rice and plant biophysical and biochemical properties as different phenological stages and play important roles in the growth and development rice.(Cheng et al., 2017; Jiang et al., 2019; Yu et al., 2013). Over the last 40 years, there has been increasing capability of satellites and more recently drones to capture electromagnetic radiation at different parts of the spectrum, from optical, near-infrared and shortwave infrared which are essential for the estimation of yield indicators and forecasting yield. Sensors mounted on satellites are equipped with wide synoptic view and possess the capability of capturing extensive areas at a single pass, potentially saving human and financial cost associated with manual data collection techniques(Mosleh et al., 2015b). Satellite images from remote sensing platforms provide the opportunity to provide detailed and unbiased spatial information of an area, most of which human efforts cannot effectively offer or reconcile. In addition, sensors mounted on drones provide fine spatial resolution and real-time monitoring ability of airborne remote sensing, suitable for monitoring yield and yield indicators for applications that characterize changes in crop attributes over time.(Chauhan et al., 2019). Satellite and drone remote sensing platforms offer repetitive and revisit capabilities; this can be daily, weekly, monthly or yearly, providing an avenue for studying phenological growth patterns of rice without the influence of cloud. With the recent advancement in satellite and drone sensors, emphasis on improving the monitoring of the accuracy of yield indicators during critical growing stages of rice as well as accurately estimating yield will not only be beneficial for researchers, but will provide important information for farmers, agronomist and agricultural institutions in Nigeria.

Therefore, this thesis is focused on understanding the dynamics of irrigated dry season rice with a view to monitoring yield and yield indicators across spatial scales. In particular, the research focuses on the influence of satellites spatial scales for monitoring yield from

smallholder farm scale, as they hold the key to rice self-sufficiency in Nigeria and sub-Saharan Africa (Lowder et al., 2016) and further upscaling to landscape scales.

1.2 Thesis Aims and Contributions

The overarching aim of the study is to assess the potential of remote sensing technologies for monitoring rice yield and the phenological patterns of yield indicators of dry season irrigated rice. This was tackled through exploring the potential of drone and satellite remote sensing platforms and techniques for estimating rice biomass, LAI and yield across a range of spatial, spectral and temporal resolutions. To achieve this, the research adopted the alternative thesis format in answering the following research (Figure 1-1) objectives:

Objective 1: To analyse the current state of remote sensing for monitoring irrigated rice yield and yield indicators (Above Ground Biomass and Leaf Area Index), and to determine the gaps in knowledge. The literature review focused on the monitoring Above Ground Biomass (AGB), the dynamics of monitoring Leaf Area Index and yield from remote sensing platforms and techniques, highlighting the strengths and weaknesses of each platform and methodologies. In terms of monitoring Above Ground Biomass at field scale, the literature suggests the use adoption of drone-based platforms for monitoring yield. However, with the recent availability of camera sensors on board drones, the significance of these cameras for estimating Above Ground Biomass have yet to be established. In terms of yield estimation across different spatial scales, remote sensing platforms were also investigated for estimation of high-resolution yield, with emphasis on the strengths and weakness of each platform. The review showed the potential of Sentinel-2 for high resolution yield estimation due to the high spatial, spectral and temporal resolution. However, the suitability of the full potential of Sentinel 2 varying spatial and spectral resolutions for estimating between and within field variability of yield have yet to be assessed. Finally, I explored the remote sensing platforms, particularly focusing on the retrieval methods currently being adopted for the retrieval of Leaf Area Index during different phenological phases of rice growth. Sentinel-2 was identified as an ideal platform for monitoring LAI across different scales. Furthermore, in terms of the methodological approach for the estimation of LAI, the hybrid method, which combined Radiative Transfer Models with machine learning algorithms (Gaussian Process Regression) was identified as a potentially suitable approach for the estimation of the seasonal dynamics of LAI. However, no study has established for a fact the suitability of the methodological approach for estimating the seasonal dynamics of irrigated rice in Sentinel-2.

These gaps in literature were used to define the research questions to determine the direction of the thesis.

Objective 2: To determine the relative merits of structural and multispectral information from cameras for estimating mid-late season rice above ground biomass from very high spatial resolution drone imagery.

The structural properties of RGB cameras to generate plant height from Crop Surface Models are exciting for the estimation of rice Above Ground Biomass (AGB). Studies have also identified the significant potential of more spectrally sophisticated drone sensors (multi-spectral cameras) with the capacity of generating Vegetation Indices and Texture Metrics for the estimation of rice AGB. However, the comparative advantage of the structural properties of RGB-based sensors compared to the spectral properties of Multispectral based sensors are yet to be established. The research question was identified as "What are the relative merits of using data either from a drone-mounted consumer-grade RGB, a scientific grade multispectral camera, or their combined use, for estimating rice mid-late season above ground biomass?".

Objective 3: To determine the potential of hybrid machine learning methods for estimating the seasonal dynamics of rice Leaf Area Index (LAI). To date, most hybrid machine learning models have adopted the inversion of Artificial Neural Network (ANN) models with physical based (Radiative Transfer Models) models. However, saturation of LAI estimates have been noted in several studies at high LAI, usually occurs during the reproductive and ripening stages of rice growth. Studies have opted to use other Machine Learning Regression Algorithms in combination with RTMs which have presented superior estimation when LAI values are high. Particularly, the GPR model has been identified in literature to outperform other Machine Learning Regression Algorithms for LAI estimation. However, the phenological dynamics of GPR hybrid model from the retrieval of LAI from Sentinel-2 is yet to be investigated. The research question was identified as "What is the potential of hybrid machine learning methods for estimating the seasonal dynamics of rice Leaf Area Index?".

Objective 4: To determine the relative importance of the spatial and spectral resolution of Sentinel-2, for estimating rice yields across a range of spatial extents.

The launch of Sentinel-2 offers the potential for the estimation of rice yield at high resolution. With the spatial resolution as high as 10m and the addition of spectral bands along the red-edge for the 20m spatial bands, the potential exists to identify the suitability of high resolution to perform better for landscape yield estimation, the inclusion of extra spectral bands to Sentinel-2 20m have yet to be explored. Although a study identified the superiority of Sentinel-2 10m or 20m using identical spectral bands, the comparison based on the additional

spectral bands in Setinel-2 20m has not been investigated. This research provided insight into the potential of baseline Sentinel-2 10m and 20m for estimating rice yield at landscape and smaller holder farm scales. The research question was identified as “What is the influence of the spatio-spectral resolution of Sentinel-2 for estimating within field variability of yield at landscape scale and between field variability of smallholder farmer plots”?

1.3 Field site

The study was carried out on a commercial rice farm in Nasarawa state, Nigeria. The site is an ideal location for this work since the climatic and ecological conditions of the study are suited to dry season irrigation farming. In addition, the farm is one of the largest and most mechanised irrigated commercial rice farms in Africa, providing the ideal avenue to monitor yield and yield indicators at irrigated rice field. For more information on the field site see Chapter 3.

1.4 Thesis Structure

This thesis comprises of seven chapters. Chapters 1, 2 and 3 are the introduction, literature review and methodology, respectively. Chapters 4, 5 and 6 present the results of the data analysis are written as research manuscripts to be submitted to international journals. Chapter 7 provides a summary discussion, conclusion, limitations and areas of possible further research. Figure 1-1 is a graphical illustration showing the various chapters of this thesis and the connection between them.

Chapter 1 provides an overview of the research. It provides a general background on the spread and consumption of rice globally with particular focus on Nigeria and sub-Saharan Africa. It explains the shift from the oil sector-based economy to the potential for Nigeria to being self-sufficient in rice production due to government policy. Finally, it discusses the potential of remote sensing platforms and approaches for the monitoring of irrigated dry season rice farming.

Chapter 2 presents a literature review on monitoring and predicting yield and yield indicators from proximal, airborne and satellite scales. It then narrows the findings when monitoring across platforms for biomass, leaf area index and yield estimation in rice. It also critically evaluates and assess the techniques adopted for yield and yield indicators estimation across different scales. Finally, the observed gaps in the literature, the rationale for the current research, the research questions, aims and objectives are highlighted.

Chapter 3 outlines the methodology used in the thesis. It provides an overview of the study area in Nasarawa state, with emphasis on the location, size, population, ecology, soil geology and climate of the study area. It details the overall experimental design, data collection techniques, field sampling techniques, pre-drone flight calibration and flight plan, remote sensing satellite data and yield data.

Chapter 4 presents the result of the first research objective was "Exploiting the centimetre resolution of drone-mounted sensors for estimating mid-Late season above-ground biomass in rice". Here, I assessed the performance of a consumer-grade RGB and a multispectral camera mounted on a drone for estimating biomass during the mid-late growing stages of rice. I also assessed the added value of plant height estimates obtained from the RGB camera compared with vegetation indices and texture metrics obtained from multi-spectral cameras using regression models.

Chapter 5 presents the results of the second research question of "What is the performance of Gaussian Process Regression and PROSAIL for estimating the phenological dynamics of rice Leaf Area Index?" This chapter focused on a generic LAI model for estimating the LAI during the key phenology stages of rice from the combination of altered water and nitrogen applications on the designated experimental plots. Results of LAI estimations from GPR PROSAIL were compared with PROSAIL and Sentinel-2 Application Platform (SNAP) LAI during the different phenological stages.

Chapter 6 presents the result of the third research question, which is "What is the influence of the spatio-spectral resolution of Sentinel-2 for estimating within field variability of yield at landscape scale and between field variability of smallholder farmer plots?" The emphasis is on the spatial and spectral resolution of Sentinel-2 satellite for predicting yield at smallholder farm plots and landscape scale from yield data collected with a high sophisticated combined harvester equipped to global position system. The utility and performance were assessed using the Random Forest model, as was adopted in the first research objective. We evaluated within and between field yield variability between Sentinel 2 10m and 20m bands from images from different phenological phases of rice growth.

Chapter 7 provides a summary discussion of the results obtained from the three analysis chapters (Chapters 4, 5 & 6) with a view of harmonising all findings and evaluating how these compare with existing literature in addressing the research gaps observed. It also provides a

conclusion to the thesis, highlighting the wider implications of the findings and contributions to wider knowledge. Several limitations encountered in the course of the research are identified and areas of possible further investigation are proposed.

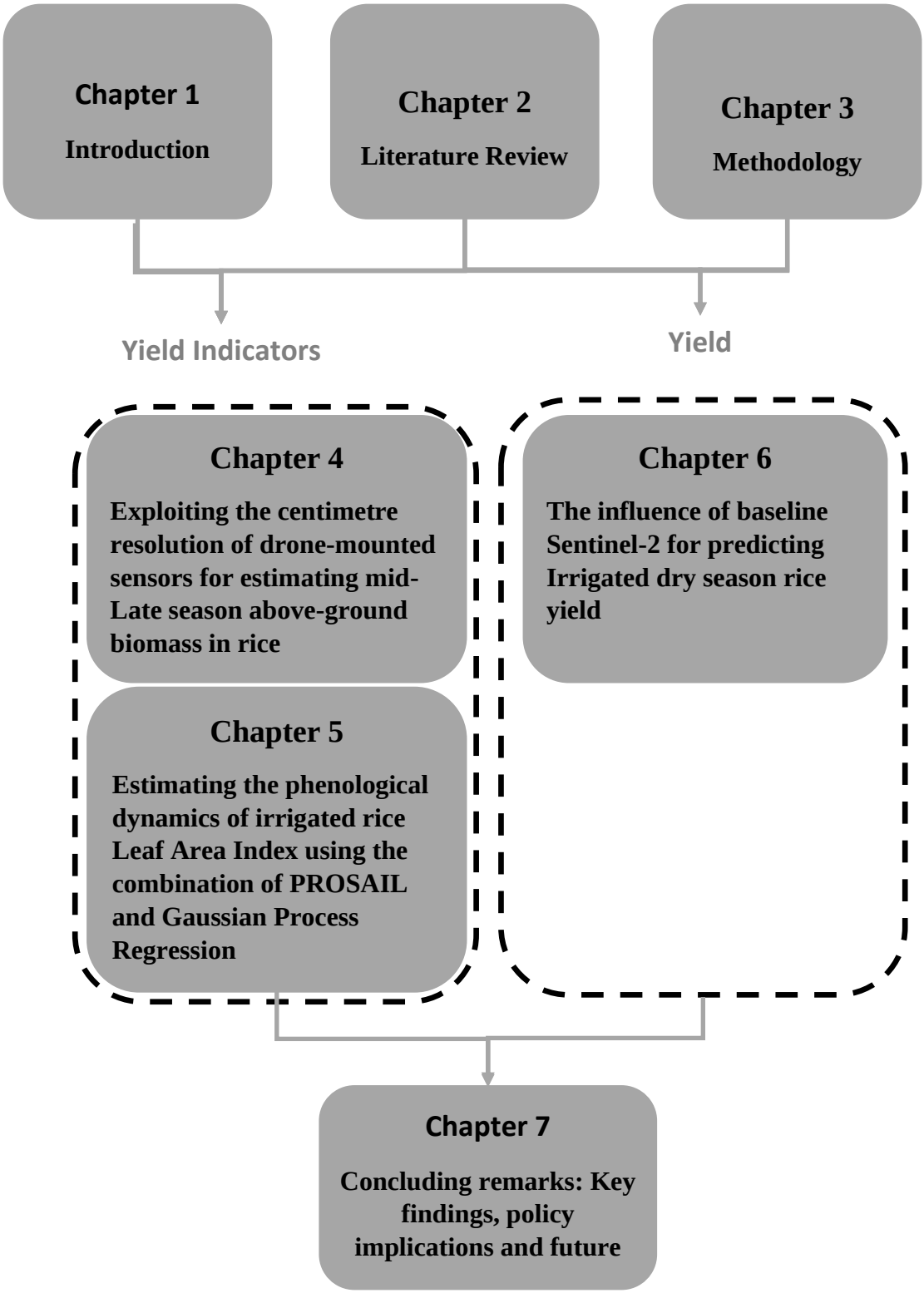

Figure 1-1: Thesis Structure

Chapter 2 Literature Review

This chapter introduces the importance of rice as a staple food source in Nigeria and the potential of remotely sensed data to provide important information on rice yield indicators and yield estimations at different scales. Specifically, the chapter reviews key remote sensing platforms and methodologies that are currently used for estimating rice biomass, leaf area index (LAI) and yield from optical remote sensing data across a range of spatial scales. In doing so, the chapter will discuss several of the most frequently used approaches and their strengths and weaknesses, providing an insight into which approaches are likely to produce the most useful results for monitoring irrigated rice. The chapter ends by highlighting current research gaps in this field, which are drawn upon to formulate the key research questions for the thesis.

2.1 The importance of rice globally and the potential of rice growth in Nigeria

Rice is an important crop for large parts of the world, with some regions heavily dependent on it (Figure 2-1). For instance, rice is a staple crop in Asia, accounting for almost 90% of global rice consumption (Statistica, 2020b). In the Americas, there is also a high rate of consumption of rice, with Latin America and the Caribbean increasing the consumption of rice by 40% within the last two decades (Statistica, 2020b). Similarly, rice is one of the most popular grains in the United States, with Americans consuming around 4.22 million metric tons of rice in the 2019/2020 fiscal year, equating to 13.5 kg per capita (Statistica, 2020). Rice consumption is also popular in the Middle East and North African countries with Saudi Arabia, United Arab Emirates, Egypt and Iran accounting for the bulk of consumption (OECD, 2018). Though not consumed as a staple food, Europe per capita annual consumption is 3.5 – 5 kg in non-rice growing countries and 6 – 18 kg in Southern Europe as of 2019 (OECD-FAO, 2019). In an African context, rice consumption increased by almost 300% between 1961 and 2013 and is steadily increasing (11 kg and 28 kg, respectively (OECD-FAO, 2019), primarily caused by a combination of high rates of population growth and changing consumer preferences.

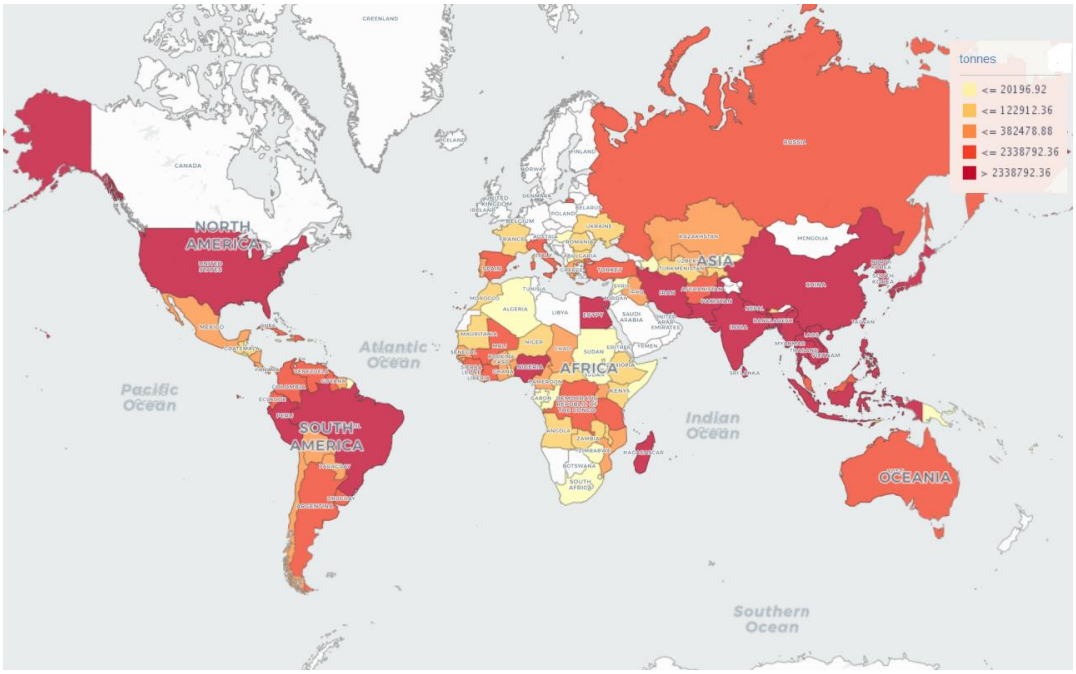

Figure 2-1: Consumption of rice by country, 2019. Source: Statistica, 2020)

Land sizes also play and important role in the growth and distribution of rice (Apata, 2016; FAO, 2018a; Silva et al., 2018). Typically, rice farms are classed into smallholder, medium and larger scale farms (Lowder et al., 2016). Smallholder farming is the dominant form of agriculture in the world, supporting a majority of vulnerable population, within some of the most diverse and threatened landscapes. According to (FAO, 2018a), eight indicators define smallholder farms and farmers. They include the farm size, production, income, pluri-activity and poverty, labour, capital and inputs, innovation and technology, access to market, and demographics. Keeping in mind the aforementioned indicators of smallholder farms, any definition of the characteristics of smallholder farmers will be dependent on the definition that each region/country adopts for itself. However, many definitions of smallholder farms tend to be led by land holding area/size, as this is often regarded as the most significant indicator of smallholder farmers (FAO, 2014; Ricciardi et al., 2018; Wolfenson, 2013). Medium and large scale farms classed based on their size, nevertheless also play a significant role in global rice security (Lowder et al., 2016).

Lowder et al. (2016) investigated the number, size, and distribution globally of farms, smallholder farms, and family farms from agricultural censuses and showed that small farms (less than 2 ha) operate about 84% of the world's agricultural land (Table 2-1). Similar results were identified by Samberg et al. (2016), whose assessment of rice farms globally indicated that smallholder units from 0-2 ha contribute more than 80% of global rice production, while smallholder rice farmers <1 ha, contribute 64% of global rice production. Samberg et al.

(2016) also identified that smallholder systems of less than 5 hectares per farming household are home to more than 380 million farming households, accounting for about 30% of agricultural land in Latin America, sub-Saharan Africa, and South and East Asia. In terms of large farms, Lowder et al. (2016) notes that the percentage of farmland available to farmers with farm sizes from 50ha+ contributes 60% of land for farming (Table 2-1).

Table 2-1: Rice farm sizes for cereal crops ranging from large to small farms

Farm size (ha)	% farms [1]	No. millions [2]	Farm land(ha) [3]	Cereals (%)	Scale
>200	2	11.4	50	17	Large
50–200			10	22	
20–50			10	7	Medium
5–20	4	22.8	10	31	Small
2–5	10	57	8		
1–2	12	68.4	12	21	
<1	72	410			

1. Of 570 million farms in 161 countries, this farm size classification is from a subset of 460 million farms (classified from international comparison tables of the 1990 & 2000 rounds of the WCA for farm sizes) by Lowder et al. (2016).

2. Assuming farm size percentages represent farm sizes worldwide, Lowder et al. (2016) estimate these numbers by multiplying 570 million farms with the percentages.

3. Author estimates from Lowder et al. (2016) – 106 country sample covering 450 million farms, representing 80% of world farms.

Although over 80% of farmers are considered smallholder farmers, Herrero et al. (2017) points to a more nuanced analysis that only 12% of land is available for cereal crops at smallholder scale. However, Samberg et al. (2016) however reports that the 12% of land held by smallholder farmers grow 64% of rice globally, which strengthens the case of smallholder rice farmers. Despite the contradicting reports on the importance of smallholder and larger rice farms for food security, Woodhill et al. (2020) argued that the fundamental dualism between smallholder farmers and much large holder farmers are important for food security because for small-scale farmers production is critical for their own income, food and nutrition security, and for localised markets, while larger scale farmers tend to meet the growing

demands of urban populations. Therefore, in order to improve yield, monitoring smallholder farms as well as much larger farms are fundamental for food security.

In Nigeria, rice is an important staple crop for improving food security and reducing poverty (Ezedinma, 2008; Okpiaifo et al., 2020; Ugalahi et al., 2016). Rice consumption patterns, driven by changes in the dietary needs of the population over the last three decades, has led to increased demand. In terms of land sizes, more than 90% of Nigeria's rice is produced by resource-poor smallholder farmers, while the remaining 10% is produced by a handful of large companies, such as Coscharis Group, Dangote and Olam (Reuters, 2020).

Rice is produced in all agroecological zones of Nigeria with the middle belt region enjoying a comparative advantage in terms of production over other parts of Nigeria due to its soil and environmental factors (Udemezue, 2018). In terms of environments, rice cultivation is categorised under four main groups: rainfed lowland (69.0%), irrigated lowland (2.7%), mangrove swamp (1%) and rainfed upland (28.3%). Rainfed farming is the most popular and accounts for 97% of rice farming in Nigeria. However, rainfed farming is heavily dependent on climate and is vulnerable to changes in temperature and rainfall (Singh, 2016), limiting yield to between 1.5 - 2 t/ha.

Nigeria is well suited towards increasing its rice growing capacity to meet growing demands since rice cultivation can occur during both the rainy and dry seasons and the irrigation potential of the country is estimated at 3.14 million ha (Ugalahi et al., 2016). In terms of irrigation potential, Nigeria has two of the largest rivers in West Africa in River Niger and River Benue, local groundwater in shallow alluvial (FADAMA) aquifers adjacent to major rivers (Ugalahi et al., 2016) and extensive ground waters in eight hydrological areas. Also, permeable (sedimentary aquifers) groundwater is distributed in about ten provinces in Nigeria with over 200 dams and 83 water projects (ongoing and proposed). This signifies the irrigation potential for multiple cultivations of rice annually, especially during the dry season months (Ugalahi et al., 2016). Yet, irrigation farming represents less than 50,000 ha despite the rich potential for irrigation farming.

In addition to the irrigation potential for growing rice, steps have been taken to improve the genotypic characteristics of rice best suited for the Nigerian climate. Measures by the then West Africa Rice Development Association (WARDA), now known as New Rice for Africa (NERICA), cross bred Asian rice (*Oryza sativa*), with African rice (*Oryza glabberima*). This was done because the African species yield was meagre (less than 2 t/ha) while the Asian rice,

which has a higher yield potential (typically 6-10 t/ha), is poorly adapted to many of the African environmental in which rice is grown (Grindley et al., 2002). NERICA varieties have the potential for yield above 6 tonnes per hectare in different rice-growing environments (Gridley et al., 2002; Jones et al., 1997), which is significantly higher than what Nigerian farmers currently harvest (Figure 2-2). In addition, the Agricultural Transformation Agenda (ATA) was an initiative set up to help boost rice through infrastructure development (Ugalahi et al., 2016), provision of extensive workers to train farmers on modern sowing practice, provision of fertiliser at subsidised rate and provision of loans.

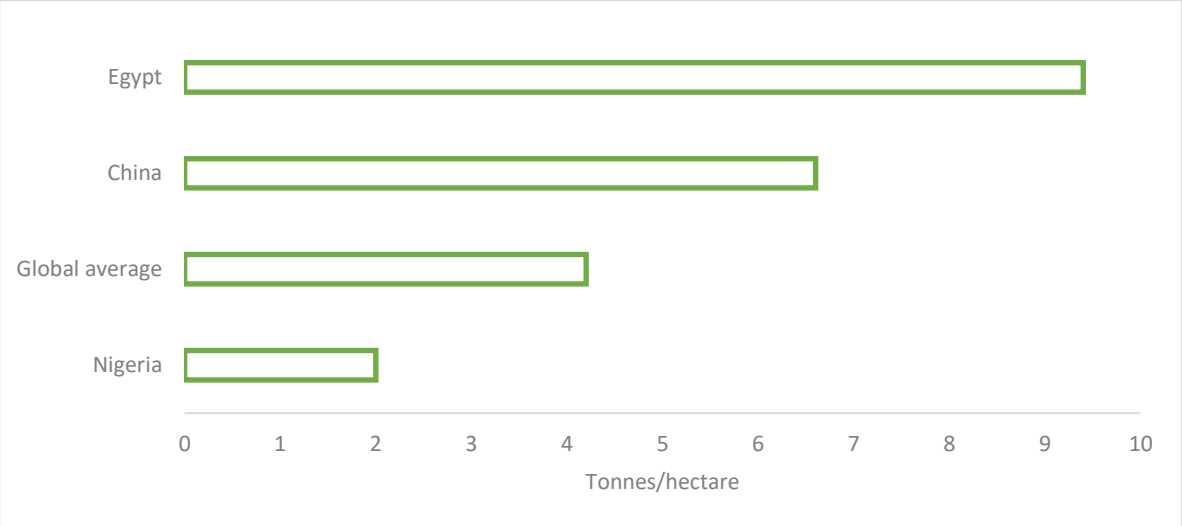

Figure 2-2: Nigeria's annual rice yield in comparison to global average, China and Egypt. Source: FAO, 2018).

Despite all the measures on the ground, with the rich potential to improve yield and be self-sufficient in rice, poor yield returns are usually the case in Nigeria. These are primarily due to farming practices involving poor selection of appropriate varieties of rice to grow the proper identification of seeds based on the soil and water requirements, reluctance to adopt the improved yield varieties, timing of sowing and harvesting, monitoring of yield indicators during the growing season and forecasting of yield amongst others have led to grossly low rice yield in Nigeria (GRiSP, 2013).

In order to bridge the yield shortfall (around 2.4 million metric tonnes of rice as at 2019), sustainable, replicable and attainable strategies must be adopted over time to improve rice yield in Nigeria. One of those steps involves understanding how yield indicators at different phenological stages can be used to predict/forecast yield (Moldenhauer et al., 2013).

2.2 The importance of phenological growth phases to rice yield

The grain yield of a rice plant is a function of the number of panicles (or heads) per plant (or per unit area), the number of filled grains per panicle, and the mean weight of individual grains. Each of these yield components is determined during the phenological growth cycle of the rice.

Rice has three main growth phases: vegetative, reproductive and ripening (Moldenhauer et al., 2013) (Figure 2-4). The vegetative phase (lasting ~55 – 75 days) is important in determining the number of panicles per plant. The vegetation phase covers the time from when the sown seeds begin to geminate until the point at which the panicle (or the head) begins to form in the base of the shoots or stems. The duration of the vegetative phase is primarily dependent on the climatic conditions and the variety of rice sown (Datta, 1981). The longer the vegetative phase the greater the number of panicles produced, with temperate regions often experiencing longer vegetative phases compared to the tropics (Guedes et al., 2015; Vergara, 1991). Management practices, such as the management of nutrient availability, are also important during the vegetative phase as such activities influence panicle formation and growth (Fageria, 2007).

The second developmental phase is the reproductive phase where the panicles continue to grow, leading to the bulging of the leaf stem that conceals the developing panicle, called the 'booting' stage. Then the tip of the developing panicle emerges from the stem and continues to grow until flowering (the formation of spikelets) begins (Kamoshita et al., 2008). This phase is important for yield estimation as it determines the number of spikelets that are produced per panicle. The number of spikelets produced depends on the level of photosynthetic activity and on there being a sufficient supply of nitrogen (Kamoshita et al., 2008). The reproductive phase lasts between 30-35 days regardless of the variety of rice grown. However, short reproductive phases result in low leaf areas available for photosynthesis and thus reducing the number of spikelets produced per panicle (Fageria, 2007).

The final development phase is the ripening phase, which starts when the crop begins to flower and ends when they mature. This developmental phase controls the final weight of a single grain of rice and typically lasts up to 30 days in the tropics (Fageria, 2007). Solar radiation is critical during the ripening phase to achieve higher yields (Fageria, 2007).

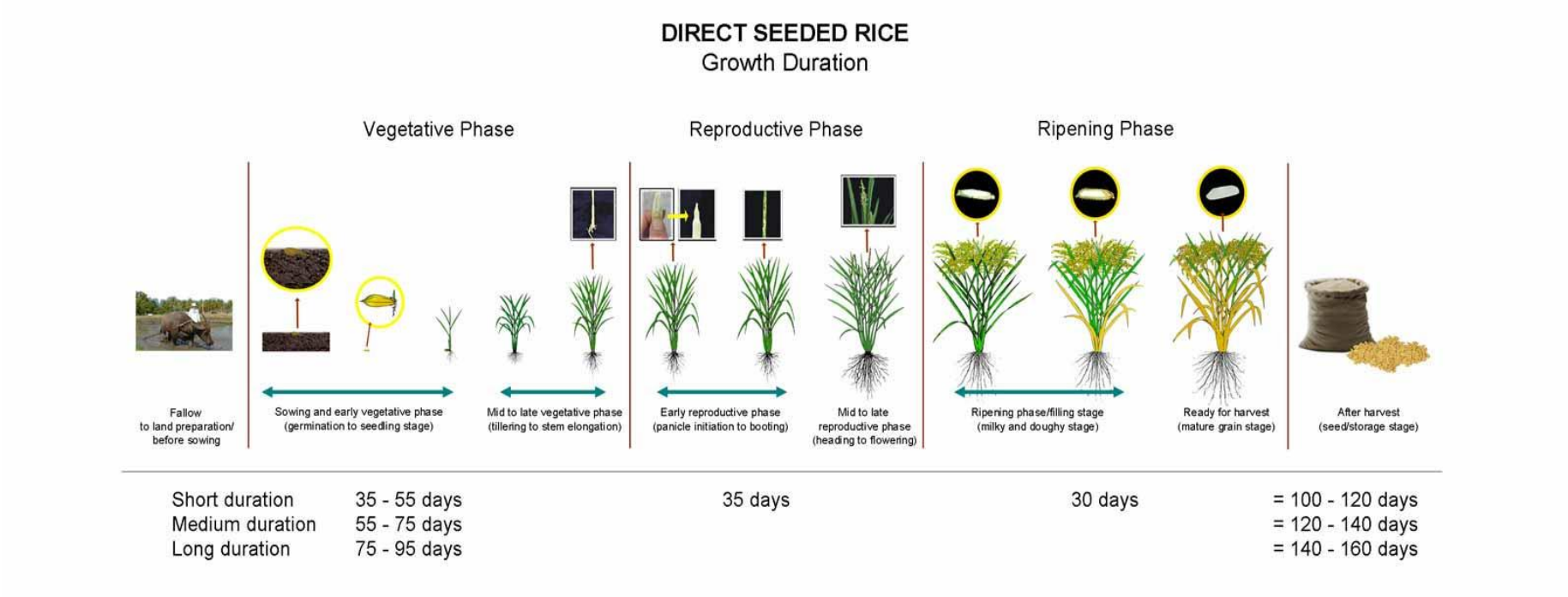

Figure 2-3: *The phenological growth duration of direct seeded rice (Source: IRRI, 2013)*

The development of rice is a sequence of different phenology phases. This implies that the condition of the plant during the vegetative phase determines relates directly to the potential number of panicles and the health of leaves functioning during the reproductive and ripening stages. Therefore, each phase is the result of the previous phase and the cause of the following phase (Dunand and Saichuk, 2014).

2.3 Estimating rice yield indicators and yield

Typically, yield is measured based on the tiller count, number of panicles, plant height, biomass, leaf area index (LAI) and yield. For instance, rice tillers are branches developed from the leaf of the main shoot or from other tillers during the vegetative phase (Figure 2-4). They determine the panicle number of rice plant which is a key component of grain yield (Krishnan et al., 2011). As such, rice grain yield is highly depended on the number tillers produced by each plant.

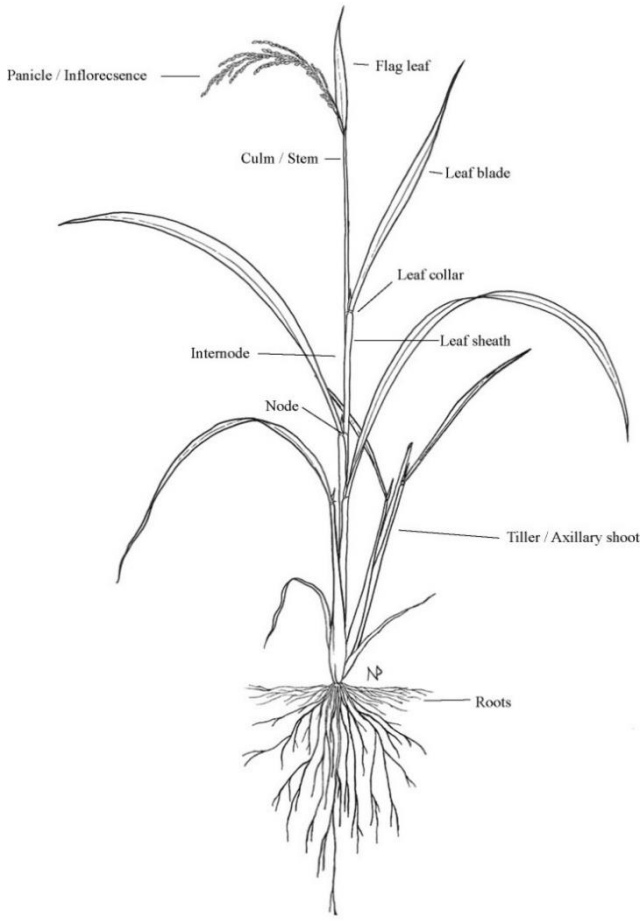

Figure 2-4: Annotated diagram of rice plant

Similarly, biomass estimation is vital for improving the agronomic management efficiency and predicting crop yield. Biomass is also a diagnostic technique to assess the fertilization necessities of nitrogen deficiencies in crops (Lemaire et al., 2009) and is typically obtained from the shoot height of the rice plant (Hasegawa, 2003). Hasegawa (2003) reported that higher yields of rice cultivars were associated with higher dry matter production from dry shoot weight and both increased dry matter and grain harvest index equally contributed to yield increases. Dry matter production used for obtaining biomass measurements have been reported to have a higher correlation with grain yield during booting, flowering, and physiological maturity growth stages which occur in the reproductive and ripening stages than at vegetative growth stages (Fageria, 2007).

In addition to biomass as an indicator of yield, plant height is an important phenotypic trait that can be used not only as an indicator of overall plant growth but also a parameter to calculate advanced yield indicators such as biomass and yield (Tilly et al., 2015; Yu et al., 2002). Plant height increases exponentially up until the stem/culm elongation stage and then quadratically till the ripening stage, providing useful information for the estimation of biomass and yield throughout different phenological phases of rice (Fageria, 2007).

LAI also plays an important role in vegetation processes such as photosynthesis and transpiration, and is connected to meteorological /climate ecological land processes. The LAI is an important parameter to estimate yields and is often utilised by many crop growth models that use net photosynthesis, assimilate partitioning, canopy mass, and energy exchange (Fageria et al., 2007). The LAI of rice increases as crop growth advances and reaches a maximum at about heading or flowering stage. The increase in LAI is caused by an increase in tiller number or leaves on each tiller and in size of successive leaves (see Figure 2-4).

Finally, directly measuring rice yield is often the most effective way of obtaining accurate yield information on rice fields. Rice yields are determined by the number of panicles and spikelet per panicle. Therefore, it is very important to understand what influences yield components and consequently grain yield. For instance, the number of panicles are determined during vegetative growth phase, the spikelet per panicle during reproductive growth phase and weight and spikelet sterility during spikelet filling or reproductive growth phase.

Rice yield can be expressed in the form of following equation by taking into account the yield components:

Grain yield (kg ha^{-1}) = Number of panicles m^{-2} × Spikelet per panicle × %filled spikelet × 1000 spikelet weight (g) × 10^{-5}

Several approaches have been adopted by farmers for monitoring and evaluating rice yields, of which, direct field observations are the most common approach for monitoring rice yield (Wopereis et al., 2009). Farmers generally visually evaluate growth performance of the crop during and after the growing season. Field measurement tools include tapes and rulers for monitoring plant height, manual harvesting for determining plant biomass and yield, and tiller counting for monitoring the quality of grain. Plant height and biomass measurements are usually conducted during the growing season, while yield harvesting occurs 30 days after the rice crop reaches the ripening stage. Whilst these monitoring approaches have been adopted by farmers in Nigeria and other rice-growing regions (Wopereis et al., 2009), they have several limitations. For example, differences in a farmers' field experience may affect the quality of measurements and proper identification of contributing factors to yield. Additionally, the time required for the measurements of yield and yield indicators manually limit the replicability these techniques for use on large rice farms. Consequently, the need for timely, accurate, recurrent, and spatially monitoring are important towards effectively monitoring yield and yield indicators of rice (Bouvet and Le Toan, 2011; Dong et al., 2015; Kuenzer and Knauer, 2013).

2.4 Optical remote sensing of rice yields and yield indicators

One approach adopted as a viable proxy for monitoring yield and yield indicators of rice is through the use of optical remote sensing (Kim et al., 2017; Kuenzer and Knauer, 2013; Niel et al., 2004; Siyal et al., 2015; Yang et al., 2017). The optical region of remote sensing spans from the visible to the Near Infrared (NIR) region of the electromagnetic spectrum (wavelength 400-2500nm). In the visible spectrum (400-700nm), electromagnetic radiation is absorbed by the rice plant pigments. In the green band (500-600 nm), comparatively less absorption occurs, producing a reflectance peak region within the visible bands that reflects the green coloration of plants perceived by the human eye.

The spongy mesophyll cells are associated with pronounced scattering of Near Infrared (NIR) radiation, leading to a high spectral reflectance in the 700-1200nm region of the spectrum (Figure 2-5). The spectral reflectance in the red region for healthy, actively growing vegetation typically decreases with the growth of the rice plant, primarily as a result of the increasing photosynthetic activity, leading to greater absorption at wavelength between 600-700nm,

while the NIR reflectance increases with increase in the rice canopy. The increase in the leaf thickness may also lead to increases in the NIR region (Mosleh et al., 2015). In between the visible and NIR lies the red edge region (Figure 2-5). This narrow wavelength range is sensitive to vegetation conditions such as Normalised Difference Red Edge (NDRE) and has been be used to support different rice yield indicators (Huang et al. 2017; Zhang et al., 2019).

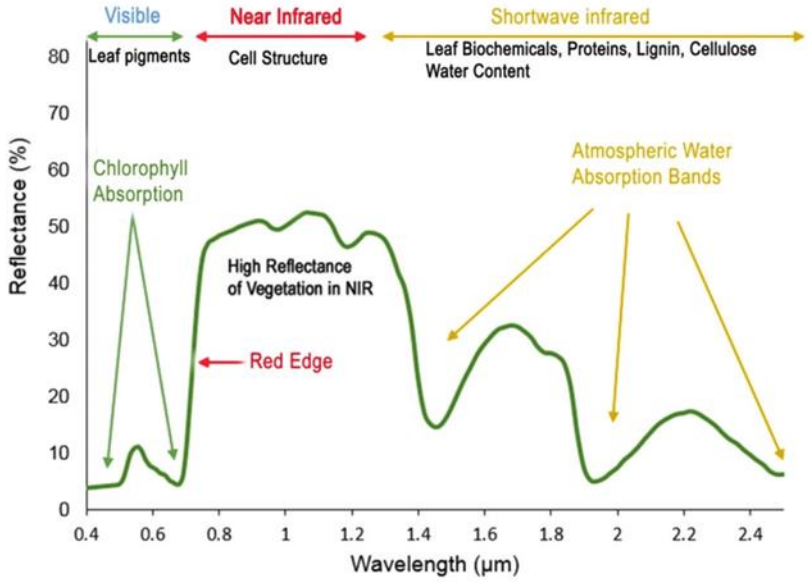

Figure 2-5: Spectral profile of healthy rice plant

Key advantages of remote sensing over more traditional in situ rice crop measurements include the provision of continuous spatial coverage over large geographic areas and the ability to acquire information during different phenology and seasons quickly often at low cost (Mosleh et al. 2015).

2.5 Concept of scale for monitoring yield and yield indicators from satellite, airborne and drones.

A number of optical remote sensing platforms have been employed to monitor irrigated rice growth and yields. These platforms and their associated imaging systems differ in terms of the spatial and spectral resolution of the imagery collected (i.e. pixel size and number of spectral bands), and their minimum return frequency (Figure 2-6). Remote sensing platforms include proximal sensing (Barmeier and Schmidhalter, 2016; Deery et al., 2014), airborne sensing (Du and Noguchi, 2017; Duan et al., 2019; Gabriel et al., 2017; W. Li et al., 2015) and satellite

sensors (Bai et al., 2019; Guan et al., 2018; Korhonen et al., 2017; Liu et al., 2020), all with varying spectral properties.

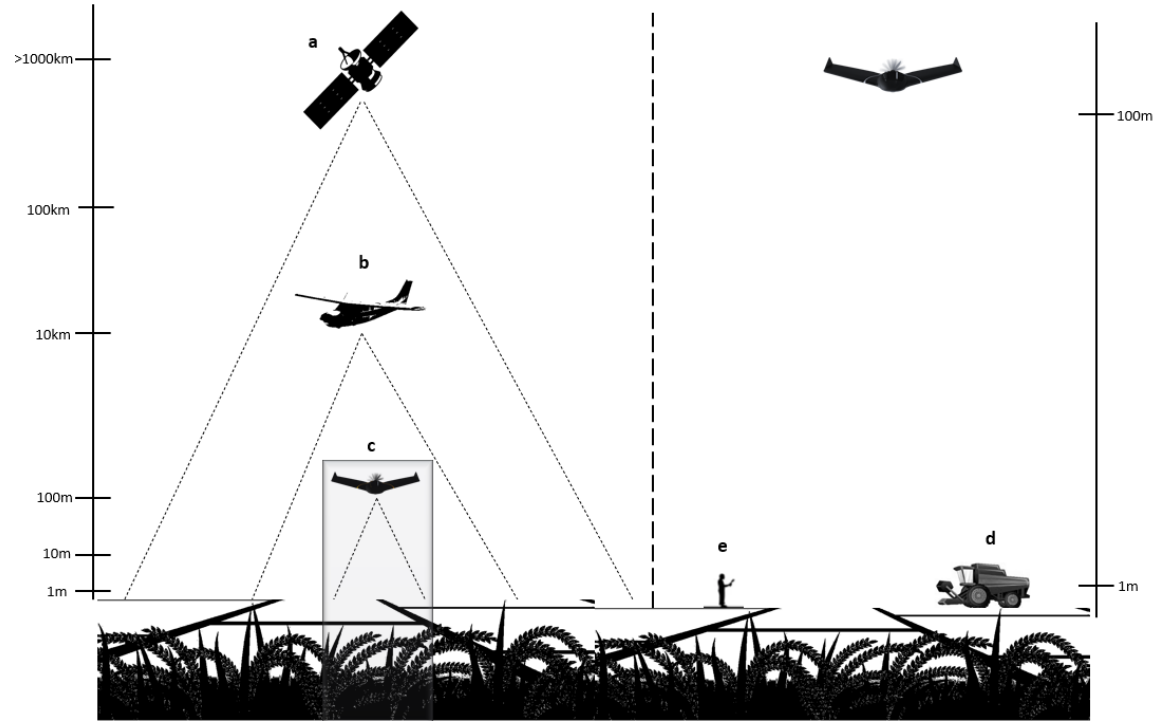

Figure 2-6: Remote sensing technologies at different spatial scales. On the left-hand side are the different aerial and spaceborne systems: (a)satellite, (b), airplane and, (c), and Unmanned Aerial Vehicles (UAV) or drones capable of providing coarse to fine resolution data at global to regional scales, respectively. At the proximal scale (right-hand side), (d) fine resolution data can be obtained using tractors equipped GPS (e) handheld devices for monitoring yield indicators.

Based on the concept of spatial scale in particular, Dungan et al. (2002) provided a balanced view of scale in spatial analysis. Spatial scale can be identified based on the extent and resolution when monitoring yield and yield indicators. The extent is the total length, area or volume that exists or is observed or analysed. On the other hand, the resolution of a data set is often taken to be the size of the smallest sampling unit or grain size of its sampling design. In the next section and throughout the thesis, when quantifying the spatial scale of satellite, airborne and drone scales, the extent and resolution are used in combination as the metrics for determining the suitability for monitoring yield and yield indicators across scales.

2.5.1 Satellite Scale

Remote sensing has evolved over time for monitoring yield and yield indicators since the early 1970's (Bauer & Cipra, 1973; Doraiswamy, Moulin, Cook, & Stern, 2003; Jewel, 1989) when Landsat 1 (originally known as Earth Resources Technology Satellite 1) was launched in 1972 with a moderate spatial resolution. Multispectral Scanner System (MSS) sensors on Landsat 1 collected imagery in the green, red and two infrared bands at a spatial resolution of 80 m and a return frequency of 18 days. Landsat 5 was launched in 1984 and collected Thematic Mapper (TM) imagery at a higher spatial resolution of 30 m and spectral resolution to Landsat 1 with spectral bands in the blue, green, red, near infrared, and infrared (including thermal) regions. Landsat has evolved over the years with the latest launch of Landsat 8 in 2013, providing archival data for monitoring rice yield (Ishiguro et al., 1993; Kontgis et al., 2015; McCLOY et al., 1987; Zhou et al., 2016). Similarly, France launched a comparable satellite (Satellite pour l'Observation de la Terre (SPOT) 1) in 1986, which collected 20 m imagery with a return frequency of up to six days in the green, red and near infrared frequencies. The SPOT satellite series continued until SPOT 5 (which was eventually decommissioned in 2015), providing a high spatial resolution images for monitoring yield and yield indicators in rice (Navarro et al., 2016, p. 5; Nguyen et al., 2012; Yang et al., 2009)

In terms of global monitoring of rice yield and yield indicators, the launch of the Advanced Very-High-Resolution Radiometer (AVHRR) in 1978 kick-started the daily monitoring of agricultural landscapes (Cracknell, 2001), eventually leading the establishment of the AgRISTARS (Agriculture and Resource Inventory Surveys Through Aerospace Remote Sensing) program in the early 1980s saddled with the tasks of monitoring agricultural fields (Becker-Reshef et al., 2010). This was followed up with the launch of other global oriented satellites like Moderate Resolution Imaging Spectroradiometer (MODIS) in 2002 with a high temporal and spectral resolution compared to the previously mentioned satellites. MODIS has extensively been utilised for monitoring rice yield and yield indicators (Caccamo et al., 2011; Alex O. Onojeghuo et al., 2018; Peng et al., 2014; Shi et al., 2013; Son et al., 2014; Xiao et al., 2005). The acquisition of MODIS satellite images on a daily basis have made the satellite pivotal for Group on Earth Observations Global Agricultural Monitoring (GEOGLAM) Initiative, which is a mandated to coordinate satellite-based monitoring of global croplands (Whitcraft et al., 2015)

The turn of the century saw increased monitoring of rice from high resolution satellite remote sensing platforms. IKONOS was launched in 1999 which collected 4 m resolution imagery in the blue, green, red and near infrared bands at a return frequency of up to 5 days. Similarly, Worldview-2 and Rapideye satellites, equipped with bands in the red edge region of the electromagnetic region, has a revisit period of 1-4 days and a spatial resolution of 1.85m providing high spatial resolution for monitoring yield and yield indicators. Huang et al. (2017) compared Worldview and Rapideye high resolution satellite with FORMOSAT-2 (which has no bands at the red edge region) for monitoring yield indicators in a rice field. Results showed that the satellites with red-edge bands improved the estimation of rice nitrogen status which has a strong relationship with biomass.

In terms of spectrally enhanced satellites, the turn of the century ushered in commercially designed satellite imaging systems with higher resolution and quicker revisits for the monitoring of rice yield and yield indicators. A notable example was the launch of a hyperspectral satellite, Hyperion, in 2002, has a high resolution hyperspectral imager capable of resolving 242 spectral bands (from 0.4 to 2.5 nm) with a 30-meter resolution and a temporal resolution of between 16-30 days. Rao et al. (2006) used Hyperion to accurately estimate vegetation LAI compared to traditional broadband multispectral data. The results from the study show a stronger relationship with LAI from Hyperion compared the Linear Imaging Self-Scanning Sensor 3- LISS III multispectral data in 4 bands. More recently, PRISMA (Hyperspectral Precursor and Application Mission) hyperspectral satellite was launched in 2019 has been launched with the capability of monitoring yield and yield indicators in crops from a wide array of spectral information (~250 bands).

The availability of optimal spatial, spectral and temporal resolution actively governs the accuracy of accessing yield and yield indicators in rice. While coarse resolution sensors (e.g. AVHRR or MODIS) provide global coverage at daily intervals, their coarse spatial resolution (> 250m) cannot capture the variabilities of smallholder and landscape scales. Satellites such as Landsat-7/8 with 30 m spatial resolution (and between 8/11 spectral bands depending on the sensor), on the other hand, have lower revisit times (~16 days) that are impractical for monitoring yield indicators frequently during the growing season. The spatial resolutions have improved in some recent commercial satellite sensors such as Worldview-2, 3 and 4. However, free access to high-resolution temporal spaceborne images becomes crucial if operational satellite-based quantitative applications are to be developed.

The spatial resolution of freely available satellite has improved in some recent satellite sensors such as Sentinel-2 (10 or 20 m) and with a temporal resolution of five days it provides the opportunity to monitor yield and yield indicators at high resolutions. Furthermore, the free availability of images at the global scale is potentially critical for monitoring rice farms in sub-Saharan Africa, which may only be possible with high resolution commercial images which are costly to purchase. Moreso, the addition of bands along the red-edge, which have shown to improve the monitoring of yield and yield indicators in rice (Kanke et al., 2016), provides new opportunities for rice monitoring. This is reflected in the ESA-funded Sentinel-2 for Agriculture (Sen2-Agri) project, which provides an open-source system based on generic time series analysis methods for crop mapping and monitoring at the global scale (Defourny et al., 2019).

2.5.2 Airborne Scale

Airborne platforms for remote sensing usually involves the use of manned aircraft or remotely-piloted aircraft systems (usually referred to as Unmanned Aerial Vehicles (UAVs) or drones) for monitoring yield and yield indicators in crops (Colomina and Molina, 2014; Zhang and Kovacs, 2012). The fine spatial resolution and real-time monitoring ability of airborne platforms suggest that it is well suited for applications that characterize changes in crop attributes over time at farm scale as oppose to regional scale. Manned airborne platforms present the earliest use of airborne estimation for monitoring yield indicators in crops (over 40 years ago) and have been extensively applied in ecology(Anderson et al., 2016; Luscombe et al., 2015) and more recently, for monitoring rice (Tilly et al., 2014; 2015). However, the cost implication of manned aircraft remote sensing has seen the decline in the number of manned aircraft platforms for monitoring of rice yield indicators and yield (Sankaran et al., 2015).

The recent development of miniature imaging instruments and an expansion of commercial drone companies facilitating data acquisition and analysis, has seen a shift from manned aircraft towards relatively low-cost systems such as drones. Compared to satellite platforms, airborne drone platforms are more flexible than satellite-based systems, in terms of flight planning, timely acquisition and flexibility (Colomina and Molina, 2014). Drones have been used for monitoring yield indicators and yield indicators from RGB cameras (Bendig et al., 2014; Lu et al., 2019), multispectral cameras (Zheng et al., 2019), thermal (Maimaitijiang et al., 2017) and Light Detection and Ranging (LiDAR) sensors (ten Harkel et al., 2020).Furthermore, the last decade has seen the increase in sensors on-board drones for

monitoring yield and yield indicators in crops (Table 2-2). These sophisticated sensors have the potential to influence improve the monitoring of yield monitoring, however, the significance of these consumer grade cameras is still to be fully understood as they are still in their infancy (Deng et al., 2018).

Table 2-2: *Common multispectral sensors on-board UAVs/drones*

Multispectral sensor	Spectral range (nm) / Central wavelength (band width) (nm)	Resolution (pixels)	Weight (g)
Sentera Quad	RGB Red: 655 (40) Red edge: 725 (25) NIR: 800(25)	1248 × 950	170
ADC Micro	Green: 520–600 Red: 630–690 NIR: 760–900	2048 × 1536	200
Buzzard	Blue: 500 (50) Green: 550 (25) Red: 675 (25) NIR1: 700 (10) NIR2: 750 (10) NIR3: 780 (10)	1280 × 1024	250
MiniMCA6	Blue: 490 (10) Green: 550 (10) Red: 680 (10) Red edge: 720 (10) NIR1: 800 (10) NIR2: 900(20)	1280 × 1024	700
XNite Canon SX230 NDVI (modified)	Blue: 385–470 Green: 500–570 NIR: 670–770	4000 × 3000	223
RedEdge	Blue: 475 (20) Green: 560 (20) Red: 668 (10) Red edge: 717 (10) NIR: 840 (40)	1280 × 960	231
Altum	Blue: 475 (20) Green: 560 (20) Red: 668 (10) Red edge: 717 (10) NIR: 840 (40), 8-14	2064 x 1544	357
Sequoia (MS)	Green: 550 (40) Red: 660 (40) Red edge: 735 (10) NIR: 790 (40)	1280 × 960	72
P4 Multispectral	Blue: 450 (16) Green: 560 (16) Red: 650 (16) Red edge: 730 (16) NIR: 840 (26)	1600×1300	468

2.5.3 Proximal Scale

Ground-based or proximal sensing systems have a number of advantages over satellite and airborne platforms: (i) ground conditions can be tailored or conditioned to examine the effects of specific crop parameters; (ii) the effect of mixed pixels that usually affects satellite and airborne platforms can be reduced significantly; and (iii) the acquisition of high spatial resolution information is not constrained by platform revisit frequency, thus enabling timely implementation of required remedial action (Moran et al., 1997). Proximal systems fall into two main categories: fixed systems, involving the mounting of sensors on permanent platforms of towers, and mobile in-field systems, which involves the use of hand held devices, sensors on moving tractors or autonomous field robots (Deery et al., 2014).

Proximal platforms have been adopted for monitoring yield (Li et al., 2015) and yield indicators (Gabriel et al., 2017; Gnyp et al., 2014) in crops and have often been adopted for validating satellite and airborne sensors (Deery et al., 2014).Proximal sensing is particularly suited to high-resolution temporal monitoring of yield and yield indicators. However, there are some limitations in its use for extensive assessment of yield and yield indicators in rice and other crops. For instance, the spatial coverage of proximal monitoring equipment is poor, even if mounted on fixed poles or moving vehicles (Chauhan et al., 2019). In such scenarios, multiple sensors are required to view entire fields, which can be prohibitively expensive.

2.6 Estimating rice yield indicators from remote sensing platforms

Two rice yield indicators usually applied for monitoring the growth dynamics of rice at various scales are aboveground biomass and Leaf Area Index. Here I focus on the two yield indicators across different scales, the methodological approaches adopted and their corresponding merits and limitations.

2.6.1 Estimating Aboveground biomass

Aboveground biomass (AGB) is an important indicator in rice production as it provides useful information for grain yield predictions for growth status monitoring (Kanke et al., 2016), as well as gross primary production estimation (Peng and Gitelson, 2011). Furthermore, the relationship between AGB and nitrogen (N) concentration determines the N dilution curve, from which the critical N concentration can be derived to calculate N nutrition index (Yuan et al., 2016), which also has potential for in-season estimation of grain yield (Ben zhao 2018). Biomass can be estimated from remotely sensed data across multiple spatial scales, ranging from the use of low-resolution MODIS data (>250m) to point-based estimations (>1cm) using

field spectrometry developed based on certain methods. Methods generally applied for obtaining AGB from optical sensors include the simple statistical analysis with vegetation indices; the net primary productivity estimation method; the crop height -based estimation method; Texture metrics; and the crop growth model method. The following sections will explore the estimation of AGB in crops from various platforms.

2.6.1.1. Satellite-based estimations of rice AGB

Satellites monitoring at spatial scales have been adopted for the estimation of AGB in crops. In instance, high temporal resolution of coarse spatial resolution sensors (e.g. MODIS) have been fused with higher spatial resolution sensors for the estimation of crop AGB (Dong et al., 2016; Liao et al., 2019; Marshall and Thenkabail, 2015; Meng et al., 2013). Meng et al. (2013) combined MODIS and the Chinese satellite, HJ-1 CCD (temporal resolution of 20 days) to generate NDVI indices using the adaptive Vegetation Fusion Model (STAVFM) for the estimation of wheat AGB. The estimation of wheat correlated well with observed AGB (R^2 = 0.87), suggesting similar applications over larger areas.

Data assimilation approaches have also been adopted for the estimation of AGB from the fusion of MODIS and higher resolution images. Dong et al. (2016) applied similar fusion methods to the aforementioned study using the Simple Algorithm for Yield Estimation Model (SAFY). A good agreement was achieved between the estimated and field measured biomass by assimilated LAI derived from the fusion of both MODIS and Landsat 8 as opposed to Landsat 8 alone (R^2 = 0.77; RMSE = 231g/m^2). Liao et al. (2019) fused MODIS with Landsat 8 and MODIS data to measure corn and soybean AGB using the SAFY model. Results showed good agreement for AGB estimation (corn, RMSE = 147.87 g/m^2; wheat, RMSE = 120.25 g/m^2).

Despite the fusing of MODIS with much higher spatial resolution sensor, mixed pixel representation which invariably leads to misclassification of fields make them unsuitable for high resolution yield mapping. Moreover, Liao et al. (2019) identified discrepancies at peak crop phenological phases in the peak phases when acquiring Landsat images (16-day interval), leading to uncertainties in the crop simulation model for estimating AGB.

More recently, finer spatial and spectral resolution satellites have been adopted for the estimation of biomass in rice and other cereal crops. Notably, Han et al. (2017) used a combination of Pleiades-1A, Worldview-2, Worldview-3, and SPOT-6 high resolution satellite imagery (< 6m) for the estimation of oilseed biomass for the entire season using

multispectral VIs in China. Results showed that the normalized difference vegetation index (NDVI) in conjunction with a linear regression model was able to predict field-scale oilseed rape biomass through the seasonal growth dynamics. Kross et al. (2015) also successfully used high resolution satellite imagery in the form of RapidEye (5m) to estimate maize and soybean biomass in Canada using vegetation indices. However, the main limitation of high-resolution satellite imagery for biomass monitoring is that they are usually commercial, which means that high costs associated with the purchasing of imagery often prevents the acquisition of multiple images over time (Alex Okiemute Onojeghuo et al., 2018b).

2.6.1.2. Airborne-based (Manned Aircrafts) estimations of rice AGB

Airborne platforms have increasingly been adopted for the estimation of biomass. Notably, remotely piloted airplanes equipped with LiDAR using plant height, hyperspectral and multispectral sensors and a combination of both have been successfully used for biomass estimation in crops (Li et al., 2015; Luo et al., 2019, 2016; Tilly et al., 2015, 2014; Wang et al., 2017). Tilly et al. (2014) utilised terrestrial laser scanning (TLS) to monitor plant height on paddy rice fields in China. The high density of measurement points allows the establishment of crop surface models with a resolution of 1 cm, which can be used for deriving plant heights. For both sites, strong correlations (each R^2 = 0.91) between TLS-derived and manually measured plant heights confirm the accuracy of the scan data. A biomass regression model was then established based on the correlation between plant height and biomass samples from the field experiment (R^2 = 0.86). Similarly, Tilly et al. 2015 adopted the aforementioned approach in multiple growing seasons for the estimation of rice AGB. Biomass regression models were established based on strong coefficients of determination between plant height and dry biomass (R2 = 0.66 to 0.86 and 0.65 to 0.84 for linear and exponential models, respectively).

Similar to AGB estimation from LIDAR, hyperspectral sensors have been combined with LiDAR data onboard remotely piloted aircrafts for the estimation of biomass in other cereal crops (e.g. maize) crops. Luo et al. (2019) utilised plant height and vegetation indices using LiDAR and hyperspectral respectively for the estimation of maize AGB. The results showed the strong relationships between LiDAR variables and maize biomass (R^2 = 0.87. The study also found that combined LiDAR variables and vegetation indices derived from hyperspectral imagery produced a better prediction of biomass (R^2 = 0.91) when compared to LiDAR data alone, and the prediction accuracies improved by 4.4%. The combined hyperspectral imagery

and LiDAR data provided complementary information and therefore improved prediction accuracies of these biomass in a cereal crop.

Li et al. (2015) particularly noted the strong correlation between plant height from LiDAR data with maize AGB during the critical growing phases. While plant height was been identified with maize AGB during the critical growing phases, Wang et al. (2017) identified improved estimation of maize AGB from the combination of plant height obtain from LiDAR data and hyperspectral sensors (R^2 = 0.88, RMSE = 321.09 g/m^2, RMSECV = 337.653 g/m^2) compared to plant height estimates (R^2 = 0.83, RMSE = 374.655 g/m^2, RMSECV = 393.573 g/m^2) and hyperspectral data alone

However, challenges still remain with this method. Acquisition of airborne data is expensive (Gonzalez et al., 2010) making repeated acquisition of data for monitoring AGB a challenge for farm stakeholders.

2.6.1.3. Proximal remote sensing- based estimations of AGB

As an alternative to acquiring fine spatial resolution imagery, a number of studies have used proximal near-surface sensors for estimating crop biomass at the field scale often through the use of handheld hyperspectral sensors (Fu et al., 2014; Gnyp et al., 2014; Thenkabail et al., 2000) or multispectral radiometers (Casanova et al., 1998; Prabhakara et al., 2015). However, monitoring biomass across entire fields over the course of a growing season using handheld platforms is time-consuming and logistically challenging. An alternative to handheld monitors are the use of mobile and static sensors for estimating plant biomass that are mounted on tractors or mobile sensors (Bai et al., 2016; Watanabe et al., 2017). A typical example is the phenomobile powered by a hydraulic drive system, equipped with three LIDAR sensors, four RGB cameras, hyperspectral camera, an adjustable height boom and a real-time kinetic (RTK) GPS, with a 2 cm accuracy for position accuracy (Deery et al., 2014). This mobile platform has successfully been used in wheat in experimental trial plots for estimating canopy height, counting spikes in wheat, and monitoring plant stress (Deery et al., 2014). Another mobile platform is the PhenoTrac4, which is equipped with three active sensors, a passive hyperspectral sensor and RTK GPS for positioning and has been used to evaluate plant nitrogen uptake, grain yield and plant dry weight (Barmeier and Schmidhalter, 2017, 2016). The advantage of a mobile platform over the handheld sensors is their ability to evaluate multiple traits and multiple rows in parallel, thus reducing the time and cost (Bai et al., 2016).

However, these motorised platforms are expensive to buy and require technical "know-how" to operate (Bai et al., 2016).

2.6.1.4. Drone-based estimations of AGB

When measuring AGB from drone mounted platforms, RGB and Multispectral/hyperspectral sensors have often adopted for the estimation of AGB in crops (Table X (Bendig et al., 2014 Cen et al., 2019; Lu et al., 2019). Digital Surface Models (DSM), from which crop model surfaces can be developed, can be obtained from RGB sensors. The generation of Crop Simulation Models (CSMs) help determine plant height, which has been identified to have a strong relationship with crop AGB, especially during the mid-late growth stages of crop growth (Bendig et al., 2014; Lu et al., 2019). Bendig et al. (2014) reported strong correlations between plant height from CSMs and barley fresh biomass (R^2 = 0.81) and dry biomass (R^2 = 0.82). Similarly, Jiang et al. (2019) reported strong relationship the estimation of rice AGB and plant height obtained from CSMs (R^2 = 0.77; RMSE = 224.69g/m^2). However, Lu et al. (2019) identified a lower coefficient of determination and higher RMSE when predicting wheat biomass (cereal crop) during the reproductive and ripening phases of winter wheat using RGB images, which is considered the critical phase for biomass monitoring in rice (refer to section 2.2 and 2.3). The reasons for the underestimation could be explained by recurring wind in the field that might blow the leaves leading to lodging (weakening of the stem to the point they can no longer support the weight of the grain), which could have affected the particular wheat variety used for the study leading to underestimation of plant height and thus, AGB (Du and Noguchi, 2017). Therefore, underestimating plant height and thus biomass necessitate further investigation to monitoring of rice AGB during the critical growing phases.

More recently, drone-mounted multispectral sensors with spectral bands associated with the red-edge and near infrared (NIR) regions of the electromagnetic spectrum have been used for the estimation of biomass in rice and cereal crops. These spectrally enhanced cameras have been used for the estimation of biomass via the calculation of vegetation indices (Han et al., 2019; Maimaitijiang et al., 2017) and more recently, texture metrics. The texture metrics proposed by Haralick et al. (1973) is a grey level co-occurrence matrix texture algorithm and has commonly been adopted as the texture metrics for monitoring texture from crops from different spectral bands (Liu et al., 2019; Yue et al., 2019; Zheng et al., 2019). Zheng et al. (2019) showed the mean matrix in the NIR band to have the strongest correlation with rice biomass during the late growing phase compared to the red edge and visible texture bands.

Although Yue et al. (2019) did not consider the mean texture matrix for analysis, results showed texture matrix in the NIR band to have a strong correlation with yield.

Vegetation indices (VIs) have commonly been adopted for the estimation of biomass in rice and other crops at centimetre scale using multispectral cameras. Liu et al. (2019) applied four vegetation indices for the estimation of oilseed during the reproductive phase in China. The normalized difference vegetation index (NDVI) and red edge chlorophyll index ($CI_{rededge}$) showed the strongest relationship with AGB at the mid growth phase. Zheng et al. (2019) assessed of eight vegetation indices with the exclusion of the $CI_{red\ edge}$ when monitoring rice AGB. Rice AGB from the optimized soil adjusted vegetation index (OSAVI), which is a ratio of bands in the NIR and visible, performed best in the estimation of rice AGB at the mid-late growing stages.

Whilst vegetation indices have been used to estimate of rice AGB (Duan et al., 2019; Huang et al., 2015; Jiang et al., 2019; Zheng et al., 2019), they often suffer from the saturation effects during the heading and ripening stages of rice growth as biomass is mixed with panicles and stems as opposed to panicles during the vegetative stage (Cheng et al., 2017; Zheng et al., 2019). For instance, Normalized Difference Vegetation Index (NDVI) underestimates high biomass density due to this saturation effect (Fu et al., 2014; Kumar and Mutanga, 2017). However other VIs generated from the near infrared and red edge bands have presented more accurate estimations of rice AGB during the late growth stages. Zheng et al. (2019) demonstrated that the optimised soil adjusted vegetation index (OSAVI) exhibited a significantly positive relation with rice AGB during the late growing stage (R^2 = 0.65) compared to NDVI, green normalised vegetation index (GNDVI) and Modified triangular vegetation index 2 (MTVI 2). VIs generated from the red-edge and the near-infrared region have performed more favourably for the estimation of mid-late season AGB. For example, Maimaitijiang et al. (2017) examined the performance of VIs for estimating AGB 70 days after sowing and identified the Near Difference Red Edge Index (NDRE) to have the strongest relationship with AGB compared to NDVI and GNDVI. Therefore, further investigation of VIs during the reproductive and ripening phases is critical for monitoring rice AGB.

The combination of VIs and texture metrics have also shown to improve the estimation of rice AGB using the multispectral camera. For example, Zheng et al. (2019) demonstrated that the combination of texture metrics with bands in the NIR region and OSAVI vegetation indices produced the highest estimation accuracy for all phases of growth (R^2 = 0.78 and RMSE =

1.84 t/ha) and different phases (R^2 = 0.84 and RMSE = 1.06 t/ha for pre-heading stages and R^2 = 0.65 and RMSE = 1.94 t/ha for post-heading stages) compared to VIs and texture metrics alone in rice. Liu et al. (2019) also showed the combination off VIs and texture metrics using multivariate regression models to improve the estimation of biomass in oilseed crops. However, the cost implication of acquiring multispectral sensors to off the shelf RGB cameras, (though significantly cheaper than commercial images in the long-term) makes the practicability of farmers using them challenging (Jin et al., 2020b).

Although several studies have shown the potential of spectrally enhanced sensors in estimating crop AGB during the entire season and during the reproductive and ripening stages (Zheng et al., 2019; Yue et al., 2019), to date there have yet to be any studies that have investigated rice AGB using multispectral and RGB cameras in the mid to late growing stages (which are closely related to eventual yield outcomes). As such, the potential and relative merits of using drone-mounted consumer-grade RGB imagery and/ or scientific grade multispectral imagery for estimating rice mid-late season aboveground biomass remains to be investigated.

2.7 Estimating rice leaf-area index (LAI) from remote sensing platforms

Monitoring yield indicators such as LAI are fundamental to assessing the crop response to management practices and yield patterns (section 2.3). LAI can be retrieved from proximal, airborne and satellite sensors. When estimating high resolution LAI, proximal and airborne sensors are appropriate for mapping LAI over field and landscape areas, however the practicability of replicating this at region or global scales are impracticable because of issues relating to scale and frequency of acquisition. On the other hand, satellite platforms are better suited for global retrieval of LAI. For example, moderate spatial resolution satellites such as MODIS (see further discussion in section 2.5.1) have been used for global retrieval of LAI (Shi et al., 2013; Weiss et al., 2007). However, the spatial resolution of the sensors are such that they cannot be used for retrieval of LAI due to mixed pixels (Son et al., 2016). High spatial resolution satellites such as Landsat have a temporal resolution of 16 days, limiting the availability of images for monitoring LAI during different phenological phases. Very high resolution satellites on the hand, are impracticable due to the cost attached for regional and global monitoring of LAI.Sentinel-2 as highlighted in section 2.5.1 has a high temporal, spectral and temporal resolution and serves as platform for monitoring high resolution LAI from field scale to global scale (Pipia et al., 2019).

Irrespective of the scale, LAI retrieval is grouped into two broad categories: (i) statistical (variable-driven); (ii) physical (or radiometric data-driven) (Baret and Buis, 2008). However, since the turn of the 21st century, methodological approaches have expanded into a number of subcategories and combinations. Verrelst et al. (2015a) categorised LAI retrieval methods into four categories. They include parametric regression methods, non-parametric regression, physically based methods and hybrid models (Figure 2-7). The strengths and weaknesses of each method will be discussed in the following sub-sections.

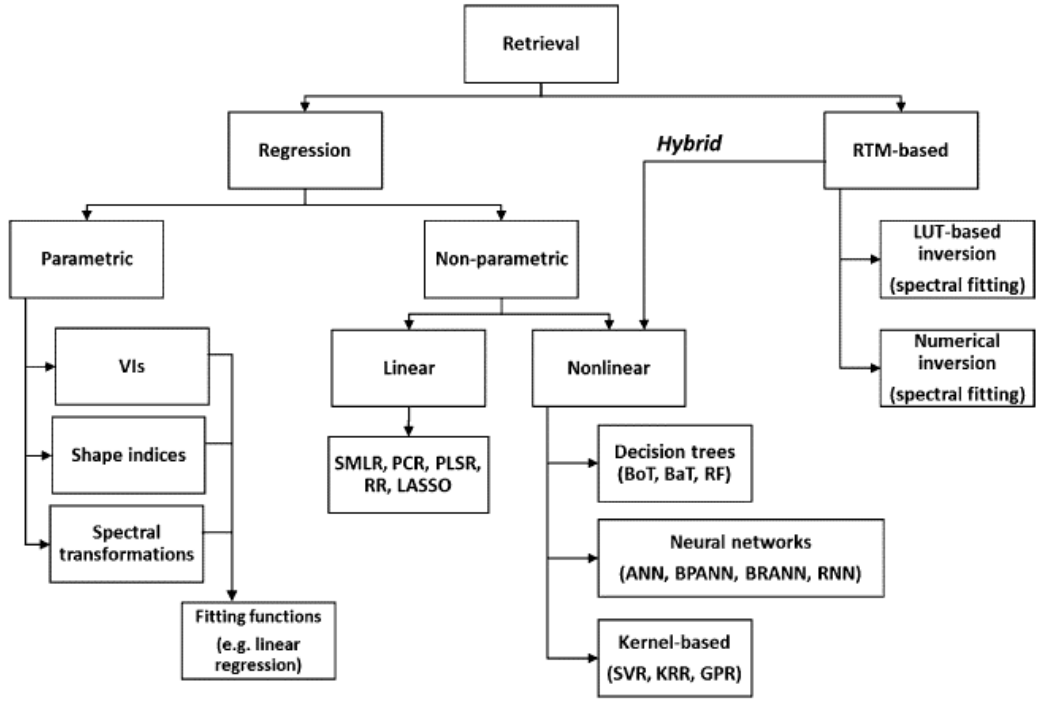

Figure 2-7: Schematic overview of the main retrieval methods (adopted from Verrelst et al. (2018))

2.7.1 Parametric Regression Model

The parametric regression model approach has been the most popular and widely adopted approach for estimating LAI from optical sensors. This approach involves the use of spectral features to reduce undesired effects, such as the variations of other leaf or canopy properties, soil reflectance, atmospheric composition, and sun and viewing geometry (Verrelst et al., 2015c). Parametric regression model approaches are achieved through the mathematical combination of spectral bands regressed with a biophysical variable using a fitting function, usually referred to as vegetation indices (VIs).

Most VIs used in generating LAI estimates combine reflectance in the visible and NIR wavelengths. This is because the reflectance in the visible portion of the electromagnetic

spectrum helps control the perturbation effect of background soil, whereas reflectance in the NIR domain allows for a large dynamic range of detection (Pinty et al., 2009). The normalized difference vegetation index (NDVI) is by far the most widely used index in the literature for estimating rice LAI from moderate (Xiao et al., 2005), high (Liu et al., 2012) and very high (Bsaibes et al., 2009) resolution images. However, NDVI approaches reach saturation asymptotically under conditions of moderate-to-high LAI (Gitelson, 2004).

Alternative VIs have been developed to minimize soil effects, such as the development of the soil adjusted vegetation index (SAVI) (Huete, 1988), the optimized SAVI (Rondeaux et al., 1996), and the modified SAVI (Qi et al., 1994). Additionally, other indices have been adopted to improving the sensitivity of VIs at high LAI and to reduce atmospheric perturbation such as Enhanced Vegetation Index (EVI) (Huete et al., 2002; Jiang et al., 2008). Wardlow et al. (2007) found that EVI exhibited greater sensitivity during the reproductive phases of crops, especially at the peak growing stage compared to NDVI values. The development of sensors with extra bands along the red-edge curve has led to the development of red-edge reflectance. They include Normalised Vegetation Red-edge (Gitelson and Merzlyak, 1994), chlorophyll index (Gitelson et al., 2003a) and Inverted red-edge chlorophyll index (Frampton et al., 2013). The significant advantage of the VIs based on the red-edge is that they are less influenced by canopy structures, hence making them suitable for building a single generic model (Adeluyi et al., 2019; Frampton et al., 2013; Xie et al., 2019a). However, the relationships between LAI and VIs are not always consistent for crops with different canopy structures (Kross et al., 2015; Viña et al., 2011).

Due to their empirical nature, these regression models are developed under various experimental setups, at different scales (leaf, plant, canopy), for different sensors (e.g. broadband vs. narrowband) and under different environmental conditions. Consequently, parametric models cannot be translated into other observation configurations without losing predictive power. Their performance can be hampered by disruptive disturbing factors, e.g., differences in surface properties and sun and viewing geometry. Hence, while being successful in the extraction of vegetation variables designed for local conditions, they are of limited applicability in a broader operational setting.

The main advantage of VIs is their simplicity because they require only a small set of spectral bands, reducing the computation time required to generate results. However, since parametric approaches are based on relatively simple mathematical definitions – as opposed to more

advanced methods (Non-parametric models) – and uncertainty intervals for the retrieval on a per-pixel basis are not provided. With the absence of uncertainty estimates, the performance of parametric regression methods is difficult to ascertain in an operational environment. Therefore, parametric methods are inadequate to provide global LAI products. Table 2-4 shows the strengths and weakness of the parametric method.

2.7.2 Non-parametric Regression Models

Non-parametric regression models adopt the use of a learning phase acquired from training datasets. This method combines different data structures in a non-linear way hence an explicit selection of spectral bands or transformations are not required (Verrelst et al., 2015a). However, in the case where models are too flexible, overfitting of the training model may occur. To tackle issues with overfitting, model weights are defined by jointly minimising the training set approximation error while limiting model complexity. The non-parametric regression models can be further categorised into linear and non-linear non-parametric models and will be discussed in the following sub-sections.

2.7.2.1. Linear non-parametric models

Linear non-parametric models (Figure 2-7) are multivariable linear models capable of handling multi-spectral datasets. However, when input data quantity is limited with regards to dimensionality of the dataset, linear nonparametric models become problematic. To cope with the collinearity, a dimensionality reduction approach is often adopted. In terms of their application, Darvishzadeh et al. (2008) used the stepwise multiple linear regression (SMLR) to estimate LAI. Results showed superiority in the estimation of LAI from the multivariable linear models compared to univariable models such as NDVI and SAVI. In addition to SMLR, Principal Component Analysis (PCA) has also been adopted for the estimation of LAI in crops (Chaurasia and author, 2004; Fei et al., 2012). Other linear non-parametric models perform better than SMLR for the estimation of LAI. For instance, partial least squares regression (PLSR), one of the most widely applied non-parametric approaches, has been shown to generate more accurate estimates compared to VIs (Cho et al., 2007; Darvishzadeh et al., 2008b; X. Li et al., 2014; Li et al., 2016). Darvishzadeh et al. (2008) showed that PLSR outperformed SMLR and VIs for the estimation of LAI. Similar results were identified when PLSR were compared against other non-parametric regression for the estimation of LAI from Sentinel-2 simulated data (Verrelst et al., 2015c). Other linear non-parametric model like ridge regression (RR) and least absolute shrinkage and selection operator (LASSO) have not seen

as much uptake for the estimation of LAI compared to previously mentioned non-linear regression methods. Lazaridis et al. (2010) compared RR and LASSO methods to PLSR and showed that these non-parametric methods performed particularly well. Despite the results obtained from non-parametric linear models, these methods have not been incorporated into operational and global retrieval methods as compared to non-linear non-parametric models (Verrelst et al., 2015a).

2.7.2.2. Non-linear non-parametric models

Non-linear non-parametric methods, often referred to as Machine Learning Regression Algorithms (MLRA), are important methodologically because of their capability to capture non-linear relationships of image features without explicitly knowing the underlying data distribution (Verrelst et al., 2018, 2015a). Therefore, they are developed without assuming a particular probability density distribution, which is why they are suitable for different types of data and are structured in such a way that they can incorporate prior knowledge. Three families of machine learning models are usually applied for the estimation of LAI from earth observation satellites: Artificial Neural Network-based, decision tree-based, and kernel-based regression methods (Figure 2-7).

The Artificial Neural Network-based regression models are a connection of layered structures of artificial neurons. These artificial neurons are pointwise non-linear function applied to the output of a linear regression. Since artificial neurons are interconnected with different links, an individual artificial neuron will exhibit similarities to those obtained in linear regression. Hence, the collective interconnection patterns between different artificial neuron layers, alongside the learning processes for updating the weights of the connection and the activation functions which convert the artificial neurons weighted inputs, is referred to as Artificial Neural Network (ANN) (Atkinson and Tatnall, 1997; Bacour et al., 2006). Results from ANN for estimation of LAI have been identified to be superior to parametric models for the estimation of rice and other crops (Chen et al., 2015; Hongliang Fang and Shunlin Liang, 2003; F. Wang et al., 2019). However, ANNs are largely determined by their design in the sense that too few or too many layers of artificial neurons may significantly reduce the accuracy of estimation.

Decision tree-based regression models are a class of very powerful MLRAs. Frequently applied in classification, decision tree-based models have just recently been applied in regression analysis. Decision tree learning models are based on a set of hierarchical connected

nodes, with each node representing a linear decision on a specific input feature. Of the decision tree-based models, the Random Forest MLRA (Breiman, 2001) are considered the most powerful. Random forest models are an ensemble of trees, where each tree contributes with a single vote for the assignment of the most frequent class to data (Breiman, 2001). Random forest builds on multiple regression trees independently by using different bootstrapped sample subsets of training samples. Random forest models have been used for the estimation of LAI in sugarbeet and potato (Siegmann and Jarmer, 2015; Vuolo et al., 2013). Although random forest has some advantages compared to other machine learning regression algorithms, it is difficult to use in datasets with missing data (Pal, 2005).

Another commonly adopted model class used for the estimation of LAI are the Kernel-based regression methods. Kernel-based methods provide a framework for developing non-linear techniques and possess useful properties in the case where a low number of training samples, outliers and noise are found in the dataset (Gómez-Chova et al., 2011; Tuia et al., 2018).

Kernel-based methods are suitable for the extraction of non-linear information from spectral data. Three main regression models are commonly adopted for the estimation of LAI: Support Vector Regression (SVR) (Vapnik, 1998); the Kernel Ridge Regression (KRR) (Suykens and Vandewalle, 1999); and the Gaussian Process Regression (GPR) (Rasmussen and Williams, 2006). SVR models are the earliest and most popular model which are normally adopted for classification purposes from the mid-1990s (Support Vector Machine (SVM)). They have been successfully adopted for the estimation of LAI (Camps-Valls et al., 2009; Durbha et al., 2007). However, when compared with other machine learning methods, such as random forest, SVR estimation were less accurate (Siegmann and Jarmer, 2015). Similar to SVR, KRR models initially made waves in the classification field before its emergence in regression analysis. Studies have used the KRR approach for the estimation of LAI. (Verrelst et al., 2012b) investigated the performance of KRR against other MLRA models and were found to be robust for the estimation of LAI. This primarily due to their relatively simple design which requires only one hyperparameter to be tuned. Additionally, KRR models are capable of dealing with collinearity in the event where numerous bands are present. Likewise, GPR models have been successfully implemented for the estimation of LAI within the last decade. Notably, Verrelst et al. (2012a) compared GPR with parametric methods. Results here showed better performances from GPR, offering additional information on band relevancy for each variable, the weighted relevant spectra contained in the training dataset and the probabilistic outputs, i.e. a mean estimate and associated uncertainty interval. When compared against other MLRA,

GPR models slightly outperform other models but were computationally demanding compared to KRR (Verrelst et al., 2012b, 2015c).

An overview of the strengths and weaknesses of non-parametric regression methods are listed in Table 2-4.

Table 2-3: Strength and Weaknesses of non-parametric method for LAI estimation

Retrieval Approach	Strengths	Weaknesses
Parametric method	- Simple and comprehensive regression models; limited knowledge of the user require - Fast processing - Computationally inexpensive	- Boundary conditions are defined based on the level of selected bands, formulations and regression function - Models tend to be specific to the dataset used for model characterization) - Models are sensor-specific models (i.e., a direct transfer to other sensors is usually not possible) - Only one variable can be accounted for at a time - Uncertainty estimates are not provided. Hence the quality of the output maps remains unknown - Need for collecting field data (i.e., Measurement campaigns are necessary)

Non-parametric method	- Some MLRAs cope well with datasets showing redundancy and high noise levels - Once trained, imagery can be processed time efficiently	- Training can be computationally very demanding - Some regression algorithms are difficult (or even impossible) to train with a high number of samples
	- Some of the non-parametric methods (e.g. ANNs, decision trees) can be trained with a high number of samples (typically > 1,000,000)	- Expert knowledge is required, e.g. for tuning. However, toolboxes exist automating some of the steps
	- Some MLRAs provide insight in model development (e.g. GPR: relevant bands; decision trees: model structure)	- Most of the methods are considered black boxes
	- Some MLRAs provide multiple outputs (e.g. PLRS, ANN, SVR, GPR and KRR) - Some MLRAs provide uncertainty intervals (e.g. GPR)	- Some regression algorithms elicit instability with datasets having statistics deviating from the datasets used for training - Need for collecting field data (i.e. measurement campaigns are necessary)

Physical based Models	- Reputation of physically-based methods (however, note the impact of regularization factors)	- Computationally demanding due to the per-pixel based approach (however, solutions based on a priori information have been developed)
	- Generally, and globally applicable (e.g. MODIS products)	- Retrieval quality depends on the quality of the RT models, prior knowledge and regularization
	- Capability to provide multiple outputs	- Quite complex approach: requires parameterization and optimization procedures
	- Yields additional information about uncertainty of the retrievals (e.g. through spectral residuals)	- The imposed upper/lower boundaries in the LUT have a logical consequence in that estimated variables cannot go beyond the boundaries imposed. This contradicts somewhat the physical approach as the prior information has an overwhelming influence (Baret and Buis, 2008)
		- LUT-based inversion methods are often strongly affected by noise and measurement uncertainty (Liang, 2007)

2.7.3 Physically-based Models

Physically-based models provide an explicit connection between biophysical variables and canopy reflectance, through the modelling of radiation transfer within the canopy or leaf, based on physical laws (Figure 2-7). These models are categorised based on their complexities and are grouped into four categories: kernel-based, turbid medium, geometrical, and computer simulation models. The kernel-based model are simple Radiative Transfer Models (RTM) that estimate the directional reflectance of the land surface based on the sun-surface-sensor geometry and forward/backward scattering shape of the anisotropic reflectance pattern (Rahman et al., 1993; Roujean et al., 1992). The turbid medium model simulates the canopy as turbid parallel layers above a ground surface (Kuusk, 2001). Turbid models are best suited for dense canopies with small vegetation elements such as crops, grasses and forest. An example of a model adopted in this category is the PROSAIL model (Figure 2-8) (Berger et al., 2018; Jacquemoud et al., 2009), which combines the PROSPECT leaf optical properties model (Jacquemoud and Baret, 1990) and the Scattering by Arbitrarily Inclined Leaves canopy bidirectional reflectance model (Verhoef, 1984). For geometric optical models, the description of canopy architecture is based on different geometric objects based on a given distribution and optical properties (Chen and Leblanc, 1997). However, intrinsically, geometric models are only accurate in the visible part of the electromagnetic spectrum, where absorption by vegetation is high (Chen et al., 2000). Computer simulation models are complex models that rely explicitly on the canopy architecture, trace photon interactions with the environment and are configured to simulate inhomogeneous and urban landscapes (Disney et al., 2006; Roupsard et al., 2008).

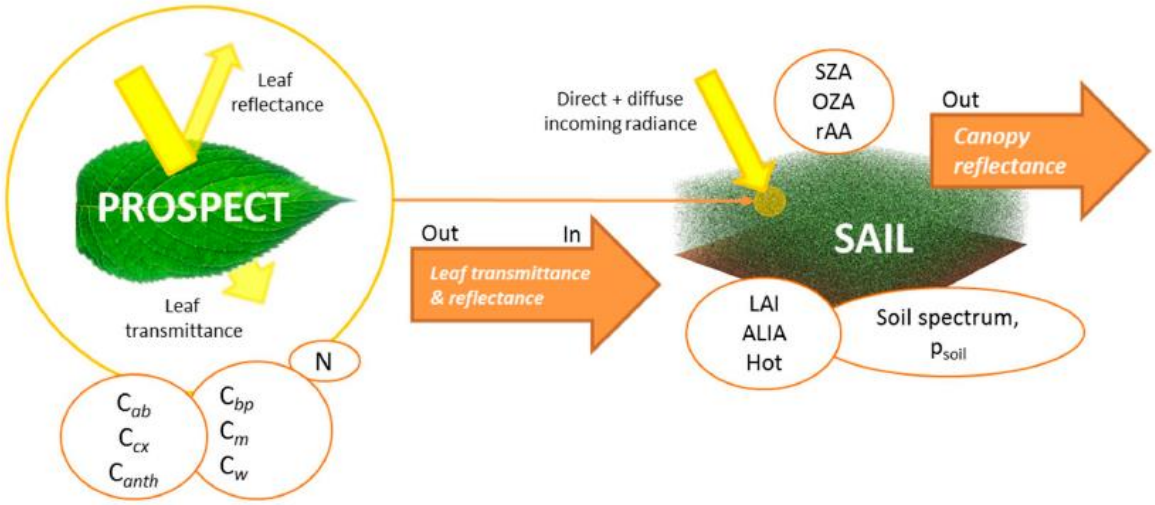

Figure 2-8: Calculation of canopy reflectance using the coupled PROSPECT + SAIL models. Variables are further explained in Chapter 5 Source: Berger et al (2018).

Irrespective of the complexity of the models, in principle, only a coupled leaf-canopy RTM and an inversion routine are required for the retrieval of RTM LAI, where the approach is generic and generally applicable. Nonetheless, these approaches are not straightforward for several reasons. Firstly, an RTM should be selected such that a trade-off between realism and inversion possibility of the RTM can be established. As discussed above, more complex models tend to be more realistic, but require more variables, thereby making them more challenging to invert, whereas simpler models are easy to invert but less realistic. Secondly, RTMs are invertible only when an inversion solution is unique and dependent—in a continuous mode—on the variables to be extracted. However, these boundaries are not met because the inversion of canopy RTMs are usually undermined and ill-posed because the number of unknowns can be much larger than the number of independent observations. Hence, physical based models for the retrieval of LAI properties are a challenging task. To cope with the underdetermined problem of optimizing the inversion process, several strategies were proposed. They include iterative numerical optimization methods, look-up table (LUT) and hybrid approaches.

The iterative numerical optimization method represents a classical approach to invert RTMs in image processing (Jacquemoud et al., 1995; Zarco-Tejada et al., 2001). The optimization method consists in reducing a cost function, which estimates the difference between measured and estimated variables by successive input variable iteration. However, optimization algorithms are

computationally demanding and time consuming when working the inversion of large-scale remote sensing data. Furthermore, optimization techniques require regularization techniques are required to achieve accurate results (Zarco-Tejada et al., 2001).

LUT on the other hand are engineered to speed up the inversion process. This is achieved by generating spectral reflectance from a large range of combinations of variable values ranges. As such, the inversion issues are reduced to the identification of the modelled reflectance set that most closely resembles the measured one. This is achieved by querying the LUT and subsequently applying a cost function. A cost function minimizes the summed differences between simulated and measured reflectance for all wavelengths. The main advantage of LUT-based inversion over numerical optimization is their computational speed, since the computationally demanding part of the inversion process is completed before the inversion itself (Dorigo et al., 2007). For these reasons, LUT-based inversion models are typically used as a preferred solution in RTM inversion studies (Verrelst et al., 2015a). Other strategies have been adopted to further improve the LUT-based inversion by mitigating the ill-posed problem. They include the use of prior knowledge, introduction of cost functions, and the use of artificial noise. Despite the comparative advantage of the LUT method over the iterative numerical optimization approach, its drawback lies in its computational burden resulting from too many per-pixel iterations. An overview of the strengths and weaknesses of physically-based methods are listed in Table 2-4.

2.7.4 Hybrid Regression Approach

Hybrid models are based on the combination of physical based models and usually the MLRA approach. Hybrid models adopt the generic level associated with physical based approach and complements with the flexibility and computational approaches from machine learning regression models towards the estimation of LAI. One comparative advantage of the hybrid model is that it uses all available data to train (non-linear) non-parametric regression compared to the LUT, which attempts to simulate as close as possible to the measured LAI.

Hybrid models have made it into the operational processing chains with the sole purpose of generating LAI and other biophysical parameters using ANN (Bacour et al., 2006). Bacour et al. (2006) pioneered this approach that was based the inversion of ANN into RTM and ever since has been the core routine in various processing chains. For example, the MERIS vegetation algorithm is based on the training of ANNs with a database containing simulations from canopy and

atmosphere RTMs (PROSAIL). Similarly, the CYCLOPES products are processed in a similar ways to the MERIS product using SPOT-VEGETATION sensor (Baret et al., 2007). More recently, the Sentinel-2 Application Platform (SNAP) has adopted the same mechanism for the retrieval of LAI on a global scale (Weiss and Baret, 2016). However, while the ANNs have been applied extensively for the operational estimation of LAI, limitations still exist with this approach. For instance, LAI estimates from CYCLOPES were seen to be less accurate when LAI values were greater than 4 due to the saturation effect in radiative transfer models simulation and the ANN algorithms (Bacour et al., 2006; Weiss et al., 2007). Secondly, ANN models are usually referred to as 'black box' models, implying that they behave relatively unpredictably when used with input spectra deviating from what has been input during the training stage (Rivera et al., 2014).

Based on the limitations associated with the ANN models, other studies have applied other MLRAs with RTM for the estimation of LAI. Notably, Campos-Taberner et al.(2016) applied the inversion of the PROSAIL radiative transfer model through the GPR, ANN and KRR methods using multitemporal Landsat and SPOT5 data for the estimation of rice LAI. Results showed better results generated from GPR models compared to the KRR and ANN models. Furthermore, Upreti et al. (2019) in their estimation of wheat LAI showed superior estimates using a GPR model compared to ANN applied in the SNAP toolbox. That said, further validation is required to confirm the performance of GPR models to already existing operational processing LAI models. Additionally, it remains to be seen whether rice LAI can be reliably estimated from GPR and ANN using Sentinel-2.

2.7.5 Measuring the Phenological Dynamics of LAI

Having reviewed the importance of the phenological stages of rice in section 2.1, this section reviews the ability of current techniques to contribute towards a better understanding of the seasonal dynamics of LAI.

Previous studies have focused on understanding the phenological dynamics of LAI in rice and other crops over the entire growing season (Qiao et al., 2019; L. Wang et al., 2019) as they provide in-season information of yield limiting factors such as nitrogen and irrigation application. Wang et al. (2019) compared statistical based models (parametric and non-parametric models) for the understanding the seasonal dynamics of rice. They argued that these approaches were robust for

understanding the LAI changes that occur during different phenological phases. Likewise, Qiao et al. (2019) argued that vegetation indices could be adopted for understanding the phenological changes of LAI in cereal crops. While these approaches may have yielded good results, the models adopted will require re-calibrations when conducted in other farm regions, therefore limiting the replicability of these approach.

Campos-Taberner et al. (2016) on the other hand investigated the seasonal dynamics of rice LAI using GPR hybrid models from SPOT and Landsat satellites. However, no study has validated the GPR and ANN model from alternating management regimes, which are important towards understanding yield limiting factors using Sentinel-2 satellite. The robustness of these retrieval methods under alternating farming treatments, over different phenological stages has yet to be established. Therefore, the thesis explores the phenological dynamics of estimating LAI in an irrigated rice farm using Sentinel-2 data.

2.8 Estimation of rice yields

This section will look at the estimation of yield at varying spatial extents from satellite platforms using two yield estimation approaches. The review excluded proximal and airborne platforms due to issues related to scale (Dungan et al., 2002).

2.8.1 Satellite Estimation of rice yield

Low spatial resolution satellites (< 250m) have been used to predict yield in rice and other crops. The Advanced Very High-Resolution Radiometer (AVHRR), a low-resolution satellite (1.1 km spatial resolution) has been utilised to predict yield. For instance, Bastiaanssen and Ali (2003) utilised AVHRR data to predict regional rice yield in Pakistan. Validation results at county data scale showed a RMSE of 551 kg/ha, although AVHRR is basically too coarse a resolution for field scale crop yield estimations. In addition to AVHRR, the Moderate Resolution Imaging Spectroradiometer (MODIS) (≤ 250m) has been utilized extensively for yield estimation because of the temporal and spectral resolution of the sensor. Ren et al. (2008) predicted crop production using a MODIS-NDVI based model at regional scale with a 250 m spatial resolution in China. Predicted yield using MODIS-NDVI results showed that the relative errors of the predicted yield were between 4.62% and 5.40% and that the RMSE (214.16 kg ha/1) was lower than the RMSE (233.35 kg ha/1) of agro-climate models at country scale. Similarly, Sakamoto et al. (2013)

estimated rice yield using empirical time-series MODIS model, suggesting the suitability of MODIS for suggest MODIS is capable of predicting yield at the regional scale. However, the spatial resolution of low spatial resolution satellite sensors makes them unsuitable for field to landscape scale yield monitoring.

In an attempt to overcome the spatial limitations of low resolution satellite sensors, medium to high spatial resolution satellites have been adopted extensively for the prediction and estimation of yield (Gilardelli et al., 2019; Guan et al., 2018; Siyal et al., 2015). Notably, Landsat has been the preferred option for many researchers due to the free availability of data spanning more than 40 years. Jin et al. (2017) used Landsat imagery integrated into a scalable satellite-based crop yield mapper to predict maize yield at county level in Midwestern US states, with results capturing 75% of the yield variation in 3 states in United States.

Kang and Özdoğan (2019) also used Landsat to downscale county-level yield statistics to 30-meter resolution yield maps, which can inform between and within field maize yield variability. Despite results showing the suitability for predicting yield at high spatial resolution, Landsat temporal resolution of 16 days, reduces the acquisition of images especially between 50 -90 Days After Sowing (DAS) for rice, which has been identified as a crucial for predicting yield (Fageria, 2007). Although measures have been adopted to fuse the daily temporal resolution obtained from MODIS and 30m spatial resolution from Landsat (Feng Gao et al., 2006; Gevaert et al., 2015), the performance depends on the characteristic landscape patch size and degrades somewhat when used on extremely heterogeneous landscapes (Feng Gao et al., 2006).

Other medium to high resolution satellites like SPOT (Satellite Pour l'Observation de la Terre) at 10m have been used for predicting yield. Noureldin et al. (2013) created rice yield forecasting models using satellite imagery in Egypt. Here validation results indicated that using NDVI combined with leaf area index (LAI) produced the model with highest accuracy and stability during the two rice seasons. However, the discontinuation of the SPOT 4 satellite and commercialization of SPOT 5,6 and SPOT 7 (now Azersky) serves as a limitation to the satellites used for crop yield estimation. Similarly, the commercialization of other very high-resolution satellites such as KOMPSAT, GeoEye, Worldview series Pleiades-1, are ideal for high resolution yield prediction. However, very high spatial resolution images may not be suitable for predicting yield in regions such as developing countries due to the financial implications of acquiring images.

The launch of Sentinel-2 in 2015 by the European Space Agency (ESA), creates new opportunities for agricultural monitoring, by making it possible to view agricultural fields in 12 spectral bands at a 10 – 20 m spatial resolution, with global coverage and a 5-day revisit frequency, and is compatible with the current and historical Landsat and SPOT 4 missions (Serrano et al., 2000). The Sentinel-2 satellite has on board bands from the visible to the shortwave infrared: four bands at 10 m, the classical broadband visible blue (490 nm), green (560 nm), red (665 nm), and near infrared (842 nm); six bands at 20 m, three narrow bands in the vegetation red edge spectral domain (705, 740 and 775nm).

The addition of spectral bands along the red-edge curve opens up opportunities for the estimation of yield, as well as yield indicator monitoring (Drusch et al., 2012). For instance, Sentinel-2 has been used to accurately estimate yield indicators like Leaf Area Index (Korhonen et al., 2017; Sinha et al., 2020; M. Zhang et al., 2019), chlorophyll content (Ansper and Alikas, 2019; Clevers et al., 2017; Delloye et al., 2018), fraction of vegetation cover (Djamai et al., 2019) and biomass (Darvishzadeh et al., 2019; Pahlevan et al., 2020; Punalekar et al., 2018). Similarly, Sentinel-2 is better suited for irrigated rice monitoring during the dry season as issues with cloud are less pronounced compared to the rainy season, which affect the transmission of radiation between satellite and sensor targets (Coluzzi et al., 2018). However, Kanke et al. (2016) assessment of Sentinel-2 20m using red-edge indices improved the estimation of yield prediction in rice compared to indices without red-edge bands. Evaluating this trade-off, and specifically its implications in the context of yield estimation at different spatial scales (e.g. plot-level yield versus yields averaged over a larger spatial area), is the main focus of this study. In doing so, I address a key gap in scientific knowledge about how to best leverage Sentinel-2 imagery for rice yield estimation at farm to landscape scales, considering in particular the relative of Sentinel-2 spatial and spectral properties at different scales of estimation.

2.8.2 Methods for Predicting Yield from Satellite Platforms

Yield estimation at the individual field and landscape level is an imperative task for agricultural research and application (Zaks and Kucharik, 2011). Primarily, yield estimation falls into two categories: data assimilation approaches (Jin et al., 2018; Kang and Özdoğan, 2019a; Thorp et al., 2012a) and empirical (Ahmad et al., 2020; Bolton and Friedl, 2013; Hunt et al., 2019; van Klompenburg et al., 2020).

The data assimilation approach integrates, both in space and time, canopy state variables with various information using remote sensing methods for optimizing crop parameters in crop models (Jin et al., 2018). The process involves integrating observed variables (from remote sensing data resources), state variables (from a complete crop model system), model parameters (described relationships between the observed variables and state variables) and output variables (yield in most of the data assimilation) (Delécolle et al., 1992). The integration approaches usually adopted include calibration method, forcing method, and updating methods (Dorigo et al., 2007; Jin et al., 2018; Kang and Özdoğan, 2019a; Moulin et al., 1998). Pagani et al. (2019) used a rice crop model (WARM model) and remote sensing information was used for predicting rice yield in three European countries. Results explained between 21 - 89% of the inter-annual yield variability from eight rice cultivars. Similarly, Gilardelli et al. (2019) assimilated LAI data obtained from Sentinel-2 and Landsat into the WARM model to forecast rice yield. The assimilation of remotely sensed LAI into model parameters increased the accuracy of the system with MAE and RRMSE 0.66 t/ha and 13.8% respectively, whereas, without data assimilation, they were 0.82 t ha-and 15.7%.

Although these studies showed promising results for the estimation and prediction of yield, data assimilation approaches of yield mostly rely on model specifications that relate to various environmental stresses, which can hardly be fully corrected by only assimilating LAI. Also, using sophisticated crop growth models, such as Decision Support System for Agrotechnology Transfer (DSSAT) (Jones et al., 2003) and World Food Studies (WOFOST) (de Wit et al., 2019), to perform data assimilation for yield estimation requires specific complicated interactions between environmental factors and management practices, explicit information on soil properties and weather variables, as well as cultivar-specific parameters that are not normally available to farmers, preventing their use in yield estimation applications (Jin et al., 2018; Kang and Özdoğan, 2019a; Lambert et al., 2018)

The empirical methods on the other hand rely on in situ or synthetic yield data to train parametric or non-parametric models, such as machine learning algorithms (Hunt et al., 2019; Lambert et al., 2018; van Klompenburg et al., 2020), to evaluate actual yield and can be applied at large scales increasingly congruent with the reality of smallholder agricultural systems (Lambert et al., 2018). Hunt et al. (2019) used the Random Forest MLRA and Sentinel-2 to accurately predict wheat yield in the UK at landscape scale. Similarly, Kayad et al. (2019) applied similar methods for the

estimation of maize yield in Northern Italy. Consequently, achieving robust smallholder/landscape yield predictions is important in developing countries, notably where subsistence agriculture still determines food security, and for profitable farmer participation in more contract-oriented agricultural areas.

The practicability of using empirical models are further enhanced with the availability of validation yield data innovations in farming technology, providing an opportunity for farmers to measure, observe and respond to the spatial and temporal variation in crops. These precise measurement approaches aim to ensure accurate targeting of agricultural interventions. A key component of precision monitoring has been the incorporation of high-accuracy GPS technology into farm machinery, such as the combine harvester. With the inclusion of sophisticated on-board yield monitors, there is now an opportunity to access fine-resolution mapping of within-field variation in crop yields.

The availability of high-resolution satellites opens up the opportunity to access the potential of predicting within field variability at landscape scale, while also evaluating within field variability at smallholder farms. The thesis explored the possibility of predicting rice yield using empirical models.

2.9 Summary and Gaps in Literature

This literature review has provided insight on the importance of rice globally, with specific focus on Nigeria. It has highlighted the potential of growing rice in Nigeria based on the natural resources and initiative adopted by the Nigerian government. However, the review has highlighted the factors behind low yield outcomes of rice in Nigeria. The review further highlighted the importance of each phenological phase of rice growth in relation to actual yield productivity. Remote sensing approaches were identified as a suitable means of monitoring yield and yield indicators from different remote sensing platforms. The review focused on optical remote sensing for monitoring rice aboveground biomass, leaf area index and yield.

When considering the estimation of rice above ground biomass at fine high resolution, the review highlighted the superiority airborne (drones) platform for the estimation of field scale AGB estimation as compared to satellite, airborne (remotely piloted aerial vehicles) and proximal sensors as a result of the acquisition cost and their high spatial and temporal resolutions. Further

investigation highlighted the characteristics of drone-mounted sensors for the estimation of rice AGB. Notably, the structural properties of RGB sensor to generate plant height from crop surface models are an exciting development for the estimation of rice AGB. Previous studies have also identified the significant potential of more spectrally sophisticated drone sensors (i.e. multi-spectral cameras) that have the capacity of generating vegetation indices and texture metrics for the estimation of rice AGB. However, the comparative advantage of the structural properties of RGB-based sensors compared to the spectral properties of multispectral based sensors are yet to be established. This thesis serves to also provide a comprehensive comparison of both types of sensors for estimating AGB during the reproductive to ripening stages of rice, which are considered critical for biomass formation. From literature review, I identified they key research question as "What are the relative merits of using data either from a drone-mounted consumer-grade RGB, a scientific grade multispectral camera, or their combined use, for estimating rice mid-late season above ground biomass?"

Similarly, the literature review also reviewed leaf area index as a yield indicator of rice. The review focused on the estimation of LAI from field to global scale and identified the advantages of satellite platforms over airborne and proximal platforms. Of the satellite platforms, Sentinel-2 satellite was identified as potentially the most suitable satellite for upscaling LAI monitoring at field to global scale. Subsequently, I reviewed various retrieval methods for estimating rice LAI. LAI retrieval methods were grouped into parametric, non-parametric, physical based and hybrid models. Parametric models were identified to be less computationally demanding compared to other retrieval methods, but are site specific and require re-calibration when executed in other rice farms. Non-parametric models present a more robust approach for LAI retrieval and results, in most cases, are superior to parametric models. However, non-parametric models require collection of field data for training the model. Physical based models on the other hand are more robust as these models generic and globally accepted, reducing the need for re-calibration based on location. On the other hand, these models are complex and require parameterization and optimization procedures. Although strategies to mitigate the ill-posed nature of physical models, the imposed upper and lower boundaries from the commonly adopted LUT affect the accuracy of LAI retrieval. To somewhat tackle this, the combination of physical based models (e.g., Radiative Transfer Models) and non-parametric models (e.g., MLRA) have been adopted for the global operational retrieval of LAI. To date, most hybrid models have adopted the inversion of ANN models with

physical based models. However, saturation of LAI estimates has been noted in several studies, especially at high LAI, which usually occurs during the reproductive and ripening stages of rice growth. The reason being that saturation affects the model at high LAI values. LAI also often difficult to train because of their multi-parameter complexity and are black box in nature. Studies have opted to use other MLRAs in combination with RTMs which have presented superior estimation when LAI values are high. Particularly, the GPR model has been identified in literature to outperform other MLRAs for LAI estimation. However, the phenological dynamics of GPR hybrid model for the retrieval of rice LAI phenology from Sentinel-2 is yet to be investigated.

Finally, I reviewed yield estimation from satellite platforms for the estimation of yield from smallholder to landscape scales. As identified with the estimation of LAI across scales, Sentinel-2 was identified as potentially suitable for monitoring high resolution yield based on the free availability of satellite images at high spatial, spectral and temporal resolution. However, based on varying spectral resolutions of Sentinel-2 10m and 20m spatial resolutions, a research gap was based on the spatio-spectral influence of baseline Sentinel-2 for estimating within field variability of yield at landscape scale and between field variability of smallholder farmer plots. Furthermore, I identified the approaches used for estimating yield in rice using earth observation satellites, which include data assimilation of remote sensing data in crop simulation models and empirical models. Crop models have been identified to be more robust than empirical models for predicting yield at smallholder scale, however, they are difficult to implement in scales much larger than smallholder farm scales. On the other hand, the simplicity of empirical models in combination with machine learning models and availability of high-resolution images opens the opportunity to predict yield at smallholder and much larger scales. Therefore, the research question established for monitoring yield was “What is the influence of the spatio-spectral resolution of Sentinel-2 for estimating within field variability of yield at landscape scale and between field variability of smallholder farmer plots?

Chapter 3 Methodology

The methodology chapter describes the characteristics of the study area and all datasets used in addressing the research objectives. It also explains the pre-processing operation and quality assurance checks performed on the data to assess their quality and suitability. It goes further to explain the experimental design of the 2.5 ha field experiment, as well as the conventional farming practice over 1150 hectares of irrigated rice farming at Olam farm. Research objectives 2 and 3 (highlighted in section 1.2) are associated with the 2.5-hectare experimental campaign conducted in the 2017-18 dry season field campaign, addressing the relative merits of structural and multispectral information for estimating mid-late season above ground rice biomass from drone imagery and the phenology dynamics of LAI retrieval using Sentinel-2. Research objective 4 was achieved using in the 2018-19 dry season field campaign, addressing the relative importance of the spatial and spectral resolution of Sentinel-2 for estimating rice yields across a range of spatial extents. Field sampling techniques to coincide with drone and satellite imagery overpass were explicitly highlighted with the rationale for each decision. This chapter also outlines the image processing methods and data pre-processing used during data analysis.

3.1 Study Area

The study was conducted in Nasarawa State, situated in the central part of Nigeria otherwise referred to as the middle belt region of Nigeria. The state lies between longitude 6°57'16" E to 9°33'51" E and latitude 7°46'17" N to 9°18'47" N (Figure 3-1). The population of Nasarawa State according to the 2006 census report was 1,863,275, with a population density of 65 people/sq km. Nasarawa State is a cosmopolitan state, with diverse people from different backgrounds co-habiting peacefully. The main indigenes are: Koro (Migili), Eggon and Kambari, Gbagyi, Mada, Gwandarawa, Afo, Hausa and Nidre. Agriculture is the main economic activity in Nasarawa State (Agidi, 2018). Farming is subsistence and generally rain-fed cultivation of annual crops. Although there are many rivers in the state, the population engaged in irrigation farming is low(Salau, 2012).

Crops grown include grains such as rice, wheat, soybeans, beans, maize and millet, and tuber crops such as yam and cassava. Smallholder farmers undertake the bulk (80%) of crop production in Nasarawa State, most of whose labour force, management and capital originate from the households (Akwa et al., 2007). The average number of farm plots per household ranges between

3 -30 plots, which is between 0.4 - 5.0 hectares (Salau, 2012) primarily due to land available and capacity for cultivation by each household.

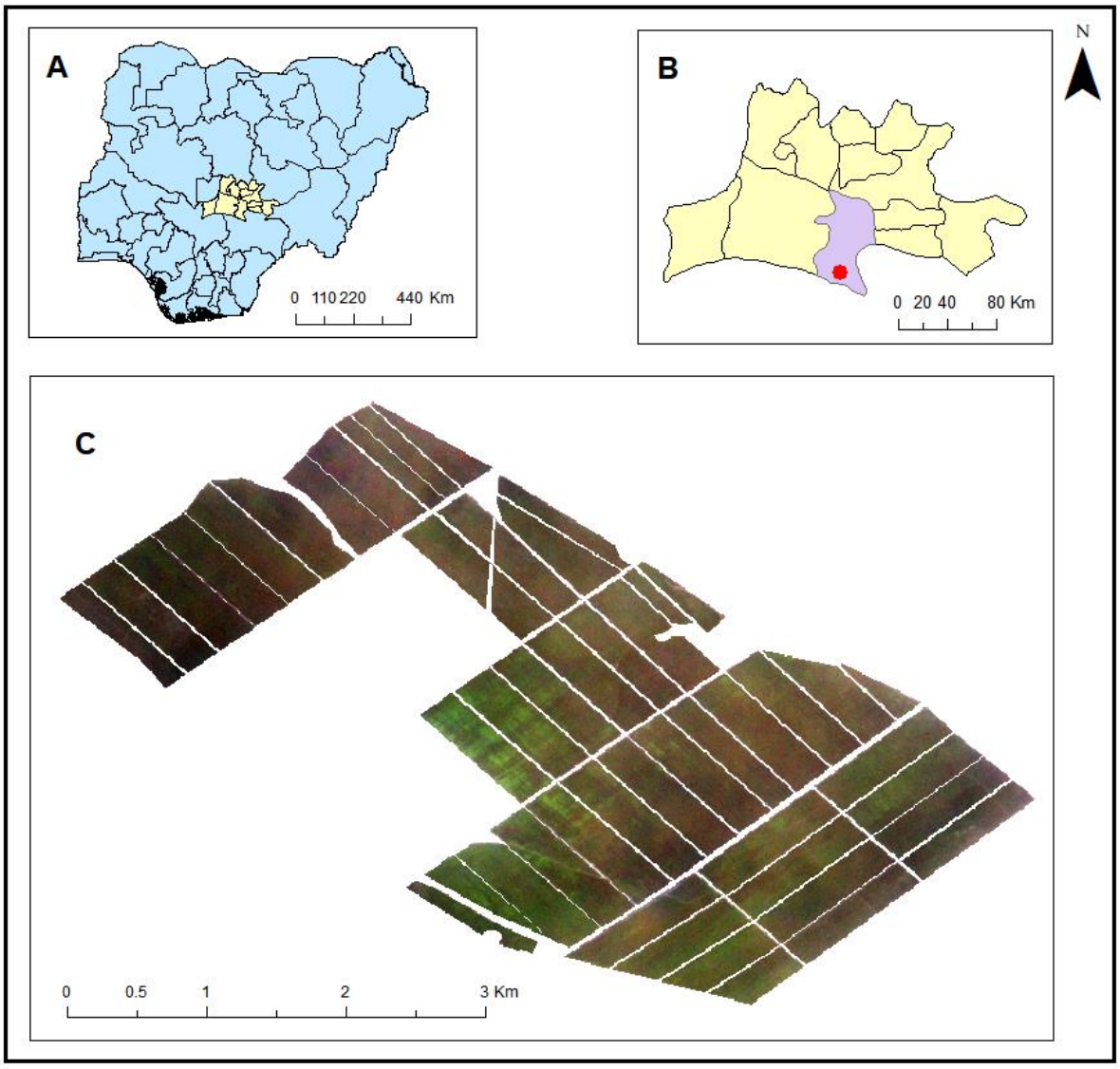

Figure 3-1: (a) Nasarawa state highlighted within Nigeria, (b) the study area location highlighted in Doma local government area, (c) 1150ha Olam rice farm where the field campaigns were implemented. .

In terms of soil and geology, Nasarawa state is richly endowed with fertile soils from soil materials of alluvial deposits in most of the southern part of the state, to a more structured and developed Oxisols and Ferrisols in the northern part of the state, with underdeveloped soils on hillslopes and entrenched river valleys (Agidi, 2018). The dominant parent materials for soils in the state are derived from Cretaceous sandstone, siltstone, shale, limestone and ironstone of the Precambrian

to Cambrian. The soil in Nasarawa is derived mainly from basement complex formation of sedimentary rocks. Lateritic crust occurs in extensive areas on soils on the basement complex, while hydromorphic soils are common along the Benue trough and flood plains of major rivers. Many of the major soil orders have been identified across the state and include: Ultisols, Alfisols, Entisols, Inceptisols, Vertisols and Oxisols (Agidi, 2018). Studies have shown the soil in Nasarawa to be suitable for the cultivation of rice (Kyat and Idoga, 2018).

The vegetation of Nasarawa State lies within the guinea savanna ecoregion of West Africa, which is a derivative of the tropical deciduous forest that existed centuries ago. Three distinct vegetation types can be seen in the state according to Tarfa et al. (2019) which are: Southern Guinea savannah and Northern Guinea Savanah. The region enjoys a rainy season that lasts for about 6 to 7 months (April-October) with peak rainfall in July. In the rainy season, the grasses and leaves are green and fresh, while in the dry season, they die through withering or bush fire (Agidi, 2018).

The fieldwork campaign, which underpins the results presented throughout the thesis, was undertaken at Olam rice farm, in Nasawara State (https://www.olamgroup.com/products-services/olam-global-agri/rice.html). Olam rice farm is located in Doma Local Government Area in Nasarawa state. Located in Rukubi village about 60 km from Doma, Olam farm sits on 10,000 hectares of land, although less than 5,000 hectares are currently cultivated (refer to Figure 3-1). Olam rice farm is currently the largest and most mechanized rice farm in Nigeria and Africa. The farm which started operation in 2012 is mechanised with high powered farm machines, some fully automated. With an irrigation water channel that allows water flow from the River Benue where the farm draws its water, rice production at Olam is not defined by seasons, providing the opportunity to grow rice during the dry season months.

3.1.1 Rice varieties

Development of the lowland NERICAs was initiated from cross-breeding specific African rice varieties, known for their resistance to rainfed lowland stresses, with popular – but susceptible – Asian rice varieties. The lowland NERICA development was facilitated through the cross-breeding approach with national programs in West and Central Africa to accelerate the selection process and achieve wide adaptability of the rainfed lowland NERICA(Gridley et al., 2002).

Sixty lowland NERICA varieties (NERICA-L), with a yield potential of 6 to 7 t/ha and excellent resistance to significant lowland stresses are available. Two of the varieties were selected for this research the include NERICA L34 and NERICA 61. Table 3-1 elaborates on the merits of the genetically enhanced species and the reason for adopting them.

Table 3-1: *Characteristics of NERICA varieties. NERICA is the combination of Asian and African species of rice* Source: (Gridley et al., 2002)

Characteristics of NERICA varieties	
1	Wide and droopy leaves that help to smother leaves in early growth.
2	Strong stems that can support heavy heads of grain.
3	More tillers with longer grain-bearing panicles than either parent and non-shattering grains.
4	Stems with secondary branches on their panicles that can carry up to 400 grains.
5	Early maturity, 30-50 days earlier than currently grown cultivars.
6	A good height that allows easy harvest of panicles.
7	Good tolerance to drought.
8	Resistance or tolerance to Africa's most serious pests and diseases - African rice gall midge, rice yellow mottle virus and blast (*Magnaporthe grisea*).
9	Tolerance to acidic soils but responsive to limited organic and inorganic fertilizers.

3.2 Overview of field campaigns

The fieldwork consisted of two dry season field campaigns in 2017-2018 and again in 2018/2019. The objective of the first field campaign was to alter the application of nitrogen and water applications in order to obtain variations in LAI, above ground biomass and plant height between subplots. A factorial design experiment was used, in which treatments of nitrogen and water were varied and field measurements of LAI, biomass, plant height and canopy reflectance were made. The objectives of the second field campaign conducted in 2018/2019 were to obtain yield measurements using the combined harvesters. During this campaign, yield was collected on the following season from a 1150ha portion from Olam farm (refer to section 3.2.2).

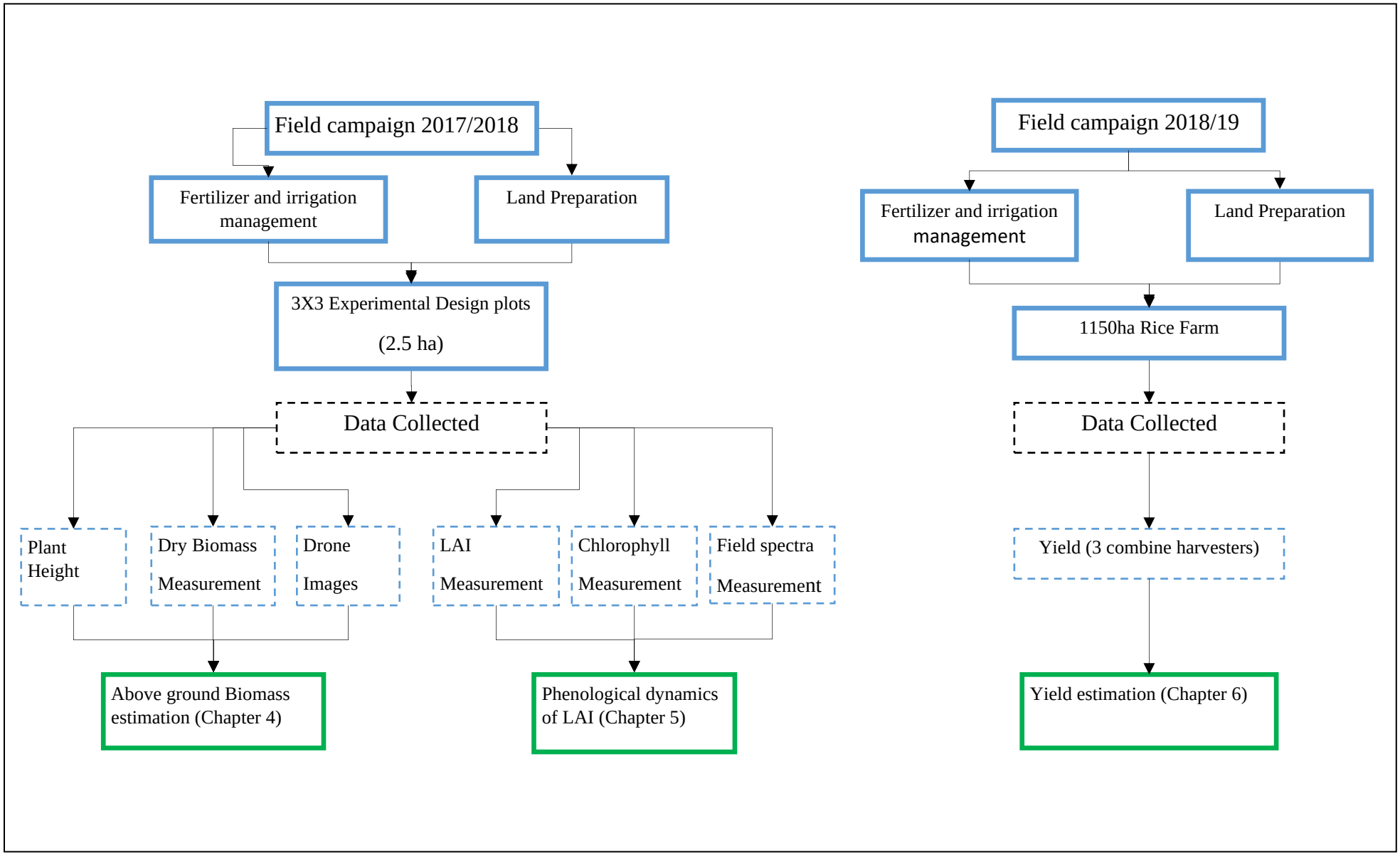

Figure 3-2: Methodological flowchart of field data collection for the thesis in 2017/18 and 2018/19

3.3 Field campaign 1 for 2017/18

To explore the use of different remote sensing products and platforms for evaluating the relative merits of the structural and multispectral information from drone cameras for estimating mid-late season above ground rice biomass and estimating the seasonal dynamics of rice Leaf Area Index, I developed and implemented rice production experiments on a portion of a commercial farm (Olam farm) in a single growing season (2017/18), which lasted for 117 days from 23/12/2017 to 17/04/2018 – the dry season in this part of Nigeria. Data collected from these experiments was used as the basis for analyses presented in Chapters 4 (Biomass) and 5 (LAI) of the thesis.

The field experiment composed of a randomized split-plot design where levels of irrigation and nitrogen fertilization were varied to generate spatial and temporal variability in crop chlorophyll content and leaf area index (LAI). The fully factorial design consisted of three irrigation regimes and three nitrogen (N) application rates. Treatments were arranged in three blocks (replications). Within each block there were three plots (77 m x 30 m), each containing three sub-plots (25 m x 30 m). A 2 m and 1 m wide alley was used to separate the plots and sub-plots; respectively. Irrigation regimes were controlled at the plot scale, whereas fertilisation regimes were controlled at the sub-plot (Figure 3-3). The study varied the application of nitrogen and water in order to obtain high variability between subplots.

Soil water potential was monitored at the Alternate Wetting and Severe Drying (AWSD) and Alternate Wetting and Moderate Drying (AWMD) plots using a 30 cm tensiometer (Irrometer Tensiometer). Tensiometers act like a clone of the root, allowing the soil moisture to interact with the instrument through the ceramic tip. Soil water tension outside of the instrument tries to remove the water from it, which creates a measurable tension inside the column(Wang et al., 2016a). Readings at 15–20 cm soil depth were recorded at 1200 h each day. When soil water potential reached the threshold (-10 KPa and -15 for AMWD and AWSD regimes; respectively), a flood with 5–10 cm water depth was applied. The amount of irrigation water was monitored with a flow meter (LXSG-50 Flowmeter, Shanghai Water Meter Manufacturing Factory, Shanghai, China) installed in the irrigation pipelines located between each of the blocks. Each plot was irrigated/ drained independently.

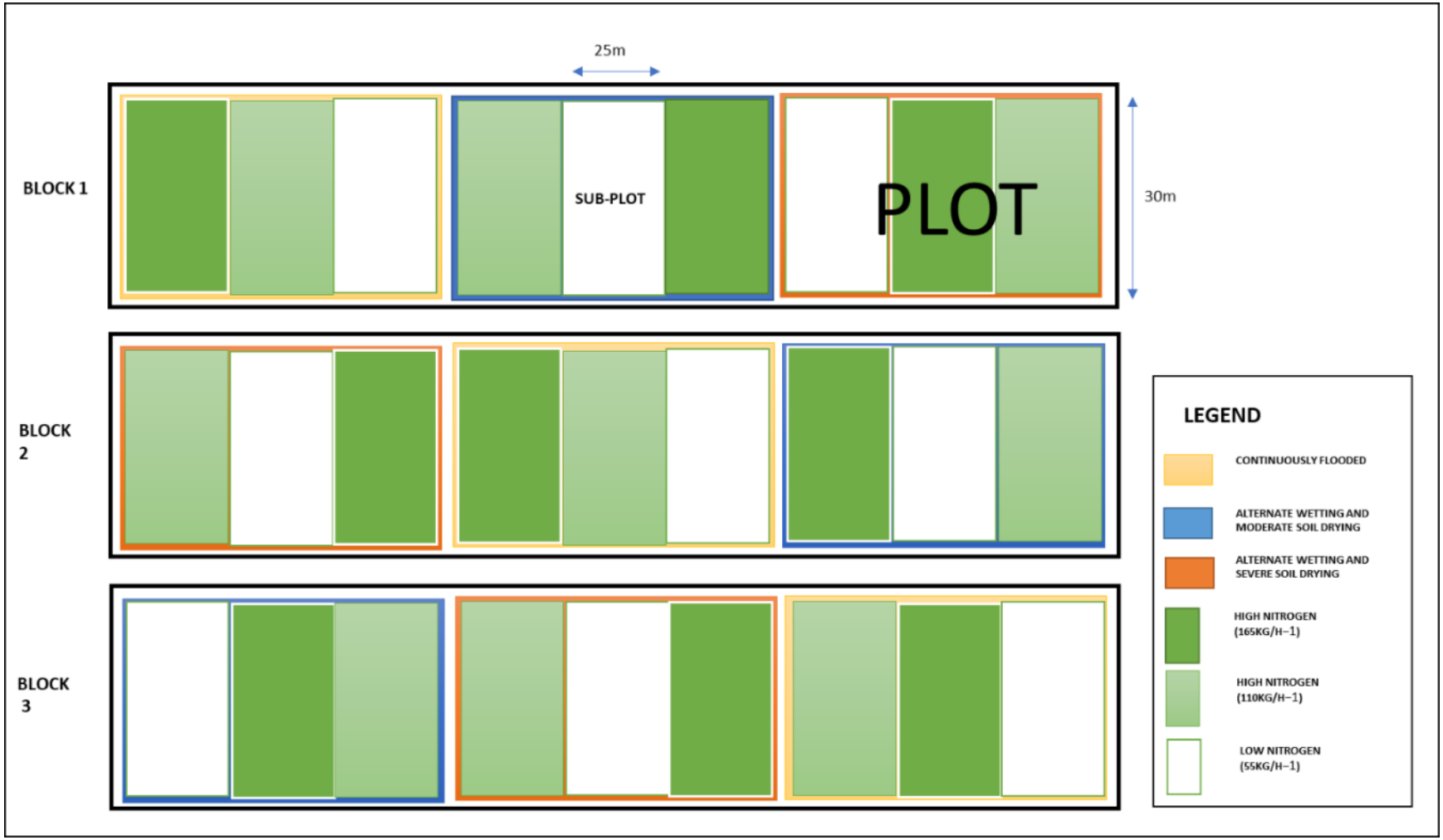

Figure 3-3: Experimental set-up for data collection. The site was divided into 3 blocks. Each block was divided into 3 plots with each plot having 3 sub-plots. The treatment for each plot were divided into continuous flooding, alternative wetting and moderate drying, and alternative wetting and severe drying. The nitrogen applications were classed as high nitrogen, normal nitrogen and low nitrogen.

Nitrogen treatments consisted of three N application rates (55, 110, and 165 kg ha^{-1}) (Figure 3-4) and represented low (LN), normal (NN), and high (HN) levels of Nitrogen respectively. Nitrogen as urea was applied at seeding stage (25 Days After Sowing (DAS)), early tillering (40 DAS) and at panicle initiation (55 DAS) (Refer to section 5.2.4). The proportion of N split across these three growth stages was 30%, 40% and 30%, respectively. This was achieved using the broadcast method of application. These application methods are in line with previous published literature on Nitrogen Applications in rice(Bijay-Singh and Singh, 2017; Liu et al., 2016).

Figure 3-4: The application of water and Nitrogen at the experimental plots during the 2017/18 season.

3.3.1 *In situ* measurements of leaf area index (LAI)

In situ LAI measurements were obtained for the validation of the LAI models generated for monitoring the phenological dynamics of irrigated rice in Chapter 6. Measurements were conducted from January 30th to March 26th 2018 (Table 3-2).

Table 3-2: Field Measurements and data used for calibration and verification of the retrieval scheme.

Phenology phase	Date	Days After Sowing (DAS)	Spectrometer data	LAI	Chl	Biomass	Plant height
Vegetative	30-01-18	37	✓	✓	✓		
	04-02-18	42	✓	✓	✓		
	14-02-18	52	✓	✓	✓		
	19-02-18	57	✓	✓	✓		
Reproductive	24-02-18	62	✓	✓	✓		
	06-03-18	72	✓	✓	✓		
	16-03-18	82				✓	✓
Ripening	26-03-18	92	✓	✓	✓	✓	✓

Leaf area index was measured indirectly using a LAI-2200 Canopy Analyzer (LI-COR, Lincoln, NE, USA). LAI-2200 Canopy Analyzer (LI-COR, Lincoln, NE, USA) consists of a fisheye lens (148° of field of view) divided into five concentric rings with zenith angles of θ: 7°, 23°; 38°, 53° and 63°. For measuring rice LAI, a 45° view cap was used to block off the operator from the instrument's field of view as well as part of influence of the direct light on the sensor (Stroppiana et al., 2006).

LAI 2200c consists of a console and provision for one of two optical sensors, with the wand serving as the data collection component of the LAI-2200C. The wand keypad includes two buttons that are used for logging data, switching between A and B readings, and power on/off the optical sensor. A sequence of readings was determined “on-the-fly” by using the A/B key on the wand keypad. LAI measurement was collected within each of the five 1 m^2 quadrats which were established within each sub-plot (25 x 30 m; Figure 3-5) (Figure 3-5). On each sampling date, one above-canopy and four below canopy measurements radiation measurements were collected (Figure 3-5) along a transect. All measurements were collected

either in the early morning or late afternoon to ensure diffuse lighting conditions (Fang et al., 2014).

Figure 3-5: LAI measurements showing the Wand and console collecting above and below LAI readings

Individual readings were subsequently imported into the instruments processing software (FV 2200 version 2.1.1), to compute LAI measurements.

The LAI-2200C relies upon four assumptions: all light is absorbed by the foliage, the foliage is randomly distributed, the foliage orientation is random, and the foliage elements are limited by the view ring. Although no real canopy conforms exactly to these assumptions due to offsetting errors (Reichenau et al., 2016), such as illumination conditions (direct versus diffuse illumination), variations in the instrument footprint, saturation of the optical signal in dense canopies (gap fraction saturates as LAI approaches to 5–6, (Gower et al., 1999), simplification of leaf optical properties (Hyer and Goetz, 2004), poor performances of some instruments (e.g. AccuPAR, LAI-2000) for short canopies (although LAI-2200C is better suited for short canopies), and the ability of the sampling scheme to capture canopy spatial heterogeneity (Weiss et al., 2004). However, with optimum LAI instrumentation performance has led to obtaining accurate LAI measurements using LAI-2000/2200 in rice (Fang et al., 2014; Stroppiana et al., 2006), thus, we adopted the approaches by the two studies for measuring LAI.

3.3.2 *In situ* chlorophyll measurements

Chlorophyll data were used to for parametrisation of the PROSAIL radiative transfer model used to estimate LAI using a combined radiative transfer and machine learning model (see chapter 6 and Figure 3.2).

Five plants within each of the five 1 m^2 quadrats per sub-plot (section 3.2.1) were selected for leaf chlorophyll content (Cab). (Figure 3-6). Chlorophyll was measured non-destructively using a chlorophyll content meter (atLEAF+, FT Green, Wilmington, DE), which measured relative leaf level chlorophyll content. Measurements were collected on the same days as LAI (section 3.2.2; Table 3-2).

The atLEAF+ sensor is a handheld device, which uses a logarithmic ratio between red and NIR light transmission (650, 900 nm). The red and NIR regions take advantage of the relationship between high absorption by chlorophyll of red radiant energy and high reflectance of near-infrared energy for healthy leaves and plant canopies. Several studies have used the atLEAF+ to monitor leaf chlorophyll content in crops (Novichonok et al., 2016; Padilla et al., 2018). Strong correlations have previously been observed between the atLEAF+ instrument and the more expensive SPAD 502 meter (Zhu et al., 2012). The atLEAF+ meter readings were subsequently converted to leaf chlorophyll content (mg/cm^2) using the manufacturers calibration equations.

3.3.3 Plant height

Plant height measurements were measured to evaluate the performance of RGB sensor structural plant height estimation (see section 3.4.2).

Manual measurements of plant height were undertaken using a 2 m rule (Table 3-2; Figure 3-6). Plant height was measured for five individuals plants within each of the five $1m^2$ quadrats as previously used to estimate LAI and chlorophyll content (Figure 3-6); (Watanabe et al., 2017).The five plant heights were subsequently averaged to produce a single mean plant height per sub-plot (n=27). As with LAI and Chl measurements, plant height measurements were conducted during the reproductive and ripening stages of rice growth. (Table 3-2)

Figure 3-6: Chlorophyll and Plant height measurement on the experimental plot in 2017/18 season

3.3.4 Rice biomass measurements

Biomass measurements were used to evaluate the estimation of the rice AGB from RGB and Multispectral cameras. Results from the estimation was used in chapter 4(Table 3-2; Figure 3-7).

Biomass measurements were obtained immediately after the collection of plant height on two collection dates in March (Table 3-2). On each sampling occasion, plants, within a 0.4 x 0.4 m area were destructively harvested from the sampling region of each sub-plot (Figure 3-7. The fresh biomass samples were cleaned, the roots clipped, and stem, leaves and ears were weighed prior to oven-drying at 80 $^{\circ}$C for 72 hrs or more depending on the moisture content of the plant. The samples were then weighed to ascertain dry biomass (kg/m^2).

Figure 3-7: Destructive biomass collection and drying from the 27 experimental plots

3.3.5 Canopy spectral measurements and processing

The purpose for obtaining spectral measurements was for building the PROSAIL radiative transfer model for the estimation of LAI dynamics in chapter 6.

Canopy reflectance was measured using an ASD Field spec Spectro-radiometer (400 to 2500 nm wavelength range), on dates to coincide with LAI and chlorophyll measurements (section 3.3.1, 3.3.2; Table 3-2) from the experimental plots in the 2017/18 dry season campaign. On each sampling occasion from the experimental plot, five spectral measurements were collected and averaged for each of the five 1 m^2 quadrats per subplot (Figure 3-8). The five averaged spectral reflectance per quadrat were averaged to account for the spectral measurement for each subplot. Measurements of a white spectralon panel (FSF, Edinburgh, United Kingdom) were also conducted through optimization measures to convert spectral measures of radiance to reflectance prior to the collection of field spectra on each subplot. Optimisation measures were taken to adjust the sensitivity of the instrument's detectors according to the specific illumination conditions at the time of measurement. For consistency, optimisation occurred at the start of measurement for each subplot. However, in some cases where sudden increase or decrease in sun illumination, optimisation occurred immediately. Additionally, when cloud passed over the experimental plots, we waited for a large enough clear spell before collecting measurements. A total of 69 soil spectral samples were obtained from the experimental plots. Log sheets were used to maintain accurate documentation of any changes in solar irradiance and to make notes of every filename and corresponding surfaces.

All spectra were collected between 10:00 and 14:00, to ensure that the canopy was exposed to full sunlight (Figure 3-8), using an 18-degree field of view fore optic, held 1 m above the plant canopy.

Reflectance values were calculated by post-processing using the FSF template ASD Raw Reflectance Data Template_Ver 03.XLT. The atmospheric water absorption bands (1350 – 1460 nm and 1790 – 1960 nm) were subsequently removed, as reflectance data were noisy in these regions (Appendix 1). Distinct wet and dry soil spectral reflectance measurements from the experimental plots were also during the field campaign.

To match the spectral bands of Sentinel-2, spectral data were resampled to match the Sentinel-2 MSI bands using the sensors Spectral Response Function (SRF) as defined within the freely available ARTMO (Automated Radiative Transfer Models Operator) software (Verrelst et al., 2012c).

Figure 3-8: Collection of spectral data using the ASD spectrometer and a white reflectance panel through optimization measures to convert spectral measures of radiance to reflectance

3.3.6 Drone Imagery and processing

A SenseFly eBee drone, equipped with the a SensFly RGB (S.O.D.A) camera and Multispectral Sequoia camera were utilised to capture images of the field experiment (apx 2.5ha (Figure 3-9, section 3.2.1) for the estimation of rice AGB during the reproductive (16th March) and ripening (26th March) stages of rice growth (Table 3-2). This was undertaken to in order to fulfil the research objective of determining the relative merits of the structural and multispectral information from cameras for estimating mid-late season above ground rice biomass from drone imagery. On each flight date the drone was flown twice using the same flight plan; first with the RGB camera mounted on board and then with the multispectral Sequoia camera. 125 images were acquired with the SODA camera while 500 images were acquired from the sequoia camera.

The commercially available fixed-wing eBee (SenseFly, Cheseaux-Losanne, Switzerland; Figure 3-12) is a hand-launched, autonomous flying drone with an electric motor-driven pusher propeller. It has a 110 cm (43.3 in) wingspan and a weight of about 1.1 kg (2.4lb), including RGB camera, inertial measuring unit, GPS and battery payloads. The maximum flight time

(with RGB camera) is approximately 59 min, which results in a coverage was of approximately 40 km^2 (15.4 mi^2) per flight when weather conditions are not above 30˚c.

The eBee plus flight plan managed through SenseFly's eMotion software and the flight monitored using an autonomous flight plan mirroring a 'lawnmower' design. The software requires initial parameterization to determine the flight plan, take-off and landing point and to monitor the environmental conditions and its effect on the UAV. The software then automatically calculates the number of flight lines needed to cover the area of interest based on the flight height, with flight height was set to 120m. Similar flight plans were used for both cameras to ensure consistency and repeatability.

Figure 3-9: The ebee plus drone in preparation for take-off. The LED green solid green light indicates ready to take-off'. B. The researcher monitoring of the flight plan with a laptop of the experimental field along with the field experiment team.

Ground Control Points (GCPs, 10 in total), in the form of black and white checked 1m by 1m targets, were permanently installed and evenly distributed across the field site (Figure 3-10). The centre of GCP coordinates were recorded by a Trimble Geo 7X GPS (www.trimble.com).

Figure 3-10: Experimental plots showing the location of targets spread across the field.

3.3.6.1. SODA Sensor Optimised for Drone Applications RGB Camera

The Ebee plus drone is equipped with a senseFly SODA camera (senseFly SA, Cheseaux-sur-Lausanne, Switzerland) which is designed specifically for visualisation (Table 3-3). The small, ultra-light, and fully configurable camera has built-in dust and shock protection features a 20-megapixel RGB sensor with a 1-inch sensor.

Table 3-3: Technical specifications of the senseFly's S.O.D.A. Digital Camera

Parameter	Value
Optical sensor size	116.2 mm^2
Image size	5742*3648 pixel
Focal length	10.6 mm
Pixel size	3 cm

Proprietary Pix4D software was used to generate 3D point clouds and orthomosaics using all 125 images collected for a specific day for generating plant height and discrete spectral bands. A standard three-step semi-automated processing workflow was used (Figure 3-11). For correct scale, orientation and geographic location of generated products, GCPs were incorporated by identifying where they each occurred.

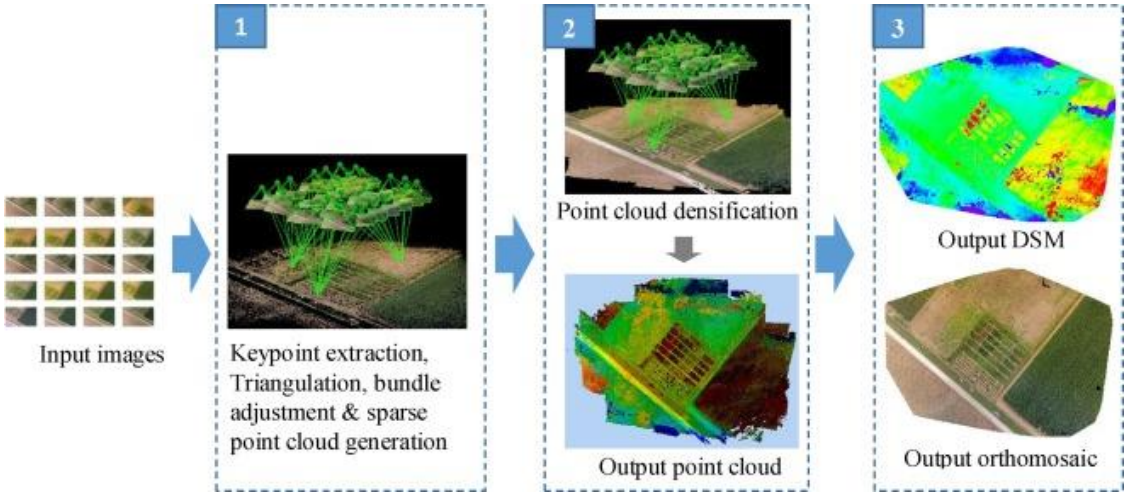

Figure 3-11: Pix4D processing workflow: 1 Initial processing of key point extraction, triangulation, bundle adjustment and sparse point cloud generation; 2. Point cloud densification; 3. Digital surface model (DSM) and orthomosaic generation. Source: Malambo et al., 2018

Pix4d undistorts each of the original images, correcting the lens distortion of the camera based on the camera model (S.O.D.A camera). After a first pass to search for automatic feature tie-points through matching pairs of images using aerial grid, the manual ground control points (GCPs) were used to anchor the images against the ten ground references, which were measured by Trimble Geo 7XGPS. For the initial processing of the images, the standard calibration method from Pix4d was applied to the images (Table 3-4). The automatic tie points and GCPs are then used in the bundle block adjustment before the density point cloud is constructed. In Pix4D, the bundle block adjustment is calculated using the relationship between overlapping images, keypoints, GCPs, and the specific internal camera parameters and adjustments are applied to images within each specific block. The final processing steps were the generation of the 3D textured mesh, surface models including the digital surface model (DSM) and digital terrain model (DTM), and the orthomosaic. The orthomosaic is obtained from the DSM and corrected for perspective, with the value of each pixel calculated as an average of the pixels in the corresponding images (Appendix 2).

Table 3-4: Three step work flow for processing the S.O.D.A camera images from Pix4d software

1. Initial processing	2. Point cloud densification	3.DSM & orthomosaic generation
Keypoint image scale: Full	Point density: Optimal	Ground resolution: Automatic
Calibration method: Standard	Image scale: ½ of original	Use noise filtering: Yes
		Surface smoothing: Sharp

3.3.6.2. Sequoia Multispectral Sensor

Multispectral imagery was collected with a Parrot Sequoia camera, which captures four discrete spectral bands: green (wavelength = 550nm, bandwidth = 4 0nm), red (660 nm, 40 nm, red-edge (735nm, 10nm) and near-infrared (790nm, 40nm) at a resolution of 11 cm. The parrot sequoia multispectral sensor is a self-calibrating system that incorporates an integrated irradiance sensor using the sun angle correction radiometric calibration technique. The sun angle correction radiometric calibration technique was possible to apply to the eBee drone because the orientation between the camera and the sunshine sensor is fixed and known. A grey balance radiometric calibration target (also called calibrated reflectance panel) was used to calibrate the camera before each flight. The sunshine sensor allows sunlight information to be logged and captured throughout the flight. Utilizing these irradiance values, the system automatically calibrates all output images along with assigning geolocation information from the Parrot Sequoia's onboard GPS, IMU, and Magnetometer. Because the sunshine sensor records information in real time during each flight, Sequoia-derived reflectance values vary relatively insignificantly with the weather conditions(Deng et al., 2018).

During the initial processing stage, the calibrated images and the 500 images from the four spectral bands were imported in Pix4d for further processing. The sequoia camera is equipped with four multispectral sensors, and the aerial triangulation of each of the sensors are processed at the same time, accounting for each sensor's lens distortion. Thereafter, a reconstruction of the surface was produced via a dense point cloud using multi-view stereo matching (Deng et al., 2018). Finally, individual orthorectified images were combined into a 4-band multispectral orthomosaic image to obtain the UAV orthophoto of the entire area. Due to the fact that each spectral band was processed considering its own characteristics, band-to-band alignment was achieved.

3.4 Field campaign 2 2018/19: Yield monitoring

Yield data collection were conducted across Olam farm in Nasarawa during the 2018/19 irrigation dry season farming. The objective of this second field campaign was to obtain yield data with spatial co-ordinates from a combined yield harvester. Data collected during this field campaign included were used to evaluate the yield models generated from Sentinel-2 data.

Forty-eight plots were created across the entire farm (~ 1150 ha) which ranges in size from 20ha to 35ha. The farm consists of NERICA Faro 61 and NERICA Faro 44 varieties of lowland

aerobic rice due to their resilience to drought and weed infestations. Both varieties have early maturing yield (<110 – 120 days) and are commonly used for irrigation rice production in Nigeria.

Prior to sowing, land preparation was conducted. The first step for land preparation involved burn stubbing. Burn stubbing involves intentionally setting fire to the straw stubble that remains after grains have been harvested from prior season(Kumar et al., 2015). Burn stubbing provides rapid and complete residue removal, especially for those practicing multiple cropping (Bijay-Singh et al., 2008; Bijay-Singh and Singh, 2017). Although studies have argued that this approach is important for clearing residual rice straw due to simplicity and economic implication compared to other approaches (Chawala and Sandhu, 2020), open burn stubbing residues also contributes to global warming through emissions of greenhouse gases (GHGs) such as carbon dioxide (CO2), methane (CH4), and nitrous oxide (N_2O) (Gadde et al., 2009; Gupta et al., 2004). Notwithstanding this, strategic burning of stubbles, based on sound agronomic principles, may be a valid option(Kumar et al., 2015). Burn stubbing provides rapid and complete residue removal, especially for those practicing multiple cropping (Bijay-Singh et al., 2008; Bijay-Singh and Singh, 2017). Thereafter, tillage of the soil was prepared by mechanical agitation using ploughing, heavy disking and harrowing methods. The importance of the implementation of tillage for improving soils response to fertilizer and for improving yield has been shown in literature(Ahmed et al., 2020). Afterwards, last stage of land preparation was the development of cross bunds. For each of the 48 plots, 50cm by 30 cm bunds were constructed. These bunds were compacted and properly sealed to prevent water seepage through cracks and holes. The final stage of land preparation before sowing was soil rolling. Soil rolling was conducted to smoothen the field to create better water reception from the surrounding soil layers and for faster germination.

For irrigation during the dry season, dams were constructed at strategic locations on the farm to cater for the supply of water during the growing season. Water was drenched from River Benue (apx 5km from the farm) and stored in the dams. Border irrigation was selected as the irrigation method for three reasons. Border irrigation are suited to the larger mechanized farms, suitable slope (>2%) and homogenous loam or clay soils with medium infiltration rates(Rai et al., 2017). The farm met the above criteria, hence the adoption of the border irrigation regime.

Next stage involved the sowing of rice on the field. Two rice varieties were sown on the field. The NERICA Faro 61 and NERICA Faro 44 varieties were cultivated on the farm due to their

ability to grow in the event of drought and weed infestation. These varieties both have early maturing (<110-120 days) and have been successfully used for irrigation farming(Nguezet et al., 2013). Seed rate was set at 40kg per hectare and were applied using a polish m-18 dromader plane.

After sowing, three applications of herbicides were administered during the vegetative stage to prevent competition of nutrients from weeds. Bispyribac sodium was applied 15 DAS, Weed infestation decreased the rice yield by 75.2% (Jabran et al., 2012). The application of cyhalofop butyl herbicide was done 30 DAS, while (Antralina et al., 2015; Anwar et al., 2013). To manage best and diseases, pesticide was applied at the beginning of reproductive stage (60-65 DAS) via the application of fungicide.

3.4.1 Yield measurements

The purpose of obtaining yield data was for model development and testing evaluate baseline Sentinel-2 for estimating rice yield (Table 3-5; Figure 3-9). The results were to address the research objective of ascertaining the influence of Sentinel-2 baseline data for accurately predicting Irrigated dry season rice yield across scales

High resolution point yield data were obtained from 3 combine harvesters equipped with differential GPS (DGPS) receivers. Data were obtained over a period of 10 days (18/03/19 – 28/13/19) due to the size of harvesting area. Prior to collection of the yield data from the combine harvesters, each combine harvester was calibrated based on recommendations from CASE IH 9230 manual guide(Case IH, 2018).

Table 3-5: Sentinel-2 and yield harvesting dates for predicting yield during the 2018/19 rice irrigated dry season.

Phenophase	Date	Days After Sowing (DAS)	Sentinel-2 MSI imagery	Harvest
Vegetative	21/12/2018	35	✓	
	26/12/2018	40	✓	
	5/01/2019	50	✓	
	20/01/2019	55	✓	
Reproductive	14/02/2019	80	✓	
	19/02/2019	85	✓	
Ripening	11/03/2019	105	✓	

Harvest	18-28/03/2019	112- 122	✓

Multiple calibration processing was deemed necessary prior to harvest for precise yield data collection. These steps are important to generate accurate yield data from the combine harvesters. Firstly, the mass-flow sensor vibration was calibrated. This was to ensure that the proper head was attached to each of the combined harvesters, that the combined harvester was empty of rice grain and that the combine harvester was running at full revolutions per minute (RPM). The temperature calibration was necessary to ensure accurate grain moisture estimates from the moisture sensor in the clean grain elevator. This was done when all the combine harvesters were sitting in the shaded garage for at least 3 – 5 hours. Thereafter, a thermometer was used to estimate the ambient air temperature. During harvest, calibration was equally conducted. Each combine harvester was regularly monitored to ensure the DGPS signals were not lost. Re-calibration was considered necessary if more than a 5 percent difference in weight calibrations errors or an increase in temperature greater than 10 degrees. In the event of broken paddles or loose tightening elevator chain, re-calibration was necessary.

Figure 3-12: CASE IH 9230 combined harvester harvesting rice during the 2018/19 irrigated rice dry season farming

3.4.2 Sentinel-2 Multi-Spectral Imager

Sentinel-2 data was used for the study because of the potential to acquire high spatial resolution images frequently over the phenological growing stage of rice. Sentinel -2 images were acquired for dates spanning both field campaigns. Sentinel-2 data was used for analysis in chapter 5 (LAI retrieval) and chapter 6 (yield estimation).

Sentinel-2 is a European Space Agency (ESA) and European Commission satellite launched under the Copernicus joint initiative programme. The Sentinel-2 mission comprises of two satellites, launched into orbit in 2015 (Sentinel-2A) and 2017 (Sentinel-2B), respectively. The combination of both satellites provides images every five days. Each sensor carries a Multi-Spectral Imager (MSI) which has a swath width of 290 km and provides data in 13 spectral bands spanning from the visible and near-infrared region to the shortwave infrared region, including four bands at 10 m, six bands at 20m and three bands at 60m spatial resolution (Drusch et al., 2012). Sentinel-2 also incorporates three bands in the red-edge region, centred at 705 nm, 740 nm and 783 n;m respectively. Sentinel-2 MSI images were obtained for free from the Copernicus Open Access Hub web portal (https://scihub.copernicus.eu/).

For the 2017-2018 season, Sen2Cor Level-2A processor was used to correct single date Sentinel-2 Level-1C products (digital number image) for the atmospheric effects and generating Level-2A surface reflectance product using SNAP (Sentinel Application Platform) Toolbox environment. The SNAP toolbox processor is designed to estimate the biophysical and biochemical properties for retrieval of LAI, canopy water content, fraction of photosynthetically active radiation absorbed by the green elements of the canopy and fraction of vegetation cover (Weiss and Baret, 2016). The principles governing the retrieval of the properties are also based on the PROSAIL radiative transfer model adopted for this study (see section 5.2.6.4). The Artificial Neural Network (ANN) is selected as the non-parametric model for model inversion. Based on the ANN model (Weiss and Baret, 2016), LAI values were retrieved from pure pixels (pixels found in each experimental subplot, 30 x 25 m) in each of the seven Sentinel-2 images used for the study (Table 3-2, Figure 3-3. At least one pure pixel was used in determining the spectral reflectance value from the experimental subplots (n=27).

Sentinel-2 images obtained for monitoring the 2018-2019 1150ha rice farm were already atmospherically and radiometrically corrected, hence there was no need to replicate the steps adopted for the previous season. Eight Level-2A Sentinel-2 cloud free images were acquired during the vegetative, reproductive and ripening phases of irrigated rice growth (Table 3-3). Further details on the analysis of the Sentinel-2 images for the generation of yield models are found in section 6.2.4.

Chapter 4 Exploiting the centimetre resolution of drone-mounted sensors for estimating mid-late season above ground biomass in rice

Abstract

Above-ground biomass (AGB) is an important indicator for improving agronomic management efficiency and yield monitoring in crops. In particular, rice AGB during the mid(reproductive) and late (ripening) phases are responsible for the panicles per given area; the number of spikelets or grains per panicle; the percentage of filled kernels and grains; and the weight of each grain. Consequently, proper monitoring of rice AGB, particularly during the mid to late growing phases are important for accurate estimation of rice yield. To this end, monitoring AGB at centimetre scale have become implementable by the use of sensors on-board Unmanned Aerial Vehicles (UAVs) or drones. RGB sensors with the capability of generating plant height estimations from digital surface models provide a viable option for monitoring rice AGB. The advancement in miniature Multi-Spectral Imager (MSI) sensors capable of generating vegetation indices (VIs) and texture metrics (TM) also provides the opportunity to ascertain the capability of the sensor to estimate rice AGB, particularly during the growth phases. The study compares the potential and relative merits of using drone-mounted consumer-grade RGB imagery and/ or scientific-grade multispectral imagery for estimating rice mid-late season above-ground biomass. Plant height estimates, generated from the RGB sensor were compared with in-situ measurements of biomass using a simple linear regression (SLM) model. On the other hand, VIs, TM and their combination were accessed using the Random Forest model for estimating rice AGB. We also accessed the combination of both sensors for estimating rice AGB. Results testing model quality statistically showed plant height (R^2 = 0.72; RMSE = 1.07 t/ha; MAE = 0.93 t/ha) estimates from the RGB camera performed better than VIs (R^2 = 0.59; RMSE = 1.31 t/ha; MAE = 1.06 t/ha), TM (R^2 = 0.43; RMSE = 1.58 t/ha; MAE = 1.22 t/ha) and the combination of VIs and TM when estimating rice AGB at the mid to late growing stages. When combining plant height and VIs from both cameras to estimate AGB, results suggest that the combination using random forest models improve the estimation of rice AGB. The combination of TM, VIs and PH estimates produced the most statistically accurate estimates (R^2 = 0.74; RMSE = 1.02 t/ha; MAE = 0.82 t/ha). Our findings suggest that the Plant height estimates from the RGB sensor produce a more accurate estimation of AGB compared to the MSI camera. However, the most accurate estimations are seen when both sensors are combined for the estimation of rice AGB at the mid to late growth phase.

Keywords: Drone, Above-ground biomass, sensors, plant height, texture metrics, vegetation indices, rice

4.1 Introduction

Rice (*Oryza sativa,* Asian rice*; Oryza glaberrima,* African rice) is one of the major staple crops of the world and is responsible for the dietary needs of over 700 million people in sub-Saharan Africa (Ndjiondjop et al., 2010). The ability to monitor yield and yield indicators of rice is imperative towards maximizing yield potential and catering to the growing population in sub-

Saharan Africa(Senthilkumar et al., 2018). Above-ground biomass (AGB), one of the indicators of yield, is closely related to crop nutrition status and yield (Fu et al., 2014). Four factors are responsible for understanding yield patterns in rice. They include the number of panicles per given area; the number of spikelets or grains per panicle; the percentage of filled kernels and grains; and the weight of each grain. These factors have a strong relationship with yield and are determined during the mid (reproductive stage) and late (ripening stage) growing stages (Fageria, 2007; Laza et al., 2004). The ability to accurately estimate AGB during the reproductive and ripening stages of rice growth is of particular importance for estimating rice yields (Chen et al., 2019; Jeng et al., 2006). Destructive sampling is commonly used approach to measure rice biomass (Mosleh et al., 2015a). However, destructive sampling is time-consuming, often inaccurate, and requires labour-intensive ground-based visits and aren't spatially explicit (Kuenzer and Knauer, 2013).

As an alternative, remote sensing has shown huge potential to estimate AGB across extensive areas using a diversity of sensors, techniques and at a variety of spatial and temporal resolutions (Ali et al., 2015; Chao et al., 2019; Gitelson et al., 2003b; Kumar and Mutanga, 2017). A remote sensing approach for monitoring AGB in crops are the use of proximal sensors for the estimation of crop AGB at field scale using handheld hyperspectral sensors (Fu et al., 2014; Gnyp et al., 2014; Thenkabail et al., 2000) and multispectral radiometers (Casanova et al., 1998; Prabhakara et al., 2015). However, the proximal sensor approach are limited in the sense that they cannot be applied efficiently over large areas. More recently, onboard Manned Aerial Vehicles using LiDAR (light detection and ranging) have been adopted for the estimation of biomass using plant height.(W. Li et al., 2015; Tilly et al., 2014). Though LiDAR can also obtain high estimation accuracy, those data sources are often expensive and need extensive experience in data processing (Mulla, 2013). Satellite imagery on the other hand have been utilised to estimate biomass over large areas(Dong et al., 2017; Han et al., 2017; Meng et al., 2013), however, they are often constrained by insufficient temporal-spatial resolution.

Over the last decade, Unmanned Aerial Vehicles (UAVs), also referred to as drones have increasingly become a tool for precision agriculture (Deng et al., 2018; Freeman and Freeland, 2015; Jay et al., 2017). The flexibility of drone platforms is such that data can be collected frequently throughout the growing season, and when cloud cover in the upper atmosphere may hinder the collection of satellite data (Yue et al., 2019), making it particularly suitable for agricultural applications that require crop data to be captured at multiple points within the growing season. Drone imagery derived from a range of different sensors, has shown great

potential for rice biomass estimation (Cen et al., 2019; Jiang et al., 2019; Yang et al., 2019; Zheng et al., 2019). From a structural standpoint, plant height information can be used to estimate rice AGB especially for high canopy densities (Cen et al., 2019; Jiang et al., 2019), as plant height is closely associated with plant stability and yield potential (Herrero-Huerta et al., 2020). Similarly, the emergence of sophisticated software equipped with structure for motion approaches (i.e. Pix4D, Switzerland) has enabled efficient creation of 3D point clouds and super high detail orthophotos provides the opportunity to estimate accurately from the structural crop properties primarily derived from consumer-grade RGB sensors(Souza et al., 2017). Although spectral information, which has shown to have a positive relationship for the estimation of AGB in crops(Liu et al., 2019; Marshall and Thenkabail, 2015), spectral data obtained from RGB sensors are often uncalibrated and require complex radiometric processes if the data are to be used to track changes in crop status over time. (Iqbal et al., 2018; O'Connor et al., 2017).

Multispectral sensors have now become sufficiently miniaturised over the last decade, allowing the sensors to be mounted on board drones, which open up the possibility to make use of spectral information. The addition of spectral bands in the near-infrared region and red-edge can provide additional information on the growth and vigour of plants. There are two approaches commonly adopted for estimating AGB from drone-mounted multispectral sensors: (i) the calculation of vegetation indices (VIs) from two or more spectral bands provides partially analytical gauges on vegetation activity, capable of identifying the phenological variations of rice and other green plants across scales and (ii) texture analysis (TA), which measures of variability in pixel values among neighbouring pixels for a defined analysis window.

Whilst vegetation indices have been used to estimate rice AGB (Duan et al., 2019; Huang et al., 2015; Jiang et al., 2019; Zheng et al., 2019), they often suffer from the saturation effects during the heading and ripening stages of rice growth as biomass is mixed with panicles and stems as opposed to panicles during the vegetative stage (Cheng et al., 2017; Zheng et al., 2019). For instance, Normalized Difference Vegetation Index (NDVI) underestimates high biomass density due to this saturation effect (Fu et al., 2014; Kumar and Mutanga, 2017). However other VIs generated from the near infrared and red edge bands have presented more accurate estimations of rice AGB during the late growing stages. Zheng et al. (2019) demonstrated that the optimised soil adjusted vegetation index (OSAVI) exhibited a significantly positive relation with rice AGB during the late growing stage (R^2 = 0.65)

compared to NDVI, green normalised vegetation index (GNDVI) and Modified triangular vegetation index 2 (MTVI 2). VIs generated from the red-edge and the near-infrared region have performed more favourably for the estimation of mid-late season AGB. For example, Maimaitijiang et al. (2017) examined the performance of VIs for estimating AGB 70 days after sowing and identified the Near Difference Red Edge Index (NDRE) to have the strongest relationship with AGB compared to NDVI and GNDVI.

The calculation of textural metrics, which characterise the spatial variation of reflectance values as a function of scale (i.e. texture analysis), from spectral reflectance data, has recently emerged as an additional approach for the estimation of crop AGB from optical imagery (Liu et al., 2019). Textural approaches potentially provide additional insights into the plant canopy (Lu and Batistella, 2005) as studies have proved that texture to a better predictor of biomass than spectral variables (Lu and Batistella, 2005; Sarker and Nichol, 2011). Whilst textural metrics can also be calculated from consumer-grade RGB sensors, the uncalibrated nature of the spectral information mean that they are limited for monitoring change over time (Lu et al., 2019).

Several attempts have been made to improve the estimation of rice AGB from the structural and spectral characteristics from drone sensors (Bendig et al., 2015; Cen et al., 2019; Liu et al., 2019; Lu et al., 2019; Zheng et al., 2019). Liu et al. (2019) combined texture metrics and vegetation indices for the estimation of oilseed AGB. Results demonstrated that the incorporation of texture metrics to VIs provided more accurate estimations of AGB in winter oilseed rape than the models based solely on VIs. However, the combination of structural properties from plant heigh estimates were not accounted for in the study. Furthermore, Cen et al. (2019) combined plant height data from an RGB sensor and VIs from an MSI sensor to improve the estimation of rice. Despite Cen et al. (2019) improvement in the estimation of rice AGB, emphasis on quantifying the significance of the combination of the sensors has not been explicitly identified during the reproductive and ripening growing stages of biomass, as these stages serve as critical yield indicators for the estimation of yield. Also, despite their potential and reduced cost of MSI sensors, they still remain relatively expensive for farmers and agronomist especially in developing countries. It's important to know whether that additional cost brings with its greater predictive accuracy of AGB at the points in time when farmers need to know those measures most. Therefore, this study focuses on quantifying the relative merits of consumer-grade RGB sensor's to more expensive multispectral sensors, for estimating rice mid-late season AGB.

The overall aim of this paper is to compare the potential and relative merits of using drone-mounted consumer-grade RGB imagery and/ or scientific grade multispectral imagery for estimating rice mid-late season above ground biomass. Specifically, using data during the mid-late growing seasons, we will (i) determine the extent to which estimates of plant height, derived from a RGB sensor can estimate rice AGB, (ii) determine the performance of spectral information derived from a multispectral sensor for estimating rice AGB; (iii) ascertain whether the predictive performance of plant height data is improved with the addition of spectral information obtained from a multi-spectral sensor.

4.2 Materials and Methods

4.2.1 Study Area and Experimental Design

To explore the use of different remote sensing sensors for monitoring rice AGB, biomass measurement from the field were obtained and implemented on a rice farm (Olam farm) in a single growing season (2017/18) (Figure 4-1). The experiment was conducted during the dry season from December 2017 to April 2018, during which time the temperature ranged from 17°C in December to almost 40°C in late March. The experiment used a factorial design and consisted of three irrigation regimes; three nitrogen (N) application rates applied across three repeated blocks. Irrigation consisted of (i) alternate wetting and moderate soil drying, (ii) alternate wetting and severe soil drying and (iii) continuously flooded. Nitrogen application rates were 55 kg ha^{-1}, 110 kg ha^{-1}, and 165 kg ha^{-1}, representing low, normal and high amounts of nitrogen respectively. Nitrogen, in the form of urea was applied at the seedling stage, early tillering (approx. 40 Days After Sowing (DAS) and at panicle initiation (i.e. on the first appearance of the differentiated apex) until maturity as per conventional farming practice. Each of the three replicated blocks contained three plots (77 m x 30 m). Each plot contained three subplots (30 x 25 m) giving a total of 27 sampled subplots covering a range of growth conditions (Figure 4-1c). The NERICA 61 (Faro 34) variety of rice, which is best suited for

lowland irrigation farming, was planted in each plot in December 2017 and harvested in April 2018.

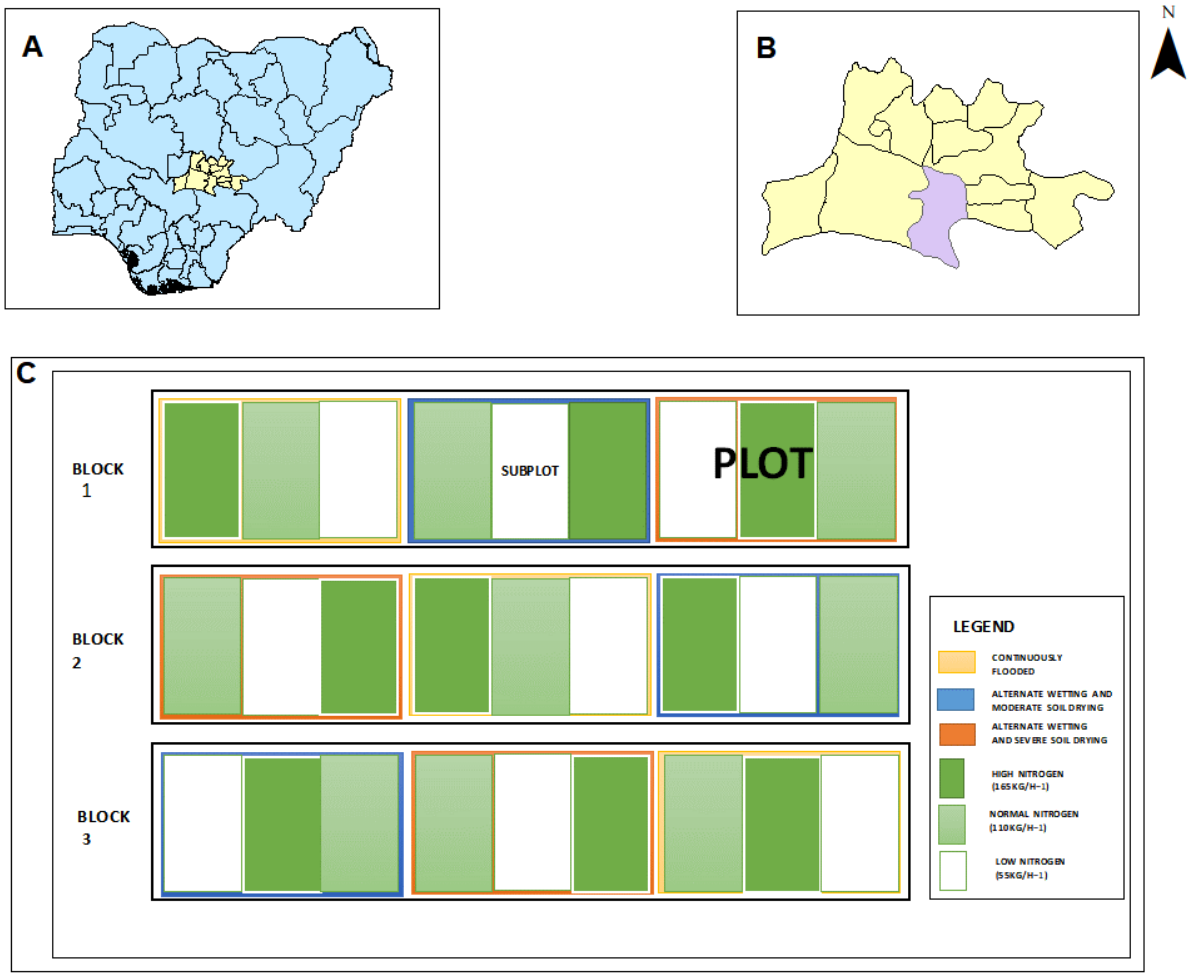

Figure 4-1: A. Map of Nigeria highlighting Nasarawa state. B. Nasarawa stats with local government Areas. C. Experimental set-up for data collection. The site was divided into 3 blocks. Each block was divided into 3 plots with each plot having 3 subplots. The treatment for each plot were divided into continuous flooding, alternative wetting and moderate drying and alternative wetting and severe drying. The nitrogen applications were classed as high nitrogen, normal nitrogen and low nitrogen.

4.2.2 Field Measurements

4.2.2.1.Plant height

Plant height was measured in five 1 x 1 m quadrats located within each of the 27 subplots immediately prior to destructive biomass sampling (Table 4-1). Within each quadrat, manual measurements of plant height were undertaken using a 2 m rule. Mean plant height per subplot was subsequently determined by averaging the height of the five individuals plants obtained from each of the 1 x 1m quadrants(Watanabe et al., 2017).The plant heights method were subsequently replicated on the other experimental subplots. (n=27).

4.2.2.2. Above ground biomass

Biomass measurements were obtained immediately after collection of plant height on data collection days as shown in Table 1. On each sampling occasion, a destructive sample of 0.4 × 0.4 m above-ground biomass was collected from each of the subplots. Plants within the 0.4 x 0.4m of rice plants were randomly harvested from the sampling region of each subplot (Figure 4-1). The fresh biomass samples were cleaned, the roots clipped, and stem, leaves and ears were weighed prior to oven-drying at 80°C for around 72 hrs, depending on the moisture content in the plant. After the drying of the sampled mass was obtained, samples were weighed to ascertain dry biomass.

Table 4-1: Acquisition dates of data collection for rice Above Biomass Estimation

Date	Plant Height Measurement	Biomass Harvest	UAV Flight Date	Sowing	Growing Stage
23-12-2017				✓	Vegetative Stage
16-03-2018	✓	✓	✓		Reproductive Stage
26-03- 2018	✓	✓	✓		Ripening Stage

4.2.3. Acquisition and pre-processing of drone images

Figure 4-2 presents a flow chart depicting the analytical approach taken in this study. An autonomous flight plan mirroring a 'lawnmower' design was constructed using the proprietary drone software, Emotion to determine the flight plan, take-off and landing point and to monitor the environmental conditions and their effect on the drone All images were obtained at a flight altitude of 120 m with afront overlap of 70% and side overlap of 60% to ensure image redundancy for post-processing. Ten Ground Control Points (GCPs), in the form of black and white checked 1 m by 1 m targets, were permanently installed and evenly distributed across the field site. The GCP coordinates were recorded by a Trimble Geo 7X GPS (www.trimble.com). On each flight date the drone was flown twice using the same flight plan; first with the RGB sensor mounted on board and then with the multispectral Sequoia sensor. A total of 125 images were acquired with the S.O.D.A sensor while 500 images were acquired from the sequoia sensor for flight.

Proprietary Pix4D software was used to generate 3D point clouds and orthomosaics using all images from the RGB sensor. Pix4d undistorts each of the original images, correcting the lens distortion of the sensor based on the sensor model (SODA sensor). After a first pass to search

for automatic feature tie-points through matching pairs of images using aerial grid, the manual ground control points (GCPs) were identified in the imagery and used to anchor the images against the ten ground references.

The automatic tie points and GCPs are then used in the bundle block adjustment before the density point cloud is constructed. In Pix4D, the bundle block adjustment is calculated using the relationship between overlapping images, keypoints, and GCPs, and the specific internal camera parameters and adjustments are applied to images within each specific block. The final processing steps were the generation of the 3D textured mesh, surface models including the digital surface model (DSM), digital terrain model (DTM), and the orthomosaic (Malambo et al., 2018). The orthomosaic is obtained from the DSM and corrected for perspective, with the value of each pixel calculated as an average of the pixels in the corresponding original images.

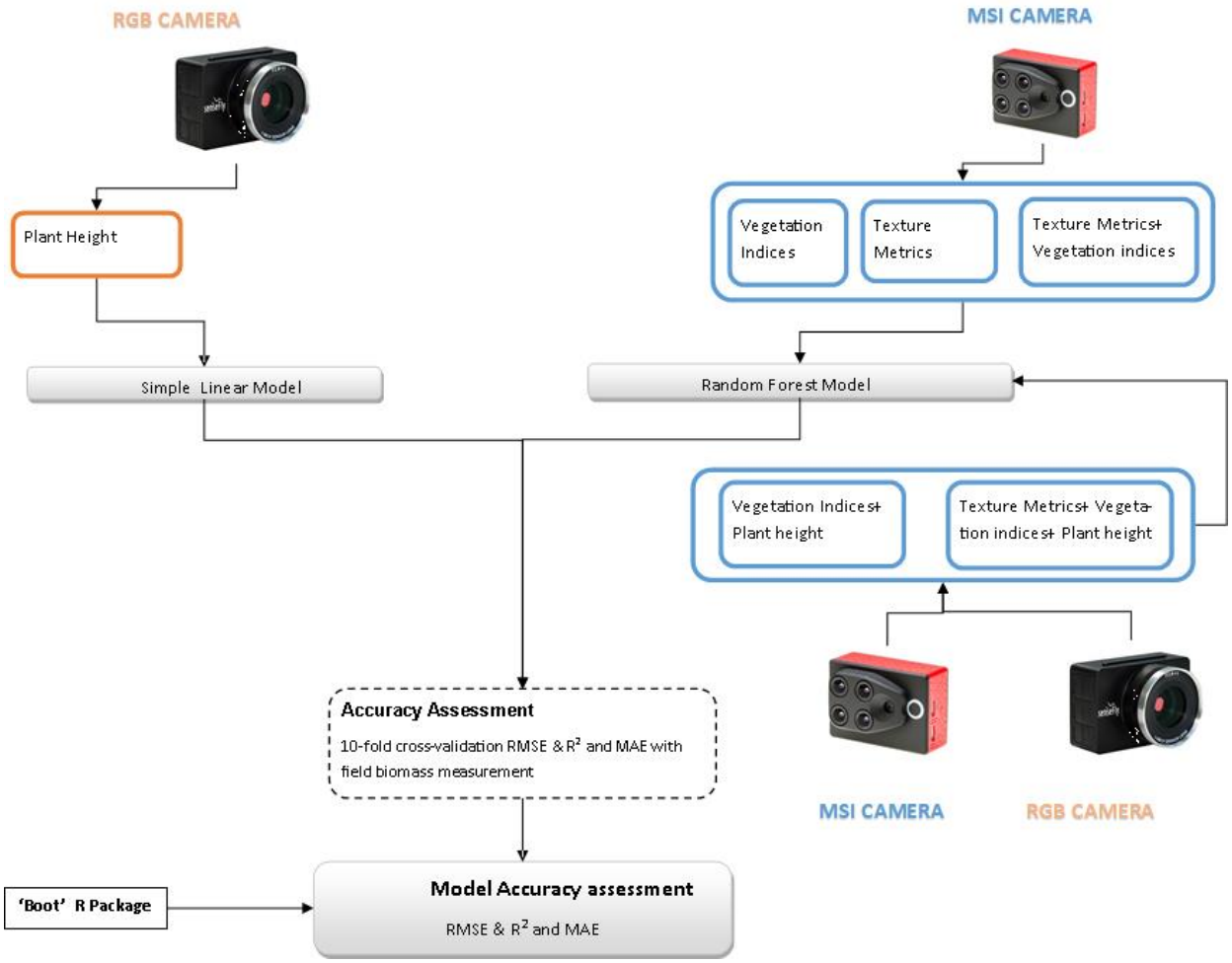

Figure 4-2: Overview of the approach used to estimate rice Above ground biomass using the RGB and Multispectral sensors on-board the Ebee plus drone.

The sequoia sensor captures four discrete spectral bands: (wavelength = 550nm, bandwidth = 4 0nm), red (660 nm, 40 nm, red-edge (735nm, 10nm) and near-infrared (790nm, 40nm). The sequoia multispectral sensor is a self-calibrating system that incorporates an integrated irradiance sensor using the sun angle correction radiometric calibration technique. The sun angle correction radiometric calibration technique was possible to apply to the eBee drone because the orientation between the camera and the sunshine sensor is fixed and known. A grey balance radiometric calibration target (also called calibrated reflectance panel) was used to calibrate the camera before each flight. The sunshine sensor allows sunlight information to be logged and captured throughout the flight. Utilizing these irradiance values, the system automatically calibrates all output images along with assigning geolocation information from the Parrot Sequoia's onboard GPS, IMU, and Magnetometer. Because the sunshine sensor records information in real time during each flight, Sequoia-derived reflectance values vary relatively insignificantly with the weather conditions(Deng et al., 2018).

During the initial processing stage, the calibrated images and the 500 images from the four spectral bands were imported in Pix4d for further processing. From the four multispectral sensors on the sequoia camera, the aerial triangulation of each of the sensors are processed at the same time, accounting for each sensor's lens distortion. Thereafter, a reconstruction of the surface was produced via a dense point cloud using multi-view stereo matching (Deng et al., 2018). Finally, individual orthorectified images were combined into a 4-band multispectral orthomosaic image to obtain the UAV orthophoto of the entire area. Due to the fact that each spectral band was processed considering its own characteristics, band-to-band alignment was achieved. The experimental plot acquired from the multispectral sensor and randomly selected spectral profiles from different experimental plots were generated to show the spectral reflectance curve for experimental subplots (n = 3). Although radiometric calibration issues have been associated with the sequoia sensor (Fawcett et al., 2020), selected spectral profiles were unique as they represented the spectral properties from different applications of nitrogen and water (Figure 4-3). Therefore, the study was based on the assumption that the sequoia camera is suitable for estimating the spectral profiles of each subplot.

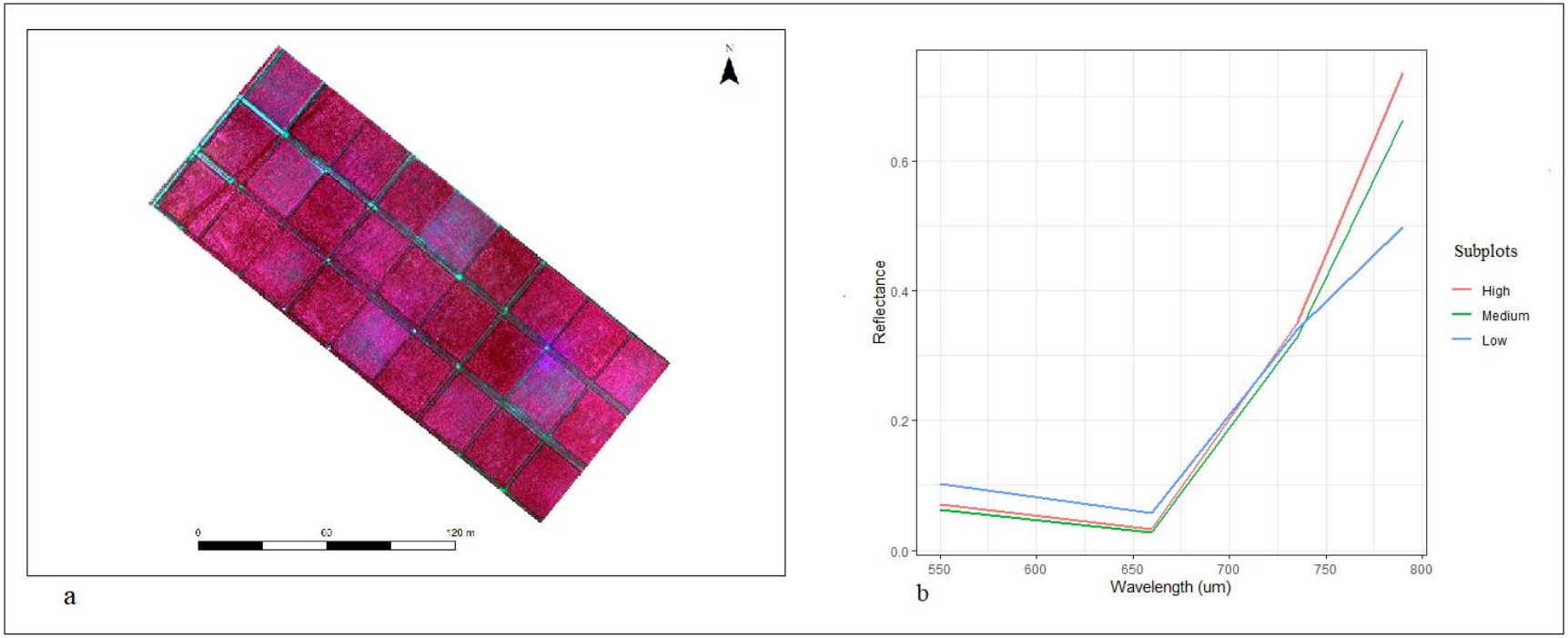

Figure 4-3: A. Sequoia sensor Near-Infrared, Red and Green bands layerstacked showing the spectral profiles of each of the 27 subplots on the 16th of March. B. Spectral reflectance (nm) profiles obtained from experimental plots (n = 3) related to high, medium and low treatments at each subplot

4.2.4. Estimating plant height from RGB imagery

Mean plant height per subplot was estimated using the 3 cm resolution DSM generated from the RGB imagery. A boundary shapefile containing each of the 27 subplots was used to identify the subplot locations. To determine average plant height within each subplot, each subplot was split into ten segments, leaving out the segments at the edges of the subplots, therefore, eight segments were used for further analysis. Segmenting the subplots was important because plant height measurements were collected at different parts of the subplot during the field campaign (example given in Figure 4-4) and due to the uneven heights observed within some subplots. The upper height boundaries (95th percentile) for each of the eight segments were averaged to produce a mean plant upper height per subplot. To determine the ground level, gaps within each subplot were identified were visible (minimum of 4), and used to determine the average ground level per subplot. Finally, subplot mean plant height from eight segments was calculated by the segment average upper boundary subtracted by the plot average ground level.

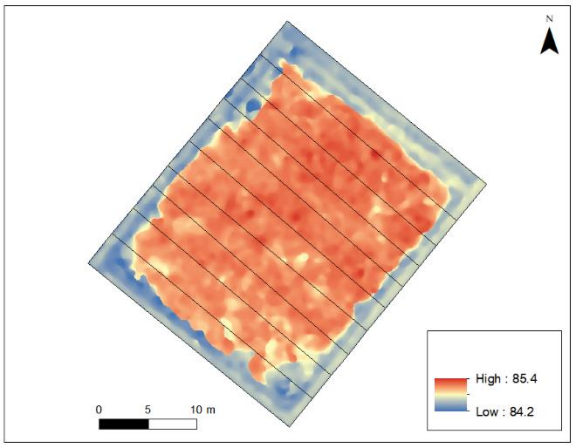

Figure 4-4: Plant height (in meters) extracted from segmented plots with the exclusion of segments at the edges due to the edge effect from adjacent subplots with different treatments

4.2.5. Vegetation indices and textural metrics

Vegetation indices were obtained from the multispectral bands while textural metrics were obtained from each of the spectral bands on the sequoia sensor on each of the sampling dates.

A set of five vegetation indices known to be sensitive to canopy structure and biomass were extracted from the multispectral orthorectified imagery (Table 4-2). We extracted the spectral values from each pixel in each of the subplots and then averaged them for each subplot. Pixel

values were not extracted from a 2 m buffer along the length and width of each subplot to reduce plot edge-effects.

Eight grey level co-occurrence matrix (GLCM; Haralick et al., 1973) texture measurements (Table 4-2) were generated for each of the four spectral bands of the MSI imagery, resulting in 32 texture metrics. The selected GLCM texture metrics were chosen as previous studies have shown them to be useful for estimating biomass in crops (Yue et al., 2019; Zheng et al., 2019). To calculate texture metrics, pixel pair sampling distances were chosen with respect to the expected spatial frequencies present in the image. Texture metrics are calculated using a 3 x 3 pixel (9 x 9 cm) moving kernel across each band of the orthomosaic image. We extracted the texture metrics values from each of the eight grey level co-occurrence matrix in each of the subplots and then averaged them for each subplot. Similar to the selection of vegetation indices, pixel values were not extracted from a 2 m buffer along the length and width of each subplot to reduce plot edge-effects.

Table 4-2: Vegetation indices and texture metrics derived from the multispectral camera. Texture metrics were obtained per spectral band for the green, red, red-edge and near infrared bands

Index	Acronym	Equation/Description	Reference
Green Normalized Difference Vegetation Index	GNDVI	$(NIR - G)/ (NIR + G)$	(Gitelson et al., 1996)
Normalized Difference Vegetation Index	NDVI	$(NIR - R)/ (NIR + R)$	(Rouse, 1974)
Red Edge Normalized Difference Vegetation Index	NDRE	$(NIR$ – RED-EDGE$)/ (NIR$ + RED-EDGE)	(Gitelson and Merzlyak, 1994)
Optimized Soil Adjusted Vegetation Index	OSAVI	*(NIR - R) / (NIR + R + 0.16)*	(Rondeaux et al., 1996)
Chlorophyll edge Index	$CL_{red\text{-}edge}$	*(NIR / RED-EDGE) - 1*	(Gitelson et al., 2003a)
Mean	MEA	*The average of pixel values in an image*	(Haralick et al., 1973)
Variance	VAR	*The deviation of pixel values in an image*	
Homogeneity	HOM	*How close the distribution of elements in the GLCM is to the diagonal of GLCM. As homogeneity increases, the contrast, typically, decreases*	
Contrast	CON	*A measure of intensity or grey level variations between the reference pixel*	

		and its neighbour. Large contrast reflects large intensity differences.
Dissimilarity	DIS	*A measure of how dissimilar pixels are computed using the absolute values of the greyscale differences. Higher values indicate a greater degree of dissimilarity amongst pixel brightness levels.*
Entropy	ENT	*The randomness or the degree of disorder present in the image. The value of entropy is the largest when all elements of the co-occurrence matrix are the same and small when elements are unequal*
Second Moment	SEM	*The local uniformity of the grey levels. When pixels are very similar the second moment value will be large.*
Correlation	COR	*A measure of the linear dependency of grey level values in the co-occurrence matrix. Values approach 1 or -1 indicate that pixels brightness values between pixels is strongly linearly correlated*

4.5.1. Statistical analyses

Rice AGB was estimated from both data acquisition dates using two approaches: Random forest (RF) and Simple Linear Regression Model. The RF model was used to estimate AGB using spectral information derived from the multispectral sensor, and when combining data from both the multispectral and RGB sensors.

RF is a non-linear parametric model that constructs and subsequently averages a large number of randomized, de-correlated decision trees for classification or regression purposes (Breiman, 2001). Each decision tree is trained using a subset of the various input variables with two thirds of these samples. RF has three unique qualities which make it ideal for this study. Firstly, RF builds on regression trees independently by using different boot strapped subsets of training samples. This reduces outliers in the data set as each tree relies on its own subset, reducing the sensitivity of the model. Secondly, a randomly chosen independent variable among the entire set of independent variables are split at each node of the tree (Liaw and Wiener, 2007) and the model selects a subset of trees with the least error as the final output. This ensures the Random Forest model is robust against overfitting (Rodriguez-Galiano et al., 2012). From the bagging

approach, the RF model chooses sample subsets from the training samples with replacement (i.e. bootstrap) which implies that the model can perform when sample dataset is small. Random Forest was selected for estimating biomass as studies have shown the suitability of the model for estimating biomass in rice, have been used to estimate rice AGB (Jiang et al., 2019) and other crops (Liu et 2019; Lu et al., 2020).

In this study, five RF models were developed as shown in Figure 2 from the MSI sensor and the combination of the MSI and RGB sensors. A model selection approach was used to find the most parsimonious model that is not fitting noise (parsimony = 0.05). This allowed us to select the most important variables for the model. To quantitatively assess the performance of the RF models with *in-situ* field biomass measurements, the 10-k fold cross validation model was selected to determine model predictive performance. The aim of k-fold cross-validation is to employ unseen data to estimate the performance of an algorithm. Thus, the benefit of k-fold cross-validation is that it can utilize all samples as training and testing samples, leading to lower biased or lower optimistic estimate for the performance of the machine learning algorithm (Kuhn and Johnson, 2013). To quantitatively assess the performance of the RF models with in-situ field biomass measurements, we calculated the coefficient of determination (R^2) and root mean square error (RMSE) and mean absolute error (MAE). The P-values were calculated to show the standard errors and significance of each one of the parameters in the model These evaluation metrics have been widely used to estimate the predictive power of regression models (Elarab et al., 2015; Yi et al., 2014).

In addition to the RF models, the Simple Linear Regression Model (SLM)(Montgomery et al., 2012) was adopted to describe the relationship between the field biomass measurements and Plant height from the RGB sensor because it only had one input parameter.

To test if model quality was statistically better for the SLM to the RF models, a bootstrap test was performed using the function "boot" available in the R package 'boot' (Canty & Ripley, 2014). Test variables were calculated by comparing the R^2, RMSE and MAE values of SLM model to the ones produced by each of the RF models (Lopatin et al., 2016). A one-sided test was performed between SLM and RF values based on 500 bootstrap samples to determine the which model was statistically better. The level for significance was set to $\alpha = 0.05$.

4.3. Results

4.3.1. Relationships between RGB derived plant height and above ground biomass

Plant height estimated from the RGB digital surface model was significantly ($p < 0.0001$) correlated with in situ measurements ($R^2 = 0.7$; RMSE = 6.09 cm, MAE = 5.11 cm). The plant height derived from the RGB imagery tended to be slightly higher than measured height for some of the lower measured heights and vice versa for the plant with the highest measured heights (Figure 4-5).

Biomass estimation, derived from RGB imagery, was significantly correlated with in situ measures of above ground biomass (Figure 4-5; Table 4-2; $R^2 = 0.72$; $p < 0.0001$; RMSE = 1.04 t/ha, MAE = 0.91 t/ha).

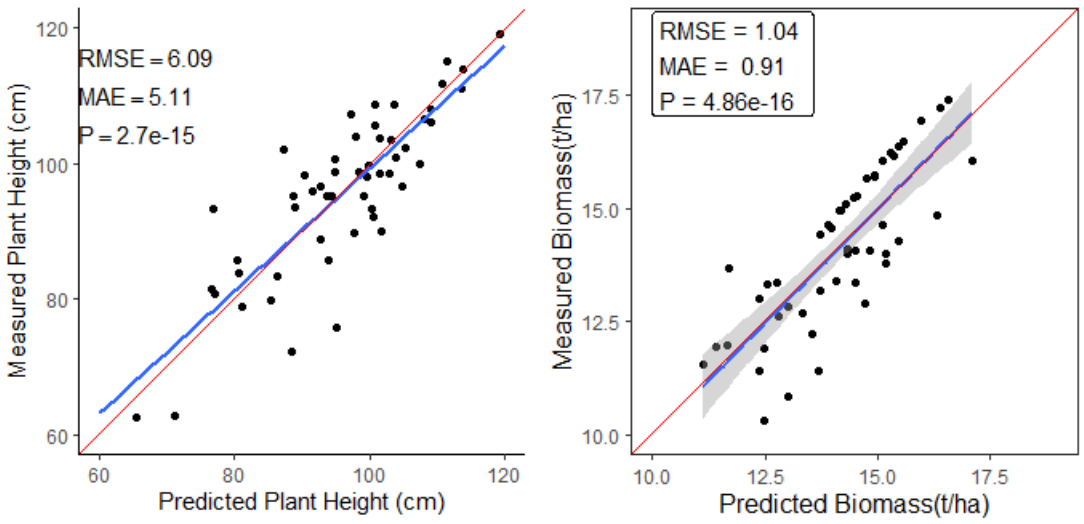

Figure 4-5: A. Relationship between measured plant height and estimated plant height generated from RGB point cloud data (n = 54). B. Comparison between measured Biomass and the Predicted Biomass from DSMs generated with UAV images using the k=fold cross validation method (n=54). The diagonal represents the 1:1 line. metrics Solid red line are regressions, blue line is corresponding to 95% confidence intervals, and shaded areas the corresponding 95% prediction intervals).

Table 4-3: Evaluating mid-late rice AGB from Plant Height (PH), Texture Metrics (TM) *and Vegetation Indices (VI) derived from RGB and MSI sensors.*

Sensor	No of Variables	Type of model	R^2	RMSE (t/ha)	MAE (t/ha)
Multispectral	5	VI	0.63	1.22	1.00
	32	TM	0.46	1.48	1.31
	37	VI +TM	0.60	1.26	0.91
RGB	1	PH	0.72	1.04	0.97
Multispectral + RGB	6	VI + PH	0.75	1.03	0.83
	40	VI+TM+PH	0.79	0.97	0.74

4.3.2. Relationships between MSI derived vegetation indices and texture metrics with above ground biomass

Three independent RF models were generated to determine the utility of (i) spectral indices, (ii) spectral texture metrics and (iii) a combination of vegetation indices and texture metrics; for estimating mid- to late season rice AGB.

4.3.2.1. Vegetation Indices

The RF model predicted 63% of the variance in measured biomass ($p < 0.001$; RMSE = 1.22 t/ha; MAE = 1.00; Figure 4-6; Table 4-4). The model shows a pattern of overestimation of rice AGB at low values of measured biomass (< 14 t/ha), while underestimating biomass and greater than 15 t/ha. From the five VIs tested (Table 4-3), the NDRE, OSAVI and GNDVI indices were identified as the most important for predicting rice ABG based on the parsimony applied to RF model, while the NDVI or the $CI_{red\text{-}edge}$ indices were omitted in building the RF model.

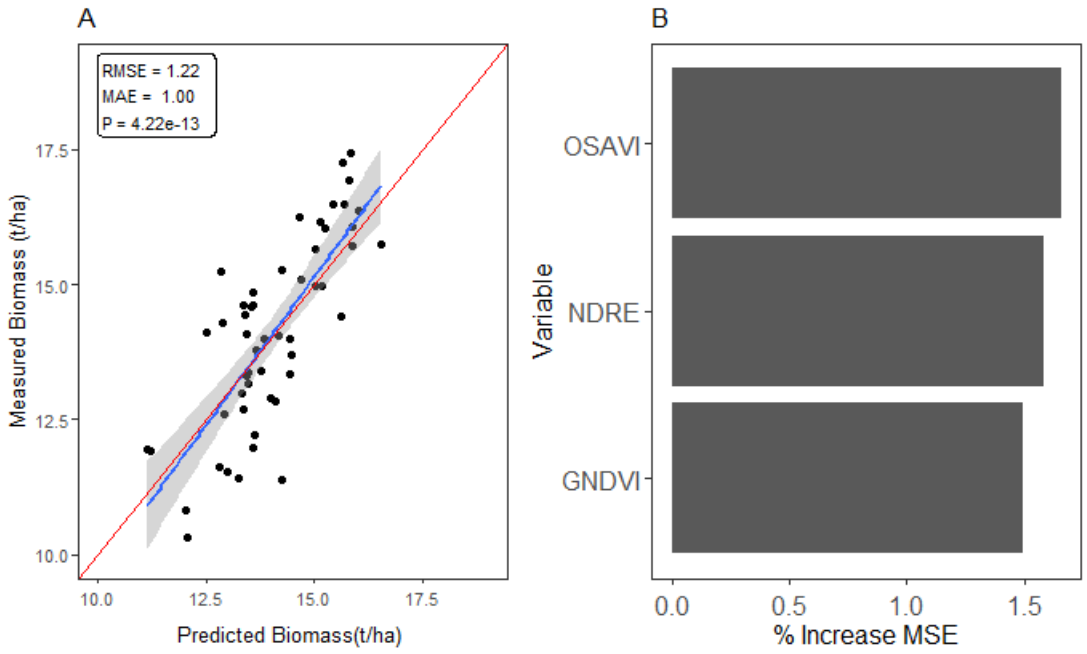

Figure 4-6: A. Measured versus Estimated Biomass from the most significant Vegetation Indices. Solid red line represents the 1 to 1-line, blue line is corresponding to the regression line and shaded areas the corresponding 95% prediction intervals. B. Variable Importance plot ranking the most significant to the least significant vegetation index.

4.3.2.1. Textural metrics

The relationships between rice AGB and GLCM-based texture measurements associated with different spectral bands were found to be poor for the majority of texture measurements. Only 10 of the 32 input variables used to generate the textural metrics model were selected by applying the parsimony to the model. It is important to note that some of the variables were potentially omitted because they were co-correlated with others (see Appendix 3). The RF model was able to predict 46% of the variance in measured biomass with an accuracy of RMSE of 1.46 t/ha and MAE of 1.13, indicating moderate (albeit statistically significant P <0.001) relation between texture metrics and mid-late rice AGB estimation. Textural metrics obtained from the NIR and Red spectral bands were the most important for estimating, accounting for 70% of the metrics selected by the final RF model. Mean NIR reflectance was identified as the most significant metric whereas Dissimilarity green, Homgeneity red and Entropy NIR contributed the least to AGB estimations (Figure 4-7).

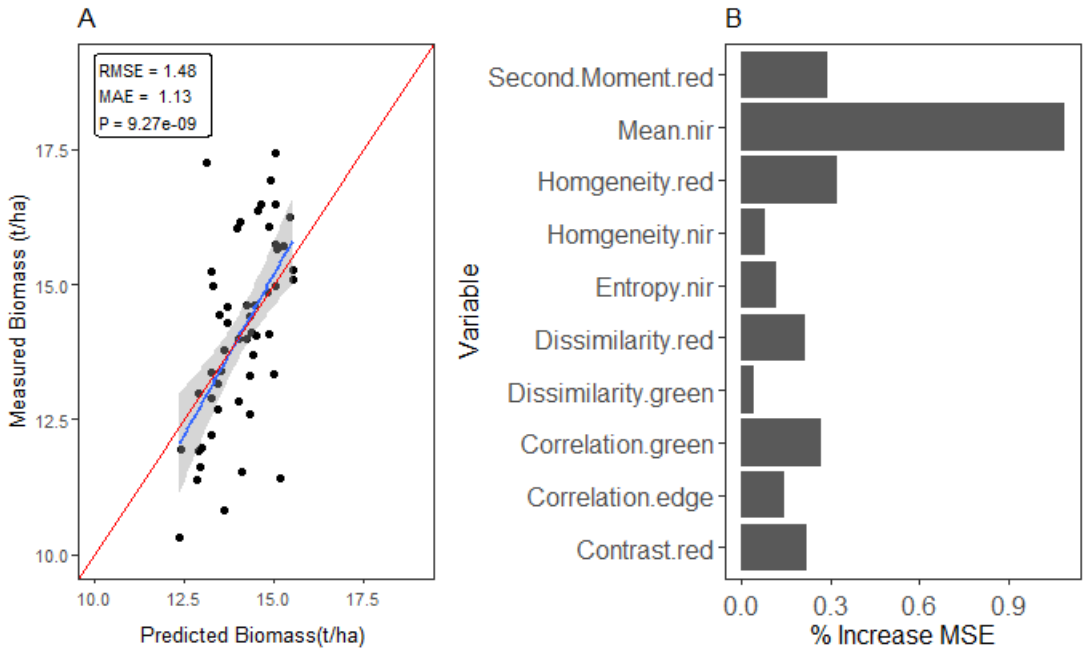

Figure 4-7: Measured versus Estimated Biomass from the most significant texture metric bands variables (n=54). Solid red line represents the 1 to 1-line, blue line is corresponding to the regression line and shaded areas the corresponding 95% prediction intervals. B. Variable Importance plot ranking the most significant to the least significant texture metric.

4.3.2.2. Relationships between the combination of vegetation indices and texture metrics with above ground biomass

The third model was developed using the combination of vegetation indices and texture metrics using the RF model. The parsimonious selection process removed 31 of the 32 texture variables and 2 of the 5 vegetation indices, leaving four selected variables from the combination of vegetation indices and textural metrics (Figure 4-8). The selection criteria for selection of vegetation index were consistent as the three vegetation indices utilised in Figure 4-7 were the same vegetation indices selected when combining vegetation indices with texture metrics. Likewise, the most significant texture band (mean (NIR), from Figure 4-8 was the only texture metrics selected from combing vegetation indices and texture metrics. However, model performance was not improved compared to the combination of both spectral properties derived from Texture metrics and VIs for estimating mid-late AGB as compared to VIs alone with model less accurate with RSME (1.26 t/ha).

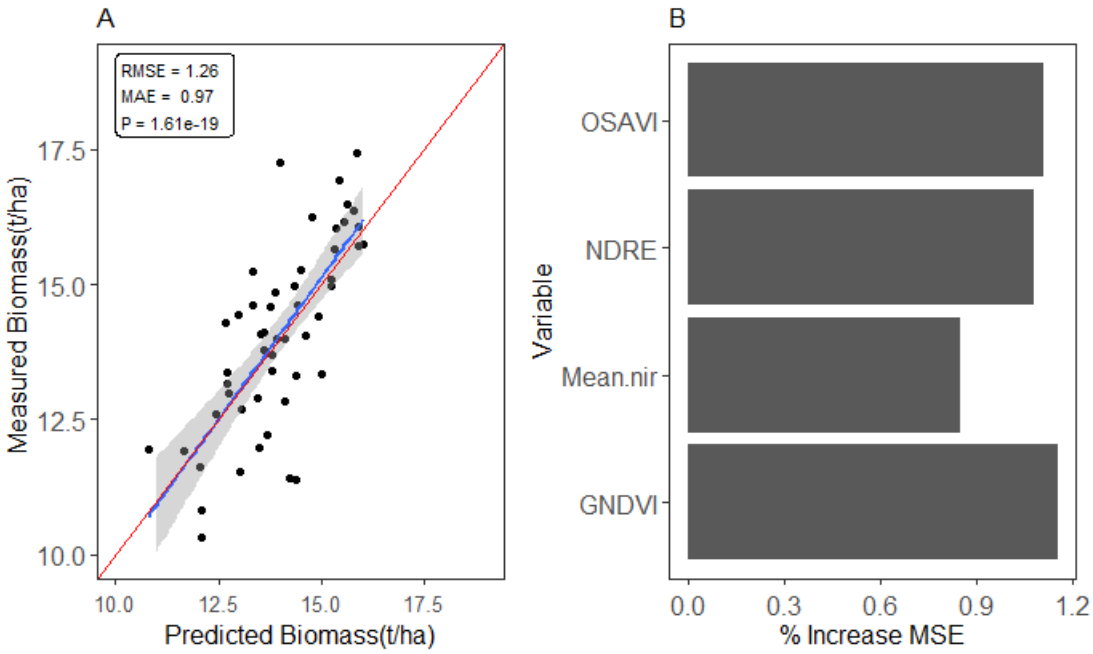

Figure 4-8: A. *Measured versus Estimated Biomass from the most significant Vegetation Indices and texture metrics variables (n=54). Solid red line represents the 1 to 1-line, blue line is corresponding to the regression line and shaded areas the corresponding 95% prediction intervals. B. Variable Importance plot ranking the most significant to the least significant combination of vegetation indices and texture metrics.*

4.3.3. Relationships between the combination of vegetation indices, texture metrics and plant height with above ground biomass

To determine the utility of estimating AGB by combining structural data from the RGB sensor with the multispectral sensor imagery, two models were investigated; (i) the combination of vegetation indices from the MSI sensor with plant height from RGB sensor and; (ii) the combination of Texture metrics and vegetation indices from the MSI sensor with plant height estimates from the RGB sensor for estimating rice AGB.

The regression model built based on the combination of vegetation indices and plant height was able to predict 75% of the variance in measured biomass, with the model RMSE and MAE were 1.03t/ha and 0.83 t/ha respectively (Figure 4-9). In terms of the most important variables selected for the model, the NDRE, OSAVI and GNDVI vegetation indices were consistently chosen from the available vegetation indices. In addition to the selected vegetation indices, the plant height variable was selected for building the model, with results indicating plant height as the most significant variable for estimating rice AGB during the mid-late growing stage.

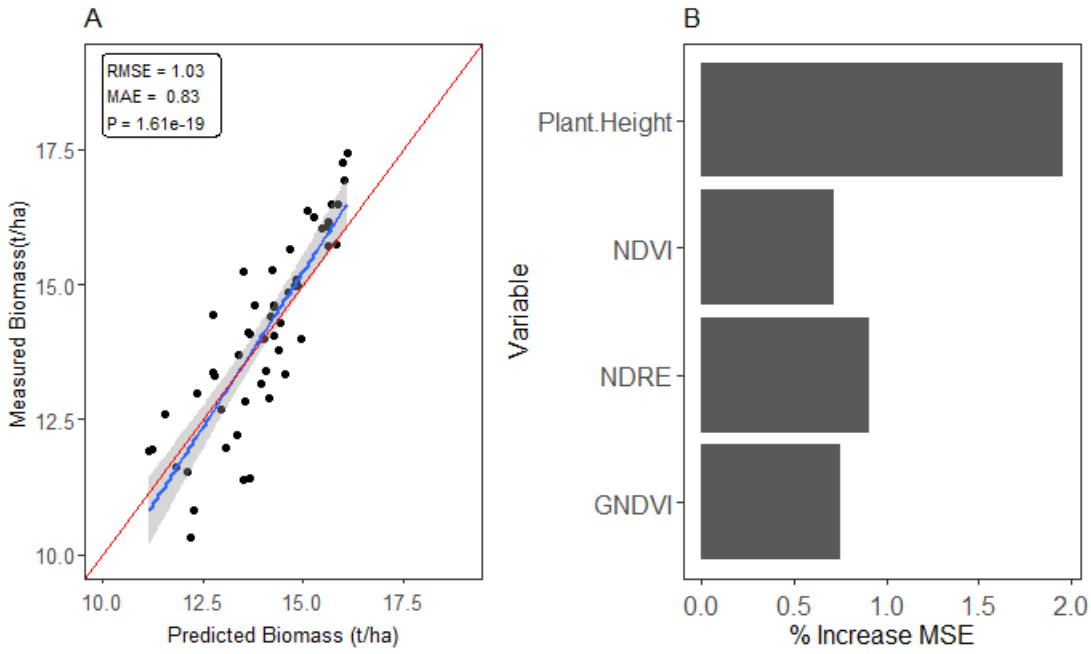

Figure 4-9: *Measured versus Estimated Biomass from the most significant plant height and vegetation indices variables (n=54). Solid red line represents the 1 to 1-line, blue line is corresponding to the regression line and shaded areas the corresponding 95% prediction intervals. B. Variable Importance plot ranking the most significant to the least significant combination of vegetation indices and plant height.*

When texture metrics, vegetation indices and plant height were combined together, the model showed lower model error, with the RMSE and MAE errors reported as 0.94 t/ha and 0.74 t/ha respectively, while the model measured biomass variance was 79%. The automation parsimonious process applied to the RF model pruned the model variables from 40 to 12. Of the 12 variables included in the final model process, plant height, five vegetation indices and six texture metrics were selected. The texture metrics were dominated by metrics in the red and NIR bands with 5 out of the 6 bands within the spectral region (Figure 4-10).

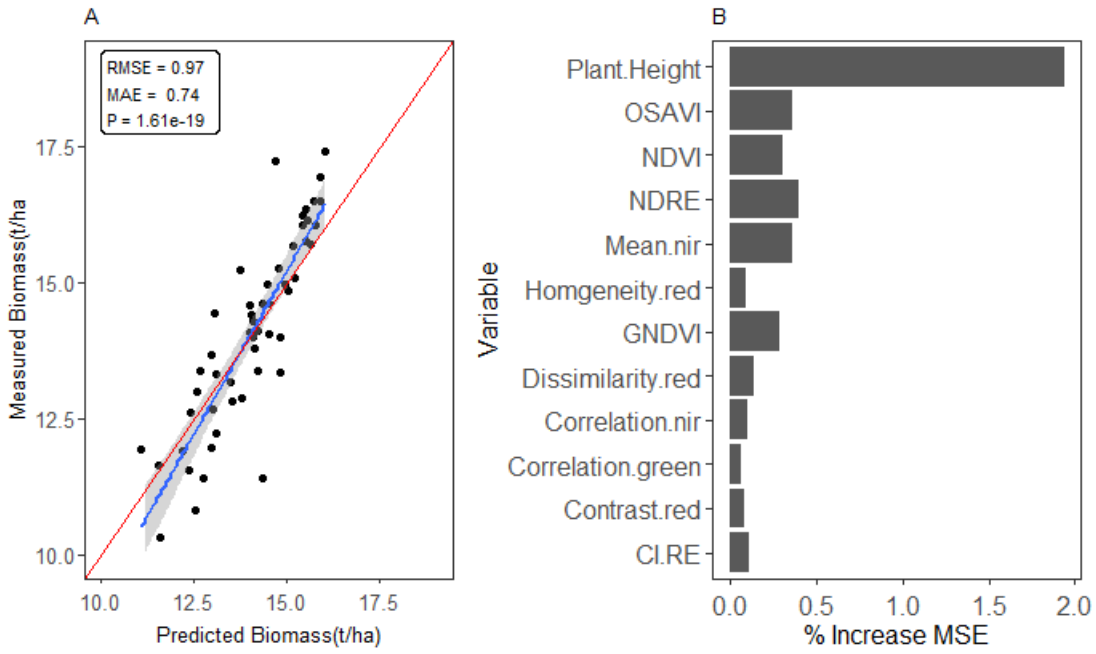

Figure 4-10: Measured versus Estimated Biomass from the most significant plant height and vegetation indices and texture metrics variables (n=54). B. Variable Importance plot ranking the most significant to the least significant combination of plant height and vegetation indices and texture metrics variables. Solid red line represents the 1 to 1-line, blue line is corresponding to the regression line and shaded areas the corresponding 95% prediction intervals.

4.3.4. Comparison between RGB and MSI sensors for estimating Above Ground Biomass

We investigated the statistical differences in model quality between the plant height model developed using the SLM model with the five RF models developed from texture metrics, vegetation indices and plant height using the bootstrap approach (Table 4-4).

When comparing the model quality measures between SLM plant height and RF vegetation indices using the bootstrap test, SLM was significantly better than RF for biomass estimation from the R^2, RMSE and MAE (Table 4-4). Similar results were observed when comparing the model quality of plant height generated from the SLM compared with the texture metrics model and the combination of texture metrics and vegetation indices. We can infer from the results that the RGB sensor using plant heights estimates provide better model quality, with the SLM results indicating lower model error and a much higher model variance (Table 4-4).

Table 4-4: Results for bootstrap test to check for statistical differences in model quality measures R^2, RMSE and MAE obtained by RF and linear model for biomass. Number of bootstrap samples= 500

Model	Variables	R^2	RMSE (t/ha)	MAE (t/ha)
Simple Linear Model	PH	0.72	1.07	0.93
Random Forest Models	VI	0.59	1.31	1.06
	TM	0.43	1.58	1.22
	VI + TM	0.54	1.38	1.08
	VI +PH	0.73	1.07	0.86
	VI + TM +PH	0.74	1.02	0.82

The combination of the RGB and MSI sensors using plant height and vegetation indices presented similar model accuracy albeit a lower mean absolute error. On the contrary, the inclusion of texture metrics variables improved the quality of the model, with lower RMSE and MAE errors (Figure 4-10). The results show that the combination of plant heigh estimates from the RGB sensor with texture metrics and vegetation indices from the MSI sensor provide the most accurate estimation of rice AGB during the mid-late growing stages of rice development. However, the improvement was not identified to be significantly different from estimated obtained from plant height estimates using SLM.

4.4. Discussion

This study evaluated the relative importance of using data from drone-mounted consumer grade RGB sensor, a scientific grade multispectral sensor and the added value of their combined use for estimating rice AGB during the mid (reproductive) to late (ripening) stages. The findings of this study are discussed in three different categories. First, we discuss RGB sensor for estimating rice AGB using plant height estimates. Second, we debate the comparative differences of using the MSI sensors on-board the drone for estimating rice AGB. Third, we evaluated the added value of the MSI sensor to the RGB sensor compared to using the RGB sensor in isolation for estimating rice AGB statistically.

When comparing the accuracy of the RGB sensor for estimating plant height from DSM with actual field measurements, results from Figure 4-3 showed high variability with measured plant height and a low RMSE. These results are particularly significant when rice plant height

grow above 1m meter during the reproductive and ripening stages, making it difficult to obtain manual plant height measurements. Likewise, the significance of the result is amplified considering the fact that manual assessment of crop height is time consuming; thus, only a small portion of the rice field can be measured consistently over time, leading to inaccuracies. Although limited studies have shown the relationship between plant height estimates obtained from drones with actual field measurements in rice fields, Cen et al. (2019) and Jiang et al. (2019) presented similar results for the estimation of plant height estimates of rice using drones. Our results suggest that plant height estimates, derived from consumer-grade three band RGB sensors can be used to estimate rice AGB during the mid-late growing stages. Plant height estimates were able to capture the variability within each plot (appendix 3) even though the AGB in cereal crops encompasses with leaves, stems and panicles, which play a significant factor in AGB during the mid-late growing season (Lu et al., 2019). For the estimation of rice AGB, results from Figure 4-5b show a strong relationship between plant height and rice AGB, indicating the suitability of the RGB camera alone for the estimation of rice AGB during the reproductive and ripening phases. Contrary to the results of plant height for estimating rice AGB, Cen et al. (2019) results suggest that plant height may not to ideal for estimating rice AGB during the late growing stages as results show low correlation between plant height and biomass. On the other hand, Tilly et al. (2015) results tally with ours as plant height was successfully utilised for estimating rice AGB over multiple growing seasons.

In a bid to identify the relative importance of the MSI sensor for estimating rice AGB, the merits of vegetation indices and texture metrics approaches were investigated. During the selection process based on the parsimony of the RF models for the vegetation indices, the NDRE, OSAVI and GNDVI vegetation indices were consistently selected as the most significant indices. The GNDVI also performed significantly better than NDVI which was omitted in the selection process of the first three RF models. The GNDVI results were similar to the NDRE models which confirms the findings that green and red edge reflectance's are sensitive to a wide range of chlorophyll levels than the red reflectance (Carter and Knapp, 2001; F. Li et al., 2014).. Additionally, the red edge band could be influenced by stress induced increase in fluorescence, and thus the sensitive is higher to stress induced chlorophyll changes than the green band (F. Li et al., 2014). However, the $CI_{red\text{-}edge}$ results were in variance to NDRE estimates of rice AGB during the late growing stages. The reason may be that rice biomass growth in the reproductive and ripening stages causes a decrease in the plant green intensity, leading to a decline in the chlorophyll content of rice AGB (Jia et al., 2004;

Saberioon et al., 2014) which affects the $CI_{red\text{-}edge}$ index . When considering the significance of OSAVI, our results confirm the significance of OSAVI index for estimating mid-late AGB in rice. This may have been as a result of the alteration of nitrogen application and water applied to different subplots which provided varying soil reflectance especially in plots where crop canopy was not dense. The OSAVI index suitability for estimating rice at the mid-late growing stages were in agreement with Zheng et al. (2019) estimation of rice AGB during the same stages.

Texture metrics, which are related to the spatial spread of dark and bright pixels in an image (Haralick et al., 1973), have recently been introduced as a technique for estimating biomass for field-scale rice farms because of the ultra-high-resolution possessed by sensors on drones (Liu et al., 2019; Yue et al., 2019; Zheng et al., 2019). However, our results suggest limited potential for textural metrics as a predictor of rice AGB. The modelled derived solely from texture metrics showed the highest error in rice AGB estimation (RMSE = 1.48 t/ha). Similar results were observed in Zheng et al. (2019) estimation of rice during the mid-late growing stage using texture metrics. Despite the results obtained using the texture metrics, the Mean NIR band was identified to be the most significant variable and showed a positive correlation with biomass (Appendix 3), corresponding to results obtained by Zheng et al., (2019) and Lu and Batistella (2005). Alternative testing of the model using the combination of texture metrics and vegetation index did not improve the estimation of rice AGB during the mid-late growing stages, although the selection of the most important variables were consistent for vegetation indices (Figure 4-6) and texture metrics (Figure 4-7). Contrary to the results reported in Liu et al., (2019), combining texture metrics and vegetation indices reduced the predictive accuracy of our model (Fig 4-9). One reason for the poor performance of this combined model may be attributed to, the textural metrics are very scale and scene dependent, because information on the canopy structure carried in single pixels vary for images with different ground resolution, thereby leading to a huge alteration in the distribution of dark and bright areas on the images (Yue et al., 2019).

The added significance of the combination of the MSI sensor to the RGB sensor for estimating rice AGB was identified. When combining plant height estimates with vegetation indices, Figure 4-9 shows stronger relationship with rice AGB compared to other RF models. Although the combination of the spectral and structural properties provides more details for understanding the rice AGB canopy (Han et al., 2019), the saturation effect experienced suggest that at the latter growing stages from VIs may have affected the estimation significance

of the combination of both techniques for estimating rice AGB. These results agree with Bendig et al. (2015) who showed lower estimation of AGB in a cereal crop (barley) from the combination of plant height and vegetation indices from the vegetative stage to the ripening phase. Similarly, Lu et al., (2019) identified a decline in the RF model performance at the late growing stage of a cereal crop (wheat), although a combination of vegetation indices and plant height improved the estimation accuracy. The combination of texture metrics, vegetation indices and plant height explained the highest model variability and least RMSE and MAE errors. The results suggest that the addition of some texture metrics bands to vegetation and plant height slightly improve the estimation of rice AGB although when texture metrics are combined with vegetation indices, the model was not improved compared to vegetation indices alone. This may be as a result of the addition of the structural property obtained from plant height to the spectral properties of vegetation indices and texture metrics which provides additional information about rice AGB characteristics.

When comparing the statistical differences in model performance, plant height estimates obtained from SLM models performed better than vegetation indices, texture metrics and their combination using RF model. The results suggest that the RGB sensor are more suitable for estimating rice AGB during the mid-late growing stages compared to the more sophisticated MSI sensors. However, the combination of both the RGB and MSI sensors using the RF model were statistically better, albeit the results being statistically significant. Rice AGB estimation during the mid-late growing stage has a strong relationship with yield outcomes(Jin et al., 2020a; Li et al., 2020; Serrano et al., 2000), therefore, accurate estimation prior to harvest can help farmers and agronomist project yield more accurately. Nevertheless, the cost implication of purchasing a multispectral sensor may change the narrative of the significance of improvement. To a well-established farmer or agronomist looking to make marginal improvements which could result in significant economic results at the end of the growing season, the purchase of a multispectral sensor may be the right step to take. However, a farmer venturing into rice farming may prefer to stick with the RGB sensor since rice AGB estimation are still significant. Therefore, we can infer from the results that multispectral sensors improve the estimation of rice ABG, though the significance may be relative to the finance and yield expectation of the farmer or agronomist.

4.5. Conclusion

This study evaluated the relative importance of using data from drone-mounted consumer grade RGB sensor, a scientific grade multispectral sensor and their combined use for

estimating rice AGB during the reproductive and ripening stages. We initially accessed the performance of plant height generating from DSM using the RGB sensor for the estimation of rice AGB. Accuracy of biomass estimation obtained from the RGB sensor using SLM were statistically compared with vegetation indices, texture metrics and the combination of vegetation indices and texture metrics obtained from the RF model. Results showed plant height as a more significant estimation parameter to vegetation indices and texture metrics for the estimation of rice AGB. Thereafter, the added advantage significance of texture metrics and vegetation to plant height for estimating rice biomass during the reproductive and ripening stages of rice was evaluated. The addition of vegetation indices improves the model and was statistically more accurate than plant height estimates from the SLM. Furthermore, the addition of the texture metrics to the vegetation and plant height using the RF model further improved the model and was statistically better than SLM plant height estimates. That said, we can infer from the study that the full potential of a multispectral sensor can further improve the estimation of rice AGB at the critical growing stages on a drone platform. Conversely, the improvement in relation to the economic implication of purchasing a multispectral sensor is relative based on income of farmers and agronomists to yield improvement. A cheaper alternative may be the adoption of a consumer grade sensor over a multispectral sensor for the estimation of biomass at the critical growing stages as opposed to both sensors.

The limitation of this study is the small sample size (54 samples). Although random forest is capable dealing with small sample sizes, a higher number of sampling points would improve the accuracy of the prediction. Additionally, assessing the performance of different rice cultivars across multiple growing seasons would further assess the performance of the model for estimating yield during the reproductive and ripening stages of rice.

Chapter 5 Estimating the phenological dynamics of irrigated rice leaf area index using the combination of PROSAIL and Gaussian Process Regression

Abstract

The development of rice is a sequence of different phenology phases. This implies that the condition of the plant during the vegetative phase relates directly to the health of leaves functioning during the reproductive and ripening phases which are important for monitoring yield. Leaf Area Index (LAI) is an important indicator of rice yields and the availability of this information during key phenological phases can support more informed farming decisions. The primary objective of the study was to demonstrate the advantage of a hybrid model which combines the PROSAIL model and Gaussian Process Regression (GPR) machine learning algorithm for estimating the phenological dynamics of irrigated rice developed from field spectral data used for simulating Sentinel-2 MSI spectral bands and later compared with Sentinel-2 LAI imagery during the vegetative, reproductive and ripening phases. To achieve this, the PROSAIL radiative transfer model was adopted to simulate a look-up table (LUT) and associated variables acquired from an experimental field in Nasarawa state, Nigeria. The LUT was then used to train the GPR model and was compared with LAI generated from the SNAP toolbox, which is based on the PROSAIL model and Artificial Neural Network (ANN) machine learning algorithm. Data was collected during the dry season from a rice farm in Nigeria where nitrogen and water application were altered, which was used as validation for the LAI models. Our resulted demonstrated that when estimating LAI during the entire growing season, the hybrid GPR model outperformed the hybrid ANN model (R^2 = 0.82, RMSE = 1.65; and R^2 = 0.66, RMSE = 3.89 respectively). During the phenological phases, the hybrid GPR model predicted more accurate with less model errors in the vegetative (R^2 = 0.67), reproductive (R^2 = 0.7) and ripening (R^2 = 0.59) phases compared to the hybrid ANN model in the vegetative, reproductive and ripening phases. When monitoring LAI phenological profiles of both hybrid models, the hybrid-GPR and ANN models underestimated LAI during the reproductive and ripening phases although the ANN model underestimations were significantly greater than those for the hybrid GPR model. Our results highlight the potential of hybrid GPR models for estimating the phenological dynamics of irrigated rice from Sentinel-2 data as they provide more accurate estimation of LAI patterns from varying nitrogen and water applications compared to hybrid ANN models

Keywords: Leaf Area Index, Sentinel-2, Gaussian Process Regression, Rice, Phenology, Radiative transfer model

5.1 Introduction

Grain crops are the main source of nutrition and food for populations around the world, with rice accounting for over 40% of consumption globally (Muthayya et al., 2014). Sub-Saharan Africa has one of the fastest rates of increase in rice consumption, with Nigeria accounting for 23% of the total consumption in the region (O'Donoghue and Hansen, 2017). However, sub-

Saharan countries are reliant on expensive rice imports due to chronically low national yields (FAO, 2018b; von Grebme et al., 2013) leading to huge financial burden on these countries.

A wide range of factors have been proposed as causes of large rice yield gaps observed in Nigeria and the wider sub-Saharan Africa region, including inadequate use of and access to inputs (e.g. water, nutrients, pest and diseases) (Fahad et al., 2017; Wahid and Close, 2007), limited farm mechanization and a lack of expertise amongst smallholder farmers about best agronomic management practices (Hengsdijk and Langeveld, 2009). Limited access to water for irrigation and fertilizers (including nitrogen), in particular, are key factors limiting productivity and resilience of rice production in sub-Saharan Africa and other smallholder farming regions globally (Ju et al., 2009; Wang et al., 2016b). Consequently, there is a growing need to monitor rice yields to address productivity gaps, including those caused by water stress and fertility limitations. Crop phenological phases inform how farm managers make decisions about application schedules (Sakamoto et al., 2005), . Effective monitoring of the growth dynamics of rice crops at different phenological phases is required to help yield prediction by informing farmers as to when management interventions are necessary (Fageria, 2007). Consequently, regular monitoring of crop phenology is an important step towards improving crop productivity (Mercier et al., 2020).

Satellite remote sensing has been proposed as a potential low-cost and scalable tool for monitoring and mapping of crop yields (Gilardelli et al., 2019; Kang and Özdoğan, 2019b), growth status (Pipia et al., 2019; Thorp et al., 2012b; Xie et al., 2019b, 2018) and stress (Bandaru et al., 2016; Banerjee et al., 2018) in agricultural environments. Key to satellite-based yield estimation approaches is the ability to accurately recover estimates of crop leaf area index (LAI) throughout the growing season. LAI is defined as half of the all-sided green leaf area per unit ground area (Chen and Black, 1991; Zheng and Moskal, 2009) and is a key biophysical parameter that reflects the physiological processes of plants, and thus is an important proxy for crop development. LAI is commonly measured directly, with destructive sampling, or indirectly, for example with digital hemispherical photography or the LAI-2000/2200 Plant Canopy Analyzer (Fang et al., 2014; Lena et al., 2016). Yet, these approaches have shortcomings for measuring LAI across large spatial extents and at frequent points in time in terms of time, labour input and cost. Satellite remote sensing represents a reliable and faster alternative to detect spatiotemporally-explicit trends in LAI. For example, the moderate resolution imaging spectroradiometer (MODIS) LAI products are suited for monitoring at regional to global scales and have been applied in various studies (Fensholt et al., 2004; Gao

et al., 2008; Jiang et al., 2010). However, the spatial resolution of MODIS (250m) hampers its adoption when monitoring LAI at much finer resolutions, e.g. at field scale. More recently, the launch of the European Space Agency's Sentinel-2 satellites provide a suitable platform for timely monitoring of LAI during different phenological phases due to the high spatial, spectral and temporal resolution (Drusch et al., 2012).

A broad range of methods have been developed for the retrieval of LAI from satellite imagery, which can be broadly categorized into statistical, physically-based and hybrid methods (Verrelst et al., 2015a). Statistical methods are divided into parametric methods, such as vegetation index (VI) approaches, and non-parametric methods such as machine learning regression algorithms. VI-based models assume an explicit relationship between spectral observations in two or more bands and measured LAI (Clevers and Gitelson, 2012; Gitelson, 2004; Verrelst et al., 2008). The successful application of this approach has been demonstrated to a range of vegetation canopies (Darvishzadeh et al., 2008a; Nguy-Robertson et al., 2012; Xie et al., 2014). Notably, VIs developed using reflectance in the red-edge region of the spectrum (RE-based VIs), such as the red-edge based NDVI and Inverted Red-Edge Chlorophyll Index (Frampton et al., 2013), have shown to estimate LAI effectively. Yet, VI-based developed models are often location, sensor and time-specific, making their application over large spatial extents challenging (Baret and Buis, 2008; Verrelst et al., 2015a).

Statistical non-parametric methods, on the other hand, assume a non-explicit relationship between spectral bands and LAI, commonly derived using non-parametric regression approaches such as machine learning regression algorithms (MLRA). MLRAs have the potential to generate adaptive, robust relationships and, once trained, in theory do not need additional information to be applied in other locations. Typically, machine learning algorithms can cope with the strong nonlinearity of the functional dependence between the LAI and reflected radiance (Verrelst et al., 2018). However, they can behave unpredictably when used with spectral data exhibiting characteristics not observed during the model training phase and may tend towards over-fitting of the training dataset (Baret and Buis, 2008; Darvishzadeh et al., 2008a; Rivera et al., 2014; Weiss et al., 2000).

Physically-based LAI retrieval methods use Radiative Transfer Models (RTM) and offer an explicit connection between canopy reflectance and plant biochemical and biophysical characteristics (Jacquemoud et al., 2009). The physical modelling approach takes into account the canopy architecture, illumination, soil background and viewing geometries. RTMs have

frequently been applied to retrieve crop biophysical parameters from a range of different sensors (Berger et al., 2020; Darvishzadeh et al., 2008a; Dorigo et al., 2007; Estévez et al., 2020). Nevertheless, the physically-based approach is not straightforward due to the trade-off between the reality and inversion possibility of the RTM made, hence, a common approach to simplify the inversion problem is by creating a Look Up Table (LUT) (Darvishzadeh et al., 2008a; Weiss et al., 2000). The LUT approach simulates multiple model realizations and stores both inputs and output spectra as a LUT. Yet, the imposed upper/lower boundaries in the LUT is such that estimated variables cannot go beyond the boundaries imposed, therefore, undermining the physical approach (Baret and Buis, 2008). Additionally, the potential irregularity of green tissues in the canopy, referred to as clumping (Chen and Black, 1992), which assumes that the canopy is spatially homogeneous, leading to underestimation in high LAI values (Duveiller et al., 2011).

More recently, hybrid methods have emerged to circumvent some of the limitations of empirical and radiative transfer approaches. Hybrid methods combine the generalization level of the physically-based radiative transfer approach with the flexibility and computational efficiency of machine learning algorithms (Verrelst et al., 2018). The Artificial Neural Network (ANN) represents the most frequently adopted MLRA used in hybrid models due to their efficient interpolation capacity. They have received much attention in biophysical variable retrieval and are currently operational as the LAI retrieval method for Sentinel-2 imagery (e.g. available within the Sentinel Application Platform (SNAP) biophysical processor toolbox). However, hybrid ANN models are often difficult to train because of their multi-parameter complexity and are black box in nature (Lunagaria and Patel, 2019). Alternative approaches such as the use of hybrid Gaussian processes regression (GPR) (Rasmussen and Williams, 2006) have provided encouraging results in the framework of biophysical parameter estimation (Campos-Taberner et al., 2016; Lázaro-Gredilla et al., 2014; Verrelst et al., 2015b). For instance, Campos-Taberner et al. (2016) used hybrid GPR from simulated Sentinel-2 bands from SPOT 5 for monitoring rice crop growth patterns. Nevertheless, SPOT 5 is spectrally inferior to Sentinel-2, with no provision of the spectral band in the red-edge region, which is important for LAI estimation (Xie et al., 2019b).

It is therefore important to validated the hybrid GPR and ANN models from alternating management regimes, which are important towards understanding yield limiting factors using Sentinel-2 satellite. The robustness of these retrieval methods under alternating farming treatments, over different phenological stages has yet to be established.

This study aims to determine the potential a hybrid PROSAIL - GPR model for estimating the phenological dynamics of irrigated rice LAI from Sentinel-2. We compare the performance of GPR from simulated Sentinel-2 data with Sentinel-2 LAI generated using an ANN, considering performance across a range of different phenological phases of rice growth to understand the intra-seasonal differences in LAI retrieval accuracy from the respective approaches. To achieve this, we address the following research objectives: (i) Evaluate the performance of hybrid GPR for estimating rice LAI across the entire vegetation active period and at key phenology phases of rice growth; and (ii) compare the relative performance of the hybrid GPR and hybrid ANN for estimating LAI during the different phenology phases of rice.

5.2 Data and Methods

5.2.1 Study Area

This study uses data from experimental plots located within a large rice farm (Olam farm) in the village of Rubuki about 60 kilometres from Doma in Nasarawa State, in the North-central region of Nigeria (Figure 5-1). Lowland rice is the major agricultural crop in the region, which is one of the main grains producing regions in Nigeria. The study area has a tropical humid climate with two distinct seasons: the wet (rainy) season lasts from the end of March to October, while the dry season is experienced between November and February. Maximum temperatures can reach 39 °C (March), while minimum temperatures can drop to as low as 17 °C (December/January).

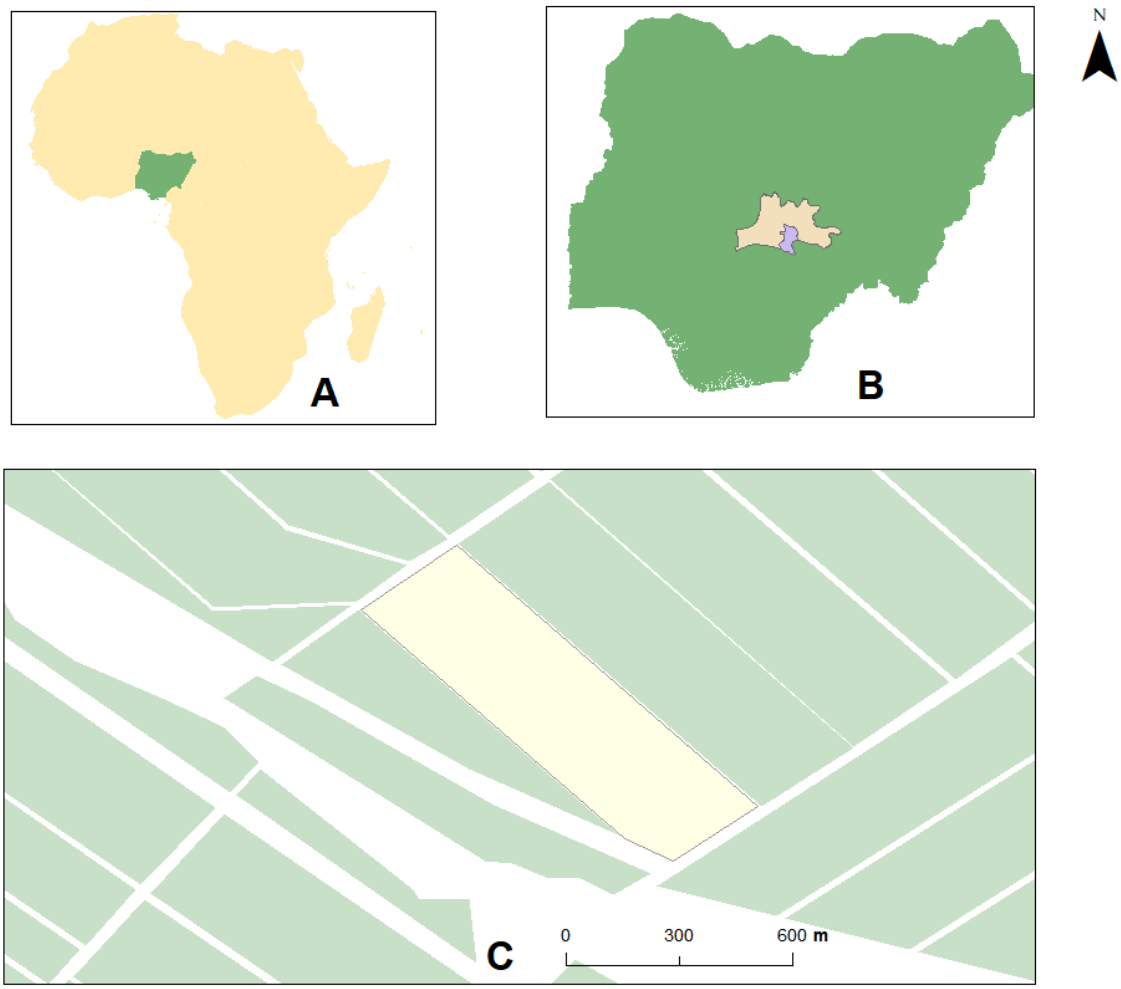

Figure 5-1: Study Area A: Nigeria. B. Specifically highlighting Doma. C. Farm showing experimental Area. The green rectangle represents the location of the 9 experimental plots

5.2.2 Experimental Design

Rice was cultivated within 27 experimental plots from December 2017 to April 2018, following a randomized split-plot design where levels of irrigation and nitrogen fertilization were varied to generate spatial and temporal variability in crop chlorophyll content and leaf area index (LAI), which is a key requirement for comparing alternative LAI retrieval approaches. The fully factorial design consisted of three irrigation regimes and three nitrogen (N) application rates. Treatments were arranged in three blocks (replications), with three plots each with three sub-plots situated within each block (3 plots x 3 sub-plots x 3 blocks = 27 sampling plots) (Figure 5-2). Each plot was 77 m long and 30m wide separated by a 2 m wide alley. Each subplot was 30 m long and 25 m wide separated by a 1 m alley (Figure 5-2).

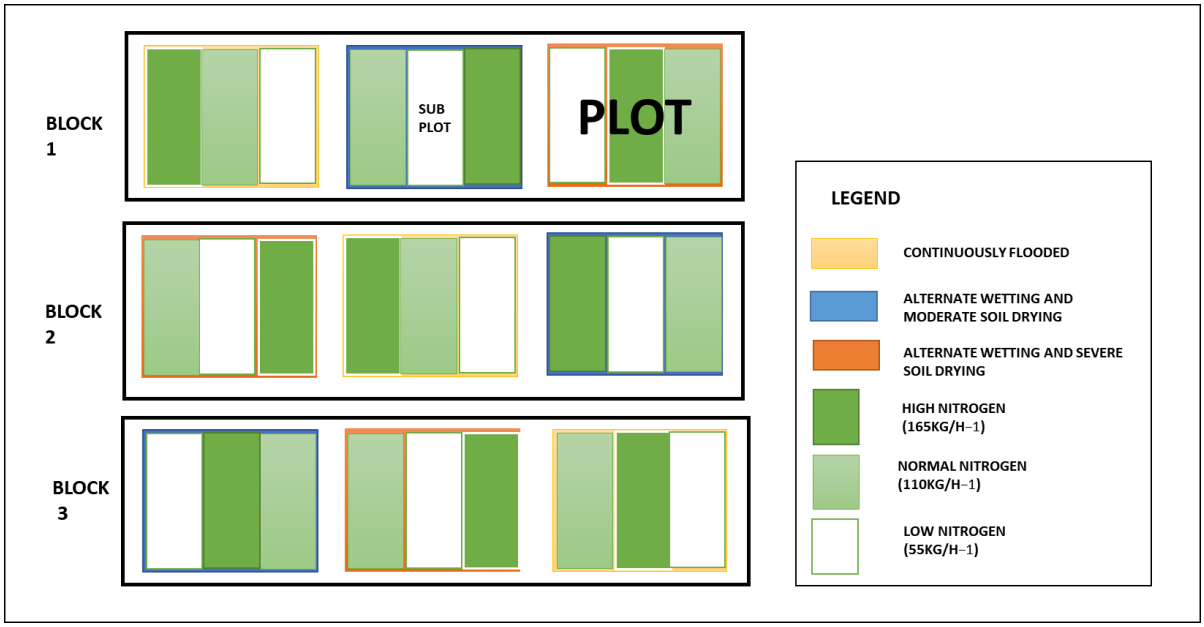

Figure 5-2: Experimental set-up for field data collection. The site was divided into 3 blocks. Each block was divided into 3 plots with each plot having 3 sub-plots. The treatments for each plot were divided into continuous flooding, alternative wetting and moderate drying and alternative wetting and severe drying. The nitrogen applications were classed as high nitrogen, normal nitrogen and low nitrogen.

5.2.3 Irrigation and Nitrogen Regimes Application across the Phenological phases on experimental Plots

Irrigation treatments consisted of three irrigation regimes, which were: (1) alternate wetting and moderate soil drying (AWMD); (2) alternate wetting and severe soil drying (AWSD); and (3) continuously flooded (CF). Except for drainage mid-season, the CF regime maintained a continuous flood with 5–10 cm water depth until one week before the final harvest as per recommended farming practices. Soil water potential was monitored at 15–20 cm soil depth with a tensiometer consisting of a sensor of 5 cm length. One tensiometer was installed in each plot of AWMD and AWSD regimes, and readings were recorded at 1200 h each day. When soil water potential reached the threshold of -10 and -15 kilopascals for AWMD and AWSD regimes respectively, a flood with 5–10 cm water depth was applied to the plots. The amount of irrigation water was monitored with a flow meter (LXSG-50 Flow meter, Shanghai Water Meter Manufacturing Factory, Shanghai, China) installed in the irrigation pipelines. Both irrigation and drainage systems were built between blocks. Each plot was irrigated or drained independently.

Nitrogen application treatments consisted of three N rates including 55, 110, and 165 kg ha^{-1}, and representing low amount (LN), normal amount (NN), and high amount (HN) of N,

respectively. Nitrogen as urea was applied at seeding phase, early tillering and at panicle initiation (the first appearance of differentiated apex). The proportion of nitrogen application was split into 30%, 40% and 40% respectively, for each of the three phenological phases (vegetative, reproductive and ripening).

5.2.4 Field Measurements

Within each sub-plot, five 1 m^2 quadrats were established for LAI measurements and the collection of field reflectance spectra. On each of the seven sampling dates (Table 1) LAI was measured within each quadrat using an LAI-2200 Plant Canopy Analyzer (LI-COR, Lincoln, NE, USA). A 45° view gap was used to avoid direct sunlight within the sensor and minimize the effects of the illumination and background conditions (Stroppiana et al., 2006). On each occasion, one above-canopy and four below-canopy radiation measurements were collected. All measurements were collected either in the early morning or late afternoon to ensure diffuse lighting conditions.

A chlorophyll content meter (atLEAF+, FT Green, Wilmington, DE) was used to non-destructively measure relative leaf level chlorophyll content. Measurements were collected on the same days as LAI. The atLEAF+ sensor is a handheld device which uses a logarithmic ratio between red and NIR light transmission (650, 900 nm; respectively). The red and NIR regions take advantage of the relationship between high absorption by chlorophyll of red radiant energy and high reflectance of near-infrared energy for healthy leaves and plant canopies. Several previous studies have used the atLEAF+ to monitor leaf chlorophyll content in crops (Novichonok et al., 2016; Padilla et al., 2018) and have compared it to the more widely used SPAD-502 meter (Konica Minolta, Inc., Tokyo, Japan) for estimating chlorophyll content (Zhu et al., 2012). Although studies have shown more accurate estimations of chlorophyll from SPAD (Novichonok et al., 2016; Padilla et al., 2018), results from Zhu et al. (2012) indicated strong correlations among laboratory leaf chlorophyll (Chl) content, SPAD values, and atLEAF values. The chlorophyll data generated were solely used to help parametrize PROSAIL (Section 2.6.1).

Canopy spectral measurements were collected using an ASD Field Spec spectroradiometer (Analytical Spectral Devices, Inc., Boulder, CO, USA). A fibre optic cable connected to the ASD with an 18° FOV was used to measure spectra from 1 m above the plant canopy at nadir. Measurements of a white spectralon panel (FSF, Edinburgh, United Kingdom) were used to

convert spectral measures of radiance to reflectance. Five spectral measurements were collected and averaged for each 1 m^2 quadrat. All measurements were made on clear, sunny days between 10:00 and 14:00. The spectral data were resampled to ten Sentinel-2 bands using the band spectral response functions available within the ARTMO software (Verrelst et al., 2012c).

LAI, Chl and spectral measurements from each of the five quadrats per sub-plot were subsequently averaged to provide one set of LAI, Chl and spectral values for each sub-plot (n = 27) per sampling date (n = 7) (Table 5-1).

Table 5-1: *Field measurements and data used for calibration and verification of the retrieval scheme. The Sentinel-2 data were acquired on the same day field measurements were conducted. Spec data – Spectral data; LAI – Leaf Area Index; Chl - Chlorophyll*

Phenology	Growth phase	Date	Days After Sowing (DAS)	ASD data	LAI	Chl	Sentinel-2
Vegetative	Early Tillering	30-01-18	37	✓	✓	✓	✓
	Tillering	04-02-18	42	✓	✓	✓	✓
	Stem Elongation	14-02-18	52	✓	✓	✓	✓
	Stem Elongation	19-02-18	57	✓	✓	✓	✓
Reproductive	Panicle Initiation	24-02-18	62	✓	✓	✓	✓
	Heading	06-03-18	72	✓	✓	✓	✓
Ripening	Milk	16-03-18	92	✓	✓	✓	✓

5.2.5 Sentinel-2 data acquisition and processing

The Sentinel-2 mission comprises of two satellites launched into orbit in 2015 (Sentinel-2A) and 2017 (Sentinel-2B), respectively. The combination of both satellites provides images every five days. Each satellite carries a Multispectral Imager (MSI) with a swath width of 290 km, and provides data in 13 spectral bands spanning from the visible and near infrared region to the shortwave infrared region, including four bands at 10 m, six bands at 20m and three bands at 60m spatial resolution (Richter et al., 2012). Sentinel-2 incorporates three bands in the red-edge region, centred at 705, 740 nm and 783 nm, respectively. Sentinel-2 MSI images were obtained from the Copernicus Open Access Hub (https://scihub.copernicus.eu/) with

dates corresponding with the dates of field measurements. The Sen2Cor Level-2A processor was used to correct Sentinel-2 Level-1C products (digital number image) for atmospheric effects to generate Level-2A surface reflectance products using the SNAP Toolbox. To retain the red-edge region in the atmospherically corrected images, we chose 20 m as the spatial resolution to resample the data to during the atmospheric correction. Details of the spectral bands retained after pre-processing can be found in Table 2.

Table 5-2: Sentinel-2 MSI band settings.

Sentinel-2 Bands	B2 – Blue	B3 – Green	B4 – Red	B5 – Vegetation Red Edge	B6 – Vegetation Red Edge	B7 – Vegetation Red Edge	B8 – NIR	B8A – Narrow NIR	B11 – SWIR	B12 – SWIR
Central Wavelength (µm)	0.49	0.56	0.665	0.705	0.74	0.783	0.842	0.865	1.61	2.19
Resolution (m)	10	10	10	20	20	20	10	20	20	20
Bandwidth (nm)	65	35	30	15	15	20	115	20	90	180

5.2.6 LAI Retrieval

Two different approaches were used to calculate LAI from Sentinel-2 imagery, (i) using a hybrid retrieval strategy from the combination of the physical based model (PROSAIL) and the GPR and (ii) using the hybrid ANN model deployable with the SNAP toolbox.

5.2.6.1. Physical based modelling

The PROSAIL model was used to build the database for training the LAI retrieval model. PROSAIL assumes the canopy as a turbid medium for which leaves are randomly distributed. The model (Jacquemoud et al., 2009) refers to the coupling of the PROSPECT leaf optical properties model (Feret et al., 2008) with the SAIL canopy reflectance model (Verhoef, 1984) and has been widely validated and used for LAI estimation (Darvishzadeh et al., 2008a; Sehgal et al., 2016; Zhang et al., 2016). PROSPECT-4 simulates leaf reflectance and transmittance for the optical spectrum (400 to 2500 nm), as a function of biochemistry and anatomical structure of the canopy and its leaves. It consists of four-leaf parameters: leaf structure, leaf chlorophyll content, equivalent water thickness and dry matter content (Feret et al., 2008).

4SAIL calculates top-of-canopy reflectance. The 4SAIL input variables are: LAI, leaf angle distribution, the diffuse/direct irradiation ratio, a hotspot parameter and the sun-target-sensor geometry.

A LUT was generated using the PROSAIL model to retrieve LAI. The LUT was generated for six fixed parameters (Table 5-3): LAI, Cab, Cm, Cw, ALA and Sun-sensor azimuth angle. Two thousand random combinations of these parameters were generated within pre-defined parameter ranges based on the collected field data. LAI, Cab, Cm and Cw were sampled using a distribution function suggested by Weiss et al. (2000). Cm, Ca, ALA and Sun-sensor azimuth angle were sampled assuming uniform distributions (Verrelst et al., 2015c)

A dataset of 69 distinct wet and dry soil samples, collected using the ASD spectrometer during the field campaign were also included in the PROSAIL simulations (Verrelst et al., 2019).

Table 5-3: Range and distribution of input parameters used to establish the synthetic canopy reflectance database for use in the LUT

Model parameters		**Range**	**Mean/standard deviation**
Leaf parameters: PROSPECT-4			
N	Leaf structure index	1.2-2.5	
LCC	Leaf Chlorophyll Content	10.0 - 55	35/20
Cm	Leaf dry matter content	0-0.03	
Cw	Leaf water content	0-0.05	
Canopy variables: 4SAIL			
LAI	Leaf area index	0.2 -9	5.5/4
soil	Soil scaling factor	0-1	
ALA	Average leaf Angle	40-80	
HotS	Hot spot parameter	nil	

The PROSAIL model top of the canopy1 1 full spectra (at 1 nm resolution) were subsequently resampled using Sentinel-2 MSI spectral response functions, to the ten bands as used in the Sentinel-2 level 2 products (Table 2).

Retrieval methods based on simulated data are not affected by noise and measurement uncertainty (Liang, 2007), which can introduce additive and multiplicative band dependent (i.e. applied to individual bands) and independent (i.e. applied to all bands) errors (Verger et al., 2011). Consequently, artificial noise was introduced into the PROSAL model LUT to

account for some of the band independent uncertainties. Specifically, white Gaussian noise was added to the output spectra, based on the noise model provided in equation (1):

$$\mathcal{R}^*(\lambda) = \mathcal{R}(\lambda).\left(1 + \frac{MD((\lambda)+MI}{100}\right) + AD(\lambda) + AI \quad (1)$$

where R(λ) and R*(λ) are the raw simulated reflectance for band λ and the reflectance with uncertainties for band λ, respectively. MD and MI are the multiplicative wavelength dependent noise and the multiplicative wavelength independent noise, respectively. AD and AI are the additive wavelength dependent noise and the additive wavelength independent noise, respectively. After some testing of additive and multiplicative noise, a value of 0.01 for AD and AI, and a value of 2% for MD and MI were used for all simulated wavelength ranges. Similar noise levels were successfully used in a recent study to reduce the over-fitting on the MLRA training database (Upreti et al., 2019).

5.2.6.2. PROSAIL model inversion using Gaussian Processes Regression

The simulated canopy reflectance data from PROSAIL was subsequently used to train a GPR model by linking the spectral information to canopy LAI.

Gaussian processes regression (Rasmussen and Williams, 2006) is a nonparametric, Bayesian regression approach, and has been successfully used for the retrieval of LAI in rice(Campos-Taberner et al., 2016). GPR is a probabilistic approximation to non-parametric kernel-based regression, where both a predictive mean (point-wise estimates of LAI) and predictive variance (error bars for the LAI predictions) can be derived. GPR offers a relation between the input (e.g., spectral data) x = [x1, . . . , xB] ∈ R^B and the output variable (i.e., LAI) y ∈ R of the form:

$$\hat{y} = f(x) = \sum_{i=1}^{n} a_i \, K_\theta(x_i x) + \alpha_\circ \quad (2)$$

where $\hat{y}$ *is LAI,* $\sum_{i=1}^{n} a_i$ are the spectra used in the training phase, $a_i \in$ R is the weight assigned to each one of them, $\alpha_\circ$ is the bias in the regression function, and K_θ is a kernel or

covariance function (parametrized by a set of hyperparameters θ) that evaluates the similarity between the test spectrum and all N training spectra.

To generate kernel regression models, a kernel function K_θ to infer the hyperparameters h and model weight $\boldsymbol{a}$ is required. Hence, we used the so-called automatic relevance determination (ARD) kernel, as an alternative generalization of the isotropic SE prior:

$$K(x_i x_j) = \upsilon exp\left\{-\sum_{b=1}^{B} \frac{X_i^{(b)} - X_j^{(b)}}{2\sigma_b^2}\right\} + \sigma_b^2 \delta_{ij} \quad (3)$$

where υ is a scaling factor, B is the number of bands, and *sb* is a dedicated parameter controlling the spread of the relations for each particular spectral band *b*. Model hyperparameters are collectively grouped in h = [m, sn, s1, . . . ,sB], and model weights $a_i$can be automatically optimized by maximizing the marginal likelihood in the training set (Rasmussen and Williams, 2006; Verrelst et al., 2012b). GPR also provides information about relevance of bands (a ranking of relevant bands), which can be used for identifying the sensitive spectral regions (Campos-Taberner et al., 2016; Jochem Verrelst et al., 2016).

5.2.6.3. Sentinel-2 Application Platform for leaf area index

Among other modules, the SNAP toolbox contains a vegetation processor module that is designed for the retrieval of LAI, canopy chlorophyll content (CCC), canopy water content, fraction of photosynthetically active radiation absorbed by the green elements of the canopy, and fraction of vegetation cover (Weiss and Baret, 2016). The principles governing the retrieval of LAI are based on the hybrid model of PROSAIL adopted for this study and the ANN models adopted as the non-parametric model for model inversion (Weiss and Baret, 2016). Based on a pre-trained neural net, at least one pure LAI pixel was retrieved in each of the experimental subplots from each of the seven Sentinel-2 images (table 1), accounting for the different phenological phases of rice growth.

5.2.7 Model Accuracy

The LUT simulated with model PROSAIL was used to train GPR into LAI retrieval models applicable to Sentinel-2. In order to assess the GPR inversion process, the model was assessed using k-fold cross-validation (k = 10). For each model, the dataset was randomly divided into 10 equal-sized sub-datasets. From these sub-datasets, 10-1 sub-datasets are selected as a

training dataset and a single sub-dataset is used as a validation dataset for model testing. The cross-validation process is then repeated 10 times, with each of the 10 sub-datasets used as a validation dataset. This way, all data are used for both training and validation, and each single observation was used for validation exactly once (Verrelst et al., 2015c). The coefficient of determination (R2), the root mean squared error (RMSE) and the normalized RMSE (NRMSE in %) were used to evaluate model fit. and predictive performance against the LAI field data.

The validation of the LAI predictions against the actual measured LAI in the field (section 2.2) i.e., how well do the predicted LAI values based on field spectral reflectance match the actual LAI measured in the field was evaluated. To evaluate the performance of both the GPR and ANN (the SNAP Sentinel-2 MSI model) models (will be referred to as GPR and ANN henceforth) with in-situ data. The coefficient of determination (R2), the root mean squared error (RMSE) were used in assessing the accuracy of the models.

To account for the accuracy in monitoring the phenological dynamics of both the GPR and ANN models based on different crop management scenarios, both the GPR and ANN LAI models were compared with corresponding field observation plots of LAI phenology patterns over the growing phases of rice.

5.3 Results

5.3.1 Temporal patterns of field measured LAI in response to Nitrogen and Irrigation Treatments

LAI values varied with nitrogen and water application rates with the highest LAI values (8.67) observed in plots with HN and CF treatment and lowest values occurring in plots with LN and AWSD treatment (1.17). Within field variability was generally low, with the exception of one subplot (B1P3SP3; see Figure 5-2) which showed high variability at the stem elongation and panicle initiation phase (Figure 5-3).

Plots that were continuously flooded (CF) showed increasing LAI values across the different phenological phases despite the variation in nitrogen application within the subplots. However, LAI values within AWMD and AWSD plots declined when soil water levels were low (Figure 5-3), likely due to the effects of water stress on plant development. These reductions in LAI were observed particularly during the stem elongation phase (see Table 5-1). In 11 out of the 18 subplots where irrigation applications were altered declines in LAI values occurred during the vegetative phase. For example, at 57 Days after Sowing (DAS) showed a decline in LAI

values for plots with alternating water applications as irrigated water was allowed to drop to -10 and -15 kilopascals for the AWMD and AWSD plots respectively.

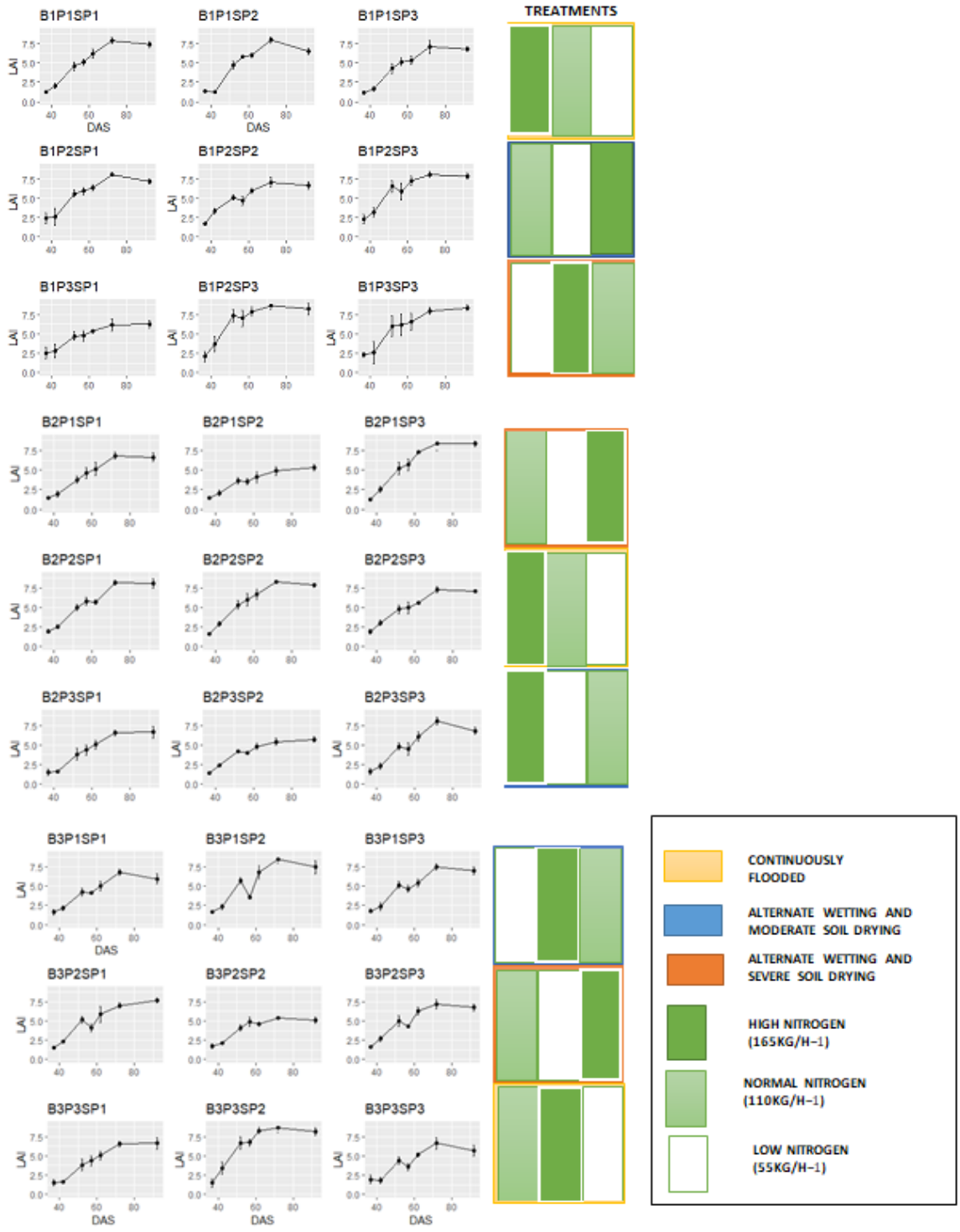

Figure 5-3:LAI phenology profile for each experimental subplot with errors bars. ***B*** *represents the block in which each plot is represented.* ***P*** *represents the Plot in which all the sub-plots are represented.* ***SP*** *represents the individual subplots found in each plot. In total, there are 27 subplots.*

When considering the nitrogen application to each subplot (Figure 5-3), it was observed that nitrogen application was an important determinant of LAI dynamics over space and time (Table 5-1). For instance, B2P1SP2 is characterised by low nitrogen application and AWSD irrigation regime while B2P1SP3 is characterised by high nitrogen application and AWSD irrigation regime. The LAI dynamics show higher LAI during the reproductive and ripening phases with high nitrogen application as compared to low nitrogen application. Similar results were observed when looking at B2P3SP2, which is characterised by low nitrogen application and AWMD irrigation treatment to B2P3SP3 subplot, characterised by normal nitrogen application and AWMD irrigation treatment. Nitrogen played a significant effect in the LAI profiles on both plots with significantly high LAI during the reproductive phase in the normal nitrogen subplots compared to low nitrogen subplot. However, each plot irrespective of nitrogen and irrigation treatment peaked during the reproductive or ripening phenological phase of irrigated rice growth.

5.3.2 PROSAIL-GPR LAI Retrieval Models Validation

The GPR model performance was evaluated against the simulated data. The hybrid GPR model explained 65% of variance in LAI estimation (RMSE 1.21)

The red-edge bands, near-infrared and short-wave infrared bands were most significant in model development, whilst the Blue and Green bands in the visible portion of the electromagnetic spectrum contributed least to the model (Figure 5-4) .

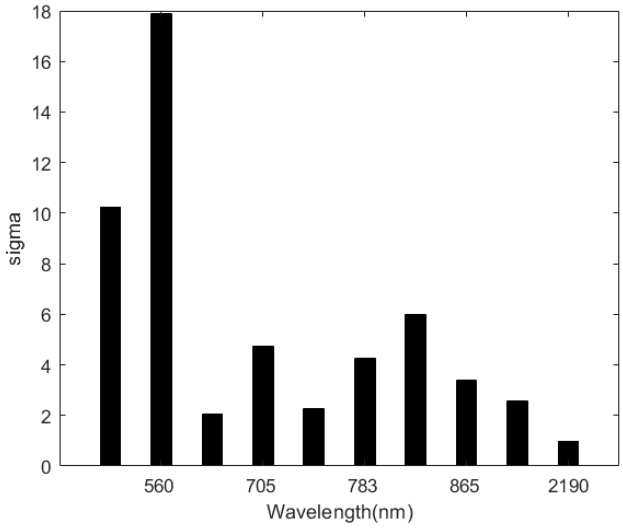

Figure 5-4: Relevance band histograms for Sentinel-2 simulated bands using GPR model. The lower the sigma the more important the band.

5.3.3 Validation of PROSAIL-GPR and Sentinel-2 LAI vs Measured LAI

When considering the performance of the hybrid models for predicting LAI phenology against in situ data, the GPR model explained 82% of LAI variation in the model with an RMSE of 1.65 for the entire season. The regression line deviated from the 1:1 line as LAI values increased, leading to underestimation at high LAI values (Figure 5-5). When validating LAI at the vegetative and reproductive phases, similar trends were identified, with regression lines deviating from the 1:1 line with increasing LAI (Figure 5-5). For the ripening phase, model results showed a relationship between measured and estimated LAI (R^2 = 0.57) however, predicted LAI values were underestimated compared to actual field observation (Figure 5).

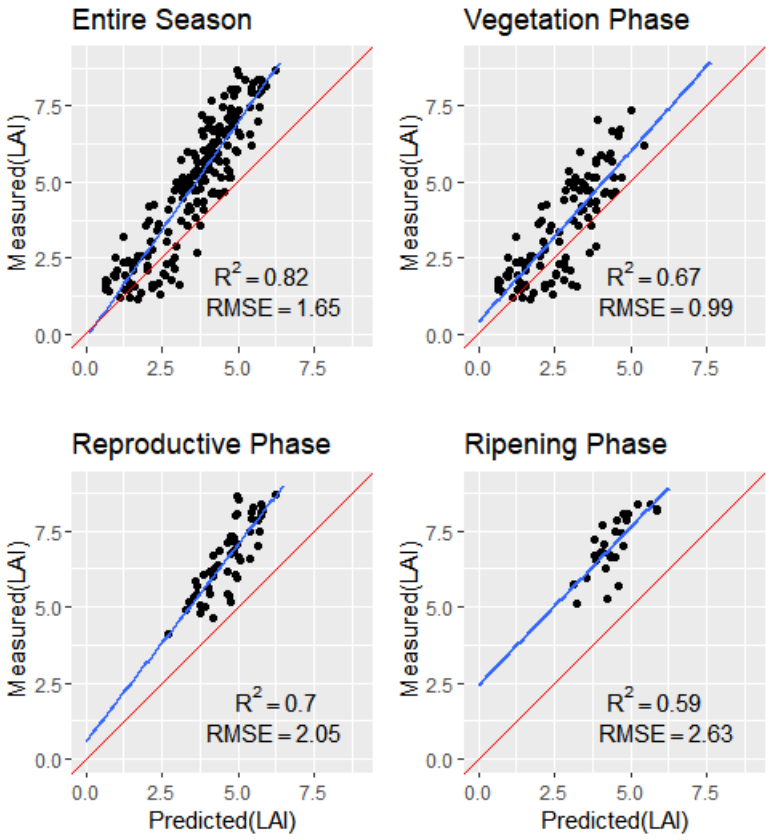

*Figure 5-5:*Measured versus predicted LAI from GPR PROSAIL for the entire season (n=189), the vegetative phase (n=108), the reproductive phase (n=54) and ripening phase (n=27).

When evaluating the ANN model with in-situ LAI measurements, the ANN model explained 66% of model variation, albeit under-estimating LAI during of entire phenological phases, leading to an RMSE value of 3.89. Similar under-estimation trends were found during the reproductive and ripening phases explaining 58% and 33% respectively (Figure 6).

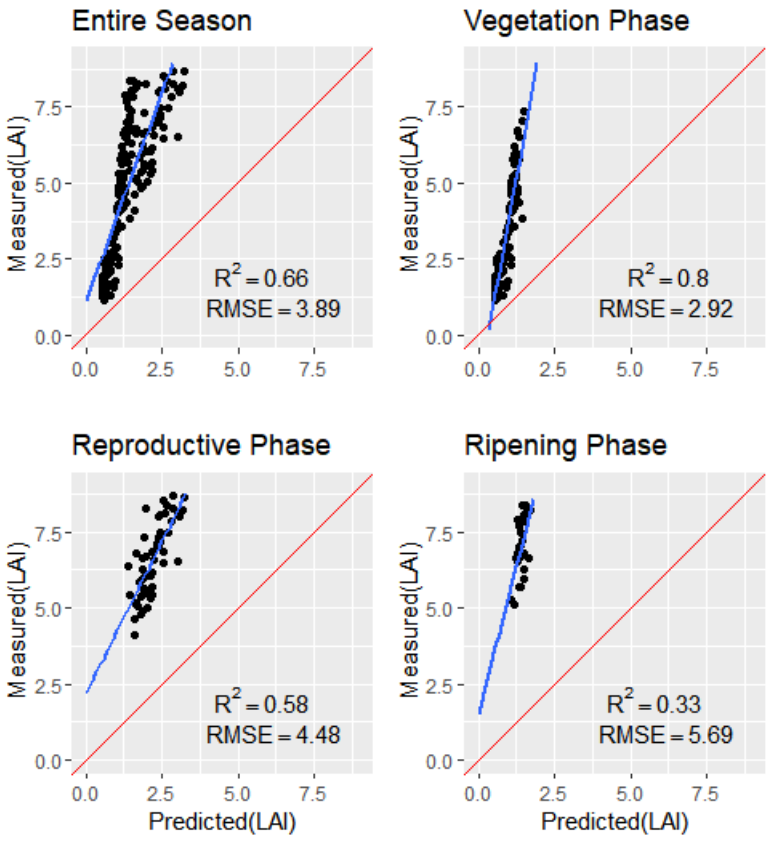

Figure 5-6 Measured versus predicted LAI from ANN model for the entire season (n=189), the vegetative phase (n=108), the reproductive phase (n=54) and ripening phase (n=27).

5.3.4 Temporal Profile of LAI across altered irrigated and nitrogen regimes

From the analysis of Low Nitrogen (LN) and Alternative Wetting and Severe Drying (AWSD) subplots, GPR and ANN showed similar profiles during the vegetative phase, however, a general under estimation was identified in both models. The transition from the vegetative to the reproductive phase showed a rapid increase of in-situ LAI. The GPR model showed much higher LAI profile transition, with a decline in LAI values observed in some plots due to the alternative wetting and drying approach adopted. However, there was still underestimation of LAI compared to in-situ measurements. On the other hand, LAI values were consistently low, with peak LAI below 2.4 with the ANN model. These peak values are usually attributed to the reproductive phase, showing a high discrepancy between actual ANN LAI phenological with in situ LAI in Figure 5-7.

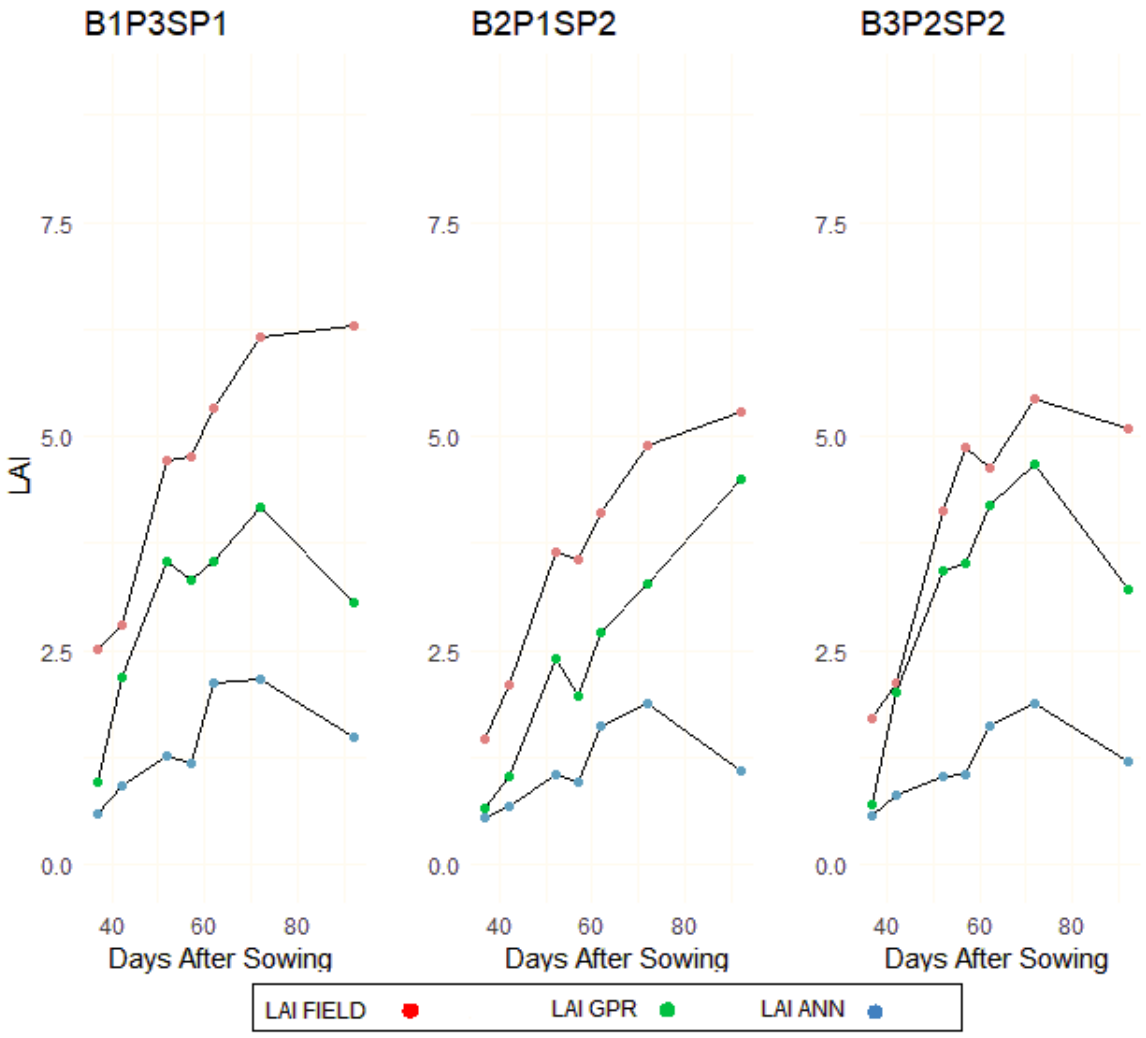

Figure 5-7: Experimental subplots characterised by Low Nitrogen and Alternative Wetting and Severe Drying (AWSD) regimes

The subplots with High Nitrogen (HN) and Continuous Flooding (CF) showed similar results for the GPR model compared to in-situ measurements (Figure 5-8). From the tillering phase, underestimation of LAI values were more evident from the ANN model compared to the measured LAI and GPR estimates. Transitioning to the reproductive phase showed a sharp rise in the LAI profile of subplots with the same nitrogen and water treatments. The GPR results exceeded LAI values of 6, although a general underestimation was the general pattern from the predictive model. In terms of the ANN model, the underestimation was more obvious from the ANN model for the three subplots during the reproductive phase. For the ripening phase, a general decline in LAI was identified compared to in situ measurements for the two hybrid models, however, the pattern of underestimation was more evident with the ANN model (Figure 5-8).

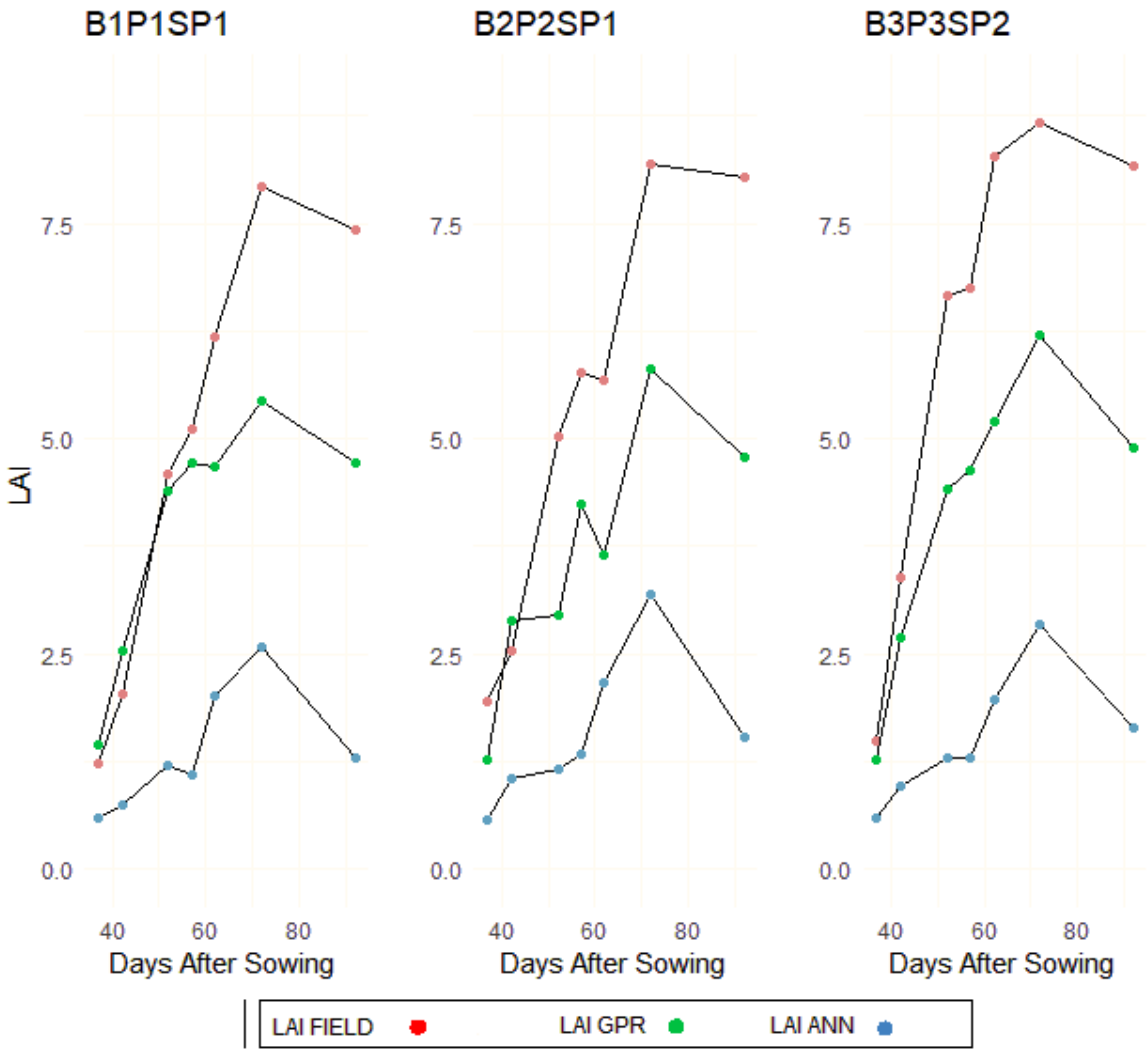

Figure 5-8: Experimental subplots characterised by High Nitrogen and Continuous Flooding (CF) regimes

We assessed plots with normal nitrogen (NN) distribution and Alternate Wetting and Moderate Drying (AWMD) plots. These plots were chosen because there may be a tendency for plots to have reduced water supply due to inadequate irrigation systems or drop in water levels at storage point when growing rice. The same patterns identified in Figure 5-7 and 5-8 were reflected in this category, except for the GPR model in the vegetative phase. For subplots B2P23SP3 and B3P1SP3, the GPR model showed overestimation in one of the plots and underestimation of LAI in the other two plots early in the vegetative phases (Figure 9). Nevertheless, underestimation was also identified in Figure 5-9 during the reproductive and ripening phases. The ANN model estimation of LAI was consistently low as identified in the other phases (Figure 5-9).

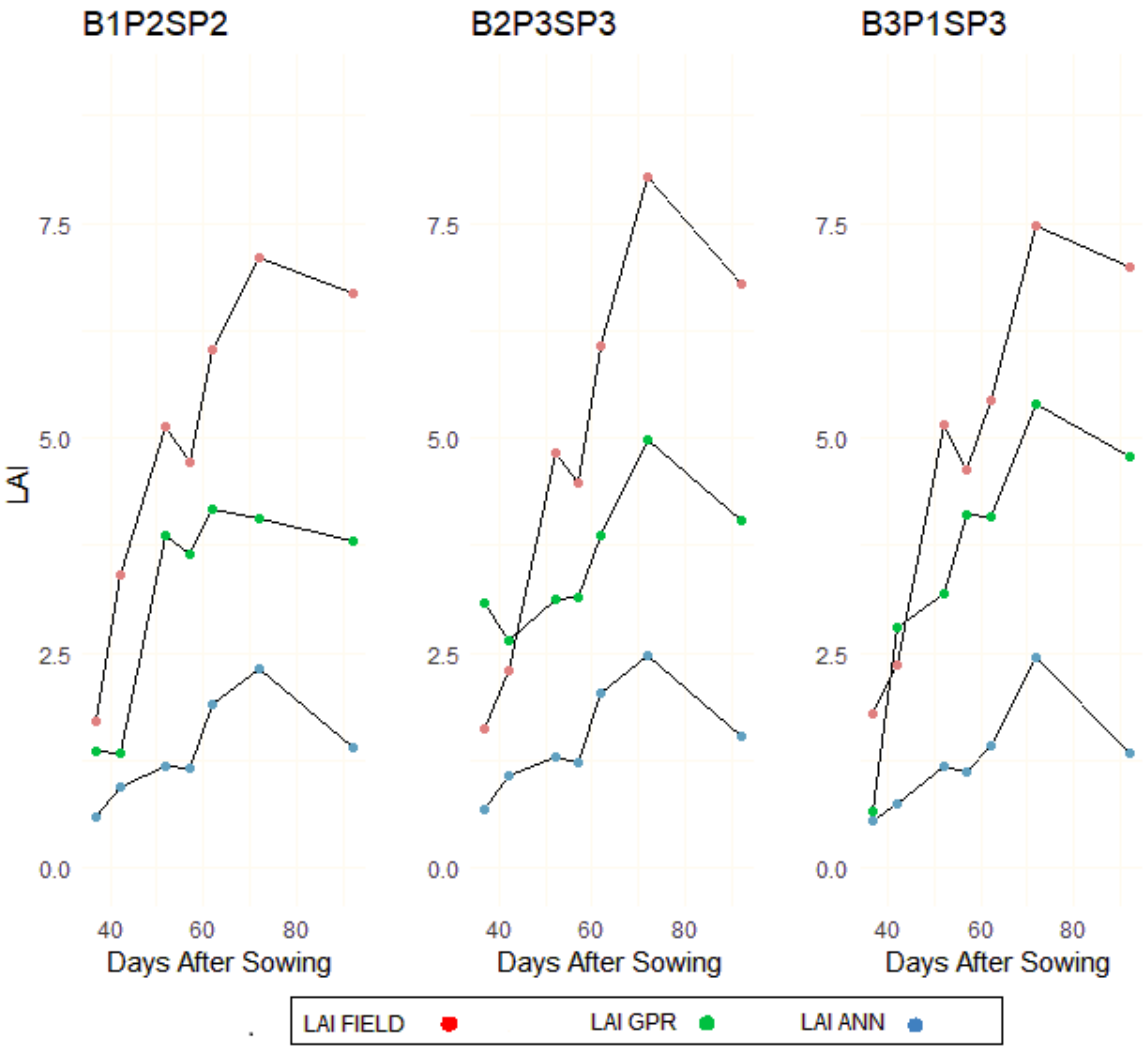

Figure 5-9: Experimental subplots characterised by Normal Nitrogen and Alternative Wetting and Moderate Drying (AWMD) regimes

In summary, ANN and GPR models generally show the same phenological profiles compared to in-situ data, however, the underestimation in ANN models was more significant when estimating the phenology patterns for different nitrogen and irrigation regimes. The same limitations were identified with the GPR model, although the GPR model estimations of rice LAI phenology showed higher variations in LAI results similar to in-situ measurements.

5.4 Discussion

LAI has been identified to have a strong relationship with yield, leading studies to investigate and estimate LAI in order to understand yield trends and patterns(Fang et al., 2014; Gilardelli et al., 2019). With the launch of Sentinel-2, acquiring high spatial, spectral and temporal resolution images as key growth phases of rice has become possible. This study focused on a

hybrid retrieval approach by combining the machine learning regression model GPR with PROSAIL simulations for estimating the phenology dynamics of rice LAI over altered irrigation and nitrogen regimes. Furthermore, we assessed the retrieval performance generated by SNAP, which consists of Artificial Neutral Network (ANN) trained by PROSAIL simulations, to understand the seasonal dynamics of rice LAI.

The GPR model showed a positive relationship (R^2 = 0.65) between the model built from Sentinel-2 data based on the spectral bands and angular configuration in terms of coefficient of determination and RMSE. The relationship of the GPR model at high LAI may have taken into account the addition of soil spectra and noise for optimization of model performance. Similar strategies have been adopted to improve the retrieval estimates of LAI (Campos-Taberner et al., 2016). However, limited variation in soil spectral led to overestimation of LAI when LAI values are low, which aligns with results suggested by Verrelst et al. (2015) as obtaining limited soil spectra variation from the experimental area would be limiting. One approach to be considered in future should capturing a larger variation in soil type, moisture content, the geometric configuration, as well as the roughness of the soil (Jacquemoud et al., 1992). From the trained GPR model, it was possible to identify the most significant spectral bands for LAI retrieval. The bands along the red edge, near-infrared and short-wave infrared, were more importance compared to the blue and green bands along the visible part of the electromagnetic spectrum as shown in Figure 5-4. The results observed were in agreement with earlier observations (Darvishzadeh et al., 2008a; Delegido et al., 2011; Verrelst et al., 2015b).

When validating the GPR and ANN models against in-situ LAI measurements, the GPR PROSAIL model exhibited a better agreement with in-situ measurements compared to ANN across the entire growing season (Figure 5-6 and 5-7). The improvement may be greater because of the transparent nature of the GPR model, which allows the use of simple to complex kernel functions for parameterisation of the model, while also providing uncertainty estimates of the mean value of prediction (Upreti et al., 2019). Further investigation into the phenology phases of growth saw improved estimation accuracy from the GPR model as compared to ANN PROSAIL during the vegetative, reproductive and ripening phases. In terms of the ANN model accuracy, the RMSE may present a bias due to trends in time series data. The ANN model displayed consistently low LAI estimates through all growing phases, leading to high model bias between estimated and predicted values of the entire season and particularly during

the reproductive and ripening phases (Figure 5-8 and 5-9), with underestimation of LAI apparent at each phenology phase.

Operational LAI products (Sentinel-2 and MODIS) have been identified to provide underestimated LAI in different seasons (Xie et al., 2019b). This was evident when assessing the phenological patterns of rice LAI in this study. LAI values remained below 4 in plots with increase irrigation and nitrogen supplies. PROSAIL models have shown to underestimate LAI in dense vegetation (Verrelst et al., 2015b), even though they have shown to be compensated when inverted with machine learning algorithms (Campos-Taberner et al., 2016). Although GPR and ANN models underestimated LAI, especially during the reproductive and ripening phases as shown in Figure 5-7, 5-8 and 5-9, the GPR phenology patterns were closely related to in-situ measurements, with some plots showing overestimation during the vegetative phase (Figure 9).

At the vegetative phase, LAI of rice subplots with adequate water supply at elevated carbon dioxide concentration increases as a result of rapid leaf production in the vegetative growth phase (Grashoff et al., 1995). This was identified in CF plots with high and normal nitrogen applications in Figure 3. This applies particularly for indeterminate growing species and under nonlimiting supply of nutrients. This was also evident in plots where water supplies were withheld for a couple of days during the vegetative phase despite a dip in LAI values. Although the GPR and ANN models identified similar field observation LAI patterns, underestimation was evident during the vegetative phase. During the reproductive phase, LAI at full heading increased with increasing nitrogen rate, which also ushers the climax of LAI values (Sharma and Yadav, 1999). Figure 5-3 shows similar results with rice LAI reaching peak in most of the subplots and the rise of LAI curve as a result of the nitrogen application. The GPR model accounted for an increase in LAI values up to 6. On the other hand, the ANN model did not exceed LAI values of 4 during the heading phases. Previous studies that have assessed the performance of the ANN model have compared model performance against LAI values less than 4 (Pasqualotto et al., 2019; Xie et al., 2019b), although LAI results have also been seen in other studies to exceed 4 with the exception for (Vanino et al., 2018; Xie et al., 2019b). Therefore, further validation of the models is imperative in other locations. The ripening phase ushered in a sharp decline of LAI due to translocation of accumulated plant reserves to the panicle (Sharma and Yadav, 1999). This was evident in the in-situ LAI measurements and the GPR and ANN models. However, underestimation was observed in the GPR model with higher underestimation in ANN LAI. The underestimation results obtained from both models

may have been as a result of changes in spectral reflectance over a relatively small portion of the experimental subplots (experimental sub-plot > 0.5ha) leading to anisotropy effects of reflectance based on the spatial resolution of Sentinel-2. Furthermore, ANNs are black box in nature, and can be unpredictable if training and validation data deviate from each other even slightly (Verrelst et al., 2015c). Whereas, GPR provides insights in bands carrying relevant information and also in theoretical uncertainty estimates, thus partially overcoming the black box problem.

Despite the superior performance of GPR for estimating LAI, GPR is computationally expensive if trained on large sets of simulations (Upreti et al., 2019; J. Verrelst et al., 2016) and will not necessarily alleviate the limitations of RTMs, such as the ill-posed inverse problem or the constrained model's capability of reproducing the measured (canopy bidirectional) spectral signals (Berger et al., 2018). Yet, GPR major benefit entails providing a comprehensive training data base for the machine learning regression model without the necessity of in-situ data collection (although this is still required for validation). Furthermore, the LUT can be modified based on the specific application by implementing existing knowledge and concepts of experienced users

Finally, to combat spectral reflectance issues due to experimental plot sizes, future studies should investigate the retrieval of GPR and ANN models over different phenology phases to understand LAI dynamics in a bid to improve global LAI estimation. Furthermore, developing models for specific regions should be investigated in future studies.

5.5 Conclusion

This study focused on determining the potential of PROSAIL and Gaussian Processes Regression (GPR) for estimating the phenological dynamics of irrigated rice LAI from Sentinel-2. We also identified the most significant bands for estimating LAI from Sentinel-2 and mapped LAI. In terms of the most significant bands, the red edge, near-infrared and short-wave infrared bands were identified as the most significant for estimating LAI from Sentinel-2. Subsequently, we compared the performance of hybrid GPR and hybrid ANN model generated from Sentinel-2 Application Platform (SNAP) for estimating the seasonal LAI dynamics of rice fields with altered nitrogen and water applications at different phases of crop growth.

The GPR model outperformed the ANN model in LAI estimation while at the same time offering uncertainty estimates. Similar results were obtained during the vegetative,

reproductive and ripening phases. Further, in the analysis of both models, ANN LAI showed gross underestimation of LAI, particularly in the reproductive and ripening phases of LAI development. On the other hand, GPR showed some overestimation during the vegetative phases. However, LAI growth curve was much closer to in-situ measurements when using GPR compared to ANN during the reproductive and ripening phases, with less underestimation. Results suggest that the GPR model can successfully estimate the phenological dynamics of rice in altered management practices. The study opens opportunities for further studies in other crop types, regions and growing seasons in other to validate and improve global LAI estimation.

Chapter 6 The influence of baseline Sentinel-2 data for predicting high resolution Irrigated dry season rice yield

Abstract

Accurate estimation of yield is essential towards attaining proper crop management, food security evaluation and policy implementation. With varying land sizes available for rice cultivation, appropriate yield estimation approaches from smallholder to landscape scales is imperative towards comprehensive yield assessment. This paper provides a novel demonstration of monitoring the spatio-spectral influence of baseline Sentinel-2 10m and 20m Multispectral Imager (MSI) for monitoring within and between field variability at smallholder and landscape scales using Random Forest (RF) models. To monitor yield, 48 management fields (combined total at 1150ha) were selected to monitor yield at landscape scale. Simulated smallholder farm plots were generated across the 48 management fields based on the following smallholder farm categories: 0 – 1 ha, 1 - 2 ha, 2 – 5 ha and 5 - 10 ha. The RF models were trained and validated using yield dataset containing over 51,000 points for 10m resolution data and over 13,000 points for 20m collected by combine yield harvester monitors. Results show that the RF model trained with the inclusion of Sentinel-2 red edge bands and Normalised Difference Red Edge (NDRE) performed better than the RF model without the red edge bands and index at 20m resolution. However, with validation data at 10m, the RF model trained with Sentinel-2 10m bands and Normalised Difference Vegetation Index (NDVI) produced the most accurate estimation of irrigated rice yield at landscape scale. Sentinel-2 MSI was able to predict between field variability of farm plots from 0 – 10 ha with model errors ranging from 0-26 – 0.41 t/ha. The results highlight the promising potential of baseline Sentinel-2 MSI for predicting within and between field variability in dry season irrigated rice farms across farm scales.

Keywords: Yield, Sentinel-2, Rice, smallholder farms, Landscape scale, Random Forest

6.1 Introduction

Rice is an important staple crop, contributing significantly to the dietary needs of households globally(OECD-FAO, 2019). Over the past three decades, sub-Saharan countries have seen consistent increase in rice demand and increased emphasis on expanding rice production in strategic food security planning policies (O'Donoghue and Hansen, 2017). With the increasing demand and expanding production of rice, it has become imperative to adopt sustainable measures of rice growth while also increasing yields. One of such measure is increasing the amount of rice grown during the dry season months to supplement rice production during the rainy season (Kurukulasuriya et al., 2006). The increasing possibility of growing rice multiple times yearly, accurately monitoring the variability of within and between field yield is not only important towards understanding yield patterns but also towards improving rice production (Kuenzer and Knauer, 2013).

The size of available farm land also plays a major role in controlling where rice is grown, both in sub-Saharan Africa and globally (GRiSP, 2013). As such, Lowder at al. (2016) classified farms sizes in hectares(ha) as small (<20ha), medium (20 – 50ha) and larger (>50ha) farms. In terms of small farms (usually referred to as smallholder), the definition of smallholder agricultural land differs amongst countries, primarily due to the socioeconomic and agroecological setting (Giordano et al., 2019). For instance, a smallholder rice farm in sub-Saharan Africa may differ from a smallholder rice farms in Asia. Farm sizes are often larger in high income countries such as Australia and United States than in those with medium to low income countries, including Ghana and Nigeria (FAO, 2014; Giordano et al., 2019). Nevertheless, over 80% of farmlands are less than 2ha in size with 72%, below 1 ha globally (Lowder et al., 2016). Although these farms are small, their number across the global is such that smallholder farms (< 2 ha) contribute more than 64% of global rice production (Samberg et al., 2016). Large farms (>50ha) also play a significant role in global rice security (Lowder et al., 2016) as the hold majority of available farms for farming with strong potential to boost rice production. Therefore, there is a need for yield monitoring techniques that work across scales, and in particular for small-scale plots that represent the main component of rice production in Nigeria and wider W Africa/SSA.

Hence, effective monitoring and timely prediction of yield across farms scales is thus needed to provide detailed information on the success of current farming practices and to identify areas that may benefit from management interventions (Samberg et al., 2016). Still, monitoring of rice yields across farms scales are often challenging as yield estimates are largely reliant upon the results of intensive field surveys that are both constrained regarding representativeness and reliability of yield estimation often leading to misrepresentation of actual yield outcomes (Lambert et al., 2018).

One alternative for monitoring rice yield is through Earth Observation (EO) satellites. Earth Observation data has been extensively used for predicting crop yields across vary scales (Azzari et al., 2017; Jin et al., 2017b; Lobell, 2013). Low spatial resolution satellites (< 250m) have been used to predict yield in rice. One such satellite is the Advanced Very High-Resolution Radiometer (AVHRR; 1.1 km spatial resolution), which has been utilised to predict rice yield. For instance, Bastiaanssen and Ali (2003) utilised AVHRR data to predict regional rice yield in Pakistan, which were validated with county data. In addition to AVHRR, the Moderate Resolution Imaging Spectroradiometer (MODIS; ≤ 250m) has been utilized for yield estimation partly due to the temporal and spectral resolution of the sensor. Ren et al. (2008)

predicted crop yield using a MODIS-NDVI based model at regional scale with a 250 m spatial resolution in China. Predicted yield using MODIS-NDVI results showed that the relative errors of the predicted yield were between 4.62% and 5.40% and that RMSE (214.16 kg ha/1) was lower than the RMSE (233.35 kg ha/1) of an agro-climate models at country scale. However, the spatial resolution of low spatial resolution satellite sensors makes them unsuitable for field to landscape scale yield monitoring.

In an attempt to overcome the spatial limitations of low-resolution satellite sensors, medium to high spatial resolution satellites have been adopted extensively for the prediction and estimation of yield (Gilardelli et al., 2019; Guan et al., 2018; Siyal et al., 2015). Notably, Landsat satellite has been the preferred option for many researchers and field observation experts due to the free availability of data, spanning over more than 40 years. While Landsat's spatial resolution makes it well suited for yield estimation in smallholder environments, accuracy of yield estimates is constrained by the long return period (16 days) between overpasses. Combined with cloud cover effects, Landsat's limited temporal resolution can lead to gaps in image acquisition during critical periods of crop growth (e.g. mid to late season for rice) reducing accuracy of resulting yield estimates (Fageria, 2007). Although measures have been adopted to fuse the daily temporal resolution obtained from MODIS and 30m spatial resolution from Landsat (Feng Gao et al., 2006; Gevaert and García-Haro, 2015; Moreno-Martínez et al., 2020), the performance depends on the characteristic size of the landscape and degrades to some extent when used on extremely heterogeneous fine-grained landscapes (Feng Gao et al., 2006). Alternatively, studies have shown the potential benefits of leveraging very-high temporal and spatial resolution from commercial satellites such as Worldview, Geoeye and IKONOS for yield estimation (Burke and Lobell, 2017). However, applicability of these approaches is constrained by both high image acquisition costs – further exacerbated by the swath width of most of the high-spatial resolution sensors (Spatial resolution 1-4m) that requires many images to be purchased for a specific production area (Joseph, 2015).

The launch of Sentinel 2A in 2015 and 2B satellites in 2017, serves to breach the gap between the provision of low and very high-resolution satellite imagery. The Multispectral Instrument (MSI) onboard the Sentinel-2 platforms, measures the Earth's reflected radiance in 13 spectral bands ranging from the visible to the infrared at spatial resolutions up to 10m. The inclusion of spectral bands located within the red edge region of the spectrum is of particular relevance given that reflectance in the red edge region is known to be closely related to vegetation chlorophyll content (Delloye et al., 2018; M. Zhang et al., 2019) and thus this region has great

potential for monitoring crop condition and yields (Drusch et al., 2012). For instance, Sentinel-2 has been used to estimate yield indicators like Leaf Area Index (Korhonen et al., 2017; M. Zhang et al., 2019), Chlorophyll Content (Ansper and Alikas, 2019; Clevers et al., 2017; Delloye et al., 2018), fraction of vegetation cover (Djamai et al., 2019) and biomass (Darvishzadeh et al., 2019; Pahlevan et al., 2020; Punalekar et al., 2018). Compared to freely available satellites like Landsat and SPOT and commercial satellites like Worldview and IKONOS with no spectral bands along the red-edge, Sentinel-2 is spectrally superior to these satellites. Sentinel-2 also has a higher temporal resolution compared to Landsat (5days compared to 16 days), which enables imagery to be acquired at multiple points in time throughout the crop growing season (cloud cover permitting). Although some commercial and freely available satellites have a higher temporal resolution (e.g. WorldView-2, 1-4 days; MODIS, 1 day), the trade-off between the spatial resolution and temporal resolution of Sentinel-2 makes them better suited for seasonal phenological yield estimation across varying scales (Segarra et al., 2020). When using Sentinel-2 for agricultural applications, a user must make a choice about whether to utilise 10m or 20m resolution imagery provided by the satellite. 10m imagery provides more spatial granularity, but comes at the cost of a reduced range of spectral bands. Evaluating this trade-off, and specifically its implications in the context of yield estimation at different spatial scales (e.g. plot-level yield versus yields averaged over a larger spatial area), is the main focus of this study. In doing so, I address a key gap in scientific knowledge about how to best leverage Sentinel-2 imagery for rice yield estimation at farm to landscape scales, considering in particular the relative spatial and spectral properties of Sentinel-2 at different scales of estimation.

Crop yield monitoring from satellite imagery is often undertaking using either crop growth models, which often combine detailed ancillary data regarding local weather, soil, plant and management practices with derived from satellite imagery or empirical models, and a spectral Vegetation Index (VI) derived from the reflectance characteristics of the crop surface (Bai et al., 2019; Feng et al., 2016; Johnson et al., 2016). Whilst yield estimations from detailed crop models often provide yield estimations with high accuracy (Ines et al., 2013; Jin et al., 2018), the practicality of this approach is often limited to smallholder farmers due to difficulties faced in obtaining the data required to run such models effectively (Burke and Lobell, 2017; Lambert et al., 2018; Lobell, 2013; Morel et al., 2014). In contrast local calibrated empirical models, based on spectral bands and vegetation indices are simple and comprehensive regression models which require baseline satellite data (i.e. spatial and spectral resolution of MSI) for

predicting yield (Lambert et al., 2018) are more suitable for monitoring at much across various scales. For instance, Jin et al. (2017b) compared a crop model calibrated with empirical data with a crop model based on data generated from the crop model. At the local scale, results of the empirically calibrated model were similar to those generated with the crop model (Jin et al., 2017b). Consequently, achieving robust smallholder landscape yield predictions is important in developing countries, notably where subsistence agriculture still determines food security, and for profitable farmer participation in more largescale rice farming.

Therefore, it remains to be seen the significance of baseline Sentinel-2 spatial and spectral properties for accurately predicting yield at landscape and based on smallholder farm scale. The aim of the study to understand the potential of Sentinel-2 MSI imagery for estimating within field variability at landscape scale and between field variability at smallholder farm dry season rice yields using the Random Forest model.

6.2 Materials and Methods

6.2.1 Study Area

The study was conducted on a homogeneous rice farm in Nasarawa state, Nigeria (for full description of the farm see Section 3.1 in Methods chapter). The predominant soil parent materials in the area are derived from the cretaceous sandstone, siltstone, shale and ironstone of the Precambrian to Cambrian (Samaila and Binbol, 2007). The study area has a tropical climate, with two distinct seasons: the wet (rainy) season lasts from the end of April to October, while the dry season is experienced between November and March. Maximum temperatures can reach 39 °C (March), while minimum temperatures in the study area can drop as low as 17 °C (December, January).

The size of the farm is 1150 ha, split into 48 fields with sizes ranging from 20 ha to 35 ha. Lowland Aerobic rice from the NERICA (NEw RICe for Africa) rice program (a combination of *Oryza sativa* + *Oryza glaberrima*) were cultivated. The NERICA Faro 61 and NERICA Faro 44 varieties were cultivated on the farm due to their ability to grow in the event of drought and weed infestation. Both varieties have early maturing harvest (< 110 – 120 days) and have been successfully used for irrigation farming (Nguezet et al., 2013). To cater for the water demands during the dry season, water was obtained from River Benue (approximately 5 km from the study site) and used to support irrigation during the growing season. Despite the commercial size of the farm, working practices are representative of smallholder farmers in the region and equally representative of regional soil and crop management practices. For

instance, the timing of application of Urea, Fertilizer and pesticides are similar to practices conducted by smallholder farmers.

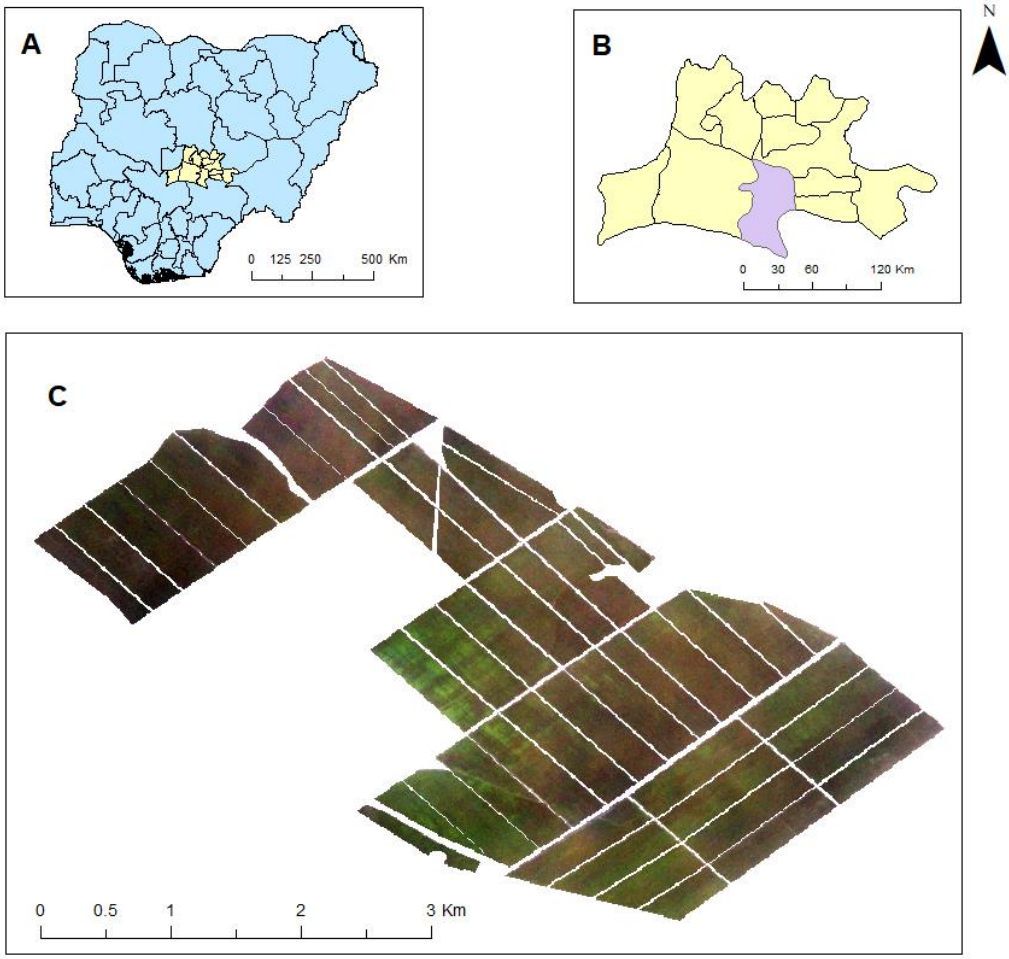

*Figure 6-1:*A. Map of Nigeria highlighting Nasarawa state. B. Doma local government area highlighted (purple) within Nasarawa state. C. 1150ha rice farm in true colour composite used as the study site for the research.

6.2.2 Rice Yield Data

Rice yield data was collected as validation for the Sentinel-2 yield estimation models from Sentinel-2 10m and 20m. Figure 6-2 represents the methodological approach adopted for the study.

High resolution point yield data were obtained from three combine harvesters equipped with Differential GPS (DGPS) receivers from the 48 fields during the period 18th to 28th of March 2019, the extended period of yield collection was due to the size of harvesting area (1150ha) and farming logistics. Prior to data collection, each of the combine harvesters was calibrated based on recommendations from CASE IH 9230 combined harvester manual(Case IH, 2018).

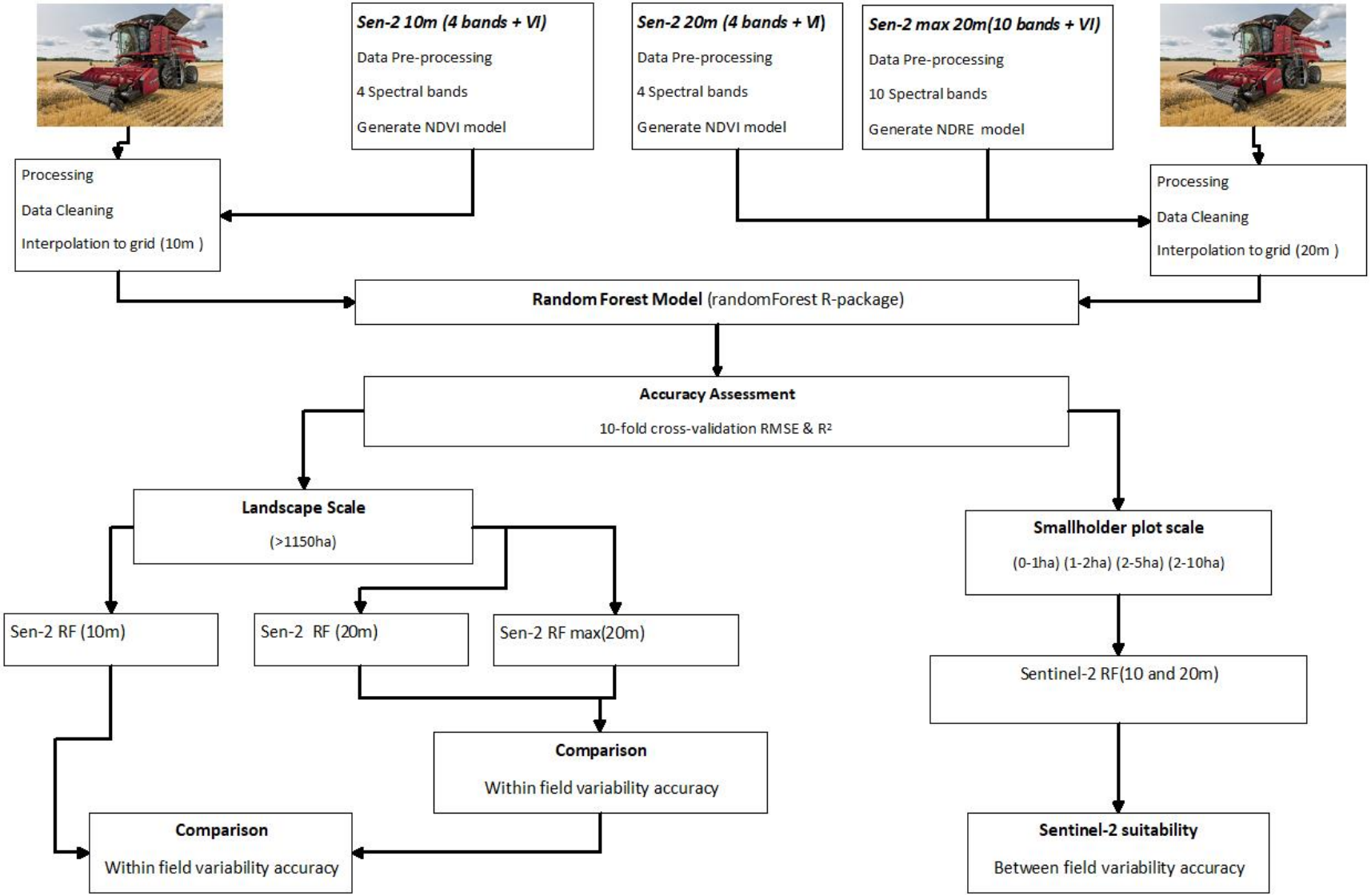

Figure 6-2: Methodological flowchart used in predicting yield at landscape and smallholder scale using Sentinel-2

The yield data were subsequently cleaned to remove values recorded when the combine harvesters speed fell outside the optimum limits to accurately measure the yield (ground speed <2 km h−1 or >8 km h−1) which may lead to inaccurate yield values (Hunt et al., 2019). The cleaned yield data were resampled to grid resolutions of 10 m and 20 m to match the spatial resolution of the Sentinel-2 MSI imagery, using an Inverse Distance Weighting function (Hunt et al., 2019). The appropriateness of mapping yields at these resolutions was supported by the relative uniformity of points and the short distances between individual yield measurements (mean nearest neighbour of 11 m). In addition, a major factor limiting the spatial resolution of yield estimations, is the width of the combine harvester's cutting head, which determines the minimum acceptable resolution for subsequent yield data aggregation. The cutting widths for the combine harvesters used in this study ranged from 9.1 m to 12.27 m, indicating that data is of sufficient resolution to be used as observational data in comparison with satellite-derived yield maps at both 10 m and 20 m spatial resolution.

The resultant 10 and 20 m spatial resolution yield maps were sub-sampled (using alternate yield pixels to reduce the impact of correlation between pixels) to generate two yield datasets (52,520 and 13,135 pixels; respectively), which were used for subsequent analyses (Figure 6-3).

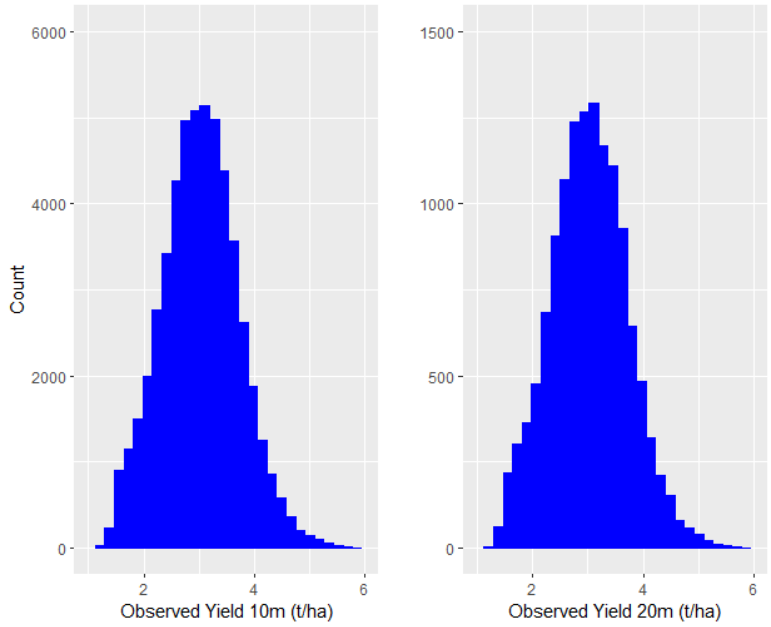

Figure 6-3: Frequency distributions for observed yields aggregated into 10m and 20m to represent the spatial resolutions of Sentinel-2

6.2.3 Simulated smallholder farm fields

The Olam farm was divided into smaller plots to represent a range of field sizes, which are representative of smallholder farms across Nigeria and sub-Saharan Africa more generally These simulated "smallholder farm fields" were subsequently used to explore the effect of farm size (spatial extent) on yield prediction accuracy from Sentienl-2 MSI data and to explore the extent to which image spatial resolution (pixel size) influenced prediction accuracies. Four categories of farm field sizes were simulated < 1 ha, 1 – 2 ha, 2 – 5 ha and 5 – 10 ha. These size categories were based on smallholder farm sizes typically found in sub-Saharan(FAO, 2014).

6.2.3.1. Plot generation

(i) 0.1 ha was set as the low threshold for farm size as representation of the lower limit of farm size.

(ii) The upper limit was set as 0.99 ha to represent the upper threshold for farm sizes ranging from 0 – 1 ha

(iii) The model was queried to generate 100 plots at an increasing order taking into consideration the distribution and orientation of the actual 48 field plots

(iv) The mean pixel values of each plot and standard deviation. Standard deviation was calculated to characterise the heterogeneity in each of the plots.

(v) Plots generated lots with an overlap of more than 20% were removed. In total, 100 small holder plots ranging from 0 – 0.99 ha were generated. Figure 6-4 gives a visual description of the plots for 0 – 0.99 ha

The sample approaches were adopted when generating plots from 1 – 2ha, 2 – 5ha and 5 – 10ha. However, due to plot overlap of more than 20% 1 – 2ha, 2 – 5ha and 5 – 10ha plots were reduced to 85, 70 and 43 respectively (Figure 6-4). For plots 5 – 10ha, plot sizes did not exceed 7.5 ha due to the farm orientation

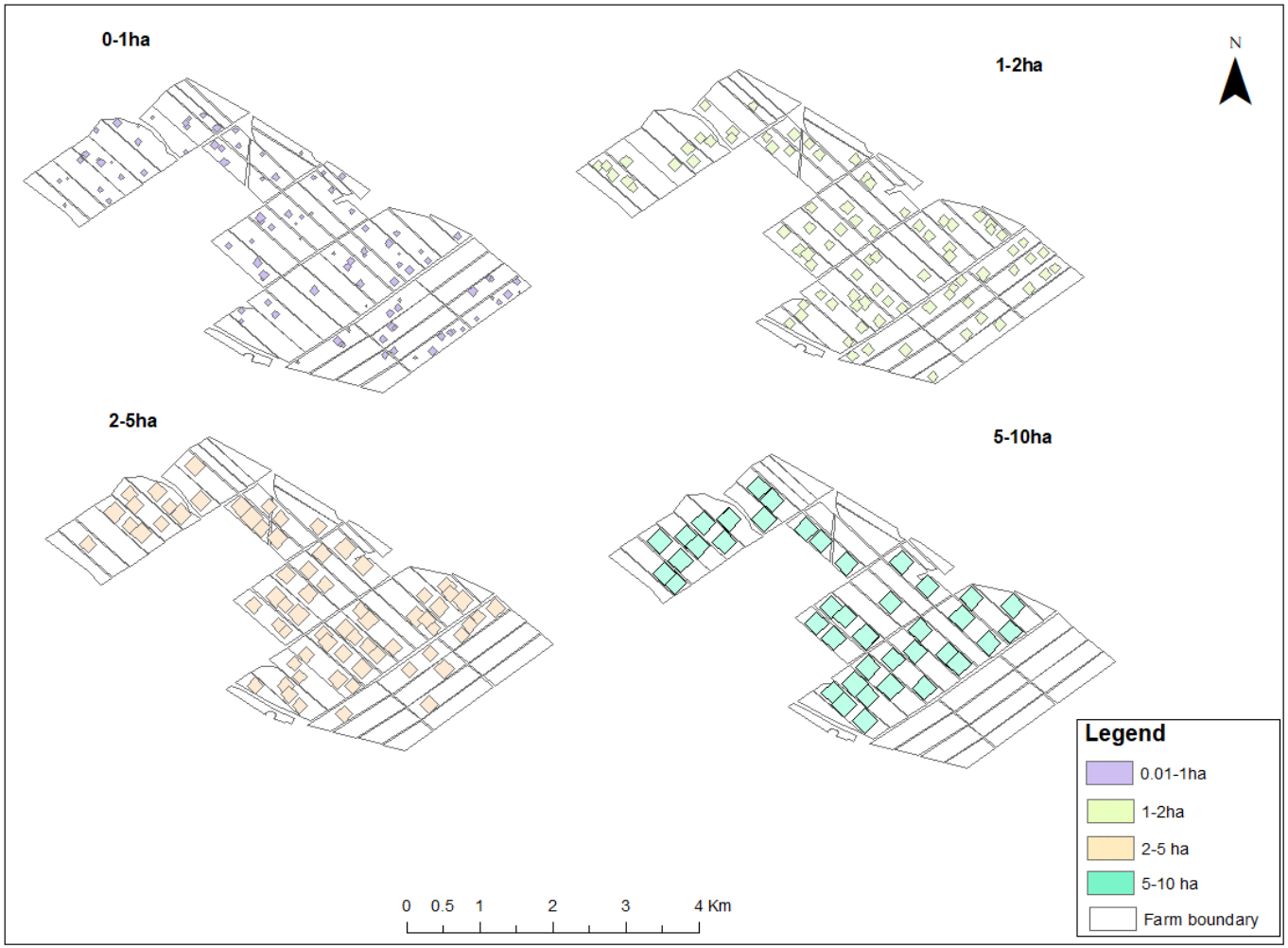

Figure 6-4: Plots Simulated small holder fields generated for 0-1ha, 1-2ha, 2-5ha and 2 -10ha size classes (n= 100, 85, 70 and 43; respectively) for yield prediction from the study area. These size classes reflect typical smallholder plots in Nigeria and sub-Saharan Africa

6.2.4 Sentinel-2 MSI Data and Vegetation Indices for building Yield Prediction Models

In order to evaluate trade-offs between Sentinel-2 10m and 20m resolution imagery, Sentinel-2 images were acquired at different phenological phases (vegetative, reproductive and ripening phases) or rice growth (Table 6-1). Of the eight images acquired for the study, four images were acquired during the vegetative stage, three during the ripening stage and one during the reproductive stage.

Table 6-1: Acquisition dates of Sentinel-2 used for the study. 8 satellite images were obtained in total, covering the different phenological phases of irrigated rice during the 2018/19 sowing season.

Phenological phase	Sampling date/period	Sowing	Sentinel-2 Acquisition	Yield
Sowing	18/11/2018	✓		
Vegetative	21/12/2018		✓	
	26/12/2018		✓	
	5/01/2019		✓	
	10/01/2019		✓	
Reproductive	20/01/2019		✓	
	14/02/2019		✓	
	19/02/2019		✓	
Ripening	11/03/2019		✓	
Harvest	18-28/03/2019			✓

The Multispectral Instrument (MSI) on board Sentinel-2 provides data in 13 spectral bands spanning from the visible (VIS) to the shortwave (SWIR) infrared region. They include four spectral bands in the VIS and near infrared (NIR) regions at 10 m spatial resolution, six spectral bands which span the red edge, NIR and SWIR regions at 20m spatial resolution and three 60m spatial resolution spectral bands located in the VIS, NIR and SWIR, primarily used for atmospheric correction and cloud detection (table 6-2). Cloud-free Sentinel-2 images (Level 2A Bottom-of-Atmosphere reflectance products) were acquired during the different phenological phases of rice growth to account for the different phases of rice growth. All data were obtained from the Copernicus Open Access Hub (https://scihub.copernicus.eu/).

Table 6-2: Sentinel-2 Multispectral Instrument (MSI) bands used in this study

Sentinel-2 Bands	Band 2 – Blue	Band 3 – Green	Band 4 – Red	Band 5 – Vegetation Red Edge	Band 6 – Vegetation Red Edge	Band 7 – Vegetation Red Edge	Band 8 – NIR	Band 8A – Narrow NIR	Band 11 – SWIR	Band 12 – SWIR
Central Wavelength (µm)	0.49	0.56	0.665	0.705	0.74	0.783	0.842	0.865	1.61	2.19
Resolution (m)	10	10	10	20	20	20	10	20	20	20
Bandwidth (nm)	65	35	30	15	15	20	115	20	90	180

Three different dataset using Sentinel-2 data were used in generating the dataset for each of the models in this study. The models were built based on the spectral bands from Sentinel-2 10m and 20m and selected vegetation indices used in previous studies to estimate yield in rice. First, the four spectral bands at 10 m spatial resolution along with the Normalized Difference Vegetation Index (NDVI) model (Rouse, 1974) from each of the data acquisition dates were used as the dataset for generating the first model called "Sen-2 10m". The addition of the spectral bands in the model was to ascertain the influence of the bands for predicting yield in rice. We selected the NDVI vegetation index as a result of the estimated accuracy reported in previous yield estimation studies (Bai et al., 2019; Balaghi et al., 2008; Guan et al., 2018; Mkhabela et al., 2011). In total, 32 spectral bands and eight NDVI variables were combined when building the Sen-2 10m model, accounting for 40 variables in the model. In order to directly compare Sentinel-2 10m to Sentinel-2 20m, the four spectral bands of Sentinel-2 were resampled to 20m. Furthermore, the NDVI vegetation indices along with the spectral bands generated from each of the acquisition dates were used in generating the dataset for the model called "Sen-2 20m". In total, 40 variables were combined in generating the dataset for the Sen-2 20m model .Third, the four resampled Sentinel-2 10m spectral bands, the six 20m resolution spectral bands on Sentinel-2 20m and the Normalised Difference Red-Edge (NDRE) (Fitzgerald et al., 2006) were used in generating the dataset for the third model called "Sen-2max 20m"as shown in Figure 6-3. NDRE model was selected because it has been successfully been adopted for estimating yield in rice (Kanke et al., 2016; Zhang et al., 2019). Ten spectral bands and the NDRE indices were generated for each of the acquisition dates and used as the dataset for the third model. In total, 80 spectral bands and eight NDRE variables were combined when building the Sen-2max 20m model, accounting for 88 variables in the

model. Spectral and vegetation index information values from each pixel from both 10m and 20m Sentinel-2 spatial resolutions were used in generating each of the models.

6.2.5 Prediction of rice yields

The Random Forest (RF) (Breiman, 2001) model adopted for estimating yield at both landscape (>1150ha) and simulated smallholder plots to understand within and between field variability using the three distinct datasets. RF is characterized by a bagging (i.e., bootstrap aggregating) approach, and has been successfully used for regression analysis in many disciplines (da Silva Júnior et al., 2019; Hunt et al., 2019; Lopatin et al., 2016). The RF algorithm first creates a pre-defined number of new training sets with random sampling and then builds a different tree for each of these bootstrapped datasets. Each decision tree is trained using a subset of the various input variables with two thirds of these samples. The remaining one third is used to generate the out-of-bag error, which is an internal validation of the final model.

We assess the performance of our three random forest models by comparing their ability to predict yields aggregated at both their nascent resolution (either 10m or 20m) and at a range of synthetically generated plot sizes (as outlined in Section 6.2.3). Model performance was assessed by comparing both the coefficient of determination and root mean squared error, calculated using a ten-fold cross-validation where the data were divided into 10 comparably sized subset (Refaeilzadeh et al., 2009).

6.3 Results

6.3.1 Variation of measured rice yields across the landscape and simulated smallholder farm fields

The summary statistics of irrigated rice yield provides a background to the number of plots generated and the ranges of yield within each of the field size categories used in the study as summarised in Table 6-3. The largest variability was seen in 1150 ha(10m), with lowest yield at 1.12 t/ha and highest yield at 6.01 t/ha. On the contrary, the lowest variability was seen in 2-5ha(10m) plots with minimum yield at 1.88 and maximum, at 3.88.

Table 6-3: Summary statistics of the measured rice yield from landscape scale and at small holder plot scale. Results generated were for both Sentinel-2 10m and 20m during the 2018-19 dry season rice farming

		Yield (tonnes/ha)			
Plot size class (Sentinel-2 10 or 20 m)	**Sample size (n)**	**Min**	**Max**	**Mean**	**Standard Deviation**
1150 ha (10m)	52520	1.12	6.01	3.02	0.7
1150 ha (20m)	13135	1.12	5.75	3.02	0.69
1 – 2 ha (10m)	100	1.58	4.36	3.09	0.57
1 - 2ha(20m)	100	1.56	4.3	3.11	0.58
2 - 5ha(10m)	85	1.66	4.55	3.03	0.56
2 - 5ha(20m)	85	1.64	4.51	3.04	0.56
2 - 5ha(10m)	70	1.88	3.83	3.03	0.45
2 - 5ha(20m)	70	1.88	3.86	3.03	0.56
5 - 10ha(10m)	43	1.71	3.76	2.94	0.47
5 - 10ha(20m)	43	1.71	3.74	2.94	0.47

6.3.2 Influence of image spatial resolution on the prediction of yield at landscape scale

The Sen-2 RF (10m), Sen-2 RF (20m) and Sen-2 RF max (20m) were validated against yield data to determine within-field variability at landscape scale. Results show that the addition of the spectral bands and the NDRE index used in Sen-2 RF max (20m) were more accurate with an $R^2 = 0.64$ and RMSE = 0.41 tonnes/ha compared to $R^2 = 0.60$ and RMSE = 0.43 tonnes/ha from Sen-RF (20m) when predicting within field variability. When predicting within field variation in yield at 10m resolution, the Sen-2 RF (10m) results indicated the significance of the spatial resolution, as the model explained 72% of model variability with lower model errors compared to the 20m Sentinel-2 RF models ($R^2 = 0.72$ and RMSE = 0.38 tonnes/ha).

When mapping the spatial variability of yield from Sen-2 RF (10m) and Sen-2 max RF (20m) against rice yield at 10 and 20m respectively, Figure 5-5 presents similar prediction patterns between observed and estimated yield in majority of the rice farm at landscape scale, particularly at the northern part of the farm were yield was between 3-4 t/ha. However, the annotated figures highlight areas with notable overestimation and underestimation of rice yield. The south-eastern part of the farm presented the highest yield, with yield exceeding 5t/ha. Although the Sen-2 max RF (20m) and Sen-2 RF (10m) models predicted high yield, spatially yield mapping from Sen-2max RF (20m) show spatially greater underestimation of yield above 5t/ha compared to Sen-2 RF (10m) when comparing with 10m observed yield. A similar trend can be seen at the central part of the farm with the lowest irrigated rice yield. Despite the higher yield variability of the 10m observed yield, Sen-2 RF (10m) yield estimates below 2t/ha were more closely related to observed yield compared to Sen-2 max RF (20m) estimates. Although, both models overestimated yield at the central part of the farm albeit the Sen-2 max RF (20m) model prediction significantly higher.

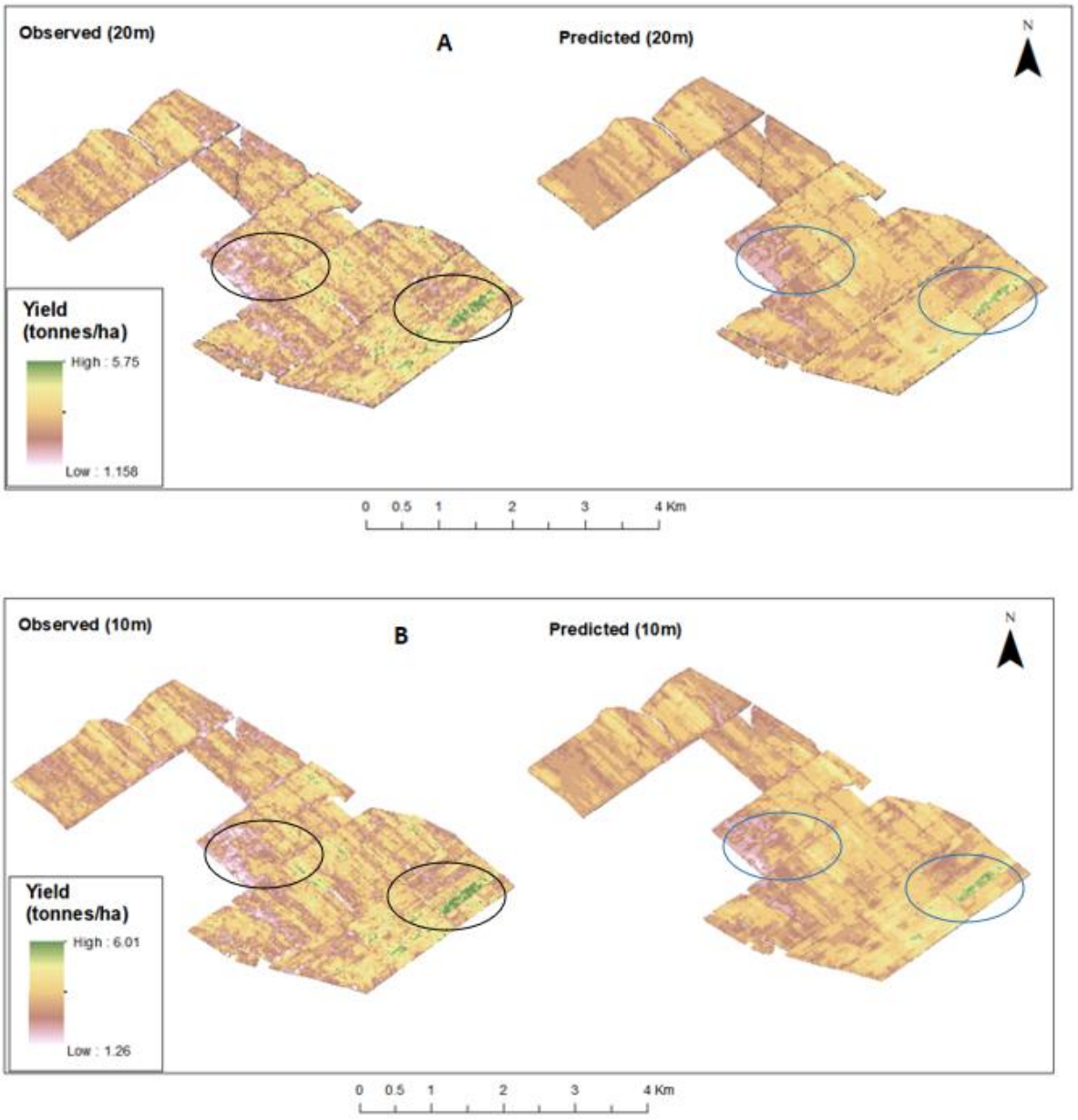

Figure 6-5: A. Spatial patterns in yield between Observed yield and Sen-2 RF (20m) of within field variability estimation with annotations highlighting high and low yield B. Spatial patterns in yield between Observed yield and Sen-2 RF (20m) of within field variability estimation with annotations highlighting high and low yield. Black annotations representing observed yield while blue annotations represent predicted yield.

Figure 6-6 and 6-7 elucidates some of the uncertainty in model accuracy with underestimation and overestimates of the yield estimation below 2t/ha and above 5t/ha. From Figure 6-6, areas with high standard error (SE) are areas categorised as high yield errors and these results are in agreement with underestimation and over estimation of yield in Figure 6-6. Despite the normal distribution identified between estimated and observed yield at 10m in Figure 6-5, observed yield values are more evenly spread between yield from 2-4 t/ha while Sen-2 RF 10m yield

values are more concentrated between 2.5 to 3.5 t/ha, increasing significantly the number of pixels with yield estimation in this region.

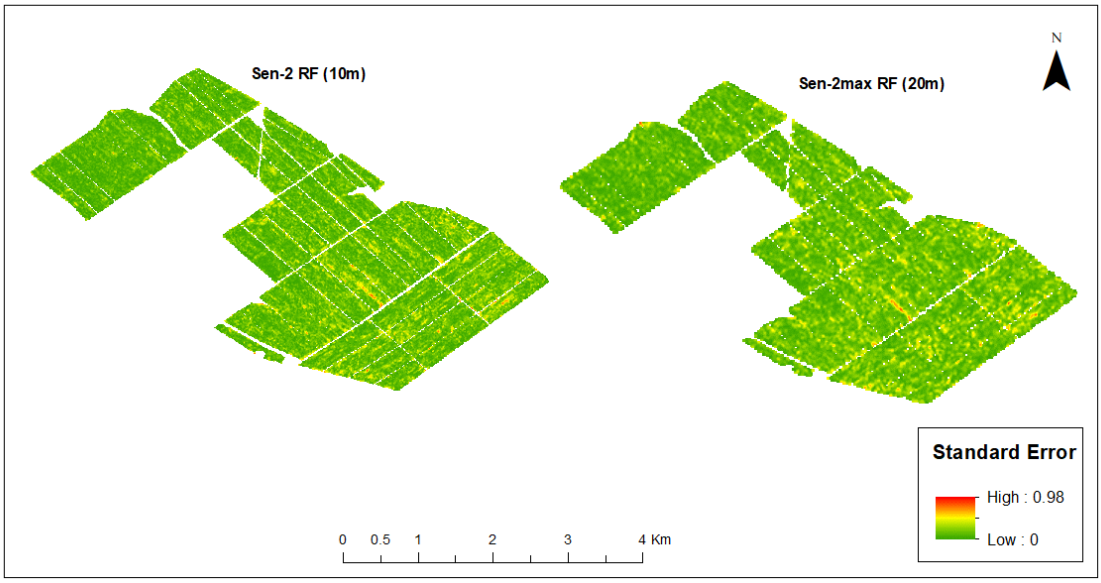

Figure 6-6: Associated uncertainties expressed as standard error (SE) for Sen-2 RF (10m) and Sen-2max RF (20m)

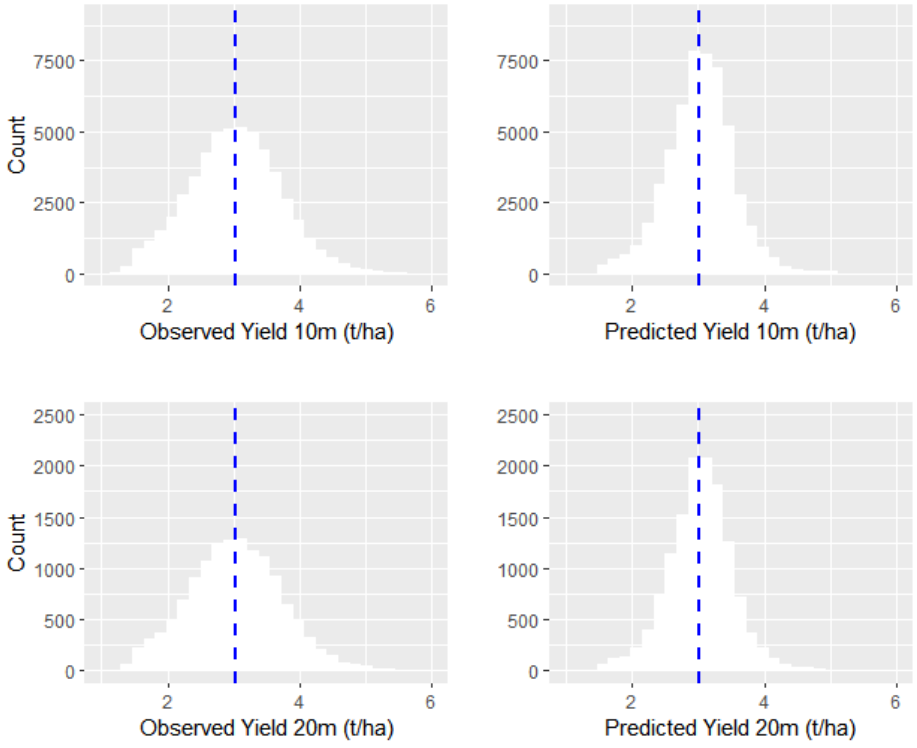

Figure 6-7: Frequency distribution of yield obtained from Sen-2 RF 10m and Sen-2max RF 20m in comparison to aggregated yield at 10m and 20m from the combined harvesters.

6.3.3. The influence of image spatial and spectral resolution on smallholder rice yield estimation from Sentinel-2

Sen-2 RF (10m), Sen-2 RF (20m) and Sen-2max RF (20m) rice yield estimation were further investigated for specific smallholder plots against plot-level yield data. Across the four simulated farm plot categories, variation yield estimation between the coefficient of determination and model error was identified (R^2 = 0.52 - 0.7 and RMSE 0.41 t/ha - 0.26 t/ha).

For the 0-1ha plots, Sen-2 RF (10m) displayed the best agreement metrics with estimated yield (R^2 = 0.55; RMSE = 0.39t/ha, $p < 0.05$) compared to Sen-2max RF (20m) (R^2 = 0.54, RMSE = 0.39, $p < 0.05$) with Sen-2 RF(20m) exhibiting the lowest predictive accuracy as compared to the other models (R^2 = 0.52, RMSE = 0.41, $p < 0.05$). However, similar yield estimations patterns were identified when yield values were below 2t/ha, resulting in reducing the estimation accuracy of the models. On the other hand, plots with yield values above 4t/ha were not accurately represented in all the models (Figure 6-8). In general, baseline Sentinel-2 data using RF models showed great potential of predicting yield at 0-1ha plots.

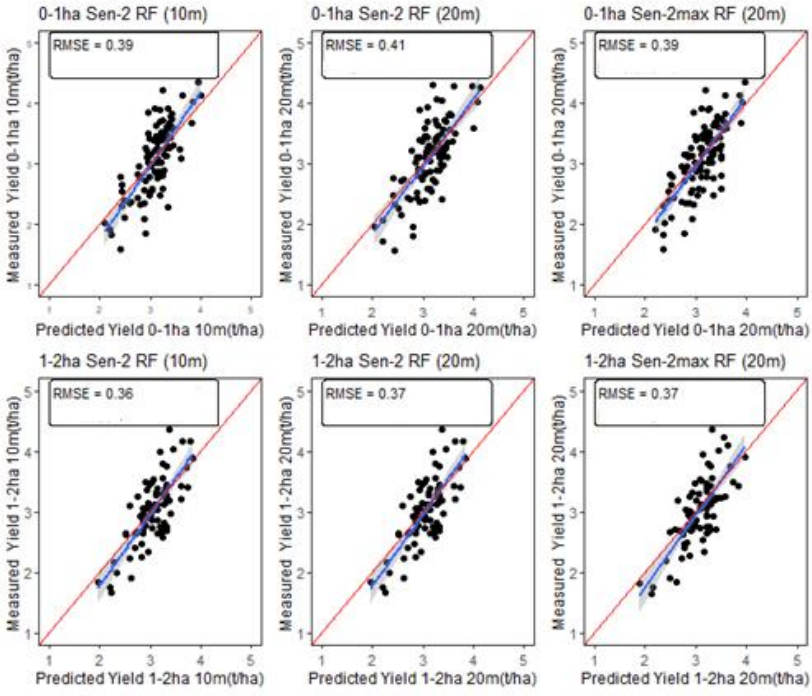

Figure 6-8: Scatter plot of estimated and measured crop yield from Sen-2RF 10m, 20m and Sen-2max RF 20m yield for small holder plots at 0-1ha (n=100) and 1-2ha (n=85)

Model performance of plots sizes at 1-2 ha presented more accurate yield estimates compared 0-1 ha plots with errors in Sen-2 RF (10m) and Sen-2 RF (20m) reducing by 0.03 t/ha and 0.04

t/ha respectively (Figure 6-9). RF models for both spatial resolutions generally underestimated irrigated rice yields of more than 4 t/ha. Compared to 0-1ha plots, 1-2ha plots only overestimated 3 plots at 2 t/ha. Sen-2 RF (10m), Sen-2 RF (20m) and Sen-2 max-RF (20m) presented very similar results for prediction of smallholder plots at 1-2ha.

Model performance for 2-5ha improved slightly for all three models (Figure 6-9, RMSE values). However, estimated yield values were concentrated between 2.5 – 3.5 t/ha, with underestimation and overestimation identified at 2.5 t/ha and 3.5 t/ha respectively.

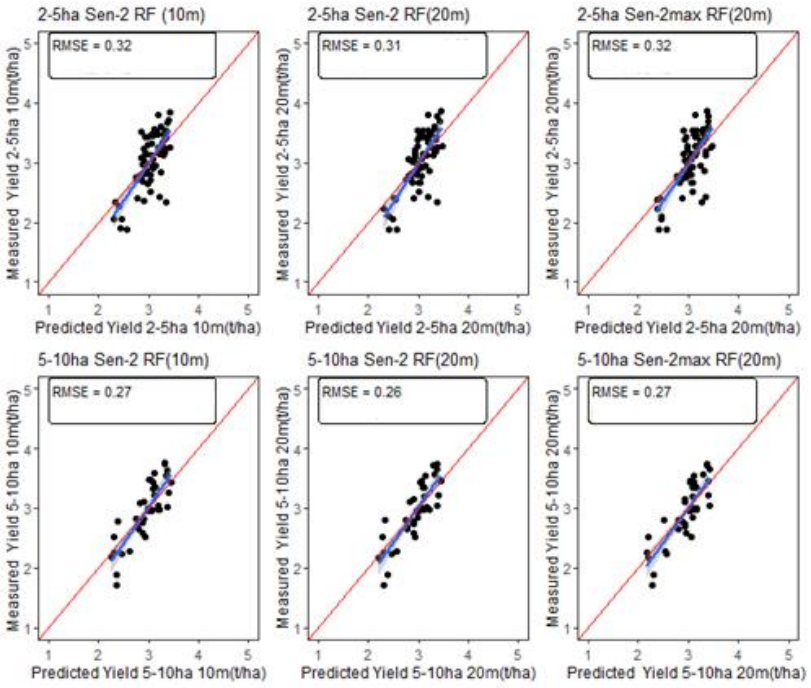

Figure 6-9: Scatter plot of estimated and measured crop yield from Sen-2RF 10m, 20m and Sen-2max RF 20m yield for small holder plots at 2-5ha (n=70) and 5-10ha (n=43)

The results from 5-10ha smallholder plots outperformed the three other plots categories with R^2 of 0.69 and 70 and a reduction in yield estimation of 0.05 t/ha for Sen-2 RF (10m) and Sen-2 RF (20m) respectively (Figure 6-11). A strong positive agreement of yield can be identified for plots between 2.5-3.5 t/ha, with an underestimation at 2t/ha and over prediction above 3.5t/ha of yield.

In terms of mapping smallholder plots, Sentinel 2 yield maps generated from the RFmodels provides the opportunity to identify between field yield difference in plot sizes typical of smallholder farming. Figure 10 demonstrates the ability of Sentinel-2 10m and Sentinel-2 20m to estimate yield at 0 – 1 ha and 5 – 10 ha respectively.

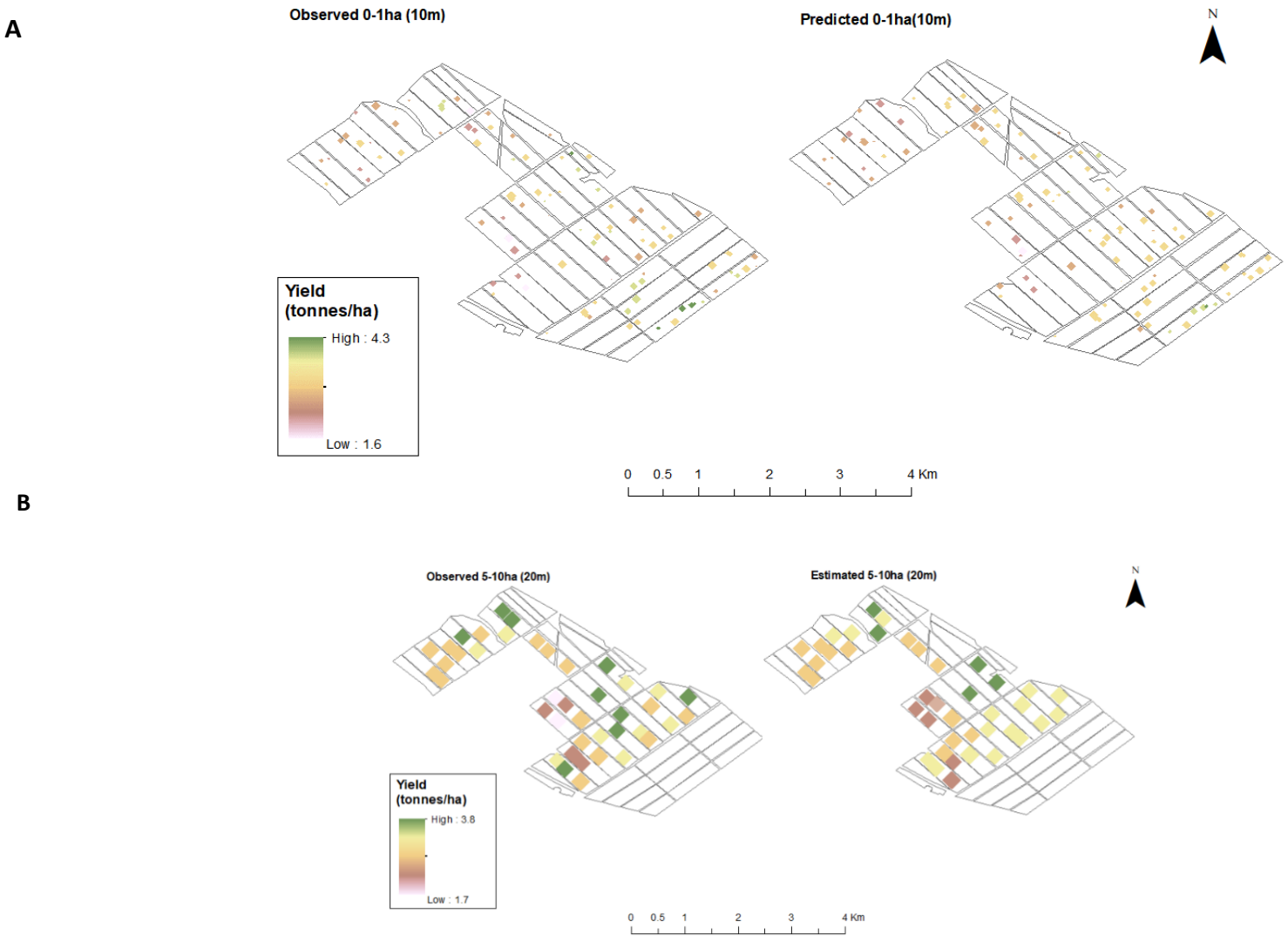

Figure 6-10: (A) Between field variability estimation of rice at smallholder plots at 0-1ha generated from Sen-2 RF 10m and aggregated yield at 10m. (B) Between field variability estimation of rice at smallholder plots at 5-10ha generated from Sen-2max RF 20m and aggregated yield at 20m

The yield estimates in each plot fell within the range of estimated yield with little discrepancies in high and low yielding plots. Figure 10-10b further demonstrates the ability of Sentinel-2max (20m) to predict yield of plots ranging between 5 – 10 ha with some understimation of yield at higher yielding plots. Both maps were able to show clusters of different yield at smallholder plots which opens oppurtunities for investigation into the factors responsible for yield variation such as environmental and crop management practices. Moreover, information on yield-limiting factors based on different management zones are important in order to improve farming pratices (Diker et al., 2004).

6.4 Discussion

This study focused on the ability of Sentinel-2 data to predict within field and between field irrigated rice yield at landscape and smallholder scale. Yield estimation was assessed based on smallholder farm plots from 0 – 1 ha, 1 – 2 ha, 2 – 5 ha and 5 – 10 ha, while landscape scale was assessed based on the >1150ha rice farm.

6.4.1 Landscape Scale

In terms of the comparison between Sen-2 RF (10m) and Sen-2 RF (20m) against corresponding high resolution yield data, the validation data played a significant role in the higher yield variability and lower RMSE and MAE errors between both models. The reason for the superior estimation results obtained from Sentinel-2 10m may be as a result of advancements in the satellite design and data processing techniques, alongside the improved combine harvester processing methods, proving better image data and reference data that enable accurate estimation of high at high resolution (Hunt et al., 2019). Our results are in line with Hunt et al. (2019) who identified the of optimum processing spatial resolution (10m) for yield prediction from Sentinel-2 data. On the contrary, in their assessment of SPOT-5 satellite data, Yang et al. (2009) showed that the 10-m, four-band imagery and the aggregated 20-m and 30m images explained 68% and 76% and 83%, respectively variability in yield. The reason for the discrepancy of results between our study and Yang et al. (2009) may be as a result of the locational accuracy of both sensors. For instance, Sentinel-2 is reported to have a locational accuracy of 20m (Drusch et al., 2012) compared to SPOT-5, which has an accuracy of 30m (Yang et al., 2009). This may partly account for the discrepancy in the image resolution versus yield accuracy in both studies. Although Durgun et al. (2020) confirmed the importance of spatial resolution of sensors compared to the temporal resolution using other sensors, this study presents the first assessment of the superiority of Sentinel-2 spatial resolution over spectral resolution for mapping high yield within field variability.

At landscape scale, direct comparison between yield performance of Sen-2 RF max (20m) and Sen-2 RF (20m) at 20m was investigated. The introduction of the full spectral resolution of Sentinel-2 20m bands with a red-edge index were assessed for predicting rice yield, with the Sen-2 RF max (20m) explained higher variability of yield with lower model error compared to Sen-2 RF (20m) (section 6.3.2). The red-edge based vegetation indices have shown to have stronger relationships with measured agronomic parameters as compared with red-based indices, which are in line with our study when using the same spatial resolution. Similar results were observed by (Kanke et al., 2016) between vegetation indices from red-based bands and red-edge bands within and grain yield. Red-based bands explaining lower variability in grain yield while the range improved using red-edge bands.

In terms of yield mapping, from Figure 6-5, field observation shows that Sentinel-2 10m more accurately identified yield gaps and the location of such gaps when validated with 10m yield data compared to Sentinel-2 20m with 20m yield data. As identified at the central portion of the farm at landscape scale, yield at the central part of the farm was between 1.8 – 2.5ha compared to the southern part of the farm where yield exceeded 4t/ha in many areas. Sen-2 RF (10m) was able to replicate more accurately the yield at both areas of the farm compared to Sen-2max RF (20m). The spatial resolution had greater influence on the RF model as the model produced more accurate yield prediction and were able to identify within field variability more accurately from 10m compared to the 20m spatial resolution of Sentinel-2. Furthermore, the reduction in standard error from Sen-2 RF (10m) to Sen-2max RF (20m) at the central and southern portions of the farm confirms the suitability of the higher resolution imagery and RF model for predicting within field variability of rice from Sentinel-2 (Figure 6-6). This provides an approach for further investigation on strategies and farming practices to be adopted by farmers and agronomist in yield limiting areas to improving rice yield.

6.4.2 Smallholder plot yield estimation

Four smallholder farm plots categories were investigated based on their size and orientation. For plot sizes ranging from 0 - 1ha, Sen-2 RF (10m) provided slight improvement in model accuracy albeit it being significant for the estimation of yield (Figure 6-8). The reason for the slight improvement may be because of the addition pixel properties, providing in-depth information on the spectral response characteristics of the plots compared to Sen -2 20m models. For instance, a 0.2ha plot contains ~18 pixels as compared to ~6 pixels from Sentinel - 2 20m which may led to a more enhanced smoothing effect of yield(Yang et al., 2009) which may reduce the variability within each plot. Results demonstrate the importance attached to

spatial resolution as against the spectral resolution for predicting yield at 0-1ha. However, when accessing smallholder plots above 5ha, the increase of smallholder plots presented similar estimation errors between Sentinel-2 10m and Sentinel-2 20m. This is because the accuracy of these models improved due to the reduced variability within each plot. Also, the added advantage of spatial and spectral resolutions of Sentinel-2 10m and 20m respectively were neutralized at the smallholder plot scale due to the smoothing effect of pixel, implying that at 5-10ha farm plots, Sentinel-2 10m and 20m bands can both be adopted for estimating the most accurate yield variability.

In terms of mapping between field variability of small holder plots (Figure 10-10), Sen-2 RF (10m) yield estimation results were similar to observed yield outcomes from the combine harvester further emphasising the added value of Sentinel-2 10m MSI for accurately identifying between field variability. Similar results were achieved when using Sen-2max RF (20m) for estimating smallholder plots at 5-10ha albeit underestimation and overestimation of some plots.

Smallholder farms play a significant role in rice production in sun-Saharan Africa. The ability to monitor rice yields at smallholder farm scales are important towards addressing the growing demand and increasing availability of rice. Also, the possibility of monitoring at smallholder scales will be strategic especially in remote areas, where repeated farm monitoring may be challenging. The results shown in this study further emphasis the increasing importance of the free availability of Sentinel-2 for estimating dry season irrigated smallholder rice yield as results show indicate the possibility of mapping rice yield at smallholder plots using the satellite.

6.4.3 Baseline Sentinel-2 data for predicting dry season rice yield

Dry season rice farming is an increasingly important technique currently being adopted to curb the spread of poverty and hunger in many developing countries. However, a major limitation to its uptake is adequate water availability, which is a crucial input for the majority of rice varieties (Belder et al., 2004; Wang et al., 2016a). With the introduction of drought resistant varieties like the NERICA 61 (Faro 34), which have been cross-bred to cope with limited amount of water, the possibility of growing rice during the dry season months has now become possible, and indeed common practice, for many farmers (Sekiya et al., 2013).

Many studies have combined information on climate and environmental factors with Earth Observation data to improve the prediction of crop variability as this provides for a more robust

identification of factors responsible for yield gaps (Jin et al., 2018; Kang and Özdoğan, 2019b; Vazifedoust et al., 2009). Though results were improved in some studies, the practicability of acquiring such robust information from the field is still challenging in many developing regions of the world. However, baseline Sentinel-2 data accounting for only satellite spectral, spatial and temporal resolution alongside vegetation indices, provided positive relationship with actual rice yield. Results show that Sentinel-2 data provides a base for the identification of dry season rice yields at landscape and smallholder freely. Although empirical approaches are site specific, requiring recalibration for different sites (Noureldin et al., 2013), and not accounting for factors that affect yield such as seed variety, weather conditions, and soil properties, Sentinel- 2 data can serve as a base for yield estimation and prediction of dry season rice. Also, the practicability of reproducing yield estimates at locations without the aforementioned yield affecting factors are more feasible from baseline Sentinel-2 data than the use of crop simulation models in regions were data availability is not available. Therefore, the spatial, spectral and temporal properties of Sentinel-2 data provide an important opportunity to identify within field variability as well as estimation of yield at of smallholder plots. This is particularly important in data deficient regions where accurate availability of environmental and climatic data may not be available. Future studies should focus on monitoring multiple dry seasons yield data for rice and other crops to the test the performance of the Sentinel-2 RF models for predicting within and between field yield in other.

6.5 Conclusion

This study demonstrates the influence of baseline Sentinel-2 data (spatial, temporal and spectral composition) for predicting high resolution yield at smallholder and landscape scales. When identifying the optimum processing spatial resolution for predicting within field variability, Sen-2 RF (10m) presented superior results in terms of a higher variability and low model error compared to Sen-2 RF (20m) when yield data at 10m is available. The introduction of additional spectral bands and red-edge based vegetation index presented more accurate results for Sen-2 Max RF (20m) compared to Sen-2 RF (20m) results, suggesting that the addition of spectral indices, especially in the red-edge region, with identical spatial resolutions will lead to improved yield estimation. However, spatial resolution remained more important factor compared to spectral resolution for estimating high resolution yield variability from Sentinel-2. In addition, Sentinel-2 shows the possibility of predicting within field variability of smallholder as low as 0-1ha, implying that the satellite can identify the variability of most of the smallholder rice fields globally. Inferring from the results, Sentinel-2 is equipped to

predict yield of farm plots <1 ha with improved results identified when smallholder plots exceed 5ha. This resolves the issues of pixel contamination often attributed to coarse resolution satellites when monitoring smallholder fields especially in developing countries. However, further validation is required in other crops and different climates.

Chapter 7 Conclusion

7.1 Introduction

This chapter discusses and summarizes the results obtained in the analysis chapters (i.e. Chapters 4, 5 and 6), which focused on monitoring yield and yield indicators (LAI, biomass) from different remote sensing platforms. The chapter highlights the important findings that emerged during this research, stressing the contribution to the existing body of knowledge within the specific focus on rice monitoring using remote sensing. The chapter also highlights the limitations encountered in the course of this research and finally areas of possible future work.

7.2 Summary of research findings

The thesis has three main aims, each related to understanding the potential of remote sensing technologies for monitoring the productivity of dry season irrigated rice in Nigeria. The research aims were as follows:

- To determine the relative merits of drone mounted sensors for estimating mid-late season rice above ground biomass from very high spatial resolution drone imagery.
- To determine the potential of hybrid machine learning methods for estimating the seasonal dynamics of rice Leaf Area Index (LAI).
- To determine the relative importance of the spatial and spectral resolution of Sentinel-2, for estimating rice yields across a range of spatial extents

7.2.1 Relative merits of drone mounted RGB and MSI sensors for estimating rice AGB during mid-late season

When monitoring rice AGB, the timing of biomass monitoring is critical for monitoring yield. From the literature, we identified the mid (reproductive) and late (ripening) growing phases of rice to play a significant role in estimating yield in rice (Fageria, 2007),therefore, influencing the phases at which we monitored rice AGB. Furthermore, emphasis was placed on very high-resolution images capable of estimating AGB at centimetre scale, leading to the adoption of drone images from airborne platforms. In addition to the scale functionality of drones, various sensors have been utilised for the estimation of AGB in rice and other crops. The consumer grade RGB, using plant height estimates and the sophisticated Multispectral cameras using vegetation indices and texture metrics, were adopted for the estimation of rice AGB.

When assessing the suitability of the RGB sensor for estimating rice AGB during the mid to late growing phases (Chapter 4), we initially investigated plant height estimates against in-situ measurements of plant heights on each of the experimental subplots. The results obtained for the estimation of plant height from the RGB camera shows a strong relationship between insitu plant height which was an important step towards identifying the suitability of plant height estimates for predicting rice ABG in the first place. Our results are in line with previous studies who estimated rice plant height from RGB sensors (Cen et al., 2019; Jiang et al. 2019). Plant height estimates generated from the RGB sensor were compared with in-situ measurements of biomass using a simple linear regression (SLM) model (R^2 = 0.72; RMSE = 1.04 t/ha; MAE = 0.97 t/ha). The results suggest the potential of plant height estimates obtained from the RGB camera as a suitable proxy for estimating rice AGB during the mid to late growing phases. Although Cen et al. (2019) results suggest the unsuitability of plant height for estimating rice AGB during the mid to late growing phases, Tilly et al (2015) results tally with this study as plant height estimates over multiple growing season results showed the suitability for estimating rice AGB.

The MSI sensor on the other hand was estimated rice AGB from vegetation indices and texture metrics like vegetation indices and texture metrics for estimating biomass from centimetre resolution platforms it at infancy. Aside from Zheng et al. (2019), this study represents one of the only studies to estimate rice AGB in rice using MSI sensors. However, the results from that texture metrics are not suitable for the estimation of rice AGB which agrees with Zheng et al. (2019) for rice and Yue et al. (2019) for wheat. The combination of both models using the random forest model didn't improve the estimation of rice AGB compared to using vegetation models. This may be attributed to the fact that textural metrics are very scale and scene dependent, therefore information on the canopy structure carried in single pixels vary for images with different ground resolution, thereby leading to a huge alteration in the distribution of dark and bright areas on the images (Yue et al., 2019).

When comparing the statistical performance of plant height using the simple linear model to texture metrics and vegetation indices using random forest models, plant height estimates performed best for rice AGB estimation indicating the suitability of the RGB to the MSI for estimating rice AGB during the key growing phases. However, the combination of both RGB and MSI sensors produced the most accurate estimation as the combination of plant height and vegetation indices improved AGB estimations (Cen et al., 2019; Bendig et al., 2015). Also, the combination of plant height, vegetation indices and texture metrics further improved the

estimation of rice AGB. This study represents the first study to investigate the combination of texture metrics, vegetation indices and plant height for the estimation of AGB in crops. On the other hand, VIs, TM and their combination were accessed using the Random Forest model for estimating rice AGB. I also assessed the combination of both sensors for estimating rice AGB.

7.2.2 Hybrid machine learning methods for estimating the phenolgical dynamics of rice Leaf Area Index

For LAI, the phenological dynamics of LAI from field scale with the potential to upscale to global scale was investigated using satellite images (Chapter 5). From satellite images, the recently launched Sentinal-2A and B satellite provides high spatial, temporal and spectral resolution, suitable for the estimation of LAI from field to global scale. We focused on the methodological approaches for estimating LAI, which include parametric, non-parametric, physical-based and hybrid approaches. The hybrid approach, which combines machine learning regression algorithms with physical based models using radiative transfer models, was identified as suitable for LAI retrieval as they are currently being adopted by Sentinel-2 Application Platform (SNAP) processor using a combination of Artificial Neutral Network and Radiative Transfer Models. Although the SNAP processor adopts the Artificial Neural Network approach, Verrelst et al. (2015) assessment of LAI retrieval methods suggests that the Gaussian Process Regression approach were more accurate to the Artificial Neural Network using simulated Sentinel-2 data. Furthermore, Campos-Taberner et al. (2016) results showed hybrid GPR model outperformed ANN and RTM for the retrieval of LAI from SPOT 5 and Landsat. The improved spectral, spatial and temporal resolution of Sentinel-2 compared to Landsat and the free availability of images to SPOT 5 necessitated the investigation of the hybrid GPR model and Sentinel-2 data for monitoring the phenological dynamics of LAI in irrigated rice fields. Also, validating LAI obtained from the established European Space Agency SNAP processor toolbox was deemed necessary.

Our findings show that the combination of GPR and RTM more accurately predicted LAI for the entire season and particularly at the reproductive and ripening phases compared to the combination of ANN and RTM. However, overestimation of LAI was observed during the vegetative phase while underestimation of LAI was identified in both models during the reproductive and ripening phases of rice LAI. LAI estimations from the ANN models were particularly low, with LAI values not exceeding 4 for the entire growing season, leading to inaccurate interpretations of LAI values during various phenological phases. Previous studies who assessed the performance of the ANN model compared model performance against LAI

values less than 4 (Pasqualotto et al., 2019; Sinha et al., 2020; Xie et al., 2019b), although LAI results have also been seen in other studies to exceed 4 with the exception for (Vanino et al., 2018; Xie et al., 2019b) indicating the need for model validation in other regions where rice is cultivated. Our findings show the possibility for the adoption of GPR models for the phenological dynamics of LAI at regional to global scales.

7.2.3 Relative importance of the spatial and spectral resolution of Sentinel-2, for estimating rice yields across a range of spatial extents

In addition to monitoring yield indicators of rice using remote sensing, the monitoring of yield itself from remote sensing is vital to farmers, agronomist and researchers. From the literature, we identified smallholder farms less than 2ha represents over 80% of rice farms globally (FAO, 2014; Lowder et al., 2016). We also identified that farms 50ha and above have access to over 85% of land for farming. Therefore, methods of monitoring rice yield across varying spatial extends are important toward bridging yield gaps. Satellite platforms were identified as the most appropriate for monitoring from smallholder to landscape scale, with Sentinel-2 serving as a potential satellite for estimating yield due to the free availability of Satellite images, as well as the high spatial, spectral and temporal resolution.

Since Sentinel-2 data has varying spatial resolutions (10m and 20m), with varying spectral properties, the study (Chapter 6) investigated the spatio-spectral resolution of Sentinel-2 10m and 20m for estimating within field variability at landscape scale and between field variability at smallholder scale (0-1, 1-2ha, 2-5, 5-10ha) using vegetation indices and spectral bands using the Random Forest model. Our findings show that Sentinel-2 10m provided the least error and highest variability of rice yield with validation data at 10m compared to Sentinel-2 20m with validation data at 20m. Similar results were achieved by hunt et al. (2019) when comparing the spatial resolutions of Sentinel-2 bands for predicting yield in wheat. Accessing the accuracy of mapping yield, Sentinel-2 10m using the Random Forest model explained more accurately, the variability in yield especially at high and low yield values compared to Sentinel-2 20m and a lower Standard Error in model performance.

When accounting for within field yield variability at smallholder plots from 0 – 10 ha, results showed the suitability of Sentinel-2 data for predicting yield. Although studies have accessed Sentinel-2 data for predicting yield (Hunt et al., 2016; Kanke et al., 2016), this study represents the pioneer study which investigated the use of Sentinel-2 data for predicting within field yield variability according to FAO (2014) classification of smallholder farms.

7.3 Significance and implications of the key findings

7.3.1 High resolution monitoring of rice AGB during the reproductive and ripening phases

The advancement in drone and sensor technologies have provided the opportunity to monitor to monitor rice AGB at very high resolution. Till now, emphasis on the estimation of the mid to late growing season have been relegated to the background although phases have been identified as critical to predicting eventual yield outcomes. As such, the emphasis of the study was on ascertaining the relative merits of RGB and MSI sensors for estimating rice AGB during the critical growing phases. The first major implication of from the study at farm scale is the importance of plant height estimates from the RGB sensor for the estimation of rice AGB during the key phenology phases compared to the MSI sensor. The significance of these findings are amplified as a result of the cost implications of acquiring the cheaper RGB sensor as opposed to more expensive and sophisticated multispectral sensor, which, during the mid-late growing phase, did not estimated rice AGB as accurately as the RGB cameras. Farmers, agronomist and researchers can opt for just the RGB camera when monitoring on their rice farms without having to incur additional cost on sensors for accurate rice AGB estimation. Particularly, the monitoring of rice AGB focused on the lowland irrigated NERICA rice variety where awareness by African governments and in particular, the Nigerian government through initiatives and schemes are being promoted to encourage rice farmers to adopt the varieties during the dry season because of their high yield potential.

In terms of the combination of both RGB and MSI sensors for monitoring rice and other crops AGB, this study and others (Cen et al., 2019; Han et al., 2019; Li et al., 2020) have shown vegetation indices and plant height to improve the estimation of rice AGB. However, this study (Chapter 4) presents the first research to show that the combination of texture metrics, vegetation indices and plant height can improve the estimation of rice AGB during the reproductive and ripening phases. These findings indicate that commercial farms with the financial capacity to monitor their farms may wish to purchase both cameras alongside a drone to improve the estimation of rice AGB. However, if the cost implication of purchasing both cameras is too much, then opting for the RGB camera should be the priority.

7.3.2 GPR (GPR hybrid) Model for monitoring the phenological dynamics of rice LAI

Accurate monitoring of yield indicators is very important for farmers, researchers and agronomist seeking to make either marginal or significant gains in yield output. Different retrieval LAI algorithms have been identified in the literature, however, the most globally implemented LAI retrieval method is the combination of the PROSAIL and ANN (ANN hybrid) using Sentinel-2 data. Previous studies have shown the GPR model as an alternative approach for the retrieval of LAI which necessitated the investigation of both monitoring the phenological dynamics of rice from both models. A key contribution identified as a result of this study is the identification of the GPR hybrid model as an alternative retrieval approach to the ANN model for estimating LAI phenological dynamics of rice using Sentinel-2 data. Evidence from the results obtained through statistical test show that more accurate estimation of LAI values can be achieved with the GPR models especially when LAI values exceed 4 mainly in the reproductive and ripening phases. GPR models have been used to accurately predict LAI using various Satellite platforms (Campos-Taberner et al., 2016), however, this research represents the first study that evaluates the model using Sentinel-2 data for monitoring rice LAI phenology. These findings stand on existing bodies of literature that have identified the suitability of Sentinel-2 data for estimating LAI (Sinha et al., 2020; Verrelst et al., 2015c; Xie et al., 2019b)

Another significant contribution to knowledge is the call for further validation of the SNAP LAI processor tool for the estimation of LAI as this processor is currently being adopted by a number of researchers, farmers and agronomist for the retrieval of LAI. With accurate LAI estimations, especially in plots with limited irrigation, nitrogen or other management applications, remote sensing technologies using the GPR retrieval estimation from Sentinel-2 can serve as a decision support tool for further diagnoses to the factors limiting LAI in farms. These results present the first comparison of the SNAP model for understanding the phenological dynamics of irrigated rice using Sentinel-2 data.

7.3.3 Estimating yield variability from Sentinel-2 data at landscape and smallholder scale

As identified with the retrieval of LAI, the availability of Sentinel-2 data not only provides the opportunity to monitor yield indicators but yield directly. To this end, this research represents the first study to access the spatio-spectral suitability of Sentinel-2 10m and 20m for predicting within field variability at landscape scale and also the possibility of Sentinel-2 for predicting

yield at smallholder rice farms (Chapter 6). The first significant contribution to knowledge is the superiority of Sentinel-2 10m for predicting within field variability at landscape scale using the spectral bands and NDVI using the random forest model compared to Sentinel-2 20m. Although Sentinel-2 20m bands contain additional spectral bands along the red-edge which have shown in other studies to improve the accuracy of predicting yield (Kanke et al., 2016), the findings from the study suggests the suitability of Sentinel-2 10m for accurately predicting yield variability in rice fields obtained through statistical test. Another significant contribution to knowledge is the suitability of Sentinel-2 (10m and 20m) data for estimating and forecasting smallholder rice farm yields based on FAO (2014) categorization of farm sizes. This study is the first to quantify the suitability of Sentinel-2 data for predicting yield based on FAO (2014) definition of smallholder farmers. Provided these farms are homogenous over a minimum area (at least 0.5ha), Sentinel-2 data is able to predict rice yield. These findings are particularly important in the context of smallholder rice farms who dominate rice cultivation sphere, with farms usually located in remote areas with limited road network. The limited availability of road network to these farms make the possibility of frequent visit to obtain yield reports a challenge to agricultural institutions saddled with the responsibility of accounting for the annual dry season yield. With the increase in government initiatives for rice farmers, the ability to track their yield over various irrigated dry seasons will provide the government with a holistic report of the estimated yield being generated by rice farmers at landscape, regional and country scale. This information will be useful towards understanding the rice produced by rice farms with a view to bridging the rice consumption deficiency in sub-Saharan countries.

Another significant contribution of the study is identifying the suitability of baseline Sentinel-2 data using random forest models for estimating rice yield when environmental and climatic data are not available. Furthermore, the results also show models using machine learning (e.g. Random Forest) to be suitable for predicting yield with baseline Sentinel-2 data only. This is significant because of the difficulty of obtaining detailed environmental and climate data of farms especially in remote villages. Without the availability of the climatic and environmental data, it becomes difficult adopting crop simulation models to predict yield. As such, the importance of this study is amplified by the possibility to acquire yield at local and regional scale without the complexities attached to crop models.

7.3.4 Significance of the results to the attainment of the objectives of the Sustainable Development Goals, the African Development Fund and the Nigerian Government

This thesis has highlighted the rich potential of remote sensing technologies for improving the productivity of rice especially for smallholder farmers. With the potential of monitoring yield indicators at remote areas, there are boundless opportunities in remote sensing for boosting rice yields.

The objectives of this thesis are directly relevant and applicable for the realisation of two targets under the 2nd objective of the SDGs ("Zero hunger – Achieve food security and improved nutrition and promote sustainable agriculture"). These are even more significant when seeking to attain zero hunger in sub-Saharan Africa and Nigeria, where poverty and hunger are prevalent. Further to the 2nd objective of the SDGs, the findings of these study have implicit links to the 9th (Industry, Innovation and Infrastructure), 12th (Responsible Consumption and Production), 13th (Climate Action) and 17th (Partnerships to achieve the Goal).

In addition to meeting the objectives some of the SDG objectives, the African Development Fund (ADF) are providing start – up grants to African youths to the tune of $120, 000 for agricultural purposes. From the findings of this thesis, the possibility of accurately monitoring yield and yield indicators provide comparative yield and profit advantage to farmers, thereby achieving the 1st, (End poverty in all its forms), 2nd (End hunger, achieve food security and improved nutrition and promote sustainable agriculture) and 6th (Ensure availability and sustainable management of water and sanitation for all) objectives of ADF.

Furthermore, with various agricultural interventions, grants and loans provided by the Nigerian government for rice cultivation, the findings of this thesis can foster the accurate monitoring of yield indicators which can have instant impact on management practices. By providing precise management practices, yield will increase, thereby directly increasing the available rice produced at a national scale and improving the financial status of smallholder farmers and large-scale farm institutions.

Therefore, through proper estimation of yield and yield indicators in rice and other crops, the possibility of attaining the respective SDG, ADF and Nigeria's goals related to food security can be achieved.

7.3.5 Collaboration with Agricultural Agencies and Organisations for improving rice productivity

From the findings of this research, there is strong potential to collaborate with agricultural agencies saddled with the task of working closely with smallholder farmers to boost their yield. By early monitoring, the possibilities of providing timely information which could be beneficial to improving the rice yield can be actualised. For instance, accurately monitoring the dynamics of LAI and providing the information to farm extension workers will provide rapid remedies/interventions towards optimizing yield for the particular rice cultivars. In the case of biomass monitoring, the information can be critical in assessing the yield potential of farmers prior to yield. This information will be important in forecasting the economic potential of rice farming for different rice seasons.

With increased interest in international organisations such as United Nations, World bank and Bill and Melinda gate foundation to improve the productivity of rice in Nigeria and Africa at large, the potential of remote sensing technologies will attract more funding bodies passionate about ending hunger and poverty in Nigeria and Africa. By providing accurate information to these bodies, it makes the deployment of finances target oriented especially to the most vulnerable farmers in urgent need of training on management practices to improve their yield. Furthermore, this will increase the interest and passion of Nigerians to go into farming knowing for a fact that the industry is lucrative and can help alleviate poverty in the worst hit areas, therefore increasing the interest in the use of technologies such as remote sensing which is not the case at the moment.

On that note, we can infer from the findings of this research that remote sensing technologies are indispensable towards synergising and complimenting the efforts of multiple rice stakeholders towards achieving a common goal rice production for the ever-increasing population in Nigeria and Africa

7.4 Limitations

Inevitably, the research has some limitations as a result of the timing of data collection, availability of equipment for monitoring and some methodologies adopted. A general limitation of the study was the inability to monitor multiple farms within the north central Nigeria due to funding, logistics and security. Below, I discuss the specific limitations based on the yield and yield indicators monitored.

7.4.1 Biomass Estimation

In terms of monitoring rice AGB, the study only monitored one season, which may present some bias in the results. Although monitoring rice in one season provided insight on application of RGB and MSI cameras for the estimation of rice AGB, inclusion of multiple growing seasons may provide additional information which may not have been observed when monitoring a single season. Also, we obtained only a single biomass collection during the reproductive and ripening phases due to sensor functionality issues during the course of the field work, limiting the study to only 54 samples for the study. For this reason, we adopted the random forest model because of the ability to deal with small sample sizes.

When estimating plant height using the RGB camera, the study did not acquire ground height measurements prior to the planting of rice. This invariably led to estimation of ground height in plots with plants at the reproductive and ripening phases, thus leading to more uncertainty in plant height measurement accuracy.

In terms of MSI sensor, standard radiometric calibration methods were applied although studies have shown that spectral reflectance from standard calibration methods may exhibit bias compared to other calibration approaches.

7.4.2 LAI Estimation

Radiative transfer models are very complex and require expertise to retrieve LAI from Satellite images. These poses are real issue in terms of transferability and readily adoption by farmers across scale because they require in-depth knowledge on spectroscopy and the underlining core principles of remote sensing. It therefore serves as a limitation in its implementation with farmers and farming stakeholders at this point.

Although this may serve as a limitation for the retrieval of LAI, the creation of a user-friendly interphase similarly to the SNAP tool box may be the most suitable approach for the estimation

of LAI. Until that is implemented, it remains challenging to adopt radiative transfer models by farmers for retrieving LAI estimating during the phenological phases.

7.4.3 Yield Estimation

In terms of yield data, the study only acquired one season of yield data due to time constraint attached to the fieldwork. Obtaining multiple yield data will be important for calibrating the model, which will present a more robust assessment of yield patterns and trends on the farm. Also, information on the climatic and environmental variables were not included in the study, which will have provided additional information to the yield models developed for the study.

The use of multiple rice cultivars is another interesting area which the study did not monitor in the first fieldwork campaign. Varying rice cultivars with different height potentials will provide further information on the suitability of plant height estimates for monitoring rice AGB at the late growing phases.

Finally, due to data commercial confidentiality, the study did not explicitly reveal the yield data. This was because of the memorandum of understanding between the farm and myself.

7.5 Possible future work

7.5.1 Inclusion of Synthetic Aperture Radar sensors for monitoring rice phenology during dry and rainy season

Optical remote sensing presents a replicable and effective way of monitoring irrigated rice yield, particularly during the dry season months. During the rainy season, cloud formation plays a significant role in the availability of Sentinel-2 images for monitoring yield and yield indicators in rice. As a result of cloud cover, there is limited availability of optical satellite images during the rainy season, owning to the fact that most rice farmers in sub-Saharan Africa depend on the rainy season rains to grow. As such, complementary images are important for rice phenology monitoring.

An alternative solution is represented by synthetic aperture radar (SAR) imagery. SAR images possess the ability to acquire images when there is cloud cover, making then very important for monitoring rice during the rainy season months (Clauss et al. 2018). Furthermore, SAR backscatter is related to the geometry and physical properties of the surface such as soil roughness, soil moisture are useful for monitoring vegetation cover (Chen et al., 2007; Guan et al., 2018; Pipia et al., 2019). For instance, Clauss et al. (2018) used Sentinel-1 data for predicting rice yield using field surveying data with statistical results showing strong

agreement with Sentinel-1 data and yield using machine learning models. In addition, the launch of Sentinel-1 data provides the opportunity to complement Sentinel-2 data for monitoring yield and yield indicators in rice. With the possibility of acquiring high resolution referenced yield data, the possibility exists to monitor rice during the dry and rainy season using the combination of Sentinel 1 and 2 data.

7.5.2 Adoption of data assimilation of remote sensing and crop models for predicting yield

This study has shown the suitability of baseline Sentinel-2 data for predicting rice yield. However, it will be interesting to see the outcome of yield estimation from fusion of satellite data and crops simulation models which account for the spatial distribution of soil properties (e.g. soil moisture), canopy state variables (e.g. LAI, biomass, nitrogen content, etc.), and meteorological data (Hansen and Jones, 2000).

Furthermore, advancements in data assimilation modelling techniques provides more efficient ways of combining crop simulation models with remote sensing data. Jin et al. (2018) review of data assimilation modelling with remote sensing spotlights updating methods such as Ensemble Kalman Filter as an assimilating technique for update LAI values retrieved from remote sensing techniques for predicting yield. Therefore, the availability of environmental and climatic data, an alternative approach to estimating yield from Sentinel 1 and 2 data and drone images.

7.5.3 Phenotyping strategies for monitoring multiple factors affecting rice yield from airborne platforms

Crop phenotyping are tailored towards accurately and precisely obtain traits linked to crop growth status, yield, and resilience to environmental stress. Jin et al. (2020) review of high throughput phenotyping shows the possibility of monitoring multiple yield, yield indicators and stress factors affecting crops simultaneously from drone in particular. With the advancement in cameras on-board drones, future studies will focus on monitoring crop lodging, nitrogen intake, plant height, LAI, biomass and yield during the same phenology window.

7.5.4 Collaboration with rice farming stakeholders in Nigeria and Africa

With the possibility of remote sensing technologies for monitoring rice productivity, further studies will collaborate with smallholder farmers and government/private stakeholders in order to established a phenological monitoring scheme for rice. In doing so, accurate and

timely data of the farms will be provided to smallholder farmers in order to help improve their yield.

Partnership with established government and Non-government Organisations saddled with the task of improving the production of rice in Nigeria using remote sensing technologies will also be an important area to further the research. By identifying the level of participation of these agencies with farmers using remote sensing technologies, they are in a better position to provide accurate intervention schemes to improve the yield performance of farmers across scales.

Finally, this approached is transferable across regions and crops as further studies should venture into monitoring other staple crops in Nigeria. From the African perspective, partnership with the African Development Bank will provide the avenue to implement the monitoring approach in Africa. In doing so, Nigeria and Africa have a much better chance towards achieving the SDG goals related to food, hunger and poverty by 2030.

Appendix

Appendix 1: Spectral reflectance curve of B1P1SP1 (High Nitrogen, Continuous Flooding) on the 30th of January and the 26th of March 2018

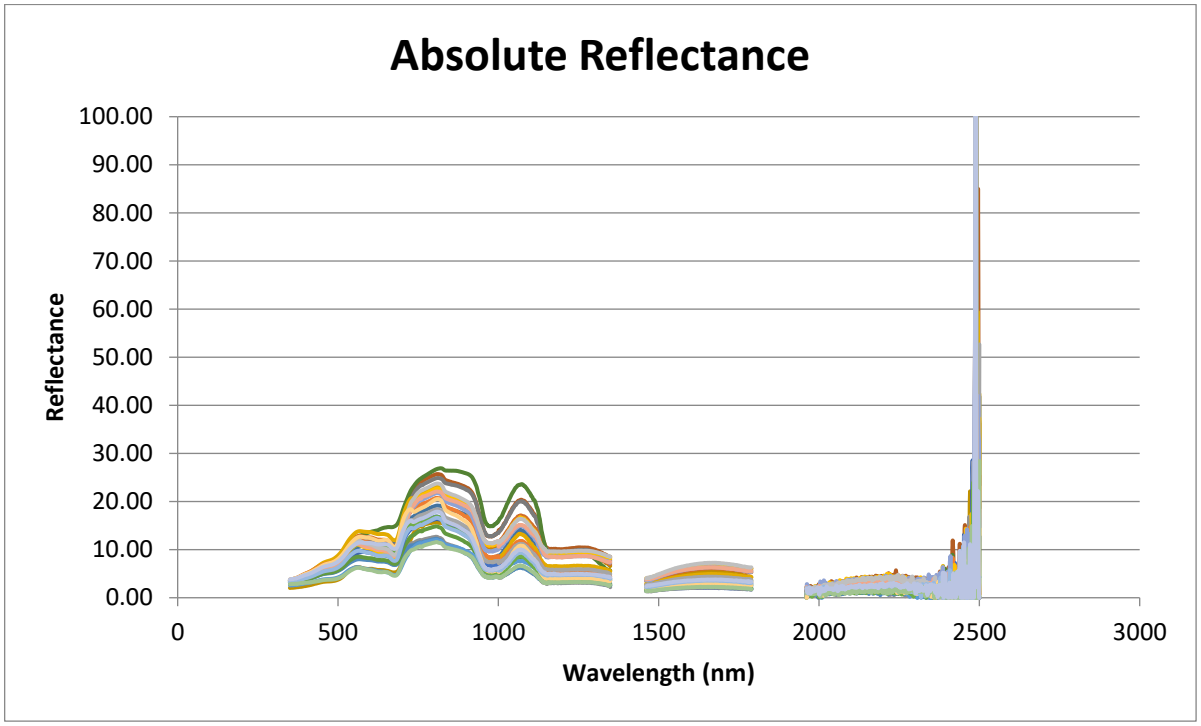

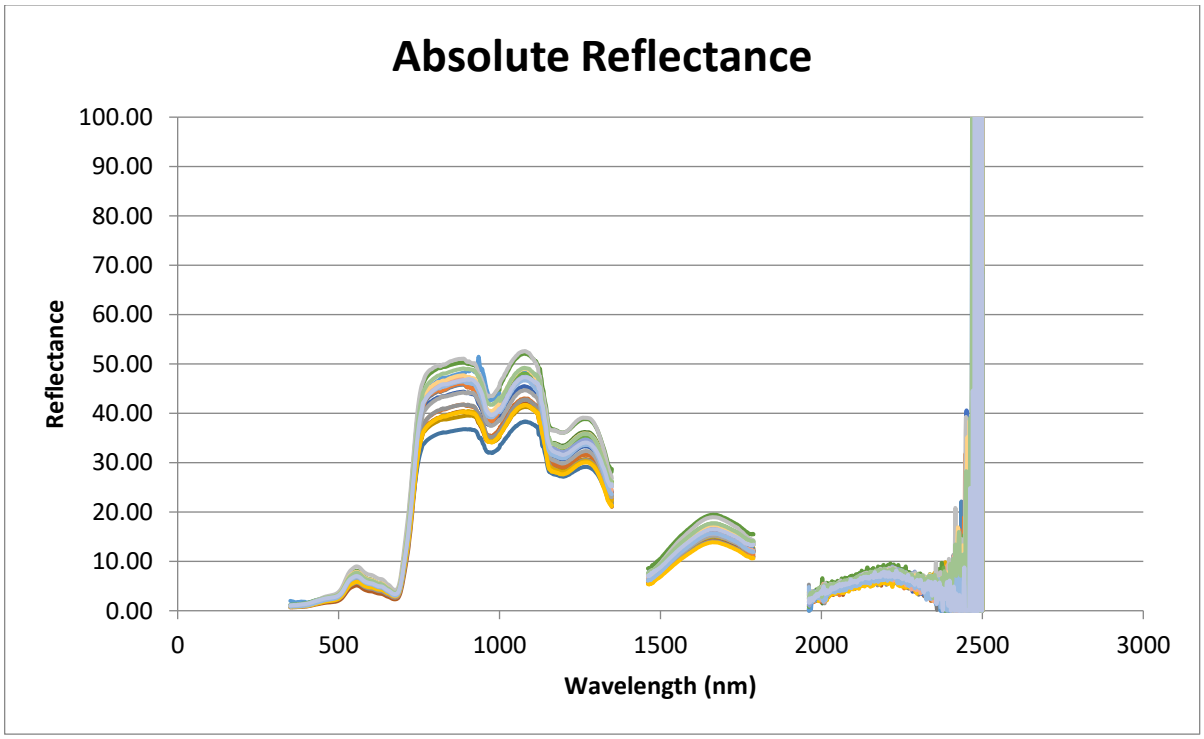

Appendix 2: Orthomosaic and the corresponding Digital Surface Model (DSM) before densification

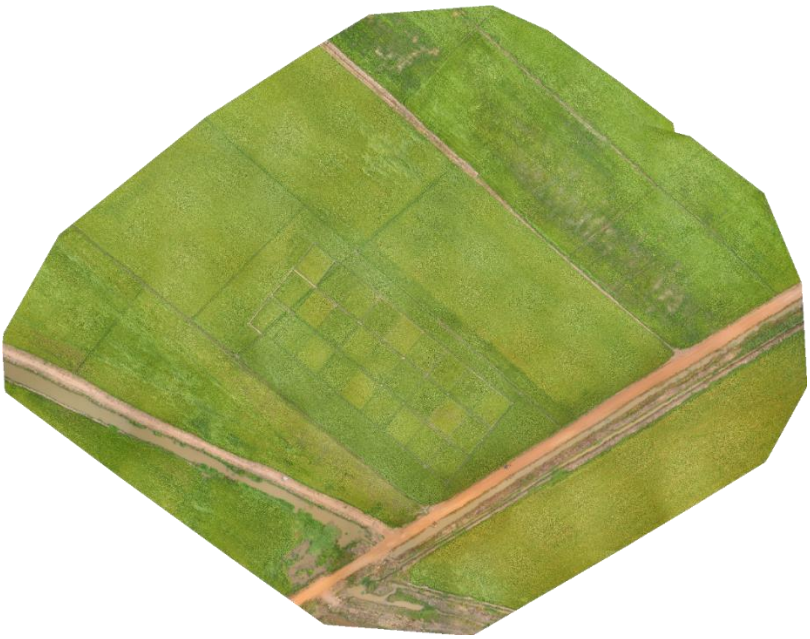

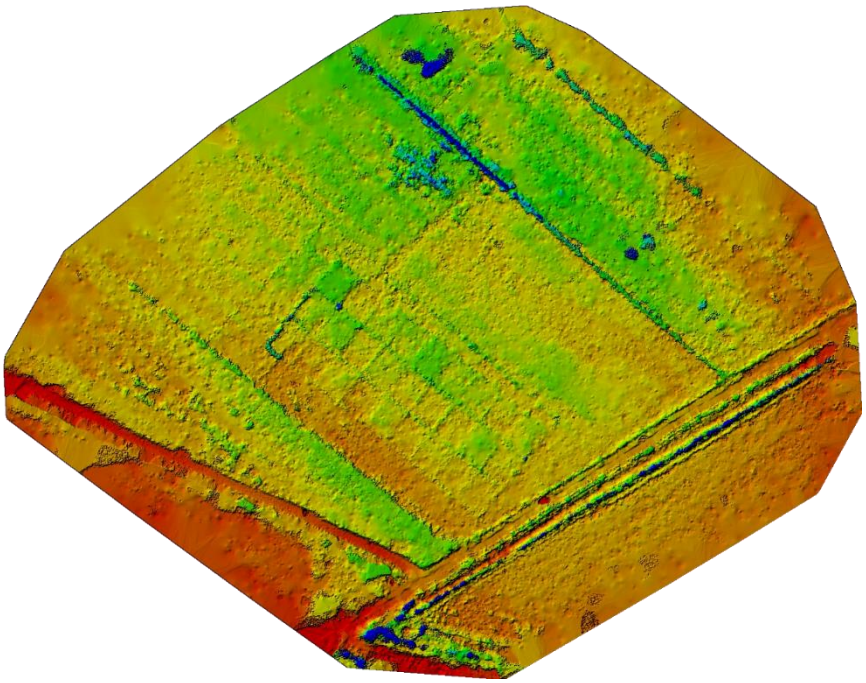

Appendix 3: Pearson correlation matrix between independent (biomass) and dependent (Plant height, vegetation indices and texture metrics) for rice aboveground biomass.

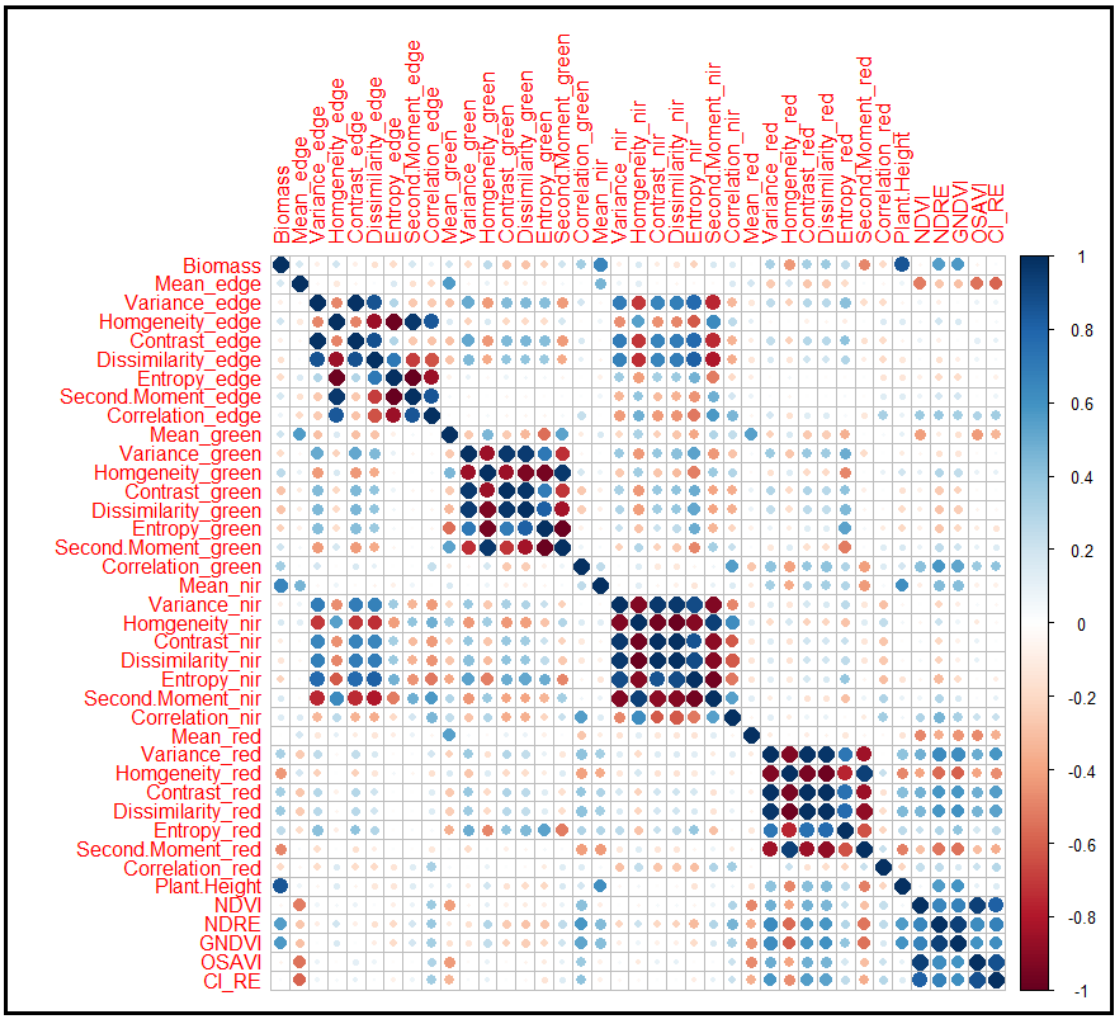

Appendix 4: Evidence of the flooding regimes adopted for the field experiment with the irrometer tensiometer install in the ground

Appendix 5: Collection of field spectra using the Field spectrometer.

Appendix 6: Researcher and field assistances preparing for drone flight after calibrating the sequoia camera with the calibration target by AIRNOV.

Appendix 7: Researcher monitoring the yield harvesting protocol during the 2018/2019 season harvest.

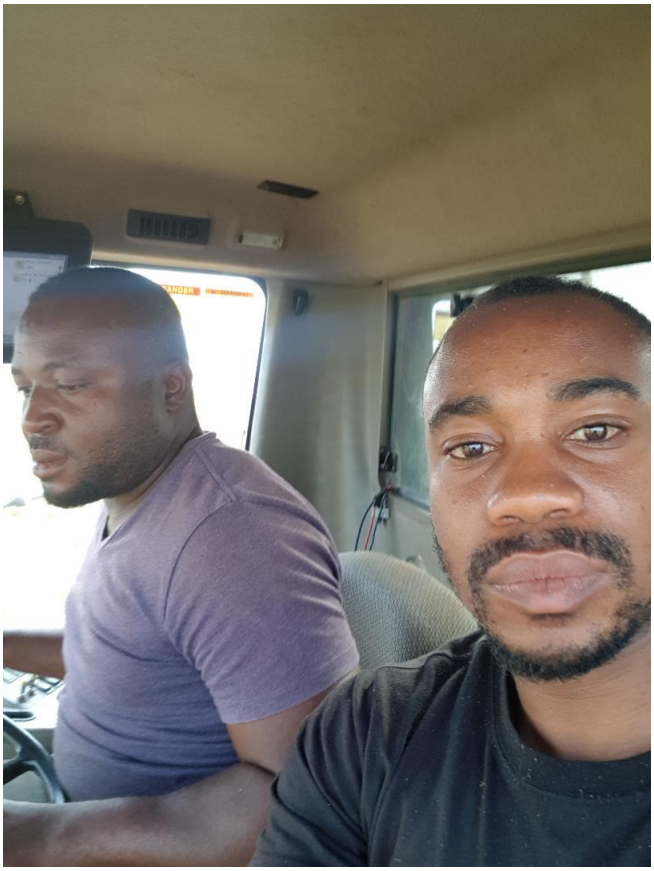

BIBLIOGRAPHY

Adeluyi, O., Harris, A., Clay, G., Foster, T., 2019. A comparison of retrieval approaches for estimating the seasonal dynamics of rice leaf area index from simulated Sentinel-2 data, in: Neale, C.M., Maltese, A. (Eds.), Remote Sensing for Agriculture, Ecosystems, and Hydrology XXI. Presented at the Remote Sensing for Agriculture, Ecosystems, and Hydrology XXI, SPIE, Strasbourg, France, p. 18. https://doi.org/10.1117/12.2533304

Agidi, V., 2018. Trends of Staple Crops Yields in Nasarawa State, Nigeria. Agric. Stud. 2, 31. https://doi.org/10.31058/j.as.2018.23014

Ahmad, I., Singh, A., Fahad, M., Waqas, M.M., 2020. Remote sensing-based framework to predict and assess the interannual variability of maize yields in Pakistan using Landsat imagery. Comput. Electron. Agric. 178, 105732. https://doi.org/10.1016/j.compag.2020.105732

Ahmed, W., Qaswar, M., Jing, H., Wenjun, D., Geng, S., Kailou, L., Ying, M., Ao, T., Mei, S., Chao, L., Yongmei, X., Ali, S., Normatov, Y., Mehmood, S., Khan, M.N., Huimin, Z., 2020. Tillage practices improve rice yield and soil phosphorus fractions in two typical paddy soils. J. Soils Sediments 20, 850–861. https://doi.org/10.1007/s11368-019-02468-3

Akintayo, O.I., Rahji, M. a. Y., Awoyemi, T.T., Adeoti, A.I., 2011. Determinants of Yield Gap in Lowland Rice Production in North-Central Nigeria. Agrosearch 11, 1–10. https://doi.org/10.4314/agrosh.v11i1.1

Ali, I., Greifeneder, F., Stamenkovic, J., Neumann, M., Notarnicola, C., 2015. Review of Machine Learning Approaches for Biomass and Soil Moisture Retrievals from Remote Sensing Data. Remote Sens. 7, 16398–16421. https://doi.org/10.3390/rs71215841

Anderson, K., Hancock, S., Disney, M., Gaston, K.J., 2016. Is waveform worth it? A comparison of LiDAR approaches for vegetation and landscape characterization. Remote Sens. Ecol. Conserv. 2, 5–15. https://doi.org/10.1002/rse2.8

Ansper, A., Alikas, K., 2019. Retrieval of Chlorophyll a from Sentinel-2 MSI Data for the European Union Water Framework Directive Reporting Purposes. Remote Sens. 11, 64. https://doi.org/10.3390/rs11010064

Antralina, M., Istina, I.N., YuyunYuwariah, Simarmata, T., 2015. Effect of Difference Weed Control Methods to Yield of Lowland Rice in the SOBARI. Procedia Food Sci., The First International Symposium on Food and Agro-biodiversity Conducted by Indonesian Food Technologists Community 3, 323–329. https://doi.org/10.1016/j.profoo.2015.01.035

Anwar, M.P., Juraimi, A.S., Mohamed, M.T.M., Uddin, M.K., Samedani, B., Puteh, A., Man, A., 2013. Integration of Agronomic Practices with Herbicides for Sustainable Weed Management in Aerobic Rice. Sci. World J. 2013. https://doi.org/10.1155/2013/916408

Apata, T., 2016. Small farms and agricultural productivity in Nigeria: empirical analysis of the effects of land tenure, fragmentation and property rights. Acad. J. Agric. Res. 4, 691–697.

Atkinson, P.M., Tatnall, A.R.L., 1997. Introduction Neural networks in remote sensing. Int. J. Remote Sens. 18, 699–709. https://doi.org/10.1080/014311697218700

Azzari, G., Jain, M., Lobell, D.B., 2017. Towards fine resolution global maps of crop yields: Testing multiple methods and satellites in three countries. Remote Sens. Environ.,

Big Remotely Sensed Data: tools, applications and experiences 202, 129–141. https://doi.org/10.1016/j.rse.2017.04.014
Bacour, C., Baret, F., Béal, D., Weiss, M., Pavageau, K., 2006. Neural network estimation of LAI, fAPAR, fCover and LAI×Cab, from top of canopy MERIS reflectance data: Principles and validation. Remote Sens. Environ. 105, 313–325. https://doi.org/10.1016/j.rse.2006.07.014
Bai, G., Ge, Y., Hussain, W., Baenziger, P.S., Graef, G., 2016. A multi-sensor system for high throughput field phenotyping in soybean and wheat breeding. Comput. Electron. Agric. 128, 181–192. https://doi.org/10.1016/j.compag.2016.08.021
Bai, T., Zhang, N., Mercatoris, B., Chen, Y., 2019. Jujube yield prediction method combining Landsat 8 Vegetation Index and the phenological length. Comput. Electron. Agric. 162, 1011–1027. https://doi.org/10.1016/j.compag.2019.05.035
Balaghi, R., Tychon, B., Eerens, H., Jlibene, M., 2008. Empirical regression models using NDVI, rainfall and temperature data for the early prediction of wheat grain yields in Morocco. Int. J. Appl. Earth Obs. Geoinformation, Modern Methods in Crop Yield Forecasting and Crop Area Estimation 10, 438–452. https://doi.org/10.1016/j.jag.2006.12.001
Bandaru, V., Daughtry, C.S., Codling, E.E., Hansen, D.J., White-Hansen, S., Green, C.E., 2016. Evaluating Leaf and Canopy Reflectance of Stressed Rice Plants to Monitor Arsenic Contamination. Int. J. Environ. Res. Public. Health 13, 606. https://doi.org/10.3390/ijerph13060606
Banerjee, K., Krishnan, P., Mridha, N., 2018. Application of thermal imaging of wheat crop canopy to estimate leaf area index under different moisture stress conditions. Biosyst. Eng. 166, 13–27. https://doi.org/10.1016/j.biosystemseng.2017.10.012
Baret, F., Buis, S., 2008. Estimating Canopy Characteristics from Remote Sensing Observations: Review of Methods and Associated Problems, in: Liang, S. (Ed.), Advances in Land Remote Sensing: System, Modeling, Inversion and Application. Springer Netherlands, Dordrecht, pp. 173–201. https://doi.org/10.1007/978-1-4020-6450-0_7
Baret, F., Hagolle, O., Geiger, B., Bicheron, P., Miras, B., Huc, M., Berthelot, B., Niño, F., Weiss, M., Samain, O., Roujean, J.L., Leroy, M., 2007. LAI, fAPAR and fCover CYCLOPES global products derived from VEGETATION: Part 1: Principles of the algorithm. Remote Sens. Environ. 110, 275–286. https://doi.org/10.1016/j.rse.2007.02.018
Barmeier, G., Schmidhalter, U., 2017. High-Throughput Field Phenotyping of Leaves, Leaf Sheaths, Culms and Ears of Spring Barley Cultivars at Anthesis and Dough Ripeness. Front. Plant Sci. 8. https://doi.org/10.3389/fpls.2017.01920
Barmeier, G., Schmidhalter, U., 2016. High-Throughput Phenotyping of Wheat and Barley Plants Grown in Single or Few Rows in Small Plots Using Active and Passive Spectral Proximal Sensing. Sensors 16, 1860. https://doi.org/10.3390/s16111860
Bastiaanssen, W.G.M., Ali, S., 2003. A new crop yield forecasting model based on satellite measurements applied across the Indus Basin, Pakistan. Agric. Ecosyst. Environ. 94, 321–340. https://doi.org/10.1016/S0167-8809(02)00034-8
Becker-Reshef, I., Justice, C., Sullivan, M., Vermote, E., Tucker, C., Anyamba, A., Small, J., Pak, E., Masuoka, E., Schmaltz, J., Hansen, M., Pittman, K., Birkett, C., Williams, D., Reynolds, C., Doorn, B., 2010. Monitoring Global Croplands with Coarse Resolution Earth Observations: The Global Agriculture Monitoring (GLAM) Project. Remote Sens. 2, 1589–1609. https://doi.org/10.3390/rs2061589
Belder, P., Bouman, B.A.M., Cabangon, R., Guoan, L., Quilang, E.J.P., Yuanhua, L., Spiertz, J.H.J., Tuong, T.P., 2004. Effect of water-saving irrigation on rice yield and

water use in typical lowland conditions in Asia. Agric. Water Manag. 65, 193–210. https://doi.org/10.1016/j.agwat.2003.09.002
Bendig, J., Bolten, A., Bennertz, S., Broscheit, J., Eichfuss, S., Bareth, G., 2014. Estimating Biomass of Barley Using Crop Surface Models (CSMs) Derived from UAV-Based RGB Imaging. Remote Sens. 6, 10395–10412. https://doi.org/10.3390/rs61110395
Bendig, J., Yu, K., Aasen, H., Bolten, A., Bennertz, S., Broscheit, J., Gnyp, M.L., Bareth, G., 2015. Combining UAV-based plant height from crop surface models, visible, and near infrared vegetation indices for biomass monitoring in barley. Int. J. Appl. Earth Obs. Geoinformation 39, 79–87. https://doi.org/10.1016/j.jag.2015.02.012
Berger, K., Atzberger, C., Danner, M., D'Urso, G., Mauser, W., Vuolo, F., Hank, T., 2018. Evaluation of the PROSAIL Model Capabilities for Future Hyperspectral Model Environments: A Review Study. Remote Sens. 10, 85. https://doi.org/10.3390/rs10010085
Berger, K., Verrelst, J., Féret, J.-B., Hank, T., Wocher, M., Mauser, W., Camps-Valls, G., 2020. Retrieval of aboveground crop nitrogen content with a hybrid machine learning method. Int. J. Appl. Earth Obs. Geoinformation 92, 102174. https://doi.org/10.1016/j.jag.2020.102174
Bijay-Singh, Shan, Y.H., Johnson-Beebout, S.E., Yadvinder-Singh, Buresh, R.J., 2008. Chapter 3 Crop Residue Management for Lowland Rice-Based Cropping Systems in Asia, in: Advances in Agronomy. Academic Press, pp. 117–199. https://doi.org/10.1016/S0065-2113(08)00203-4
Bijay-Singh, Singh, V.K., 2017. Fertilizer Management in Rice, in: Chauhan, B.S., Jabran, K., Mahajan, G. (Eds.), Rice Production Worldwide. Springer International Publishing, Cham, pp. 217–253. https://doi.org/10.1007/978-3-319-47516-5_10
Bolton, D.K., Friedl, M.A., 2013. Forecasting crop yield using remotely sensed vegetation indices and crop phenology metrics. Agric. For. Meteorol. 173, 74–84. https://doi.org/10.1016/j.agrformet.2013.01.007
Bouvet, A., Le Toan, T., 2011. Use of ENVISAT/ASAR wide-swath data for timely rice fields mapping in the Mekong River Delta. Remote Sens. Environ. 115, 1090–1101. https://doi.org/10.1016/j.rse.2010.12.014
Brady, N.C., 1981. Soil Factors that Influence Rice Production, in: Proceedings of Symposium on Paddy Soils. Springer, Berlin, Heidelberg, pp. 1–19. https://doi.org/10.1007/978-3-642-68141-7_1
Breiman, L., 2001. Random Forests. Mach. Learn. 45, 5–32. https://doi.org/10.1023/A:1010933404324
Bsaibes, A., Courault, D., Baret, F., Weiss, M., Olioso, A., Jacob, F., Hagolle, O., Marloie, O., Bertrand, N., Desfond, V., Kzemipour, F., 2009. Albedo and LAI estimates from FORMOSAT-2 data for crop monitoring. Remote Sens. Environ. 113, 716–729. https://doi.org/10.1016/j.rse.2008.11.014
Burke, M., Lobell, D.B., 2017. Satellite-based assessment of yield variation and its determinants in smallholder African systems. Proc. Natl. Acad. Sci. 114, 2189–2194. https://doi.org/10.1073/pnas.1616919114
Caccamo, G., Chisholm, L.A., Bradstock, R.A., Puotinen, M.L., 2011. Assessing the sensitivity of MODIS to monitor drought in high biomass ecosystems. Remote Sens. Environ. 115, 2626–2639. https://doi.org/10.1016/j.rse.2011.05.018
Campos-Taberner, M., García-Haro, F.J., Camps-Valls, G., Grau-Muedra, G., Nutini, F., Crema, A., Boschetti, M., 2016. Multitemporal and multiresolution leaf area index retrieval for operational local rice crop monitoring. Remote Sens. Environ. 187, 102–118. https://doi.org/10.1016/j.rse.2016.10.009

Camps-Valls, G., Munoz-Mari, J., Gomez-Chova, L., Richter, K., Calpe-Maravilla, J., 2009. Biophysical Parameter Estimation With a Semisupervised Support Vector Machine. IEEE Geosci. Remote Sens. Lett. 6, 248–252. https://doi.org/10.1109/LGRS.2008.2009077

Carter, G.A., Knapp, A.K., 2001. Leaf optical properties in higher plants: linking spectral characteristics to stress and chlorophyll concentration. Am. J. Bot. 88, 677–684. https://doi.org/10.2307/2657068

Casanova, D., Epema, G.F., Goudriaan, J., 1998. Monitoring rice reflectance at field level for estimating biomass and LAI. Field Crops Res. 55, 83–92. https://doi.org/10.1016/S0378-4290(97)00064-6

Case IH, 2018. Case Ih 9230 Manual [WWW Document]. Gist. URL https://gist.github.com/anonymous/95844a56ce38cb915639225ec8a57e88 (accessed 8.15.20).

Cen, H., Wan, L., Zhu, J., Li, Y., Li, X., Zhu, Y., Weng, H., Wu, W., Yin, W., Xu, C., Bao, Y., Feng, L., Shou, J., He, Y., 2019. Dynamic monitoring of biomass of rice under different nitrogen treatments using a lightweight UAV with dual image-frame snapshot cameras. Plant Methods 15, 32. https://doi.org/10.1186/s13007-019-0418-8

Chao, Z., Liu, N., Zhang, P., Ying, T., Song, K., 2019. Estimation methods developing with remote sensing information for energy crop biomass: A comparative review. Biomass Bioenergy 122, 414–425. https://doi.org/10.1016/j.biombioe.2019.02.002

Chauhan, S., Darvishzadeh, R., Boschetti, M., Pepe, M., Nelson, A., 2019. Remote sensing-based crop lodging assessment: Current status and perspectives. ISPRS J. Photogramm. Remote Sens. 151, 124–140. https://doi.org/10.1016/j.isprsjprs.2019.03.005

Chaurasia, S., author, V.K.D.C., 2004. Comparison of principal component inversion with VI-empirical approach for LAI estimation using simulated reflectance data. Int. J. Remote Sens. 25, 2881–2887. https://doi.org/10.1080/01431160410001685018

Chawala, P., Sandhu, H.A.S., 2020. Stubble burn area estimation and its impact on ambient air quality of Patiala & Ludhiana district, Punjab, India. Heliyon 6, e03095. https://doi.org/10.1016/j.heliyon.2019.e03095

Chen, B., Wu, Z., Wang, J., Dong, J., Guan, L., Chen, J., Yang, K., Xie, G., 2015. Spatio-temporal prediction of leaf area index of rubber plantation using HJ-1A/1B CCD images and recurrent neural network. ISPRS J. Photogramm. Remote Sens. 102, 148–160. https://doi.org/10.1016/j.isprsjprs.2014.12.011

Chen, J., Cao, F., Yin, X., Huang, M., Zou, Y., 2019. Yield performance of early-season rice cultivars grown in the late season of double-season crop production under machine-transplanted conditions. PLOS ONE 14, e0213075. https://doi.org/10.1371/journal.pone.0213075

Chen, J., Lin, H., Pei, Z., 2007. Application of ENVISAT ASAR Data in Mapping Rice Crop Growth in Southern China. IEEE Geosci. Remote Sens. Lett. 4, 431–435. https://doi.org/10.1109/LGRS.2007.896996

Chen, J.M., Black, T.A., 1992. Foliage area and architecture of plant canopies from sunfleck size distributions. Agric. For. Meteorol. 60, 249–266. https://doi.org/10.1016/0168-1923(92)90040-B

Chen, J.M., Black, T.A., 1991. Measuring leaf area index of plant canopies with branch architecture. Agric. For. Meteorol. 57, 1–12. https://doi.org/10.1016/0168-1923(91)90074-Z

Chen, J.M., Leblanc, S.G., 1997. A four-scale bidirectional reflectance model based on canopy architecture. IEEE Trans. Geosci. Remote Sens. 35, 1316–1337. https://doi.org/10.1109/36.628798

Chen, J.M., Li, X., Nilson, T., Strahler, A., 2000. Recent advances in geometrical optical modelling and its applications. Remote Sens. Rev. 18, 227–262. https://doi.org/10.1080/02757250009532391

Cheng, T., Song, R., Li, D., Zhou, K., Zheng, H., Yao, X., Tian, Y., Cao, W., Zhu, Y., 2017. Spectroscopic Estimation of Biomass in Canopy Components of Paddy Rice Using Dry Matter and Chlorophyll Indices. Remote Sens. 9, 319. https://doi.org/10.3390/rs9040319

Cho, M.A., Skidmore, A., Corsi, F., van Wieren, S.E., Sobhan, I., 2007. Estimation of green grass/herb biomass from airborne hyperspectral imagery using spectral indices and partial least squares regression. Int. J. Appl. Earth Obs. Geoinformation 9, 414–424. https://doi.org/10.1016/j.jag.2007.02.001

Clevers, J., Gitelson, A., 2012. Using the red-edge bands on Sentinel-2 for retrieving canopy chlorophyll and nitrogen content [WWW Document]. URL https://www.researchgate.net/publication/283419755_Using_the_red-edge_bands_on_Sentinel-2_for_retrieving_canopy_chlorophyll_and_nitrogen_content (accessed 2.14.17).

Clevers, J.G.P.W., Kooistra, L., van den Brande, M.M.M., 2017. Using Sentinel-2 Data for Retrieving LAI and Leaf and Canopy Chlorophyll Content of a Potato Crop. Remote Sens. 9, 405. https://doi.org/10.3390/rs9050405

Colomina, I., Molina, P., 2014. Unmanned aerial systems for photogrammetry and remote sensing: A review. ISPRS J. Photogramm. Remote Sens. 92, 79–97. https://doi.org/10.1016/j.isprsjprs.2014.02.013

Coluzzi, R., Imbrenda, V., Lanfredi, M., Simoniello, T., 2018. A first assessment of the Sentinel-2 Level 1-C cloud mask product to support informed surface analyses. Remote Sens. Environ. 217, 426–443. https://doi.org/10.1016/j.rse.2018.08.009

da Silva Júnior, J.C., Medeiros, V., Garrozi, C., Montenegro, A., Gonçalves, G.E., 2019. Random forest techniques for spatial interpolation of evapotranspiration data from Brazilian's Northeast. Comput. Electron. Agric. 166, 105017. https://doi.org/10.1016/j.compag.2019.105017

Darvishzadeh, R., Skidmore, A., Abdullah, H., Cherenet, E., Ali, A., Wang, T., Nieuwenhuis, W., Heurich, M., Vrieling, A., O'Connor, B., Paganini, M., 2019. Mapping leaf chlorophyll content from Sentinel-2 and RapidEye data in spruce stands using the invertible forest reflectance model. Int. J. Appl. Earth Obs. Geoinformation 79, 58–70. https://doi.org/10.1016/j.jag.2019.03.003

Darvishzadeh, R., Skidmore, A., Schlerf, M., Atzberger, C., 2008a. Inversion of a radiative transfer model for estimating vegetation LAI and chlorophyll in a heterogeneous grassland. Remote Sens. Environ., Earth Observations for Terrestrial Biodiversity and Ecosystems Special Issue 112, 2592–2604. https://doi.org/10.1016/j.rse.2007.12.003

Darvishzadeh, R., Skidmore, A., Schlerf, M., Atzberger, C., Corsi, F., Cho, M., 2008b. LAI and chlorophyll estimation for a heterogeneous grassland using hyperspectral measurements. ISPRS J. Photogramm. Remote Sens. 63, 409–426. https://doi.org/10.1016/j.isprsjprs.2008.01.001

Datta, S.K.D., 1981. Principles and Practices of Rice Production. Int. Rice Res. Inst.

de Wit, A., Boogaard, H., Fumagalli, D., Janssen, S., Knapen, R., van Kraalingen, D., Supit, I., van der Wijngaart, R., van Diepen, K., 2019. 25 years of the WOFOST cropping systems model. Agric. Syst. 168, 154–167. https://doi.org/10.1016/j.agsy.2018.06.018

Deery, D., Jimenez-Berni, J., Jones, H., Sirault, X., Furbank, R., 2014. Proximal Remote Sensing Buggies and Potential Applications for Field-Based Phenotyping. Agronomy 4, 349–379. https://doi.org/10.3390/agronomy4030349

Defourny, P., Bontemps, S., Bellemans, N., Cara, C., Dedieu, G., Guzzonato, E., Hagolle, O., Inglada, J., Nicola, L., Rabaute, T., Savinaud, M., Udroiu, C., Valero, S., Bégué, A., Dejoux, J.-F., El Harti, A., Ezzahar, J., Kussul, N., Labbassi, K., Lebourgeois, V., Miao, Z., Newby, T., Nyamugama, A., Salh, N., Shelestov, A., Simonneaux, V., Traore, P.S., Traore, S.S., Koetz, B., 2019. Near real-time agriculture monitoring at national scale at parcel resolution: Performance assessment of the Sen2-Agri automated system in various cropping systems around the world. Remote Sens. Environ. 221, 551–568. https://doi.org/10.1016/j.rse.2018.11.007

Delécolle, R., Maas, S.J., Guérif, M., Baret, F., 1992. Remote sensing and crop production models: present trends. ISPRS J. Photogramm. Remote Sens. 47, 145–161. https://doi.org/10.1016/0924-2716(92)90030-D

Delegido, J., Verrelst, J., Alonso, L., Moreno, J., 2011. Evaluation of Sentinel-2 Red-Edge Bands for Empirical Estimation of Green LAI and Chlorophyll Content. Sensors 11, 7063–7081. https://doi.org/10.3390/s110707063

Delloye, C., Weiss, M., Defourny, P., 2018. Retrieval of the canopy chlorophyll content from Sentinel-2 spectral bands to estimate nitrogen uptake in intensive winter wheat cropping systems. Remote Sens. Environ. 216, 245–261. https://doi.org/10.1016/j.rse.2018.06.037

Deng, L., Mao, Z., Li, X., Hu, Z., Duan, F., Yan, Y., 2018. UAV-based multispectral remote sensing for precision agriculture: A comparison between different cameras. ISPRS J. Photogramm. Remote Sens. 146, 124–136. https://doi.org/10.1016/j.isprsjprs.2018.09.008

Diker, K., Heermann, D.F., Brodahl, M.K., 2004. Frequency Analysis of Yield for Delineating Yield Response Zones. Precis. Agric. 5, 435–444. https://doi.org/10.1007/s11119-004-5318-9

Disney, M., Lewis, P., Saich, P., 2006. 3D modelling of forest canopy structure for remote sensing simulations in the optical and microwave domains. Remote Sens. Environ. 100, 114–132. https://doi.org/10.1016/j.rse.2005.10.003

Djamai, N., Fernandes, R., Weiss, M., McNairn, H., Goïta, K., 2019. Validation of the Sentinel Simplified Level 2 Product Prototype Processor (SL2P) for mapping cropland biophysical variables using Sentinel-2/MSI and Landsat-8/OLI data. Remote Sens. Environ. 225, 416–430. https://doi.org/10.1016/j.rse.2019.03.020

Dong, J., Xiao, X., 2016. Evolution of regional to global paddy rice mapping methods: A review. ISPRS J. Photogramm. Remote Sens. 119, 214–227. https://doi.org/10.1016/j.isprsjprs.2016.05.010

Dong, J., Xiao, X., Kou, W., Qin, Y., Zhang, G., Li, L., Jin, C., Zhou, Y., Wang, J., Biradar, C., Liu, J., Moore III, B., 2015. Tracking the dynamics of paddy rice planting area in 1986–2010 through time series Landsat images and phenology-based algorithms. Remote Sens. Environ. 160, 99–113. https://doi.org/10.1016/j.rse.2015.01.004

Dong, T., Liu, J., Qian, B., Jing, Q., Croft, H., Chen, J., Wang, J., Huffman, T., Shang, J., Chen, P., 2017. Deriving Maximum Light Use Efficiency From Crop Growth Model and Satellite Data to Improve Crop Biomass Estimation. IEEE J. Sel. Top. Appl. Earth Obs. Remote Sens. 10, 104–117. https://doi.org/10.1109/JSTARS.2016.2605303

Dong, T., Liu, J., Qian, B., Zhao, T., Jing, Q., Geng, X., Wang, J., Huffman, T., Shang, J., 2016. Estimating winter wheat biomass by assimilating leaf area index derived from

fusion of Landsat-8 and MODIS data. Int. J. Appl. Earth Obs. Geoinformation 49, 63–74. https://doi.org/10.1016/j.jag.2016.02.001
Dorigo, W.A., Zurita-Milla R., de Wit A.J.W, 2007. A review on reflective remote sensing and data assimilation techniques for enhanced agroecosystem modeling [WWW Document]. https://doi.org/10.1016/j.jag.2006.05.003
Drusch, M., Del Bello, U., Carlier, S., Colin, O., Fernandez, V., Gascon, F., Hoersch, B., Isola, C., Laberinti, P., Martimort, P., Meygret, A., Spoto, F., Sy, O., Marchese, F., Bargellini, P., 2012. Sentinel-2: ESA's Optical High-Resolution Mission for GMES Operational Services. Remote Sens. Environ., The Sentinel Missions - New Opportunities for Science 120, 25–36. https://doi.org/10.1016/j.rse.2011.11.026
Du, M., Noguchi, N., 2017. Monitoring of Wheat Growth Status and Mapping of Wheat Yield's within-Field Spatial Variations Using Color Images Acquired from UAV-camera System. Remote Sens. 9, 289. https://doi.org/10.3390/rs9030289
Duan, B., Fang, S., Zhu, R., Wu, X., Wang, S., Gong, Y., Peng, Y., 2019. Remote Estimation of Rice Yield With Unmanned Aerial Vehicle (UAV) Data and Spectral Mixture Analysis. Front. Plant Sci. 10. https://doi.org/10.3389/fpls.2019.00204
Dunand, R., Saichuk, J., 2014. Rice Growth and Development. La. Rice Prod. Handb. 13.
Dungan, J.L., Perry, J.N., Dale, M.R.T., Legendre, P., Citron-Pousty, S., Fortin, M.-J., Jakomulska, A., Miriti, M., Rosenberg, M.S., 2002. A balanced view of scale in spatial statistical analysis. Ecography 25, 626–640.
Durbha, S.S., King, R.L., Younan, N.H., 2007. Support vector machines regression for retrieval of leaf area index from multiangle imaging spectroradiometer. Remote Sens. Environ., Multi-angle Imaging SpectroRadiometer (MISR) Special Issue 107, 348–361. https://doi.org/10.1016/j.rse.2006.09.031
Durgun, Y.Ö., Gobin, A., Duveiller, G., Tychon, B., 2020. A study on trade-offs between spatial resolution and temporal sampling density for wheat yield estimation using both thermal and calendar time. Int. J. Appl. Earth Obs. Geoinformation 86, 101988. https://doi.org/10.1016/j.jag.2019.101988
Duveiller, G., Weiss, M., Baret, F., Defourny, P., 2011. Retrieving wheat Green Area Index during the growing season from optical time series measurements based on neural network radiative transfer inversion. Remote Sens. Environ. 115, 887–896. https://doi.org/10.1016/j.rse.2010.11.016
Elarab, M., Ticlavilca, A.M., Torres-Rua, A.F., Maslova, I., McKee, M., 2015. Estimating chlorophyll with thermal and broadband multispectral high resolution imagery from an unmanned aerial system using relevance vector machines for precision agriculture. Int. J. Appl. Earth Obs. Geoinformation, Special Issue on "Advances in remote sensing of vegetation function and traits" 43, 32–42. https://doi.org/10.1016/j.jag.2015.03.017
Estévez, J., Vicent, J., Rivera-Caicedo, J.P., Morcillo-Pallarés, P., Vuolo, F., Sabater, N., Camps-Valls, G., Moreno, J., Verrelst, J., 2020. Gaussian processes retrieval of LAI from Sentinel-2 top-of-atmosphere radiance data. ISPRS J. Photogramm. Remote Sens. 167, 289–304. https://doi.org/10.1016/j.isprsjprs.2020.07.004
Ezedinma, C., 2008. Impact of Trade on Domestic Rice Production and the challenge of Self sufficiency in Nigeria. https://doi.org/10.13140/2.1.3601.1204
Fageria, N.K., 2007. Yield Physiology of Rice. J. Plant Nutr. 30, 843–879. https://doi.org/10.1080/15226510701374831
Fahad, S., Bajwa, A.A., Nazir, U., Anjum, S.A., Farooq, A., Zohaib, A., Sadia, S., Nasim, W., Adkins, S., Saud, S., Ihsan, M.Z., Alharby, H., Wu, C., Wang, D., Huang, J., 2017. Crop Production under Drought and Heat Stress: Plant Responses and Management Options. Front. Plant Sci. 8. https://doi.org/10.3389/fpls.2017.01147

Fang, H., Li, W., Wei, S., Jiang, C., 2014. Seasonal variation of leaf area index (LAI) over paddy rice fields in NE China: Intercomparison of destructive sampling, LAI-2200, digital hemispherical photography (DHP), and AccuPAR methods. Agric. For. Meteorol. 198–199, 126–141. https://doi.org/10.1016/j.agrformet.2014.08.005

FAO, 2018a. Farm size | Family Farming Knowledge Platform | Food and Agriculture Organization of the United Nations [WWW Document]. URL http://www.fao.org/family-farming/data-sources/dataportrait/farm-size/en (accessed 6.18.20).

FAO, 2018b. FAO Rice Market Monitor (RMM) [WWW Document]. URL http://www.fao.org/economic/est/publications/rice-publications/rice-market-monitor-rmm/en/ (accessed 5.6.20).

FAO (Ed.), 2014. Innovation in family farming, The state of food and agriculture. Rome.

Fawcett, D., Panigada, C., Tagliabue, G., Boschetti, M., Celesti, M., Evdokimov, A., Biriukova, K., Colombo, R., Miglietta, F., Rascher, U., Anderson, K., 2020. Multi-Scale Evaluation of Drone-Based Multispectral Surface Reflectance and Vegetation Indices in Operational Conditions. Remote Sens. 12, 514. https://doi.org/10.3390/rs12030514

Fei, Y., Jiulin, S., Hongliang, F., Zuofang, Y., Jiahua, Z., Yunqiang, Z., Kaishan, S., Zongming, W., Maogui, H., 2012. Comparison of different methods for corn LAI estimation over northeastern China. Int. J. Appl. Earth Obs. Geoinformation 18, 462–471. https://doi.org/10.1016/j.jag.2011.09.004

Feng Gao, Masek, J., Schwaller, M., Hall, F., 2006. On the blending of the Landsat and MODIS surface reflectance: predicting daily Landsat surface reflectance. IEEE Trans. Geosci. Remote Sens. 44, 2207–2218. https://doi.org/10.1109/TGRS.2006.872081

Feng, W., Zhang, H.-Y., Zhang, Y.-S., Qi, S.-L., Heng, Y.-R., Guo, B.-B., Ma, D.-Y., Guo, T.-C., 2016. Remote detection of canopy leaf nitrogen concentration in winter wheat by using water resistance vegetation indices from in-situ hyperspectral data. Field Crops Res. 198, 238–246. https://doi.org/10.1016/j.fcr.2016.08.023

Fensholt, R., Sandholt, I., Rasmussen, M.S., 2004. Evaluation of MODIS LAI, fAPAR and the relation between fAPAR and NDVI in a semi-arid environment using in situ measurements. Remote Sens. Environ. 91, 490–507. https://doi.org/10.1016/j.rse.2004.04.009

Feret, J.-B., François, C., Asner, G.P., Gitelson, A.A., Martin, R.E., Bidel, L.P.R., Ustin, S.L., le Maire, G., Jacquemoud, S., 2008. PROSPECT-4 and 5: Advances in the leaf optical properties model separating photosynthetic pigments. Remote Sens. Environ. 112, 3030–3043. https://doi.org/10.1016/j.rse.2008.02.012

Fitzgerald, G.J., Rodriguez, D., Christensen, L.K., Belford, R., Sadras, V.O., Clarke, T.R., 2006. Spectral and thermal sensing for nitrogen and water status in rainfed and irrigated wheat environments. Precis. Agric. 7, 233–248. https://doi.org/10.1007/s11119-006-9011-z

Forum, S.W., 2013. Why Agriculture Is Nigeria's New Oil [WWW Document]. Forbes. URL https://www.forbes.com/sites/skollworldforum/2013/10/10/why-agriculture-is-nigerias-new-oil/ (accessed 5.16.20).

Frampton, W.J., Dash, J., Watmough, G., Milton, E.J., 2013. Evaluating the capabilities of Sentinel-2 for quantitative estimation of biophysical variables in vegetation. ISPRS J. Photogramm. Remote Sens. 82, 83–92. https://doi.org/10.1016/j.isprsjprs.2013.04.007

Freeman, P.K., Freeland, R.S., 2015. Agricultural UAVs in the U.S.: potential, policy, and hype. Remote Sens. Appl. Soc. Environ. 2, 35–43. https://doi.org/10.1016/j.rsase.2015.10.002

Fu, Y., Yang, G., Wang, J., Song, X., Feng, H., 2014. Winter wheat biomass estimation based on spectral indices, band depth analysis and partial least squares regression using hyperspectral measurements. Comput. Electron. Agric. 100, 51–59. https://doi.org/10.1016/j.compag.2013.10.010

Gabriel, J.L., Zarco-Tejada, P.J., López-Herrera, P.J., Pérez-Martín, E., Alonso-Ayuso, M., Quemada, M., 2017. Airborne and ground level sensors for monitoring nitrogen status in a maize crop. Biosyst. Eng. 160, 124–133. https://doi.org/10.1016/j.biosystemseng.2017.06.003

Gadde, B., Bonnet, S., Menke, C., Garivait, S., 2009. Air pollutant emissions from rice straw open field burning in India, Thailand and the Philippines. Environ. Pollut., Special Issue Section: Ozone and Mediterranean Ecology: Plants, People, Problems 157, 1554–1558. https://doi.org/10.1016/j.envpol.2009.01.004

Gao, F., Morisette, J.T., Wolfe, R.E., Ederer, G., Pedelty, J., Masuoka, E., Myneni, R., Tan, B., Nightingale, J., 2008. An Algorithm to Produce Temporally and Spatially Continuous MODIS-LAI Time Series. IEEE Geosci. Remote Sens. Lett. 5, 60–64. https://doi.org/10.1109/LGRS.2007.907971

Gevaert, C.M., García-Haro, F.J., 2015. A comparison of STARFM and an unmixing-based algorithm for Landsat and MODIS data fusion. Remote Sens. Environ. 156, 34–44. https://doi.org/10.1016/j.rse.2014.09.012

Gevaert, C.M., Suomalainen, J., Tang, J., Kooistra, L., 2015. Generation of Spectral #x2013;Temporal Response Surfaces by Combining Multispectral Satellite and Hyperspectral UAV Imagery for Precision Agriculture Applications. IEEE J. Sel. Top. Appl. Earth Obs. Remote Sens. 8, 3140–3146. https://doi.org/10.1109/JSTARS.2015.2406339

Gilardelli, C., Stella, T., Confalonieri, R., Ranghetti, L., Campos-Taberner, M., García-Haro, F.J., Boschetti, M., 2019. Downscaling rice yield simulation at sub-field scale using remotely sensed LAI data. Eur. J. Agron. 103, 108–116. https://doi.org/10.1016/j.eja.2018.12.003

Giordano, M., Barron, J., Ünver, O., 2019. Chapter 5 - Water Scarcity and Challenges for Smallholder Agriculture, in: Campanhola, C., Pandey, S. (Eds.), Sustainable Food and Agriculture. Academic Press, pp. 75–94. https://doi.org/10.1016/B978-0-12-812134-4.00005-4

Gitelson, A., Merzlyak, M.N., 1994. Quantitative estimation of chlorophyll-a using reflectance spectra: Experiments with autumn chestnut and maple leaves. J. Photochem. Photobiol. B 22, 247–252. https://doi.org/10.1016/1011-1344(93)06963-4

Gitelson, A.A., 2004. Wide Dynamic Range Vegetation Index for Remote Quantification of Biophysical Characteristics of Vegetation. J. Plant Physiol. 161, 165–173. https://doi.org/10.1078/0176-1617-01176

Gitelson, A.A., Gritz †, Y., Merzlyak, M.N., 2003a. Relationships between leaf chlorophyll content and spectral reflectance and algorithms for non-destructive chlorophyll assessment in higher plant leaves. J. Plant Physiol. 160, 271–282. https://doi.org/10.1078/0176-1617-00887

Gitelson, A.A., Kaufman, Y.J., Merzlyak, M.N., 1996. Use of a green channel in remote sensing of global vegetation from EOS-MODIS. Remote Sens. Environ. 58, 289–298. https://doi.org/10.1016/S0034-4257(96)00072-7

Gitelson, A.A., Viña, A., Arkebauer, T.J., Rundquist, D.C., Keydan, G., Leavitt, B., 2003b. Remote estimation of leaf area index and green leaf biomass in maize canopies. Geophys. Res. Lett. 30. https://doi.org/10.1029/2002GL016450

Gnyp, M.L., Miao, Y., Yuan, F., Ustin, S.L., Yu, K., Yao, Y., Huang, S., Bareth, G., 2014. Hyperspectral canopy sensing of paddy rice aboveground biomass at different growth stages. Field Crops Res. 155, 42–55. https://doi.org/10.1016/j.fcr.2013.09.023

Gómez-Chova, L., Muñoz-Marí, J., Laparra, V., Malo-López, J., Camps-Valls, G., 2011. A Review of Kernel Methods in Remote Sensing Data Analysis. https://doi.org/10.1007/978-3-642-14212-3_10

Gonzalez, P., Asner, G.P., Battles, J.J., Lefsky, M.A., Waring, K.M., Palace, M., 2010. Forest carbon densities and uncertainties from Lidar, QuickBird, and field measurements in California. Remote Sens. Environ. 114, 1561–1575. https://doi.org/10.1016/j.rse.2010.02.011

Gower, S.T., Kucharik, C.J., Norman, J.M., 1999. Direct and Indirect Estimation of Leaf Area Index, fAPAR, and Net Primary Production of Terrestrial Ecosystems. Remote Sens. Environ. 70, 29–51. https://doi.org/10.1016/S0034-4257(99)00056-5

Grashoff, C., Dijkstra, P., Nonhebel, S., Schapendonk, A.H.C.M., Geijn, S.C.V.D., 1995. Effects of climate change on productivity of cereals and legumes; model evaluation of observed year-to-year variability of the CO2 response. Glob. Change Biol. 1, 417–428. https://doi.org/10.1111/j.1365-2486.1995.tb00040.x

Gridley, H., Jones, M., Wopereis-Pura, M., 2002. Development of New Rice for Africa (NERICA) and participatory varietal selection 6.

GRiSP, 2013. Rice almanac: source book for the most important economic activities on Earth, Fourth Edition. ed. IRRI, Los Baños, Philippines.

Guan, K., Li, Z., Rao, L.N., Gao, F., Xie, D., Hien, N.T., Zeng, Z., 2018. Mapping Paddy Rice Area and Yields Over Thai Binh Province in Viet Nam From MODIS, Landsat, and ALOS-2/PALSAR-2. IEEE J. Sel. Top. Appl. Earth Obs. Remote Sens. 11, 2238–2252. https://doi.org/10.1109/JSTARS.2018.2834383

Guedes, J. d'Alpoim, Jin, G., Bocinsky, R.K., 2015. The Impact of Climate on the Spread of Rice to North-Eastern China: A New Look at the Data from Shandong Province. PLOS ONE 10, e0130430. https://doi.org/10.1371/journal.pone.0130430

Gupta, P.K., Sahai, S., Singh, N., Dixit, C.K., Singh, D.P., Sharma, C., Tiwari, M.K., Gupta, R.K., Garg, S.C., 2004. Residue burning in rice–wheat cropping system: Causes and implications. Curr. Sci. 87, 1713–1717.

Han, J., Wei, C., Chen, Y., Liu, W., Song, P., Zhang, D., Wang, A., Song, X., Wang, X., Huang, J., 2017. Mapping Above-Ground Biomass of Winter Oilseed Rape Using High Spatial Resolution Satellite Data at Parcel Scale under Waterlogging Conditions. Remote Sens. 9, 238. https://doi.org/10.3390/rs9030238

Han, L., Yang, G., Dai, H., Xu, B., Yang, H., Feng, H., Li, Z., Yang, X., 2019. Modeling maize above-ground biomass based on machine learning approaches using UAV remote-sensing data. Plant Methods 15, 10. https://doi.org/10.1186/s13007-019-0394-z

Hansen, J.W., Jones, J.W., 2000. Scaling-up crop models for climate variability applications. Agric. Syst. 65, 43–72. https://doi.org/10.1016/S0308-521X(00)00025-1

Haralick, R.M., Shanmugam, K., Dinstein, I., 1973. Textural Features for Image Classification. IEEE Trans. Syst. Man Cybern. SMC-3, 610–621. https://doi.org/10.1109/TSMC.1973.4309314

Hasegawa, H., 2003. High-Yielding Rice Cultivars Perform Best Even at Reduced Nitrogen Fertilizer Rate. Crop Sci. 43, 921–926. https://doi.org/10.2135/cropsci2003.9210

Hengsdijk, H., Langeveld, J.W.A., 2009. Yield Trends and Yield Gap Analysis of Major Crops in the World [WWW Document]. ResearchGate. URL https://www.researchgate.net/publication/43609724_Yield_Trends_and_Yield_Gap_Analysis_of_Major_Crops_in_the_World (accessed 5.6.20).

Herrero, M., Thornton, P.K., Power, B., Bogard, J.R., Remans, R., Fritz, S., Gerber, J.S., Nelson, G., See, L., Waha, K., Watson, R.A., West, P.C., Samberg, L.H., van de Steeg, J., Stephenson, E., van Wijk, M., Havlík, P., 2017. Farming and the geography of nutrient production for human use: a transdisciplinary analysis. Lancet Planet. Health 1, e33–e42. https://doi.org/10.1016/S2542-5196(17)30007-4

Herrero-Huerta, M., Rodriguez-Gonzalvez, P., Rainey, K.M., 2020. Yield prediction by machine learning from UAS-based multi-sensor data fusion in soybean. Plant Methods 16, 78. https://doi.org/10.1186/s13007-020-00620-6

Hongliang Fang, Shunlin Liang, 2003. Retrieving leaf area index with a neural network method: simulation and validation. IEEE Trans. Geosci. Remote Sens. 41, 2052–2062. https://doi.org/10.1109/TGRS.2003.813493

Huang, S., Miao, Y., Yuan, F., Gnyp, M.L., Yao, Y., Cao, Q., Wang, H., Lenz-Wiedemann, V.I.S., Bareth, G., 2017. Potential of RapidEye and WorldView-2 Satellite Data for Improving Rice Nitrogen Status Monitoring at Different Growth Stages. Remote Sens. 9, 227. https://doi.org/10.3390/rs9030227

Huang, S., Miao, Y., Zhao, G., Yuan, F., Ma, X., Tan, C., Yu, W., Gnyp, M.L., Lenz-Wiedemann, V.I.S., Rascher, U., Bareth, G., 2015. Satellite Remote Sensing-Based In-Season Diagnosis of Rice Nitrogen Status in Northeast China. Remote Sens. 7, 10646–10667. https://doi.org/10.3390/rs70810646

Huete, A., Didan, K., Miura, T., Rodriguez, E.P., Gao, X., Ferreira, L.G., 2002. Overview of the radiometric and biophysical performance of the MODIS vegetation indices. Remote Sens. Environ., The Moderate Resolution Imaging Spectroradiometer (MODIS): a new generation of Land Surface Monitoring 83, 195–213. https://doi.org/10.1016/S0034-4257(02)00096-2

Huete, A.R., 1988. A soil-adjusted vegetation index (SAVI). Remote Sens. Environ. 25, 295–309. https://doi.org/10.1016/0034-4257(88)90106-X

Hunt, M.L., Blackburn, G.A., Carrasco, L., Redhead, J.W., Rowland, C.S., 2019. High resolution wheat yield mapping using Sentinel-2. Remote Sens. Environ. 233, 111410. https://doi.org/10.1016/j.rse.2019.111410

Hyer, E.J., Goetz, S.J., 2004. Comparison and sensitivity analysis of instruments and radiometric methods for LAI estimation: assessments from a boreal forest site. Agric. For. Meteorol. 122, 157–174. https://doi.org/10.1016/j.agrformet.2003.09.013

Ines, A.V.M., Das, N.N., Hansen, J.W., Njoku, E.G., 2013. Assimilation of remotely sensed soil moisture and vegetation with a crop simulation model for maize yield prediction. Remote Sens. Environ. 138, 149–164. https://doi.org/10.1016/j.rse.2013.07.018

Iqbal, F., Lucieer, A., Barry, K., 2018. Simplified radiometric calibration for UAS-mounted multispectral sensor. Eur. J. Remote Sens. 51, 301–313. https://doi.org/10.1080/22797254.2018.1432293

Ishiguro, E., Kumar, M.K., Hidaka, Y., Yoshida, S., Sato, M., Miyazato, M., Chen, J.Y., 1993. Use of rice response characteristics in area estimation by LANDSAT/TM and MOS-1 satellites data. ISPRS J. Photogramm. Remote Sens. 48, 26–32. https://doi.org/10.1016/0924-2716(93)90004-7

Ismaila, U., Wada, A., Daniya, E., Gbanguba, A., 2012. Meeting the Local Rice Needs in Nigeria through Effective Weed Management. Sustain. Agric. Res. 2, p37. https://doi.org/10.5539/sar.v2n2p37

Ittersum, M.K. van, Bussel, L.G.J. van, Wolf, J., Grassini, P., Wart, J. van, Guilpart, N., Claessens, L., Groot, H. de, Wiebe, K., Mason-D'Croz, D., Yang, H., Boogaard, H., Oort, P.A.J. van, Loon, M.P. van, Saito, K., Adimo, O., Adjei-Nsiah, S., Agali, A., Bala, A., Chikowo, R., Kaizzi, K., Kouressy, M., Makoi, J.H.J.R., Ouattara, K., Tesfaye, K., Cassman, K.G., 2016. Can sub-Saharan Africa feed itself? Proc. Natl. Acad. Sci. 113, 14964–14969. https://doi.org/10.1073/pnas.1610359113

Jabran, K., Ehsanullah, Hussain, M., Farooq, M., Babar, M., Doğan, M.N., Lee, D.-J., 2012. Application of bispyribac-sodium provides effective weed control in direct-planted rice on a sandy loam soil. Weed Biol. Manag. 12, 136–145. https://doi.org/10.1111/j.1445-6664.2012.00446.x

Jacquemoud, S., Baret, F., 1990. PROSPECT: A model of leaf optical properties spectra. Remote Sens. Environ. 34, 75–91. https://doi.org/10.1016/0034-4257(90)90100-Z

Jacquemoud, S., Baret, F., Andrieu, B., Danson, F.M., Jaggard, K., 1995. Extraction of vegetation biophysical parameters by inversion of the PROSPECT + SAIL models on sugar beet canopy reflectance data. Application to TM and AVIRIS sensors. Remote Sens. Environ. 52, 163–172. https://doi.org/10.1016/0034-4257(95)00018-V

Jacquemoud, S., Verhoef, W., Baret, F., Bacour, C., Zarco-Tejada, P.J., Asner, G.P., François, C., Ustin, S.L., 2009. PROSPECT + SAIL models: A review of use for vegetation characterization. Remote Sens. Environ., Imaging Spectroscopy Special Issue 113, Supplement 1, S56–S66. https://doi.org/10.1016/j.rse.2008.01.026

Jay, S., Maupas, F., Bendoula, R., Gorretta, N., 2017. Retrieving LAI, chlorophyll and nitrogen contents in sugar beet crops from multi-angular optical remote sensing: Comparison of vegetation indices and PROSAIL inversion for field phenotyping. Field Crops Res. 210, 33–46. https://doi.org/10.1016/j.fcr.2017.05.005

Jeng, T.L., Tseng, T.H., Wang, C.S., Chen, C.L., Sung, J.M., 2006. Yield and grain uniformity in contrasting rice genotypes suitable for different growth environments. Field Crops Res. 99, 59–66. https://doi.org/10.1016/j.fcr.2006.03.005

Jia, L., Chen, X., Zhang, F., Buerkert, A., Römheld, V., 2004. Use of Digital Camera to Assess Nitrogen Status of Winter Wheat in the Northern China Plain. https://doi.org/10.1081/PLN-120028872

Jiang, B., Liang, S., Wang, J., Xiao, Z., 2010. Modeling MODIS LAI time series using three statistical methods. Remote Sens. Environ. 114, 1432–1444. https://doi.org/10.1016/j.rse.2010.01.026

Jiang, Q., Fang, S., Peng, Y., Gong, Y., Zhu, R., Wu, X., Ma, Y., Duan, B., Liu, J., 2019. UAV-Based Biomass Estimation for Rice-Combining Spectral, TIN-Based Structural and Meteorological Features. Remote Sens. 11, 890. https://doi.org/10.3390/rs11070890

Jiang, Z., Huete, A.R., Didan, K., Miura, T., 2008. Development of a two-band enhanced vegetation index without a blue band. Remote Sens. Environ. 112, 3833–3845. https://doi.org/10.1016/j.rse.2008.06.006

Jin, X., Kumar, L., Li, Z., Feng, H., Xu, X., Yang, G., Wang, J., 2018. A review of data assimilation of remote sensing and crop models. Eur. J. Agron. 92, 141–152. https://doi.org/10.1016/j.eja.2017.11.002

Jin, X., Li, Z., Feng, H., Ren, Z., Li, S., 2020a. Estimation of maize yield by assimilating biomass and canopy cover derived from hyperspectral data into the AquaCrop model. Agric. Water Manag. 227, 105846. https://doi.org/10.1016/j.agwat.2019.105846

Jin, X., Zarco-Tejada, P., Schmidhalter, U., Reynolds, M.P., Hawkesford, M.J., Varshney, R.K., Yang, T., Nie, C., Li, Z., Ming, B., Xiao, Y., Xie, Y., Li, S., 2020b. High-throughput estimation of crop traits: A review of ground and aerial phenotyping

platforms. IEEE Geosci. Remote Sens. Mag. 0–0. https://doi.org/10.1109/MGRS.2020.2998816
Jin, X., Zarco-Tejada, P., Schmidhalter, U., Reynolds, M.P., Hawkesford, M.J., Varshney, R.K., Yang, T., Nie, C., Li, Z., Ming, B., Xiao, Y., Xie, Y., Li, S., 2020c. High-throughput estimation of crop traits: A review of ground and aerial phenotyping platforms. IEEE Geosci. Remote Sens. Mag. 0–0. https://doi.org/10.1109/MGRS.2020.2998816
Jin, Z., Azzari, G., Lobell, D.B., 2017a. Improving the accuracy of satellite-based high-resolution yield estimation: A test of multiple scalable approaches. Agric. For. Meteorol. 247, 207–220. https://doi.org/10.1016/j.agrformet.2017.08.001
Jin, Z., Azzari, G., Lobell, D.B., 2017b. Improving the accuracy of satellite-based high-resolution yield estimation: A test of multiple scalable approaches. Agric. For. Meteorol. 247, 207–220. https://doi.org/10.1016/j.agrformet.2017.08.001
Johnson, M.D., Hsieh, W.W., Cannon, A.J., Davidson, A., Bédard, F., 2016. Crop yield forecasting on the Canadian Prairies by remotely sensed vegetation indices and machine learning methods. Agric. For. Meteorol. 218–219, 74–84. https://doi.org/10.1016/j.agrformet.2015.11.003
Jones, J.W., Hoogenboom, G., Porter, C.H., Boote, K.J., Batchelor, W.D., Hunt, L.A., Wilkens, P.W., Singh, U., Gijsman, A.J., Ritchie, J.T., 2003. The DSSAT cropping system model. Eur. J. Agron., Modelling Cropping Systems: Science, Software and Applications 18, 235–265. https://doi.org/10.1016/S1161-0301(02)00107-7
Jones, M.P., Dingkuhn, M., Aluko/snm>, G.K., Semon, M., 1997. Interspecific Oryza Sativa L. X O. Glaberrima Steud. progenies in upland rice improvement. Euphytica 94, 237–246. https://doi.org/10.1023/A:1002969932224
Joseph, G., 2015. Building Earth Observation Cameras [WWW Document]. ResearchGate. URL https://www.researchgate.net/publication/311537409_Building_Earth_Observation_Cameras (accessed 5.13.20).
Ju, X.-T., Xing, G.-X., Chen, X.-P., Zhang, S.-L., Zhang, L.-J., Liu, X.-J., Cui, Z.-L., Yin, B., Christie, P., Zhu, Z.-L., Zhang, F.-S., 2009. Reducing environmental risk by improving N management in intensive Chinese agricultural systems. Proc. Natl. Acad. Sci. 106, 3041–3046. https://doi.org/10.1073/pnas.0813417106
Kamoshita, A., Babu, R.C., Boopathi, N.M., Fukai, S., 2008. Phenotypic and genotypic analysis of drought-resistance traits for development of rice cultivars adapted to rainfed environments. Field Crops Res. 109, 1–23. https://doi.org/10.1016/j.fcr.2008.06.010
Kang, Y., Özdoğan, M., 2019a. Field-level crop yield mapping with Landsat using a hierarchical data assimilation approach. Remote Sens. Environ. 228, 144–163. https://doi.org/10.1016/j.rse.2019.04.005
Kang, Y., Özdoğan, M., 2019b. Field-level crop yield mapping with Landsat using a hierarchical data assimilation approach. Remote Sens. Environ. 228, 144–163. https://doi.org/10.1016/j.rse.2019.04.005
Kanke, Y., Tubaña, B., Dalen, M., Harrell, D., 2016. Evaluation of red and red-edge reflectance-based vegetation indices for rice biomass and grain yield prediction models in paddy fields. Precis. Agric. 17, 507–530. https://doi.org/10.1007/s11119-016-9433-1
Khir, R., Pan, Z., 2019. Chapter 2 - Rice, in: Pan, Z., Zhang, R., Zicari, S. (Eds.), Integrated Processing Technologies for Food and Agricultural By-Products. Academic Press, pp. 21–58. https://doi.org/10.1016/B978-0-12-814138-0.00002-2

Kim, M., Ko, J., Jeong, S., Yeom, J., Kim, H., 2017. Monitoring canopy growth and grain yield of paddy rice in South Korea by using the GRAMI model and high spatial resolution imagery. GIScience Remote Sens. 54, 534–551. https://doi.org/10.1080/15481603.2017.1291783
Kontgis, C., Schneider, A., Ozdogan, M., 2015. Mapping rice paddy extent and intensification in the Vietnamese Mekong River Delta with dense time stacks of Landsat data. Remote Sens. Environ. 169, 255–269. https://doi.org/10.1016/j.rse.2015.08.004
Korhonen, L., Hadi, Packalen, P., Rautiainen, M., 2017. Comparison of Sentinel-2 and Landsat 8 in the estimation of boreal forest canopy cover and leaf area index. Remote Sens. Environ. 195, 259–274. https://doi.org/10.1016/j.rse.2017.03.021
Krishnan, P., Ramakrishnan, B., Reddy, K.R., Reddy, V.R., 2011. Chapter three - High-Temperature Effects on Rice Growth, Yield, and Grain Quality, in: Sparks, D.L. (Ed.), Advances in Agronomy. Academic Press, pp. 87–206. https://doi.org/10.1016/B978-0-12-387689-8.00004-7
Kross, A., McNairn, H., Lapen, D., Sunohara, M., Champagne, C., 2015. Assessment of RapidEye vegetation indices for estimation of leaf area index and biomass in corn and soybean crops. Int. J. Appl. Earth Obs. Geoinformation 34, 235–248. https://doi.org/10.1016/j.jag.2014.08.002
Kuenzer, C., Knauer, K., 2013. Remote sensing of rice crop areas. Int. J. Remote Sens. 34, 2101–2139. https://doi.org/10.1080/01431161.2012.738946
Kuhn, M., Johnson, K., 2013. Applied Predictive Modeling. Springer-Verlag, New York. https://doi.org/10.1007/978-1-4614-6849-3
Kumar, L., Mutanga, O., 2017. Remote Sensing of Above-Ground Biomass. Remote Sens. 9, 935. https://doi.org/10.3390/rs9090935
Kumar, P., Kumar, S., Joshi, L., 2015. The Extent and Management of Crop Stubble, in: Kumar, P., Kumar, S., Joshi, L. (Eds.), Socioeconomic and Environmental Implications of Agricultural Residue Burning: A Case Study of Punjab, India, SpringerBriefs in Environmental Science. Springer India, New Delhi, pp. 13–34. https://doi.org/10.1007/978-81-322-2014-5_2
Kurukulasuriya, P., Mendelsohn, R., Hassan, R., Benhin, J., Deressa, T., Diop, M., Eid, H.M., Fosu, K.Y., Gbetibouo, G., Jain, S., Mahamadou, A., Mano, R., Kabubo-Mariara, J., El-Marsafawy, S., Molua, E., Ouda, S., Ouedraogo, M., Séne, I., Maddison, D., Seo, S.N., Dinar, A., 2006. Will African Agriculture Survive Climate Change? World Bank Econ. Rev. 20, 367–388. https://doi.org/10.1093/wber/lhl004
Kuusk, A., 2001. A two-layer canopy reflectance model. J. Quant. Spectrosc. Radiat. Transf. 71, 1–9. https://doi.org/10.1016/S0022-4073(01)00007-3
Kyat, K.M., Idoga, S., 2018. Characterization, classification and suitability ratings of soils for rainfed rice production in Rukubi, Doma, Nasarawa State, Nigeria. Int. J. Environ. Agric. Biotechnol. 3.
Lambert, M.-J., Traoré, P.C.S., Blaes, X., Baret, P., Defourny, P., 2018. Estimating smallholder crops production at village level from Sentinel-2 time series in Mali's cotton belt. Remote Sens. Environ. 216, 647–657. https://doi.org/10.1016/j.rse.2018.06.036
Laza, M.R.C., Peng, S., Akita, S., Saka, H., 2004. Effect of Panicle Size on Grain Yield of IRRI-Released Indica Rice Cultivars in the Wet Season. Plant Prod. Sci. 7, 271–276. https://doi.org/10.1626/pps.7.271
Lazaridis, D.C., Verbesselt, J., Robinson, A.P., 2010. Penalized regression techniques for prediction: a case study for predicting tree mortality using remotely sensed vegetation indicesThis article is one of a selection of papers from Extending Forest Inventory

and Monitoring over Space and Time. Can. J. For. Res. 41, 24–34. https://doi.org/10.1139/X10-180
Lázaro-Gredilla, M., Titsias, M.K., Verrelst, J., Camps-Valls, G., 2014. Retrieval of Biophysical Parameters With Heteroscedastic Gaussian Processes. IEEE Geosci. Remote Sens. Lett. 11, 838–842. https://doi.org/10.1109/LGRS.2013.2279695
Lena, B.P., Folegatti, M.V., Santos, O.N.A., Andrade, 2016. Performance of LAI-2200 Plant Canopy Analyzer on Leaf Area Index of Jatropha Nut Estimation [WWW Document]. https://doi.org/10.3923/ja.2016.191.197
Li, B., Xu, X., Zhang, L., Han, J., Bian, C., Li, G., Liu, J., Jin, L., 2020. Above-ground biomass estimation and yield prediction in potato by using UAV-based RGB and hyperspectral imaging. ISPRS J. Photogramm. Remote Sens. 162, 161–172. https://doi.org/10.1016/j.isprsjprs.2020.02.013
Li, F., Miao, Y., Feng, G., Yuan, F., Yue, S., Gao, X., Liu, Y., Liu, B., Ustin, S.L., Chen, X., 2014. Improving estimation of summer maize nitrogen status with red edge-based spectral vegetation indices. Field Crops Res. 157, 111–123. https://doi.org/10.1016/j.fcr.2013.12.018
Li, W., Niu, Z., Huang, N., Wang, C., Gao, S., Wu, C., 2015. Airborne LiDAR technique for estimating biomass components of maize: A case study in Zhangye City, Northwest China. Ecol. Indic. 57, 486–496. https://doi.org/10.1016/j.ecolind.2015.04.016
Li, X., Zhang, Y., Bao, Y., Luo, J., Jin, X., Xu, X., Song, X., Yang, G., 2014. Exploring the Best Hyperspectral Features for LAI Estimation Using Partial Least Squares Regression. Remote Sens. 6, 6221–6241. https://doi.org/10.3390/rs6076221
Li, X., Zhang, Y., Luo, J., Jin, X., Xu, Y., Yang, W., 2016. Quantification winter wheat LAI with HJ-1CCD image features over multiple growing seasons. Int. J. Appl. Earth Obs. Geoinformation 44, 104–112. https://doi.org/10.1016/j.jag.2015.08.004
Li, Z., Jin, X., Zhao, C., Wang, J., Xu, X., Yang, G., Li, C., Shen, J., 2015. Estimating wheat yield and quality by coupling the DSSAT-CERES model and proximal remote sensing. Eur. J. Agron. 71, 53–62. https://doi.org/10.1016/j.eja.2015.08.006
Liang, S., 2007. Recent developments in estimating land surface biogeophysical variables from optical remote sensing. Prog. Phys. Geogr. Earth Environ. 31, 501–516. https://doi.org/10.1177/0309133307084626
Liao, C., Wang, J., Dong, T., Shang, J., Liu, J., Song, Y., 2019. Using spatio-temporal fusion of Landsat-8 and MODIS data to derive phenology, biomass and yield estimates for corn and soybean. Sci. Total Environ. 650, 1707–1721. https://doi.org/10.1016/j.scitotenv.2018.09.308
Liaw, A., Wiener, M.C., 2007. Classification and Regression by randomForest.
Liu, J., Pattey, E., Jégo, G., 2012. Assessment of vegetation indices for regional crop green LAI estimation from Landsat images over multiple growing seasons. Remote Sens. Environ. 123, 347–358. https://doi.org/10.1016/j.rse.2012.04.002
Liu, L., Xiao, X., Qin, Y., Wang, J., Xu, X., Hu, Y., Qiao, Z., 2020. Mapping cropping intensity in China using time series Landsat and Sentinel-2 images and Google Earth Engine. Remote Sens. Environ. 239, 111624. https://doi.org/10.1016/j.rse.2019.111624
Liu, X., Wang, H., Zhou, J., Hu, F., Zhu, D., Chen, Z., Liu, Y., 2016. Effect of N Fertilization Pattern on Rice Yield, N Use Efficiency and Fertilizer–N Fate in the Yangtze River Basin, China. PLOS ONE 11, e0166002. https://doi.org/10.1371/journal.pone.0166002
Liu, Y., Liu, S., Li, J., Guo, X., Wang, S., Lu, J., 2019. Estimating biomass of winter oilseed rape using vegetation indices and texture metrics derived from UAV multispectral

images. Comput. Electron. Agric. 166, 105026. https://doi.org/10.1016/j.compag.2019.105026
Lobell, D.B., 2013. The use of satellite data for crop yield gap analysis. Field Crops Res., Crop Yield Gap Analysis – Rationale, Methods and Applications 143, 56–64. https://doi.org/10.1016/j.fcr.2012.08.008
Lopatin, J., Dolos, K., Hernández, H.J., Galleguillos, M., Fassnacht, F.E., 2016. Comparing Generalized Linear Models and random forest to model vascular plant species richness using LiDAR data in a natural forest in central Chile. Remote Sens. Environ. 173, 200–210. https://doi.org/10.1016/j.rse.2015.11.029
Lowder, S.K., Skoet, J., Raney, T., 2016. The Number, Size, and Distribution of Farms, Smallholder Farms, and Family Farms Worldwide. World Dev. 87, 16–29. https://doi.org/10.1016/j.worlddev.2015.10.041
Lu, D., Batistella, M., 2005. Exploring TM image texture and its relationships with biomass estimation in Rondônia, Brazilian Amazon. Acta Amaz. 35, 249–257. https://doi.org/10.1590/S0044-59672005000200015
Lu, N., Zhou, J., Han, Z., Li, D., Cao, Q., Yao, X., Tian, Y., Zhu, Y., Cao, W., Cheng, T., 2019. Improved estimation of aboveground biomass in wheat from RGB imagery and point cloud data acquired with a low-cost unmanned aerial vehicle system. Plant Methods 15, 17. https://doi.org/10.1186/s13007-019-0402-3
Lunagaria, M.M., Patel, H.R., 2019. Evaluation of PROSAIL inversion for retrieval of chlorophyll, leaf dry matter, leaf angle, and leaf area index of wheat using spectrodirectional measurements. Int. J. Remote Sens. 40, 8125–8145. https://doi.org/10.1080/01431161.2018.1524608
Luo, S., Wang, C., Xi, X., Nie, S., Fan, X., Chen, H., Yang, X., Peng, D., Lin, Y., Zhou, G., 2019. Combining hyperspectral imagery and LiDAR pseudo-waveform for predicting crop LAI, canopy height and above-ground biomass. Ecol. Indic. 102, 801–812. https://doi.org/10.1016/j.ecolind.2019.03.011
Luscombe, D.J., Anderson, K., Gatis, N., Wetherelt, A., Grand-Clement, E., Brazier, R.E., 2015. What does airborne LiDAR really measure in upland ecosystems? Ecohydrology 8, 584–594. https://doi.org/10.1002/eco.1527
Maimaitijiang, M., Ghulam, A., Sidike, P., Hartling, S., Maimaitiyiming, M., Peterson, K., Shavers, E., Fishman, J., Peterson, J., Kadam, S., Burken, J., Fritschi, F., 2017. Unmanned Aerial System (UAS)-based phenotyping of soybean using multi-sensor data fusion and extreme learning machine. ISPRS J. Photogramm. Remote Sens. 134, 43–58. https://doi.org/10.1016/j.isprsjprs.2017.10.011
Malambo, L., Popescu, S.C., Murray, S.C., Putman, E., Pugh, N.A., Horne, D.W., Richardson, G., Sheridan, R., Rooney, W.L., Avant, R., Vidrine, M., McCutchen, B., Baltensperger, D., Bishop, M., 2018. Multitemporal field-based plant height estimation using 3D point clouds generated from small unmanned aerial systems high-resolution imagery. Int. J. Appl. Earth Obs. Geoinformation 64, 31–42. https://doi.org/10.1016/j.jag.2017.08.014
Marshall, M., Thenkabail, P., 2015. Advantage of hyperspectral EO-1 Hyperion over multispectral IKONOS, GeoEye-1, WorldView-2, Landsat ETM+, and MODIS vegetation indices in crop biomass estimation. ISPRS J. Photogramm. Remote Sens. 108, 205–218. https://doi.org/10.1016/j.isprsjprs.2015.08.001
McCLOY, K.R., SMITH, F.R., ROBINSON, M.R., 1987. Monitoring rice areas using LANDSAT MSS data. Int. J. Remote Sens. 8, 741–749. https://doi.org/10.1080/01431168708948685
Mendez del Villar, P., Lançon, F., 2015. West African rice development: Beyond protectionism versus liberalization? Glob. Food Secur., Special Section on "Selected

papers from the 3rd Africa Rice Congress " 5, 56–61. https://doi.org/10.1016/j.gfs.2014.11.001
Meng, J., Du, X., Wu, B., 2013. Generation of high spatial and temporal resolution NDVI and its application in crop biomass estimation. Int. J. Digit. Earth 6, 203–218. https://doi.org/10.1080/17538947.2011.623189
Mercier, A., Betbeder, J., Baudry, J., Le Roux, V., Spicher, F., Lacoux, J., Roger, D., Hubert-Moy, L., 2020. Evaluation of Sentinel-1 & 2 time series for predicting wheat and rapeseed phenological stages. ISPRS J. Photogramm. Remote Sens. 163, 231–256. https://doi.org/10.1016/j.isprsjprs.2020.03.009
Mkhabela, M.S., Bullock, P., Raj, S., Wang, S., Yang, Y., 2011. Crop yield forecasting on the Canadian Prairies using MODIS NDVI data. Agric. For. Meteorol. 151, 385–393. https://doi.org/10.1016/j.agrformet.2010.11.012
Moldenhauer, K., Counce, P., Hardke, J., 2013. Rice Growth and Development. Arkansas Rice Production Handbook, ed J. T. Hardke (Little Rock, AR: University of Arkansas Division of Agriculture Cooperative Extension Service) 1–12.
Montgomery, D.C., Peck, E.A., Vining, G.G., 2012. Introduction to Linear Regression Analysis. John Wiley & Sons.
Moran, M.S., Inoue, Y., Barnes, E.M., 1997. Opportunities and limitations for image-based remote sensing in precision crop management. Remote Sens. Environ. 61, 319–346. https://doi.org/10.1016/S0034-4257(97)00045-X
Morel, J., Bégué, A., Todoroff, P., Martiné, J.-F., Lebourgeois, V., Petit, M., 2014. Coupling a sugarcane crop model with the remotely sensed time series of fIPAR to optimise the yield estimation. Eur. J. Agron. 61, 60–68. https://doi.org/10.1016/j.eja.2014.08.004
Moreno-Martínez, Á., Izquierdo-Verdiguier, E., Maneta, M.P., Camps-Valls, G., Robinson, N., Muñoz-Marí, J., Sedano, F., Clinton, N., Running, S.W., 2020. Multispectral high resolution sensor fusion for smoothing and gap-filling in the cloud. Remote Sens. Environ. 247, 111901. https://doi.org/10.1016/j.rse.2020.111901
Mosleh, M.K., Hassan, Q.K., Chowdhury, E.H., 2015a. Application of Remote Sensors in Mapping Rice Area and Forecasting Its Production: A Review. Sensors 15, 769–791. https://doi.org/10.3390/s150100769
Mosleh, M.K., Hassan, Q.K., Chowdhury, E.H., 2015b. Application of Remote Sensors in Mapping Rice Area and Forecasting Its Production: A Review. Sensors 15, 769–791. https://doi.org/10.3390/s150100769
Moulin, S., Bondeau, A., Delecolle, R., 1998. Combining agricultural crop models and satellite observations: From field to regional scales. Int. J. Remote Sens. 19, 1021–1036. https://doi.org/10.1080/014311698215586
Mulla, D.J., 2013. Twenty five years of remote sensing in precision agriculture: Key advances and remaining knowledge gaps. Biosyst. Eng., Special Issue: Sensing Technologies for Sustainable Agriculture 114, 358–371. https://doi.org/10.1016/j.biosystemseng.2012.08.009
Muthayya, S., Sugimoto, J.D., Montgomery, S., Maberly, G.F., 2014. An overview of global rice production, supply, trade, and consumption. Ann. N. Y. Acad. Sci. 1324, 7–14. https://doi.org/10.1111/nyas.12540
Navarro, A., Rolim, J., Miguel, I., Catalão, J., Silva, J., Painho, M., Vekerdy, Z., 2016. Crop Monitoring Based on SPOT-5 Take-5 and Sentinel-1A Data for the Estimation of Crop Water Requirements. Remote Sens. 8, 525. https://doi.org/10.3390/rs8060525
Ndjiondjop, M.N., Manneh, B., Cissoko, M., Drame, N.K., Kakai, R.G., Bocco, R., Baimey, H., Wopereis, M., 2010. Drought resistance in an interspecific backcross population

of rice (Oryza spp.) derived from the cross WAB56-104 (O. sativa)×CG14 (O. glaberrima). Plant Sci. 179, 364–373. https://doi.org/10.1016/j.plantsci.2010.06.006
Nguezet, P.M.D., Diagne, A., Okoruwa, O.V., Ojehomon, V., Manyong, V., 2013. Estimating the Actual and Potential Adoption Rates and Determinants of NERICA Rice Varieties in Nigeria. J. Crop Improv. 27, 561–585. https://doi.org/10.1080/15427528.2013.811709
Nguyen, T.T.H., Bie, C.A.J.M.D., Ali, A., Smaling, E.M.A., Chu, T.H., 2012. Mapping the irrigated rice cropping patterns of the Mekong delta, Vietnam, through hyper-temporal SPOT NDVI image analysis. Int. J. Remote Sens. 33, 415–434. https://doi.org/10.1080/01431161.2010.532826
Nguy-Robertson, A., Gitelson, A., Peng, Y., Viña, A., Arkebauer, T., Rundquist, D., 2012. Green Leaf Area Index Estimation in Maize and Soybean: Combining Vegetation Indices to Achieve Maximal Sensitivity. Agron. J. 104, 1336–1347. https://doi.org/10.2134/agronj2012.0065
Niel, T.G.V., McVicar, T.R., Niel, T.G.V., McVicar, T.R., 2004. Current and potential uses of optical remote sensing in rice-based irrigation systems: a review, Current and potential uses of optical remote sensing in rice-based irrigation systems: a review. Crop Pasture Sci. Crop Pasture Sci. 55, 55, 155, 155–185, 185. https://doi.org/10.1071/AR03149, 10.1071/AR03149
Njoku, P.C., 2018. Revolutionizing Agriculture Through Space Science and Technology Applications. ARIDZONEJOURNALOFENGINEERING,TECHNOLOGY&ENVIRONMENT.
Noureldin, N.A., Aboelghar, M.A., Saudy, H.S., Ali, A.M., 2013. Rice yield forecasting models using satellite imagery in Egypt. Egypt. J. Remote Sens. Space Sci. 16, 125–131. https://doi.org/10.1016/j.ejrs.2013.04.005
Novichonok, E.V., Novichonok, A.O., Kurbatova, J.A., Markovskaya, E.F., 2016. Use of the atLEAF+ chlorophyll meter for a nondestructive estimate of chlorophyll content. Photosynthetica 54, 130–137. https://doi.org/10.1007/s11099-015-0172-8
O'Connor, J., Smith, M.J., James, M.R., 2017. Cameras and settings for aerial surveys in the geosciences: Optimising image data. Prog. Phys. Geogr. Earth Environ. 41, 325–344. https://doi.org/10.1177/0309133317703092
O'Donoghue, E., Hansen, J., 2017. USDA Agricultural Projections to 2026 [WWW Document]. URL http://www.ers.usda.gov/publications/pub-details/?pubid=82538 (accessed 5.13.20).
OECD, 2018. The Middle East and North Africa: Prospects and challenges, in: OECD-FAO Agricultural Outlook 2018-2027, OECD-FAO Agricultural Outlook. OECD, pp. 67–107. https://doi.org/10.1787/agr_outlook-2018-5-en
OECD-FAO, 2019. Agricultural Outlook 2019-2028 29.
Okotie, S., 2018. Chapter 5 - The Nigerian Economy Before the Discovery of Crude Oil, in: Ndimele, P.E. (Ed.), The Political Ecology of Oil and Gas Activities in the Nigerian Aquatic Ecosystem. Academic Press, pp. 71–81. https://doi.org/10.1016/B978-0-12-809399-3.00005-7
Okpiaifo, G., Durand-Morat, A., West, G.H., Nalley, L.L., Nayga, R.M., Wailes, E.J., 2020. Consumers' preferences for sustainable rice practices in Nigeria. Glob. Food Secur. 24, 100345. https://doi.org/10.1016/j.gfs.2019.100345
Onojeghuo, Alex Okiemute, Blackburn, G.A., Huang, J., Kindred, D., Huang, W., 2018a. Applications of satellite 'hyper-sensing' in Chinese agriculture: Challenges and opportunities. Int. J. Appl. Earth Obs. Geoinformation 64, 62–86. https://doi.org/10.1016/j.jag.2017.09.005

Onojeghuo, Alex Okiemute, Blackburn, G.A., Huang, J., Kindred, D., Huang, W., 2018b. Applications of satellite 'hyper-sensing' in Chinese agriculture: Challenges and opportunities. Int. J. Appl. Earth Obs. Geoinformation 64, 62–86. https://doi.org/10.1016/j.jag.2017.09.005

Onojeghuo, Alex O., Blackburn, G.A., Wang, Q., Atkinson, P.M., Kindred, D., Miao, Y., 2018. Rice crop phenology mapping at high spatial and temporal resolution using downscaled MODIS time-series. GIScience Remote Sens. 55, 659–677. https://doi.org/10.1080/15481603.2018.1423725

Padilla, F.M., de Souza, R., Peña-Fleitas, M.T., Gallardo, M., Giménez, C., Thompson, R.B., 2018. Different Responses of Various Chlorophyll Meters to Increasing Nitrogen Supply in Sweet Pepper. Front. Plant Sci. 9. https://doi.org/10.3389/fpls.2018.01752

Pagani, V., Guarneri, T., Busetto, L., Ranghetti, L., Boschetti, M., Movedi, E., Campos-Taberner, M., Garcia-Haro, F.J., Katsantonis, D., Stavrakoudis, D., Ricciardelli, E., Romano, F., Holecz, F., Collivignarelli, F., Granell, C., Casteleyn, S., Confalonieri, R., 2019. A high-resolution, integrated system for rice yield forecasting at district level. Agric. Syst. 168, 181–190. https://doi.org/10.1016/j.agsy.2018.05.007

Pahlevan, N., Smith, B., Schalles, J., Binding, C., Cao, Z., Ma, R., Alikas, K., Kangro, K., Gurlin, D., Hà, N., Matsushita, B., Moses, W., Greb, S., Lehmann, M.K., Ondrusek, M., Oppelt, N., Stumpf, R., 2020. Seamless retrievals of chlorophyll-a from Sentinel-2 (MSI) and Sentinel-3 (OLCI) in inland and coastal waters: A machine-learning approach. Remote Sens. Environ. 240, 111604. https://doi.org/10.1016/j.rse.2019.111604

Pal, M., 2005. Random forest classifier for remote sensing classification. Int. J. Remote Sens. 26, 217–222. https://doi.org/10.1080/01431160412331269698

Pasqualotto, N., Delegido, J., Van Wittenberghe, S., Rinaldi, M., Moreno, J., 2019. Multi-Crop Green LAI Estimation with a New Simple Sentinel-2 LAI Index (SeLI). Sensors 19. https://doi.org/10.3390/s19040904

Peng, D., Huang, J., Li, C., Liu, L., Huang, W., Wang, F., Yang, X., 2014. Modelling paddy rice yield using MODIS data. Agric. For. Meteorol. 184, 107–116. https://doi.org/10.1016/j.agrformet.2013.09.006

Peng, Y., Gitelson, A.A., 2011. Application of chlorophyll-related vegetation indices for remote estimation of maize productivity. Agric. For. Meteorol. 151, 1267–1276. https://doi.org/10.1016/j.agrformet.2011.05.005

Pinty, B., Lavergne, T., Widlowski, J.-L., Gobron, N., Verstraete, M.M., 2009. On the need to observe vegetation canopies in the near-infrared to estimate visible light absorption. Remote Sens. Environ. 113, 10–23. https://doi.org/10.1016/j.rse.2008.08.017

Pipia, L., Muñoz-Marí, J., Amin, E., Belda, S., Camps-Valls, G., Verrelst, J., 2019. Fusing optical and SAR time series for LAI gap filling with multioutput Gaussian processes. Remote Sens. Environ. 235, 111452. https://doi.org/10.1016/j.rse.2019.111452

Prabhakara, K., Hively, W.D., McCarty, G.W., 2015. Evaluating the relationship between biomass, percent groundcover and remote sensing indices across six winter cover crop fields in Maryland, United States. Int. J. Appl. Earth Obs. Geoinformation 39, 88–102. https://doi.org/10.1016/j.jag.2015.03.002

Punalekar, S.M., Verhoef, A., Quaife, T.L., Humphries, D., Bermingham, L., Reynolds, C.K., 2018. Application of Sentinel-2A data for pasture biomass monitoring using a physically based radiative transfer model. Remote Sens. Environ. 218, 207–220. https://doi.org/10.1016/j.rse.2018.09.028

Qiao, K., Zhu, W., Xie, Z., Li, P., 2019. Estimating the Seasonal Dynamics of the Leaf Area Index Using Piecewise LAI-VI Relationships Based on Phenophases. Remote Sens. 11, 689. https://doi.org/10.3390/rs11060689

Rahman, H., Pinty, B., Verstraete, M.M., 1993. Coupled surface-atmosphere reflectance (CSAR) model: 2. Semiempirical surface model usable with NOAA advanced very high resolution radiometer data. J. Geophys. Res. Atmospheres 98, 20791–20801. https://doi.org/10.1029/93JD02072

Rai, R.K., Singh, V.P., Upadhyay, A., 2017. Chapter 10 - Irrigation Methods, in: Rai, R.K., Singh, V.P., Upadhyay, A. (Eds.), Planning and Evaluation of Irrigation Projects. Academic Press, pp. 353–363. https://doi.org/10.1016/B978-0-12-811748-4.00010-8

Rao, N.R., Garg, P.K., Ghosh, S.K., 2006. Estimation and comparison of leaf area index of agricultural crops using irs liss-III and EO-1 hyperion images. J. Indian Soc. Remote Sens. 34, 69–78. https://doi.org/10.1007/BF02990748

Rasmussen, C.E., Williams, C.K.I., 2006. Gaussian processes for machine learning, Adaptive computation and machine learning. MIT Press, Cambridge, Mass.

Refaeilzadeh, P., Tang, L., Liu, H., 2009. Cross-Validation, in: LIU, L., ÖZSU, M.T. (Eds.), Encyclopedia of Database Systems. Springer US, Boston, MA, pp. 532–538. https://doi.org/10.1007/978-0-387-39940-9_565

Ren, J., Chen, Z., Zhou, Q., Tang, H., 2008. Regional yield estimation for winter wheat with MODIS-NDVI data in Shandong, China. Int. J. Appl. Earth Obs. Geoinformation, Modern Methods in Crop Yield Forecasting and Crop Area Estimation 10, 403–413. https://doi.org/10.1016/j.jag.2007.11.003

Reuters, 2020. A growing problem: Nigerian rice farmers fall short after borders close - Reuters [WWW Document]. URL https://www.reuters.com/article/us-nigeria-economy-rice/a-growing-problem-nigerian-rice-farmers-fall-short-after-borders-close-idUSKBN1ZM109 (accessed 5.24.20).

Ricciardi, V., Ramankutty, N., Mehrabi, Z., Jarvis, L., Chookolingo, B., 2018. How much of the world's food do smallholders produce? Glob. Food Secur. 17, 64–72. https://doi.org/10.1016/j.gfs.2018.05.002

Rivera, J.P., Verrelst, J., Delegido, J., Veroustraete, F., Moreno, J., 2014. On the Semi-Automatic Retrieval of Biophysical Parameters Based on Spectral Index Optimization. Remote Sens. 6, 4927–4951. https://doi.org/10.3390/rs6064927

Rodriguez-Galiano, V.F., Ghimire, B., Rogan, J., Chica-Olmo, M., Rigol-Sanchez, J.P., 2012. An assessment of the effectiveness of a random forest classifier for land-cover classification. ISPRS J. Photogramm. Remote Sens. 67, 93–104. https://doi.org/10.1016/j.isprsjprs.2011.11.002

Rondeaux, G., Steven, M., Baret, F., 1996. Optimization of soil-adjusted vegetation indices. Remote Sens. Environ. 55, 95–107. https://doi.org/10.1016/0034-4257(95)00186-7

Roujean, J.-L., Leroy, M., Deschamps, P.-Y., 1992. A bidirectional reflectance model of the Earth's surface for the correction of remote sensing data. J. Geophys. Res. Atmospheres 97, 20455–20468. https://doi.org/10.1029/92JD01411

Roupsard, O., Dauzat, J., Nouvellon, Y., Deveau, A., Feintrenie, L., Saint-André, L., Mialet-Serra, I., Braconnier, S., Bonnefond, J.-M., Berbigier, P., Epron, D., Jourdan, C., Navarro, M., Bouillet, J.-P., 2008. Cross-validating Sun-shade and 3D models of light absorption by a tree-crop canopy. Agric. For. Meteorol. 148, 549–564. https://doi.org/10.1016/j.agrformet.2007.11.002

Rouse, J.W., 1974. Monitoring vegetation systems in the Great Plains with ERTS.

Saberioon, M.M., Amin, M.S.M., Anuar, A.R., Gholizadeh, A., Wayayok, A., Khairunniza-Bejo, S., 2014. Assessment of rice leaf chlorophyll content using visible bands at

different growth stages at both the leaf and canopy scale. Int. J. Appl. Earth Obs. Geoinformation 32, 35–45. https://doi.org/10.1016/j.jag.2014.03.018
Sakamoto, T., Gitelson, A.A., Arkebauer, T.J., 2013. MODIS-based corn grain yield estimation model incorporating crop phenology information. Remote Sens. Environ. 131, 215–231. https://doi.org/10.1016/j.rse.2012.12.017
Sakamoto, T., Yokozawa, M., Toritani, H., Shibayama, M., Ishitsuka, N., Ohno, H., 2005. A crop phenology detection method using time-series MODIS data. Remote Sens. Environ. 96, 366–374. https://doi.org/10.1016/j.rse.2005.03.008
Salau, E.S., 2012. A Socio-Economic Analysis of Urban Agriculture In Nasarawa State, Nigeria.
Samaila, A., Binbol, N.L., 2007. Hydrology and Water Resources | Semantic Scholar [WWW Document]. URL https://www.semanticscholar.org/paper/Hydrology-and-Water-Resources-Samaila-Binbol/a84f393c7b26b887f90279edcdb7648f2952e6a2?citationIntent=methodology#citing-papers (accessed 5.14.20).
Samberg, L.H., Gerber, J.S., Ramankutty, N., Herrero, M., West, P.C., 2016. Subnational distribution of average farm size and smallholder contributions to global food production. Environ. Res. Lett. 11, 124010. https://doi.org/10.1088/1748-9326/11/12/124010
Sarker, L.R., Nichol, J.E., 2011. Improved forest biomass estimates using ALOS AVNIR-2 texture indices. Remote Sens. Environ. 115, 968–977. https://doi.org/10.1016/j.rse.2010.11.010
Segarra, J., Buchaillot, M.L., Araus, J.L., Kefauver, S.C., 2020. Remote Sensing for Precision Agriculture: Sentinel-2 Improved Features and Applications. Agronomy 10, 641. https://doi.org/10.3390/agronomy10050641
Sehgal, V.K., Chakraborty, D., Sahoo, R.N., 2016. Inversion of radiative transfer model for retrieval of wheat biophysical parameters from broadband reflectance measurements. Inf. Process. Agric. 3, 107–118. https://doi.org/10.1016/j.inpa.2016.04.001
Sekiya, N., Khatib, K.J., Makame, S.M., Tomitaka, M., Oizumi, N., Araki, H., 2013. Performance of a Number of NERICA Cultivars in Zanzibar, Tanzania: Yield, Yield Components and Grain Quality. Plant Prod. Sci. 16, 141–153. https://doi.org/10.1626/pps.16.141
Senthilkumar, K., Tesha, B.J., Mghase, J., Rodenburg, J., 2018. Increasing paddy yields and improving farm management: results from participatory experiments with good agricultural practices (GAP) in Tanzania. Paddy Water Environ. 16, 749–766. https://doi.org/10.1007/s10333-018-0666-7
Serrano, L., Filella, I., Peñuelas, J., 2000. Remote Sensing of Biomass and Yield of Winter Wheat under Different Nitrogen Supplies. Crop Sci. 40, 723–731. https://doi.org/10.2135/cropsci2000.403723x
Sharma, N., Yadav, M., 1999. Rice. Crop yield : physiology and process [WWW Document]. Physiol. Process. URL https://www.researchgate.net/publication/322075926_Sharma_NK_RP_Singh_MS_Yadav_and_KC_Singh_1999_Forage_Production_in_Drylands_of_Arid_and_Semi-arid_Regions_Scientific_Publishers_India_Jodhpur_ISBN_81-7233-218-1_152_p (accessed 5.11.20).
Shi, J., Huang, J., Zhang, F., 2013. Multi-year monitoring of paddy rice planting area in Northeast China using MODIS time series data. J. Zhejiang Univ. Sci. B 14, 934–946. https://doi.org/10.1631/jzus.B1200352

Siegmann, B., Jarmer, T., 2015. Comparison of different regression models and validation techniques for the assessment of wheat leaf area index from hyperspectral data. Int. J. Remote Sens. 36, 4519–4534. https://doi.org/10.1080/01431161.2015.1084438
Silva, J.V., Reidsma, P., Lourdes Velasco, Ma., Laborte, A.G., van Ittersum, M.K., 2018. Intensification of rice-based farming systems in Central Luzon, Philippines: Constraints at field, farm and regional levels. Agric. Syst. 165, 55–70. https://doi.org/10.1016/j.agsy.2018.05.008
Singh, A., 2016. Managing the water resources problems of irrigated agriculture through geospatial techniques: An overview. Agric. Water Manag., Sustainable Water Resources Management: Theory and Case Studies Part I Overseen by: Dr. Brent Clothier 174, 2–10. https://doi.org/10.1016/j.agwat.2016.04.021
Sinha, S.K., Padalia, H., Dasgupta, A., Verrelst, J., Rivera, J.P., 2020. Estimation of leaf area index using PROSAIL based LUT inversion, MLRA-GPR and empirical models: Case study of tropical deciduous forest plantation, North India. Int. J. Appl. Earth Obs. Geoinformation 86, 102027. https://doi.org/10.1016/j.jag.2019.102027
Siyal, A.A., Dempewolf, J., Becker-Reshef, I., 2015. Rice yield estimation using Landsat ETM+ Data. J. Appl. Remote Sens. 9, 095986. https://doi.org/10.1117/1.JRS.9.095986
Son, N.-T., Chen, C.-F., Chang, L.-Y., Chen, C.-R., Sobue, S.-I., Minh, V.-Q., Chiang, S.-H., Nguyen, L.-D., Lin, Y.-W., 2016. A logistic-based method for rice monitoring from multitemporal MODIS-Landsat fusion data. Eur. J. Remote Sens. 49, 39–56. https://doi.org/10.5721/EuJRS20164903
Son, N.T., Chen, C.F., Chen, C.R., Minh, V.Q., Trung, N.H., 2014. A comparative analysis of multitemporal MODIS EVI and NDVI data for large-scale rice yield estimation. Agric. For. Meteorol. 197, 52–64. https://doi.org/10.1016/j.agrformet.2014.06.007
Soullier, G., Demont, M., Arouna, A., Lançon, F., Mendez del Villar, P., 2020. The state of rice value chain upgrading in West Africa. Glob. Food Secur. 25, 100365. https://doi.org/10.1016/j.gfs.2020.100365
Souza, C.H.W.D., Lamparelli, R.A.C., Rocha, J.V., Magalhães, P.S.G., 2017. Height estimation of sugarcane using an unmanned aerial system (UAS) based on structure from motion (SfM) point clouds. Int. J. Remote Sens. 38, 2218–2230. https://doi.org/10.1080/01431161.2017.1285082
Statistica, 2020a. Total global rice consumption 2020 [WWW Document]. Statista. URL https://www.statista.com/statistics/255977/total-global-rice-consumption/ (accessed 5.24.20).
Statistica, 2020b. Rice consumption by country 2019 [WWW Document]. Statista. URL https://www.statista.com/statistics/255971/top-countries-based-on-rice-consumption-2012-2013/ (accessed 5.24.20).
Stroppiana, D., Boschetti, M., Confalonieri, R., Bocchi, S., Brivio, P.A., 2006. Evaluation of LAI-2000 for leaf area index monitoring in paddy rice. Field Crops Res. 99, 167–170. https://doi.org/10.1016/j.fcr.2006.04.002
Sustainable Rice Platform (SRP), 2019. Rice facts [WWW Document]. URL http://www.sustainablerice.org/Resources/ (accessed 5.24.20).
Suykens, J.A.K., Vandewalle, J., 1999. Least Squares Support Vector Machine Classifiers. Neural Process. Lett. 9, 293–300. https://doi.org/10.1023/A:1018628609742
Tarfa, P., Ayuba, H., Onyeneke, R., Idris, N., Nwajiuba, C., 2019. Climate change perception and adaptation in Nigeria's Guinea Savanna: Empirical evidence from farmers in Nasarawa State, Nigeria [WWW Document]. URL https://scholar.google.com/scholar_lookup?title=Climate%20change%20perception%20and%20adaptation%20in%20Nigeria%E2%80%99s%20Guinea%20Savanna%3A

%20Empirical%20evidence%20from%20farmers%20in%20Nasarawa%20State%2C%20Nigeria&author=PY.%20Tarfa&author=HK.%20Ayuba&author=RU.%20Onyeneke&author=N.%20Idris&author=CA.%20Nwajiuba&author=CO.%20Igberi&journal=Appl%20Ecol%20Environ%20Res&volume=17&issue=3&pages=7085-7112&publication_year=2019 (accessed 7.19.20).

ten Harkel, J., Bartholomeus, H., Kooistra, L., 2020. Biomass and Crop Height Estimation of Different Crops Using UAV-Based Lidar. Remote Sens. 12, 17. https://doi.org/10.3390/rs12010017

Thenkabail, P.S., Smith, R.B., De Pauw, E., 2000. Hyperspectral Vegetation Indices and Their Relationships with Agricultural Crop Characteristics. Remote Sens. Environ. 71, 158–182. https://doi.org/10.1016/S0034-4257(99)00067-X

Thorp, K.R., Wang, G., West, A.L., Moran, M.S., Bronson, K.F., White, J.W., Mon, J., 2012a. Estimating crop biophysical properties from remote sensing data by inverting linked radiative transfer and ecophysiological models. Remote Sens. Environ. 124, 224–233. https://doi.org/10.1016/j.rse.2012.05.013

Thorp, K.R., Wang, G., West, A.L., Moran, M.S., Bronson, K.F., White, J.W., Mon, J., 2012b. Estimating crop biophysical properties from remote sensing data by inverting linked radiative transfer and ecophysiological models. Remote Sens. Environ. 124, 224–233. https://doi.org/10.1016/j.rse.2012.05.013

Tilly, N., Hoffmeister, D., Cao, Q., Huang, S., Lenz-Wiedemann, V., Miao, Y., Bareth, G., 2014. Multitemporal crop surface models: accurate plant height measurement and biomass estimation with terrestrial laser scanning in paddy rice. J. Appl. Remote Sens. 8, 083671. https://doi.org/10.1117/1.JRS.8.083671

Tilly, N., Hoffmeister, D., Cao, Q., Lenz-Wiedemann, V., Miao, Y., Bareth, G., 2015. Transferability of Models for Estimating Paddy Rice Biomass from Spatial Plant Height Data. Agriculture 5, 538–560. https://doi.org/10.3390/agriculture5030538

Tuia, D., Volpi, M., Verrelst, J., Camps-Valls, G., 2018. Advances in Kernel Machines for Image Classification and Biophysical Parameter Retrieval, in: Moser, G., Zerubia, J. (Eds.), Mathematical Models for Remote Sensing Image Processing: Models and Methods for the Analysis of 2D Satellite and Aerial Images, Signals and Communication Technology. Springer International Publishing, Cham, pp. 399–441. https://doi.org/10.1007/978-3-319-66330-2_10

Ugalahi, U.B., Adeoye, S.O., Agbonlahor, M.U., 2016. Irrigation potentials and rice self-sufficiency in Nigeria: A review. Afr. J. Agric. Res. 11, 298–309. https://doi.org/10.5897/AJAR2015.10284

Upreti, D., Huang, W., Kong, W., Pascucci, S., Pignatti, S., Zhou, X., Ye, H., Casa, R., 2019. A Comparison of Hybrid Machine Learning Algorithms for the Retrieval of Wheat Biophysical Variables from Sentinel-2. Remote Sens. 11, 481. https://doi.org/10.3390/rs11050481

van Klompenburg, T., Kassahun, A., Catal, C., 2020. Crop yield prediction using machine learning: A systematic literature review. Comput. Electron. Agric. 177, 105709. https://doi.org/10.1016/j.compag.2020.105709

Vanino, S., Nino, P., De Michele, C., Falanga Bolognesi, S., D'Urso, G., Di Bene, C., Pennelli, B., Vuolo, F., Farina, R., Pulighe, G., Napoli, R., 2018. Capability of Sentinel-2 data for estimating maximum evapotranspiration and irrigation requirements for tomato crop in Central Italy. Remote Sens. Environ. 215, 452–470. https://doi.org/10.1016/j.rse.2018.06.035

Vapnik, V., 1998. The Support Vector Method of Function Estimation, in: Suykens, J.A.K., Vandewalle, J. (Eds.), Nonlinear Modeling: Advanced Black-Box Techniques. Springer US, Boston, MA, pp. 55–85. https://doi.org/10.1007/978-1-4615-5703-6_3

Vazifedoust, M., van Dam, J.C., Bastiaanssen, W.G.M., Feddes, R.A., 2009. Assimilation of satellite data into agrohydrological models to improve crop yield forecasts. Int. J. Remote Sens. 30, 2523–2545. https://doi.org/10.1080/01431160802552769
Vergara, B.S., 1991. Rice Plant Growth and Development, in: Luh, B.S. (Ed.), Rice: Volume I. Production/Volume II. Utilization. Springer US, Boston, MA, pp. 13–22. https://doi.org/10.1007/978-1-4899-3754-4_2
Verger, A., Baret, F., Camacho, F., 2011. Optimal modalities for radiative transfer-neural network estimation of canopy biophysical characteristics: Evaluation over an agricultural area with CHRIS/PROBA observations. Remote Sens. Environ. 115, 415–426. https://doi.org/10.1016/j.rse.2010.09.012
Verhoef, W., 1984. Light scattering by leaf layers with application to canopy reflectance modeling: The SAIL model. Remote Sens. Environ. 16, 125–141. https://doi.org/10.1016/0034-4257(84)90057-9
Verrelst, J., Alonso, L., Camps-Valls, G., Delegido, J., Moreno, J., 2012a. Retrieval of Vegetation Biophysical Parameters Using Gaussian Process Techniques. IEEE Trans. Geosci. Remote Sens. 50, 1832–1843. https://doi.org/10.1109/TGRS.2011.2168962
Verrelst, J., Camps-Valls, G., Muñoz-Marí, J., Rivera, J.P., Veroustraete, F., Clevers, J.G.P.W., Moreno, J., 2015a. Optical remote sensing and the retrieval of terrestrial vegetation bio-geophysical properties – A review. ISPRS J. Photogramm. Remote Sens. 108, 273–290. https://doi.org/10.1016/j.isprsjprs.2015.05.005
Verrelst, J., Camps-Valls, G., Muñoz-Marí, J., Rivera, J.P., Veroustraete, F., Clevers, J.G.P.W., Moreno, J., 2015b. Optical remote sensing and the retrieval of terrestrial vegetation bio-geophysical properties – A review. ISPRS J. Photogramm. Remote Sens. 108, 273–290. https://doi.org/10.1016/j.isprsjprs.2015.05.005
Verrelst, J., Dethier, S., Rivera, J.P., Munoz-Mari, J., Camps-Valls, G., Moreno, J., 2016. Active Learning Methods for Efficient Hybrid Biophysical Variable Retrieval. IEEE Geosci. Remote Sens. Lett. 13, 1012–1016. https://doi.org/10.1109/LGRS.2016.2560799
Verrelst, J., Malenovský, Z., Van der Tol, C., Camps-Valls, G., Gastellu-Etchegorry, J.-P., Lewis, P., North, P., Moreno, J., 2018. Quantifying Vegetation Biophysical Variables from Imaging Spectroscopy Data: A Review on Retrieval Methods. Surv. Geophys. 40, 589–629. https://doi.org/10.1007/s10712-018-9478-y
Verrelst, J., Muñoz, J., Alonso, L., Delegido, J., Rivera, J.P., Camps-Valls, G., Moreno, J., 2012b. Machine learning regression algorithms for biophysical parameter retrieval: Opportunities for Sentinel-2 and -3. Remote Sens. Environ. 118, 127–139. https://doi.org/10.1016/j.rse.2011.11.002
Verrelst, Jochem, Rivera, J.P., Gitelson, A., Delegido, J., Moreno, J., Camps-Valls, G., 2016. Spectral band selection for vegetation properties retrieval using Gaussian processes regression. Int. J. Appl. Earth Obs. Geoinformation 52, 554–567. https://doi.org/10.1016/j.jag.2016.07.016
Verrelst, J., Rivera, J.P., Veroustraete, F., Muñoz-Marí, J., Clevers, J.G.P.W., Camps-Valls, G., Moreno, J., 2015c. Experimental Sentinel-2 LAI estimation using parametric, non-parametric and physical retrieval methods – A comparison. ISPRS J. Photogramm. Remote Sens. 108, 260–272. https://doi.org/10.1016/j.isprsjprs.2015.04.013
Verrelst, J., Romijn, E., Kooistra, L., 2012c. Mapping Vegetation Density in a Heterogeneous River Floodplain Ecosystem Using Pointable CHRIS/PROBA Data. Remote Sens. 4, 2866–2889. https://doi.org/10.3390/rs4092866
Verrelst, J., Schaepman, M.E., Koetz, B., Kneubühler, M., 2008. Angular sensitivity analysis of vegetation indices derived from CHRIS/PROBA data. Remote Sens. Environ.,

Earth Observations for Terrestrial Biodiversity and Ecosystems Special Issue 112, 2341–2353. https://doi.org/10.1016/j.rse.2007.11.001
Verrelst, J., Vicent, J., Rivera-Caicedo, J.P., Lumbierres, M., Morcillo-Pallarés, P., Moreno, J., 2019. Global Sensitivity Analysis of Leaf-Canopy-Atmosphere RTMs: Implications for Biophysical Variables Retrieval from Top-of-Atmosphere Radiance Data. Remote Sens. 11, 1923. https://doi.org/10.3390/rs11161923
Viña, A., Gitelson, A.A., Nguy-Robertson, A.L., Peng, Y., 2011. Comparison of different vegetation indices for the remote assessment of green leaf area index of crops. Remote Sens. Environ. 115, 3468–3478. https://doi.org/10.1016/j.rse.2011.08.010
von Grebme, K., Headey, D., Olofinbiyi, T., Wiesmann, D., Fritschel, H., Yin, S., Yohannes, Y., 2013. 2013 Global Hunger Index: The Challenge of Hunger | IFPRI : International Food Policy Research Institute [WWW Document]. URL https://www.ifpri.org/publication/2013-global-hunger-index-challenge-hunger-building-resilience-achieve-food-and-nutrition (accessed 5.6.20).
Vuolo, F., Neugebauer, N., Bolognesi, S.F., Atzberger, C., D'Urso, G., 2013. Estimation of Leaf Area Index Using DEIMOS-1 Data: Application and Transferability of a Semi-Empirical Relationship between two Agricultural Areas. Remote Sens. 5, 1274–1291. https://doi.org/10.3390/rs5031274
Wahid, A., Close, T.J., 2007. Expression of dehydrins under heat stress and their relationship with water relations of sugarcane leaves. Biol. Plant. 51, 104–109. https://doi.org/10.1007/s10535-007-0021-0
Wang, F., Wang, Fumin, Zhang, Y., Hu, J., Huang, J., Xie, J., 2019. Rice Yield Estimation Using Parcel-Level Relative Spectral Variables From UAV-Based Hyperspectral Imagery. Front. Plant Sci. 10. https://doi.org/10.3389/fpls.2019.00453
Wang, L., Chang, Q., Li, F., Yan, L., Huang, Y., Wang, Q., Luo, L., 2019. Effects of Growth Stage Development on Paddy Rice Leaf Area Index Prediction Models. Remote Sens. 11, 361. https://doi.org/10.3390/rs11030361
Wang, Z., Zhang, W., Beebout, S.S., Zhang, H., Liu, L., Yang, J., Zhang, J., 2016a. Grain yield, water and nitrogen use efficiencies of rice as influenced by irrigation regimes and their interaction with nitrogen rates. Field Crops Res. 193, 54–69. https://doi.org/10.1016/j.fcr.2016.03.006
Wang, Z., Zhang, W., Beebout, S.S., Zhang, H., Liu, L., Yang, J., Zhang, J., 2016b. Grain yield, water and nitrogen use efficiencies of rice as influenced by irrigation regimes and their interaction with nitrogen rates. Field Crops Res. 193, 54–69. https://doi.org/10.1016/j.fcr.2016.03.006
Wardlow, B.D., Egbert, S.L., Kastens, J.H., 2007. Analysis of time-series MODIS 250 m vegetation index data for crop classification in the U.S. Central Great Plains. Remote Sens. Environ. 108, 290–310. https://doi.org/10.1016/j.rse.2006.11.021
Watanabe, K., Guo, W., Arai, K., Takanashi, H., Kajiya-Kanegae, H., Kobayashi, M., Yano, K., Tokunaga, T., Fujiwara, T., Tsutsumi, N., Iwata, H., 2017. High-Throughput Phenotyping of Sorghum Plant Height Using an Unmanned Aerial Vehicle and Its Application to Genomic Prediction Modeling. Front. Plant Sci. 8. https://doi.org/10.3389/fpls.2017.00421
Weiss, M., Baret, F., 2016. S2ToolBox Level 2 products:LAI, FAPAR, FCOVER 53.
Weiss, M., Baret, F., Garrigues, S., Lacaze, R., 2007. LAI and fAPAR CYCLOPES global products derived from VEGETATION. Part 2: validation and comparison with MODIS collection 4 products. Remote Sens. Environ. 110, 317–331. https://doi.org/10.1016/j.rse.2007.03.001
Weiss, M., Baret, F., Myneni, R.B., Pragnère, A., Knyazikhin, Y., 2000. Investigation of a model inversion technique to estimate canopy biophysical variables from spectral and

directional reflectance data. Agronomie 20, 3–22. https://doi.org/10.1051/agro:2000105
Whitcraft, A.K., Becker-Reshef, I., Justice, C.O., 2015. A Framework for Defining Spatially Explicit Earth Observation Requirements for a Global Agricultural Monitoring Initiative (GEOGLAM). Remote Sens. 7, 1461–1481. https://doi.org/10.3390/rs70201461
Wolfenson, K.D.M., 2013. Coping with the food and agriculture challenge: smallholders' agenda. Food Agric. Organ. U. N. Rome.
Woodhill, J., Hasnain, S., Griffith, A., 2020. Farmers and food systems: What future for small scale agriculture? | Environmental Change Institute, University of Oxford news [WWW Document]. URL (accessed 6.18.20).
Wopereis, M., Defoer, T., Idinoba, P., Diack, S., Dugué, M.-J., 2009. AfricaRice | Participatory Learning and Action Research (PLAR) [WWW Document]. Afr.-Engl. URL https://www.africarice.org/plar (accessed 7.16.20).
Xiao, X., Boles, S., Liu, J., Zhuang, D., Frolking, S., Li, C., Salas, W., Moore, B., 2005. Mapping paddy rice agriculture in southern China using multi-temporal MODIS images. Remote Sens. Environ. 95, 480–492. https://doi.org/10.1016/j.rse.2004.12.009
Xie, Q., Dash, J., Huang, W., Peng, D., Qin, Q., Mortimer, H., Casa, R., Pignatti, S., Laneve, G., Pascucci, S., Dong, Y., Ye, H., 2018. Vegetation Indices Combining the Red and Red-Edge Spectral Information for Leaf Area Index Retrieval. IEEE J. Sel. Top. Appl. Earth Obs. Remote Sens. 11, 1482–1493. https://doi.org/10.1109/JSTARS.2018.2813281
Xie, Q., Dash, J., Huete, A., Jiang, A., Yin, G., Ding, Y., Peng, D., Hall, C.C., Brown, L., Shi, Y., Ye, H., Dong, Y., Huang, W., 2019a. Retrieval of crop biophysical parameters from Sentinel-2 remote sensing imagery. Int. J. Appl. Earth Obs. Geoinformation 80, 187–195. https://doi.org/10.1016/j.jag.2019.04.019
Xie, Q., Dash, J., Huete, A., Jiang, A., Yin, G., Ding, Y., Peng, D., Hall, C.C., Brown, L., Shi, Y., Ye, H., Dong, Y., Huang, W., 2019b. Retrieval of crop biophysical parameters from Sentinel-2 remote sensing imagery. Int. J. Appl. Earth Obs. Geoinformation 80, 187–195. https://doi.org/10.1016/j.jag.2019.04.019
Xie, Q., Huang, W., Liang, D., Chen, P., Wu, C., Yang, G., Zhang, J., Huang, L., Zhang, D., 2014. Leaf Area Index Estimation Using Vegetation Indices Derived From Airborne Hyperspectral Images in Winter Wheat. IEEE J. Sel. Top. Appl. Earth Obs. Remote Sens. 7, 3586–3594. https://doi.org/10.1109/JSTARS.2014.2342291
Yang, C., Everitt, J.H., Bradford, J.M., 2009. Evaluating high resolution SPOT 5 satellite imagery to estimate crop yield. Precis. Agric. 10, 292–303. https://doi.org/10.1007/s11119-009-9120-6
Yang, Q., Shi, L., Han, J., Zha, Y., Zhu, P., 2019. Deep convolutional neural networks for rice grain yield estimation at the ripening stage using UAV-based remotely sensed images. Field Crops Res. 235, 142–153. https://doi.org/10.1016/j.fcr.2019.02.022
Yang, Z., Shao, Y., Li, K., Liu, Q., Liu, L., Brisco, B., 2017. An improved scheme for rice phenology estimation based on time-series multispectral HJ-1A/B and polarimetric RADARSAT-2 data. Remote Sens. Environ. 195, 184–201. https://doi.org/10.1016/j.rse.2017.04.016
Yi, Q., Jiapaer, G., Chen, J., Bao, A., Wang, F., 2014. Different units of measurement of carotenoids estimation in cotton using hyperspectral indices and partial least square regression. ISPRS J. Photogramm. Remote Sens. 91, 72–84. https://doi.org/10.1016/j.isprsjprs.2014.01.004

Yu, K., Li, F., Gnyp, M.L., Miao, Y., Bareth, G., Chen, X., 2013. Remotely detecting canopy nitrogen concentration and uptake of paddy rice in the Northeast China Plain. ISPRS J. Photogramm. Remote Sens. 78, 102–115. https://doi.org/10.1016/j.isprsjprs.2013.01.008

Yu, S.B., Li, J.X., Xu, C.G., Tan, Y.F., Li, X.H., Zhang, Q., 2002. Identification of quantitative trait loci and epistatic interactions for plant height and heading date in rice. Theor. Appl. Genet. 104, 619–625. https://doi.org/10.1007/s00122-001-0772-5

Yuan, Z., Ata-Ul-Karim, S.T., Cao, Q., Lu, Z., Cao, W., Zhu, Y., Liu, X., 2016. Indicators for diagnosing nitrogen status of rice based on chlorophyll meter readings. Field Crops Res. 185, 12–20. https://doi.org/10.1016/j.fcr.2015.10.003

Yue, J., Yang, G., Tian, Q., Feng, H., Xu, K., Zhou, C., 2019. Estimate of winter-wheat above-ground biomass based on UAV ultrahigh-ground-resolution image textures and vegetation indices. ISPRS J. Photogramm. Remote Sens. 150, 226–244. https://doi.org/10.1016/j.isprsjprs.2019.02.022

Zaks, D.P.M., Kucharik, C.J., 2011. Data and monitoring needs for a more ecological agriculture. Environ. Res. Lett. 6, 014017. https://doi.org/10.1088/1748-9326/6/1/014017

Zarco-Tejada, P.J., Miller, J.R., Noland, T.L., Mohammed, G.H., Sampson, P.H., 2001. Scaling-up and model inversion methods with narrowband optical indices for chlorophyll content estimation in closed forest canopies with hyperspectral data. IEEE Trans. Geosci. Remote Sens. 39, 1491–1507. https://doi.org/10.1109/36.934080

Zhang, C., Kovacs, J.M., 2012. The application of small unmanned aerial systems for precision agriculture: a review. Precis. Agric. 13, 693–712. https://doi.org/10.1007/s11119-012-9274-5

Zhang, K., Ge, X., Shen, P., Li, W., Liu, X., Cao, Q., Zhu, Y., Cao, W., Tian, Y., 2019. Predicting Rice Grain Yield Based on Dynamic Changes in Vegetation Indexes during Early to Mid-Growth Stages. Remote Sens. 11, 387. https://doi.org/10.3390/rs11040387

Zhang, L., Guo, C.L., Zhao, L.Y., Zhu, Y., Cao, W.X., Tian, Y.C., Cheng, T., Wang, X., 2016. Estimating wheat yield by integrating the WheatGrow and PROSAIL models. Field Crops Res. 192, 55–66. https://doi.org/10.1016/j.fcr.2016.04.014

Zhang, M., Su, W., Fu, Y., Zhu, D., Xue, J.-H., Huang, J., Wang, W., Wu, J., Yao, C., 2019. Super-resolution enhancement of Sentinel-2 image for retrieving LAI and chlorophyll content of summer corn. Eur. J. Agron. 111, 125938. https://doi.org/10.1016/j.eja.2019.125938

Zheng, G., Moskal, L.M., 2009. Retrieving Leaf Area Index (LAI) Using Remote Sensing: Theories, Methods and Sensors. Sensors 9, 2719–2745. https://doi.org/10.3390/s90402719

Zheng, H., Cheng, T., Zhou, M., Li, D., Yao, X., Tian, Y., Cao, W., Zhu, Y., 2019. Improved estimation of rice aboveground biomass combining textural and spectral analysis of UAV imagery. Precis. Agric. 20, 611–629. https://doi.org/10.1007/s11119-018-9600-7

Zhou, Y., Xiao, X., Qin, Y., Dong, J., Zhang, G., Kou, W., Jin, C., Wang, J., Li, X., 2016. Mapping paddy rice planting area in rice-wetland coexistent areas through analysis of Landsat 8 OLI and MODIS images. Int. J. Appl. Earth Obs. Geoinformation 46, 1–12. https://doi.org/10.1016/j.jag.2015.11.001

Zhu, J., Tremblay, N., Liang, Y., 2012. Comparing SPAD and atLEAF values for chlorophyll assessment in crop species. Can. J. Soil Sci. 92, 645–648. https://doi.org/10.4141/cjss2011-100